Journal of Xenobiotics

Special Issue Reprint

Feature Papers in Ecotoxicology

Edited by
Valerio Matozzo and Maria Gabriella Marin

mdpi.com/journal/jox

MDPI

Feature Papers in Ecotoxicology

Feature Papers in Ecotoxicology

Guest Editors

Valerio Matozzo
Maria Gabriella Marin

MDPI

Basel • Beijing • Wuhan • Barcelona • Belgrade • Novi Sad • Cluj • Manchester

Guest Editors

Valerio Matozzo
Department of Biology
University of Padova
Padova
Italy

Maria Gabriella Marin
Department of Biology
University of Padova
Padova
Italy

Editorial Office
MDPI AG
Grosspeteranlage 5
4052 Basel, Switzerland

This is a reprint of the Special Issue, published open access by the journal *Journal of Xenobiotics* (ISSN 2039-4713), freely accessible at: https://www.mdpi.com/journal/jox/special_issues/W14Z3YX9FT.

For citation purposes, cite each article independently as indicated on the article page online and as indicated below:

Lastname, A.A.; Lastname, B.B. Article Title. *Journal Name* **Year**, *Volume Number*, Page Range.

ISBN 978-3-7258-4613-9 (Hbk)
ISBN 978-3-7258-4614-6 (PDF)
https://doi.org/10.3390/books978-3-7258-4614-6

Contents

Journal of *Xenobiotics*

MDPI

Editorial

Feature Papers in Ecotoxicology

Valerio Matozzo * and Maria Gabriella Marin

Department of Biology, University of Padova, Via Bassi 58/B, 35131 Padova, Italy; mgmar@mail.bio.unipd.it
* Correspondence: matozzo@mail.bio.unipd.it

Ecotoxicology has progressively evolved as a key scientific discipline for evaluating the impact of both traditional and emerging contaminants on ecosystems. Initially focused on the toxic effects of conventional pollutants such as heavy metals and pesticides, this field has expanded to address a wide array of emerging contaminants, including pharmaceuticals, personal care products, and microplastics, which pose complex and often subtle ecological risks [1,2]. Advances in molecular and omics technologies have enhanced the sensitivity and specificity of ecotoxicological assessments, allowing for the detection of sub-lethal and long-term effects on non-target species and communities [3]. As regulatory frameworks increasingly incorporate ecotoxicological data, this discipline plays a vital role in environmental risk assessment and the development of sustainable pollution management strategies [4].

The collection of research and review papers presented in this Special Issue, "Feature Papers in Ecotoxicology", highlight recent developments in assessing the ecological and biological impacts of various contaminants, including pesticides, nanoplastics, rare-earth elements (REEs), bisphenols, per- and polyfluoroalkyl substances (PFASs), nanomaterials, and endocrine-disrupting chemicals, in various species. These studies offer critical insights into the ecotoxicological mechanisms underlying pollutant exposure and help in identifying key knowledge gaps that must be addressed to improve environmental protection strategies.

A significant theme emerging from this Special Issue incorporates the unintended ecotoxicological consequences of materials designed to provide safer alternatives to traditional pollutants. While biopesticides are generally perceived as environmentally friendly, research on *Allium cepa* has shown that even natural and microbial formulations can exert cyto-genotoxic effects comparable to conventional pesticides, raising concerns in relation to their large-scale application. This underscores the necessity for thorough pre-market testing and long-term ecological impact studies.

Nanoplastics, another growing threat, have been found to affect marine species. The presence of additional environmental stressors, such as salinity fluctuations, can exacerbate the toxicity of contaminants such as REEs, affecting reproductive success and population dynamics in marine species. Similarly, the combination of bisphenol A (BPA) with polystyrene nanoparticles suggests that multiple stressors can have compounding effects, potentially amplifying their toxicity beyond individual exposure outcomes.

The persistence of PFASs in the environment continues to raise concerns due to their bioaccumulative properties and adverse effects on cellular and neuronal function. These findings reinforce the urgency of investigating long-term exposure impacts and developing viable remediation strategies. Likewise, bioaccumulation pathways through food webs, as observed in bivalves consuming bisphenol-exposed microalgae, highlight the need to assess risks associated with the trophic transfer of chemical pollutants.

Innovative experimental models, such as three-dimensional (3D) fish hepatocyte cultures, are proving to represent valuable tools for replicating in vivo responses to contaminants. These cell models provide new opportunities to study the molecular and biochemical effects of pollutants, facilitating more ethical and efficient toxicity screening. Similarly, studies on engineered nanomaterials, such as ZnS quantum dots, reveal how nanoparticles can disrupt primary producers such as microalgae, potentially altering entire aquatic ecosystems.

While these studies advance our understanding of ecotoxicological threats, they also expose critical knowledge gaps. There is a pressing need for the following work:

- Long-term and multigenerational studies to assess chronic and transgenerational effects of pollutants;
- Integrated multi-stressor assessments to understand how environmental factors interact with contaminants;
- Improved regulatory frameworks that account for emerging pollutants and their complex environmental interactions;
- Scalable and sustainable remediation techniques, for example, assessing the potential of bamboo-derived biochar for pollutant removal, which remains underexplored.

As environmental pollution continues to develop, so too must our approaches to mitigating its effects. The research presented in this Special Issue highlights both the urgency and the possibility of advancing ecotoxicology through interdisciplinary collaboration, innovative methodologies, and forward-thinking policies. Addressing these challenges will not only enhance scientific knowledge but also drive the implementation of meaningful environmental protection measures in an increasingly complex and contaminated world.

Funding: This research received no external funding.

Institutional Review Board Statement: Not applicable.

Informed Consent Statement: Not applicable.

Data Availability Statement: Not applicable.

Conflicts of Interest: The authors declare no conflict of interest.

List of Contributions:

1. Duta-Cornescu, G.; Dugala, M.L.; Constantin, N.; Pojoga, M.-D.; Simon-Gruita, A. Evaluation of Clastogenic and Aneugenic Action of Two Bio-Insecticides Using Allium Bioassay. *J. Xenobiot.* **2025**, 15, 35. https://doi.org/10.3390/jox15020035.
2. Eliso, M.C.; Corsi, I.; Spagnuolo, A.; Dumollard, R. Nanoplastic-Induced Developmental Toxicity in Ascidians: Comparative Analysis of Chorionated and Dechorionated *Phallusia mammillata* Embryos. *J. Xenobiot.* **2025**, 15, 10. https://doi.org/10.3390/jox15010010.
3. Dovzhenko, N.V.; Slobodskova, V.V.; Mazur, A.A.; Kukla, S.P.; Istomina, A.A.; Chelomin, V.P.; Beskhmelnov, D.D. Oxidative Stress in Mussel *Mytilus trossulus* Induced by Different-Sized Plastics. *J. Xenobiot.* **2024**, 14, 1826–1835. https://doi.org/10.3390/jox14040097.
4. Melki, S.; Ferrari, E.; Ahmed, R.B.; Spagnuolo, A.; Corsi, I. Single but Not Combined In Vitro Exposure to Bisphenol A and Nanoplastics Affects the Cholinergic Function of the Ascidian *Ciona robusta*. *J. Xenobiot.* **2024**, 14, 1930–1940. https://doi.org/10.3390/jox14040103.
5. Leite, C.; Russo, T.; Polese, G.; Soares, A.M.V.M.; Pretti, C.; Pereira, E.; Freitas, R. Effects of the Interaction of Salinity and Rare Earth Elements on the Health of *Mytilus galloprovincialis*: The Case of Praseodymium and Europium. *J. Xenobiot.* **2024**, 14, 2015–2038. https://doi.org/10.3390/jox14040108.
6. Fabrello, J.; Dalla Fontana, M.; Gaiani, N.; Ciscato, M.; Roverso, M.; Bogialli, S.; Matozzo, V. Assessing the Effects of a Diet of BPA Analogue-Exposed Microalgae in the Clam *Ruditapes philippinarum*. *J. Xenobiot.* **2024**, 14, 1221–1237. https://doi.org/10.3390/jox14030069.

7. Lagostena, L.; Rotondo, D.; Gualandris, D.; Calisi, A.; Lorusso, C.; Magnelli, V.; Dondero, F. Impact of Legacy Perfluorooctane Sulfonate (PFOS) and Perfluorooctanoate (PFOA) on GABA Receptor-Mediated Currents in Neuron-Like Neuroblastoma Cells: Insights into Neurotoxic Mechanisms and Health Implications. *J. Xenobiot.* **2024**, 14, 1771–1783. https://doi.org/10.3390/jox14040094.
8. Deng, B.; Maaloul, R.; Nowak, S.; Sivry, Y.; Yéprémian, C.; Ammar, S.; Mammeri, F.; Brayner, R. Aquatic Fate and Ecotoxicology Effect of ZnS:Mn Quantum Dots on *Chlorella vulgaris* in Fresh Water. *J. Xenobiot.* **2024**, 14, 467–483. https://doi.org/10.3390/jox14020028.
9. Alves, R.F.; Lopes, C.; Rocha, E.; Madureira, T.V. Estrogenic Responsiveness of Brown Trout Primary Hepatocyte Spheroids to Environmental Levels of 17α-Ethinylestradiol. *J. Xenobiot.* **2024**, 14, 1064–1078. https://doi.org/10.3390/jox14030060.
10. Alfei, S.; Pandoli, O.G. Bamboo-Based Biochar: A Still Too Little-Studied Black Gold and Its Current Applications. *J. Xenobiot.* **2024**, 14, 416–451. https://doi.org/10.3390/jox14010026.

References

1. Schwarzenbach, R.P.; Escher, B.I.; Fenner, K.; Hofstetter, T.B.; Johnson, C.A.; von Gunten, U.; Wehrli, B. The challenge of micropollutants in aquatic systems. *Science* **2006**, *313*, 1072–1077. [CrossRef] [PubMed]
2. Ankley, G.T.; Bennett, R.S.; Erickson, R.J.; Hoff, D.J.; Hornung, M.W.; Johnson, R.D.; Mount, D.R.; Nichols, J.W.; Russom, C.L.; Schmieder, P.K.; et al. Adverse outcome pathways: A conceptual framework to support ecotoxicology research and risk assessment. *Environ. Toxicol. Chem.* **2010**, *29*, 730–741. [CrossRef] [PubMed]
3. Van der Oost, R.; Beyer, J.; Vermeulen, N.P.E. Fish bioaccumulation and biomarkers in environmental risk assessment: A review. *Environ. Toxicol. Pharmacol.* **2003**, *13*, 57–149. [CrossRef] [PubMed]
4. Boxall, A.B.A.; Rudd, M.A.; Brooks, B.W.; Caldwell, D.J.; Choi, K.; Hickmann, S.; Innes, E.; Ostapyk, K.; Staveley, J.P.; Verslycke, T.; et al. Pharmaceuticals and personal care products in the environment: What are the big questions? *Environ. Health Perspect.* **2012**, *120*, 1221–1229. [CrossRef] [PubMed]

Journal of *Xenobiotics*

MDPI

Article

Evaluation of Clastogenic and Aneugenic Action of Two Bio-Insecticides Using Allium Bioassay

Georgiana Duta-Cornescu *, Maria Liliana Dugala, Nicoleta Constantin, Maria-Daniela Pojoga and Alexandra Simon-Gruita

Genetics Department, Faculty of Biology, University of Bucharest, Intrarea Portocalelor 1-3, Sector 6, 060101 Bucharest, Romania; dugala.maria-liliana22@s.bio.unibuc.ro (M.L.D.); nicoleta.constantin@bio.unibuc.ro (N.C.); daniela.pojoga@bio.unibuc.ro (M.-D.P.); alexandra.simon@bio.unibuc.ro (A.S.-G.)

* Correspondence: georgiana.duta-cornescu@bio.unibuc.ro

Abstract: It is well known that modern agriculture would not be able to meet the current demand for food without the help of pesticides. However, conventional pesticides have been proven to be extremely harmful to the environment, to the species they are applied to, and, ultimately, to humans. As a result, bio-pesticides have been introduced in recent years and include natural substances that control pests, such as biochemical pesticides, microorganisms used as pest control agents (microbial pesticides), and pesticide substances produced by plants containing added genetic material, known as plant-incorporated protectants (PIPs). Although these are natural products, their widespread use has led to an increased presence in the environment, raising concerns regarding their potential impact on both the environment and human health. The aim of our study was to determine the phyto- and cytogenotoxicity caused by two insecticides, both certified for use in ecological agriculture: one biochemical (BCP) and the other microbial (MP), which were applied in three concentrations (the maximum recommended concentration by the manufacturers (MRFC), 1.5X MRFC, and 2X MRFC) to the meristematic root tissues of *Allium cepa*. The results were compared to a negative control (tap water) and a positive control (a chemical pesticide (CP) containing mainly Deltamethrin). Phytotoxic and cytogenotoxic effects were analyzed at two time intervals (24 and 48 h) by measuring root length, growth percentage, root growth inhibition percentage (phytotoxicity tests), and micronuclei frequency and chromosome aberrations (anaphase bridges, chromosomal fragments, anaphase delays, sticky chromosomes, laggard/vagrant chromosomes) (cytogenotoxicity analyses), respectively. The tests conducted in this study showed that the microbial insecticide provides greater safety when applied, even at higher doses than those recommended by the manufacturers, compared with the biochemical insecticide, whose effects are similar to those induced by the chemical pesticide containing Deltamethrin. However, the results suggest that both insecticides have clastogenic and aneugenic effects, highlighting the need for prior testing of any type of pesticide before large-scale use, especially since the results of the *A. cepa* tests showed high sensitivity and good correlation when compared to other test systems, e.g., mammals.

Keywords: bio-pesticides; *A. cepa* assay; cytogenotoxicity; phytotoxicity; bio-pesticides

1. Introduction

According to the HSE (Health and Safety Executive—Britain's national regulator for workplace health and safety), pesticides, also known as 'plant protection products' (PPP),

are used to control pests, weeds, and diseases, being divided into insecticides, fungicides, herbicides, molluscicides, and plant growth regulators. They can exist in many forms, such as solid granules, powders, or liquids, and consist of one or more active substances co-formulated with other materials [1].

Pesticides are indispensable in modern agricultural production because they allow to obtain increased quantities of products. It is estimated that without the use of pesticides, there would be a 78% loss in fruit production, a 54% loss in vegetable production, and a 32% loss in grain production [2]. According to Carvalho, 2017, pesticide production increased at a rate of about 11% per year, from 0.2 million tons in the 1950s to more than 5 million tons by 2000 [3], with over three billion kilograms of pesticides used worldwide every year [4]. However, only 1% of total pesticides are effectively used to control insect pests on target plants [5], most of the amount used remaining in the environment or acting on non-targeted species [6,7]. Therefore, the indiscriminate use of pesticides has led to serious health and environmental risks [8–11]. Due to the increased concerns regarding the environmental and health effects of pesticides, intensive research efforts were put into understanding farmers' pesticide use behavior and also in developing new types of pesticides, with a minimum to no effect on the environment or non-targeted species. Currently, alternative solutions are being considered and sought after. One of the sustainable solutions is the use of bio-pesticides, as they can be less toxic than chemical pesticides, can be highly specific to the target pest, break down quickly, and have less chance of developing resistance [12].

According to the EPA (United States Environmental Protection Agency), bio-pesticides include naturally occurring substances that control pests (biochemical pesticides), microorganisms that control pests (microbial pesticides), and pesticide substances produced by plants containing added genetic material (plant-incorporated protectants) or PIPs [13]. While conventional pesticides are usually artificial synthesized chemicals that directly kill pest, the bio-chemical pesticides are naturally occurring substances that can be used to control pests through non-toxic mechanisms. Microbial pesticides consist of microorganisms (e.g., a bacterium, fungus, virus or protozoan) as the active ingredient and can control many kinds of pests, although each separate active ingredient is relatively specific for a target pest [14,15].

Even with the emergence of these new bio-pesticides, in the intensive agriculture, the continuous increase in requirements for agricultural products leads to an inappropriate, often indiscriminate, use of pesticides and fertilizers. Therefore, the lack of adequate management and studies to monitor the impact of these products both on the environment and on plants themselves can have a negative impact on human health as well [16–18].

Some of the most used methods for evaluating the toxic effect of pesticides, including insecticides, are phyto- and cytogenotoxicity assays [19,20]

Usually, phytotoxicity tests are used for assessing the impact of various compounds on seed germination and subsequent growth, while plant cytogenotoxicity tests evaluate the impact of a chemical compound on the cell cycle, chemicals that can induce different types of chromosome aberrations (CA). CA represents modifications in either chromosomal structure (due to DNA breaks, inhibition of DNA synthesis and replication of altered DNA) or in the total number of chromosomes (e.g., aneuploidy and polyploidy, as consequences of abnormal segregation of chromosomes) [21,22]. There is a large amount of research indicating that analysis of the different chromosome aberration types in all phases of the cell cycle permits a more comprehensive and accurate evaluation of the clastogenic and/or aneugenic effects of the tested agents [21,23–26] and points that modifications like chromosome bridges and breaks are indicators of a clastogenic action, whereas chromosome losses, delays, adherence, and multipolarity result from aneugenic effects [27,28].

The *A. cepa* bioassay has been used since 1930 to detect the effect of different chemical compounds on the plant genome and is still widely applied today because it is simple, reliable, cheap, and accessible [29–31]. Moreover, many studies have identified similarities between the negative effects (e.g., causing CAs) of some pesticides on cellular DNA from *A. cepa* and from various mammalian species, including humans [29–31]. For example, Fiskesjö [32], when studying the effect of a number of compounds (salt solutions, industrial wastewaters, etc.), showed that the sensitivity of the Allium test was on the same level as the test on human lymphocytes, while Rank and Nielsen [33] indicated an 82% correlation between *A. cepa* tests and carcinogenicity tests in rodents when testing the effect of five mutagenic or carcinogenic chemicals usually found in wastewater. In another study regarding the cytogenetic effect of pyrethroid insecticides, Chauhan et al. [30] reported a good correlation between the *A. cepa* test system and those on mammals (rodents' bone marrow and human lymphocytes), suggesting that the *A. cepa* test can be validated as an alternative to the mammal test systems for monitoring the genotoxic potential of environmental chemicals, such as pesticides.

A. cepa has a small genome (2n = 16) and large chromosomes, which makes it possible to observe their behavior during mitotic divisions [31,34] and allows for the evaluation of different genetic effects, as well as understanding the action mechanisms of various categories of chemical compounds [21].

In this research, the *A. cepa* bioassay was used to assess the phytotoxic and cytogenotoxic impact of two bio-insecticides administered in different concentrations (the maximum dose recommended by the manufacturers and higher). The two tested insecticides belong to two different categories: one is included in the "bio-chemical pesticides" class (BCP) and contains Spinosad, Propanediol, and 1,2 Benzothiazoline, and the other one belongs to the "microbial pesticides class" (MP) and contains *Bacillus thuringiensis*, *Lysinbacillus sphaericus*, *Bacillus subtilis* and other components), certified to be used in ecological agriculture.

The use of positive control (PC), i.e., a compound known to cause various cytotoxic and genotoxic changes, is essential [19,35,36]. Many of the insecticides used wordwide contain Delthametrin [37] and, according to the IOBC (International Organization of Biological Control) rating, Deltamethrin is placed in category 2 level of toxicity, which can be interpreted as moderately harmful [38]. Therefore, Deltamethrin was used as a positive control because, in numerous studies, it proved to be toxic to plants and animals [39–45]. The potentially harmful effects of improper use of these pesticides on the environment and humans can thus be established.

2. Materials and Methods

2.1. Plant Material

Approximately equal sized (~2–2.5 cm diameter) and healthy onion bulbs (*Allium cepa* L., 2n = 16) were purchased at a local vendor and then carefully cleaned in order not to destroy the root primordia. The experiments were performed in triplicate for each treatment applied to onion bulbs.

2.2. Insecticide Solutions

Two insecticides from distinct categories of pesticides were tested: (1) a biochemical pesticide (BCP) that contains Spinosad (22.8%), Propanediol (≥3.0–<10.0%), polyalkylene glycol (≥3.0–<10.0%), and 1,2 Benzothiazoline (<0.05%) [46] and (2) a microbial pesticide (MP) containing super concentrated extract of feeding inhibitors, *Bacillus thuringiensis* 1×10^8 CFU, *Lysinibacillus sphaericus* 1×10^8 CFU, *Bacillus subtilis* 1×10^8 CFU, and other components (20% mineral oil USP, 30% super concentrated vegetable extract, 50% glycerol, 0.5% red dye). Both insecticides are certified to be used in ecological agriculture, being

considered effective against different species from Coleoptera, Lepidoptera, Thysanoptera, and Diptera orders that attack fruit trees, vegetables, and grape crops.

The positive control was represented by a chemical pesticide (PC) containing mainly Deltamethrin (10.5%) but also 2-Methylpropanol (1.00–3.00%), 2,6-Di-tert-butyl-4-methylphenol (0.10–0.25%), cyclohexanone (1.00–40.00%), aromatic hydrocarbons (20.00%), Benzenesulfonic acid, mono-C11-13 branched alkyl derivates, and calcium salts (1.00–5.00%).

In this assay, the three concentrations used were the maximum dose recommended by the manufacturers (MRFC), 1.5X MRFC and 2X MRFC. The experimental design and concentrations are presented in Table 1.

Table 1. The percentage concentration of insecticide solutions in the two experimental variants and in the positive control.

Experimental Variant	Insecticide Concentration (%)		
	PC	**BCP**	**MP**
MRFC (1X)	0.031	0.04	2
1.5 MRFC (1.5X)	0.046	0.06	3
2 MRFC (2X)	0.062	0.08	4

MRFC = maximum recommended field concentration, 1.5X = 1.5-fold higher than MRFC, 2X = twofold higher than MRFC, PC = positive control (insecticide with Deltamethrin), BCP = bio-chemical insecticide, MP = microbial insecticide.

As negative control (NC), healthy onion bulbs grown only in tap water throughout the experiment were used.

For the preparation of the solutions for each of the three insecticides used (MP, BCP, and PC), the manufacturer's instructions were followed. For example, in the case of MP, a concentration of 2% is recommended (i.e., 100 mL of insecticide solution diluted in 5 L of water). This was considered the MRFC (1X) experimental variant. The subsequent experimental variants (1.5 MRCF and 2 MRCF) were obtained by further adding insecticide solution in the same water volume (5 L), according to the desired concentrations. The same procedure was applied to all the insecticides. Since each experimental variant was performed in triplicate, the initial volume of the solution was 5 L to avoid any potential variation in the concentration of the solutions.

2.3. Phytotoxicity Assay

Prior to initiating the test, the outer scales of the bulbs and the dry bottom plate were removed without destroying the root primordia and germinated for 24 h in tap water, until the root primordia were visible. Then, the onion bulbs were transferred into the tested insecticide solutions. The negative control was further incubated in tap water.

The bulbs were allowed to sprout and grow for another 24 h and 48 h at room temperature (25 ± 2 °C), respectively. Numbers of sprouted roots were counted after each time interval and the root lengths were measured with the help of a calibrated ruler.

After each time interval, the length of the emerged roots was measured, and growth percentage and root growth inhibition percentage were computed using the following formulas:

$$\textbf{Growth \%} = \frac{\textbf{Average root length in control plants}}{\textbf{Average root length in treated plants}} \times \textbf{100} \quad (1)$$

$$\textbf{Root growth inhibition} = \textbf{Growth \% in control plants} - \textbf{Growth \% in treated plants} \quad (2)$$

2.4. Cytogenotoxicity Assay

Six root tips, about 0.5 cm long, were randomly removed from each of the three replicates/treatment/time intervals and fixed in 3:1 absolute ethanol/glacial acetic acid for 24 h at 4 °C. The Feulgen staining, followed by the squash method, was applied to

make the cytogenetic slides. The method involves hydrolysis with 1 N Hydrochloric acid (HCl) at a temperature of 60 °C and staining with basic fuchsin. After this treatment, the chromatin of the chromosomes stains red-violet, while the ribonucleic acid in the nucleoli and cytoplasm does not stain. The best slides in terms of biological material mounting, staining, and cellular integrity were selected for further analysis, which involved examining 500 cells/microscope slides.

The microscopic slides were visualized under the optical microscope with 10X, 20X, and 60X objectives. The photography was performed digitally with the Dino-Eye Eyepiece Camera (Dino-Lite Europe, IDCP B.V, Almere, The Netherlands) using the DinoCapture 2.0 (Windows) program.

For the cytogenotoxicity assay, for both time treatments (24 h and 48 h), mitotic index (MI), the % of cells in each mitotic phase were analyzed. MI was calculated using Formula (3).

$$\mathbf{MI} = \frac{\textbf{Number of dividing cells}}{\textbf{Total number of cells}} \times \mathbf{100} \quad (3)$$

Then, micronuclei (MN) frequency and the number of chromosome aberrations (anaphase bridges, chromosomal fragments, anaphase delays, sticky chromosomes, laggard/vagrant chromosomes) were determined.

2.5. Statistical Analysis

All samples and controls were prepared in triplicate. The results are represented as the mean values ± their respective standard deviations. The phytotoxic and cytogenotoxic effects of different insecticide concentrations on *A. cepa* root cells were compared using a two-way analysis of variance (ANOVA). Means were compared with a *t*-test ($p < 0.05$), and the Bonferroni post-tests were applied to identify the statistical differences between the various test samples and the control. The Bonferroni test was applied because it is a statistical test used to reduce the instance of a false positive, being designed, in particular, to prevent data from incorrectly appearing to be statistically significant [47–50]. All statistical analyses were performed using the Data Analysis Tools in Microsoft Excel 2016. Differences between corresponding controls and exposure treatments were considered statistically significant at $p < 0.05$.

3. Results and Discussion

3.1. Root Germination and Growth Inhibition

The present study was carried out to determine the effect of different concentrations of two commercially available insecticides certified to be used in ecological agriculture, on germination and root elongation of *A. cepa* bulbs. The three tested concentrations were chosen considering the fact that today many farmers use phytosanitary products and especially insecticides in excess, often applying treatments with much higher concentrations than those recommended. This situation can be explained by the fact that using the maximum recommended doses or above can avoid or reduce the spread of insecticide-resistant insects [51].

As is shown in Table 2, the root length is negatively correlated with insecticide concentration and treatment time. For example, for BCP-treated samples, a significant reduction in the root's length was observed at each of the three tested concentrations. The mean value of this parameter, after 48 h of treatment, was 0.75 ± 0.1, 0.82 ± 0.2, and 0.57 ± 0.2 compared with the negative control (NC) (2.75 ± 1.5). The level of root growth inhibition was comparable between the plants treated with Deltamethrin (PC) and the ones treated with BCP after 48 h of treatment (Table 2) and were correlated to the **root number**: at 48 h, the number of roots for PC plants was 30.5 ± 1.5 (at 1X experimental variant), 35 ± 7.7 (at 1.5X),

and 31 ± 4 (at 2X), while for the BCP treated bulbs the values were even lower (28.5 ± 4.9; 19.5 ± 9.1, and 13.5 ± 0.7, respectively). These results indicate that the pesticides understudy were phytotoxic and that the level of this effect is concentration dependent.

Table 2. Comparative root length, root number, and root growth inhibition of *A. cepa* exposed to various concentrations of insecticides after 24 and 48 h.

Treatment			Root Length (cm) (Mean ± SD)	No. of Roots (Mean ± SD)	Root Growth Inhibition (%)
NC		**24 h**	2.2 ± 1.8	30.5 ± 2.04	-
		48 h	2.75 ± 1.5	37 ± 1	-
PC	**1X**	**24 h**	1.025 ± 0.6	46 ± 1.6	53.41
		48 h	1.075 ± 0.9	30.5 ± 1.5	60.91
	1.5X	**24 h**	0.675 ± 0.4	42 ± 0.8	69.32
		48 h	0.8 ± 0.6	35 ± 7.7	70.91
	2X	**24 h**	0.625 ± 0.3	45.5 ± 2.85	71.59
		48 h	0.55 ± 0.54	31 ± 4	80.00
BCP insecticide	**1X**	**24 h**	1.52 ± 0.1	41 ± 1.4	30.91
		48 h	0.75 ± 0.1	28.5 ± 4.9	72.73
	1.5X	**24 h**	0.93 ± 0.5	20 ± 0.1	57.73
		48 h	0.82 ± 0.2	19.5 ± 9.1	70.18
	2X	**24 h**	0.68 ± 0.2	27.5 ± 3.5	69.09
		48 h	0.57 ± 0.2	13.5 ± 0.7	79.27
MP insecticide	**1X**	**24 h**	1.85 ± 0.7	30.5 ± 9.1	15.91
		48 h	2.45 ± 0.7	34 ± 7.07	10.91
	1.5X	**24 h**	1.7 ± 0.6	29 ± 8.4	22.73
		48 h	2.42 ± 0.5	33 ± 1.6	12.00
	2X	**24 h**	2.37 ± 0.4	33.5 ± 0.7	**−4.45**
		48 h	3.3 ± 0.2	37.5 ± 0.1	**−20**

1X = MRFC = maximum recommended field concentration, 1.5X = 1.5-fold higher than MRFC, 2X = twofold higher than MRFC, SD = standard deviation, NC = negative control (distilled water), PC = positive control (insecticide with Deltamethrin), BCP = bio-chemical insecticide, MP = microbial insecticide.

The lowest level of root growth inhibition was recorded for MP, with the values ranging from 10.91% (1X variant—48 h of treatment) to a maximum of 22.73% (1.5X variant–after 48 h of treatment), values that are also correlated with the number of roots. These findings indicated that MP insecticide might have a very low to no phytotoxic effect, even when applied at a higher concentration than the one recommended by the manufacturer. Very intriguing observations were made for the 2X experimental variant, for which, at both time intervals (24 h and 48 h), higher values of root length and no. of roots were registered and, therefore, the calculated % of root growth inhibition had negative values (−4.45% at 24 h and −20% after 48 h). These results are consistent with the length and, respectively, the number of roots after 24 h and 48 h of treatment with MP 2X. Thus, after 24 h, the root length in 2X MP insecticide was 2.37 ± 0.4 cm vs. 2.2 ± 1.8 cm in NC, and after 48 h of treatment, the difference was even greater, 3.3 ± 0.2 cm vs. 2.75 ± 1.5 cm. Root number was also higher for 2X MP: 33.5 ± 0.7 after 24 h and 37.5 ± 0.1 after 48 h treatment compared with 30.5 ± 2.4 and 37 ± 1 in NC. These results might be explained by the presence, in larger quantities, of the bacteria contained in MP. Many phytostimulants are known to work through growth hormones (e.g., auxins that promote root growth, and gibberellins

that cause stem elongation and flowering) and help regulate these hormones to improve plant growth [52]. Also, certain beneficial microorganisms, like plant-growth-promoting rhizobacteria (PGPR), stimulate plant growth by producing growth-promoting substances or improving the plant's resistance to disease [53]. MP contains three microbial strains (*Bacillus thuringiensis*, *Lysinibacillus sphaericus* and *Bacillus subtilis*). There are a number of scientific papers that assessed the phytostimulation effect of *B. thuringiensis* [54,55]. Jensen et al. [56] showed that some *B. subtilis* strains can promote, in vitro, the increase of shoot and root surface area in *A. thaliana*, while Martínez et. Dussan [57] showed that *L. sphaericus* could be a key organism in some formula of biofertilizers, as it shows potential in the phytoremediation processes, in crop plant nutrition, and in growth in low nutrient and polluted soils.

In this context, it could be considered that MP had a phytostimulatory effect on root growth in *A. cepa* when it was applied ina 2X MRFC concentration.

3.2. Chromosomal Aberrations and Micronuclei Induction

The cytotoxic potential of new-generation insecticides on *A. cepa* root tip cells was investigated using microscopic analysis in order to observe disturbances on mitotic division and chromosomal aberrations. The analyses focused on cytogenetic changes both in interphase and during all stages of the mitotic division: prophase, metaphase, anaphase, and telophase.

For the four stages of the mitotic division, there was a greater variation in the percentage values of the dividing cells under the action of insecticides (BCP, MP, and PC) compared with NC, in which no significant differences were observed regardless of the duration of the experiment (Table 3).

The MI (mitotic index) of root meristematic cells decreased as insecticide concentration and exposure time increased in almost all treatments compared with the negative control (NC). These results proved the alteration exerted by insecticides on the growth and development of the meristematic cells of the root of onion bulbs, MI being an important parameter in monitoring the effect of different chemical substances on the environment and an appropriate indicator of the cytotoxicity level [21]. The highest MI values were observed in plants of NC, reaching 33.75% at 24 h and 45.25% at 48 h, which indicated normal mitotic activity. On the other hand, differences regarding the MI value varied depending on the type of insecticide used and its concentration. For example, in *A. cepa* bulbs treated with BCP, all concentrations tested (except the 0.04%, 1X, after 24 h) generated statistically significant MI decreases when compared to the negative control (Table 3). The lower MI (16.25%) was obtained for 1X experimental variant after 48 h of exposure, while for the other treatments, the values varied between 18.8% (2X after 24 h) and 21.38% (2X after 48 h). These results suggest that BCP insecticide might have an inhibitory effect on cell division.

MP treatment had a statistically significant inhibitory effect on *A. cepa* only at the 3% concentration (1.5X): MI after 24 h was 24.75 and 27.5 after 48 h compared with 33.75 at 24 h and, respectively, 45.24 at 48 h in NC (Table 3). For the 2X experimental variant (4% MP concentration), the registered MI index was lower than in controls but not statistically significant.

This effect can be explained by the fact that the insecticide has a clastogenic effect (because clastogenic agents can cause a reduction in MI [58] due to chromosomal fragmentation) but also aneugenic (because aneugenic agents, having cell division disturbing properties, can temporarily increase MI before causing cycle arrest or apoptosis [59,60]).

Table 3. Cytogenetic analysis of *A. cepa* root tips exposed to insecticides in correlation with the concentration and time of exposure.

Treatment			TNDC ± SD	MI	Pro. (%)	Meta. (%)	Ana. (%)	Telo. (%)
NC		**24 h**	270 ± 8.9	33.75	39.62	29.97	11.4	21.85
		48 h	362 ± 1.5	45.25	34.25	32.9	13.5	26.6
PC	**1X**	**24 h**	241 ± 6.2	30.13	36.51	19.08	18.6	25.7
		48 h	**168 ± 4.2** [a]	**21.13** [a]	**26.62** [a]	**30.76** [a]	**21.3** [a]	**21.3** [a]
	1.5X	**24 h**	**184 ± 8.4** [b]	**23** [b]	**26.1** [b]	**36.4** [b]	**17.4** [b]	**20.1** [b]
		48 h	**227± 4.4** [b]	**28.34** [b]	**24.66** [b]	**40.08** [b]	**16.4** [b]	**18.5** [b]
	2X	**24 h**	**20 ± 4.3** [a]	**2.5** [a]	**15** [a]	**55** [a]	**15** [a]	**15** [a]
		48 h	214 ± 9.2	26.75	28.5	36.4	14.5	20.6
BCP	**1X**	**24 h**	200 ± 7.5	25	33	21	17	29
		48 h	**130 ± 6.25** [b]	**16.25** [b]	**37.7** [b]	**25.4** [b]	**12.3** [b]	**24.6** [b]
	1.5X	**24 h**	**166 ± 3.6** [b]	**20.75** [b]	**36.1** [b]	**16.9** [b]	**17.5** [b]	**29.5** [b]
		48 h	**165 ± 3.6** [b]	**20.62** [b]	**34.5** [b]	**22.4** [b]	**17.6** [b]	**25.5** [b]
	2X	**24 h**	**151 ± 1.9** [b]	**18.8** [b]	**29.1** [b]	**25.8** [b]	**19.9** [b]	**25.2** [b]
		48 h	**171 ± 7.8** [b]	**21.38** [b]	**36.8** [b]	**13.7** [b]	**16.9** [b]	**27.5** [b]
MP	**1X**	**24 h**	253 ± 6.2	31.62	41.89	18.97	14.62	24.5
		48 h	287 ± 6.9	35.87	31.35	29.96	20.55	18.11
	1.5X	**24 h**	**198 ± 6.2** [b]	**24.75** [b]	**35.87** [b]	**22.72** [b]	**16.66** [b]	**22.72** [b]
		48 h	**220 ± 4.4** [a]	**27.5** [a]	**37.72** [a]	**22.72** [a]	**15.45** [a]	**24.09** [a]
	2X	**24 h**	219 ± 2.1	27.37	34.7	22.83	17.8	24.65
		48 h	221 ± 7.3	27.62	35.75	26.69	18.55	19.1

1X, 1.5X, 2X = experimental variants, TNDC = total number of cells in the division, SD = standard deviation, MI = mitotic index, Pro. % = % of prophases out of the total number of cells in the division, Meta. % = % of metaphases from the total number of cells in division, Ana. % = % of anaphases from the total number of cells in the division, Telo. % = % telophases out of total dividing cells, [a] = statistically significant values, $p \leq 0.05$ compared with a negative control with *t*-test and Bonferroni Correction, [b] = highly statistically significant values, $p \leq 0.01$ compared with a negative control with *t*-test and Bonferroni Correction.

In all treatment options (PC, MP, and BCP insecticides at 1X, 1.5X, and 2X concentrations), not only was the decrease in the number of dividing cells as previously outlined identified, but also various types of chromosomal aberrations were scored and centralized in Table 4. In contrast to the insecticide treatments, no CA or nuclear abnormalities were observed during mitosis in NC grown in tap water. All prophase, metaphase, anaphase, and telophase stages were clearly visible without changes in the number or structure of chromosomes.

Table 4. Chromosome aberrations on root meristematic cells of *A. cepa* after treatment with different concentrations of insecticides.

	PC						**BCP**						**MP**					
	1X		**1.5X**		**2X**		**1X**		**1.5X**		**2X**		**1X**		**1.5X**		**2X**	
	24 h	**48 h**	**24 h**	**48 h**	**24 h**	**48 h**	**24 h**	**48 h**	**24 h**	**48 h**	**24 h**	**48 h**	**24 h**	**48 h**	**24 h**	**48 h**	**24 h**	**48 h**
Chromosomal bridges	2	0	0	4	0	3	0	0	0	1	1	0	0	1	1	1	0	0
Vagrant/laggard	8	6	4	11	0	5	5	0	8	5	4	11	12	0	7	13	14	2
Other modifications *	0	0	1	2	0	0	1	0	0	0	0	0	1	0	1	0	0	0
TCA	**10**	**6**	**5**	**17**	**0**	**8**	**6**	**0**	**8**	**6**	**5**	**11**	**13**	**1**	**9**	**14**	**14**	**2**
Cells with 1 MN	0	0	0	1	23	1	5	8	6	10	4	29	3	0	2	1	0	0
Cells with 2-more MNs **	0	0	0	1	6	0	3	0	0	1	0	4	0	0	0	0	0	0
TCNM	**0**	**0**	**0**	**2**	**29**	**1**	**8**	**8**	**6**	**11**	**4**	**33**	**3**	**0**	**2**	**1**	**0**	**0**

* = chromosomal fragment and/or decoiled chromosomes; ** = we have found cells with 3 and 6 MNs; TCA = total number of chromosomal aberrations; TCNM = total number of cells with MN; 1X, 1.5X, 2X = experimental variants; PC = positive control (insecticide with Deltamethrin); BCP = bio-chemical insecticide; MP = microbial insecticide.

CAs, which include chromosomal bridges, laggard/vagrant chromosomes, chromosomal fragments, and decoiled chromosomes, indicated disturbances in the normal processes of cell division. Also, in the interphase, the presence of some cells with one or more micronuclei (MN) was observed.

Chromosome bridges and fragments are generally caused by the clastogenic action of the insecticides on DNA strands (structural aberrations), whereas lagging/vagrant

chromosomes and chromosome losses represent the result of the aneugenic effects of these pesticides, which affect the number of chromosomes due to mitotic spindle abnormalities [61]. Chromosomal bridges are associated with further chromosome breakage, aneuploidy or polyploidy and sometimes even cell cycle arrest [62]. Vagrant and laggard chromosome presence generates, invariably, an unequal number of chromosomes in the resulting cells after division [63]. Acentric fragments, lacking the centromere, are unbalanced and distributed during cell division to daughter cells, some of them being lost in successive divisions. Depending on the number of genes contained, the loss of an acentric fragment may adversely affect the phenotype or may even be incompatible with the viability of the carrier organism [64].

Identifying the appearance of MNs is a simple and efficient way of testing the possible mutagenic effect of pesticides in general. They are visible in the interphase, and their presence and number represent definite proof of the genotoxic (clastogenic and aneugenic) effects of the tested insecticides [21]. MNs are the result of unrepaired or incorrectly repaired DNA damage, that is, of chromosomal aberrations (breaks and chromosome losses) during mitotic division [65].

At 24 h, all three insecticides induced chromosomal aberrations in a concentration-dependent manner. Interestingly, after 48 h of treatment, the number of chromosomal aberrations decreased, especially for MP treatment. One possible explanation for these observations might be that, after 24 h of treatment, the insecticides induced an adaptive response conferring the protection of root cells from genotoxic stress [66]. Also, it is possible that the cells with severely damaged DNA were directed to apoptosis, while in the surviving cells, DNA repair mechanisms operated [67].

As it was expected, positive control PC, which was a Deltamethrin containing insecticide, caused, at the 1X concentration, a significant number of chromosomal bridges and laggard chromosomes without inducing MN or other major abnormalities. At the 1.5X concentration, cells with MN and chromosomal fragments were observed, while at the highest concentration, this treatment induced a larger number of 1 MN cells but also cells with 3 MN (Figure 1).

BCP induced not only laggards and vagrant chromosomes but also a large number of cells with MN. In this case, the number of abnormal cells increased in correlation with the concentration used (Figure 2). The bio-chemical insecticide (BCP) investigated in this study belongs to the Naturalyte class of pesticides, a class that includes products derived from metabolites of living organisms. The main component of this insecticide is Spinosad, which is the fermentation product of the *Saccharopolyspora spinosa* aerobic bacteria. In recent years, several studies have been published indicating that Spinosad may have genotoxic effects on non-target species [68–70] or has been associated with various ecotoxicological events [71–74].

The results obtained in the present study are in agreement with those reported by Mendonca et. all, which showed that Spinosad exerted a mutagenic effect on *Tradescantia pallida* species at concentrations of 0.626, 1.25, and 2.5 g/mL [75], even though there is no total consensus among the data identified in the literature regarding Spinosad mutagenicity.

For example, in 1997, the U.S. Environmental Protection Agency stated that Spinosad has no mutagenic effect [76], results that were sustained by Yano et al. (who reported, in 2002, that Spinosad was no carcinogenic effect, at concentrations up to 0.05% to Fischer 344 rats) [77], Stebbins (who determined that chronic exposure of mice to Spinosad, i.e., 51 mg/kg/day for 18 months resulted in no tumor formation) [78] and Akmoutsou, which showed, using SMART test, that Spinosad does not have genotoxic activity on *D. melanogaster* [68]. On the other hand, Mansour and their team determined that Spinosad has genotoxic activity on rat bone marrow cells [79], while Asida et al., in a study from 2022,

highlighted that a bio-pesticide containing Spinosad, had cytotogenotoxic effects (decrease in the mitotic index) on *A. cepa* genome [80]. The identified chromosomal aberrations were similar to those observed in the present study: sticky chromosomes, chromosome bridges, lagging chromosomes, and chromosome fragments [80]. Moreover, despite the fact that organic insecticides, such as BCP, are considered to be a safer alternative to chemical insecticides (such as those containing, e.g., Deltamethrin), there are studies showing that Spinosad, which is now registered for use in over 80 countries, poses a much greater risk to beneficial insects than previously thought, being toxic to pollinators [75]. In our study, the cytogenotoxic effects of the Spinosad-containing insecticide were mainly represented by laggard chromosomes and MN, the frequency of these aberrations being higher with the increase of insecticide concentration. BCP also determined the highest number of chromosomal aberrations among the analyzed insecticides, including PC.

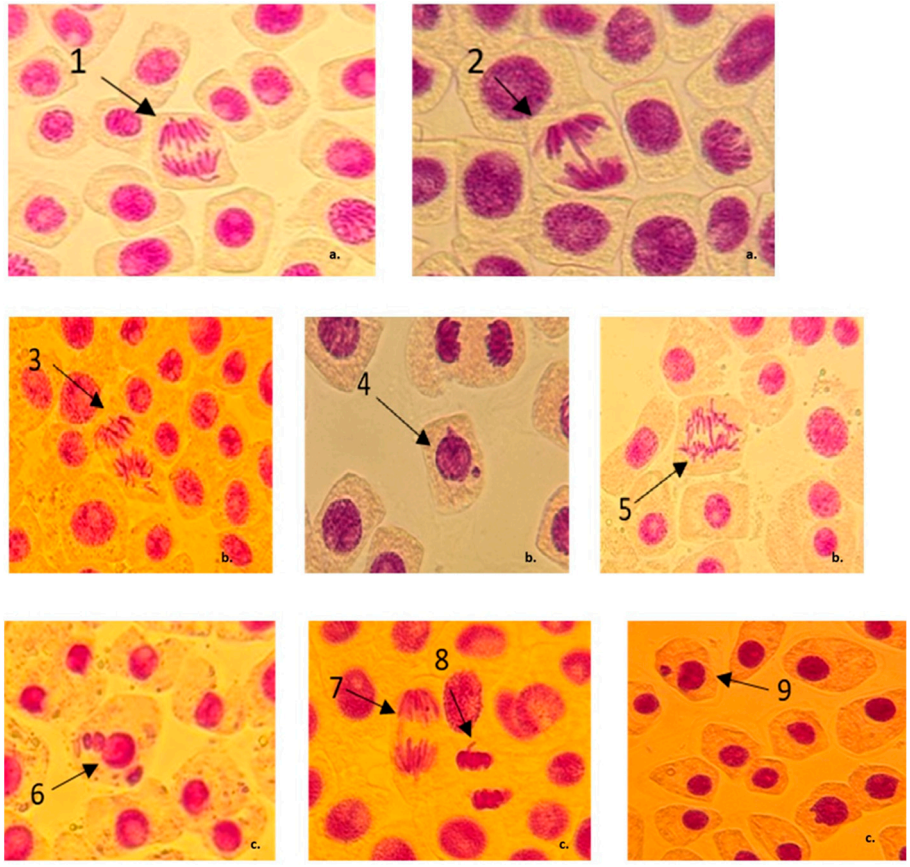

Figure 1. Chromosomal aberrations and nuclear irregularities observed in root tip cells of *A. cepa* after treatments with different concentrations of Deltamethrin-containing insecticide (PC). (**a**) MRFC concentration (1X variant): 1—anaphase with laggards and vagrant chromosomes; 2—anaphase bridge; (**b**) 1.5X concentration: 3—chromosome fragment/vagrant chromosome, 4—cell with 2 MNs, 5—anaphase bridge, (**c**) 2X concentration: 6—cell with 3 MNs, 7—laggards, 8—vagrant chromosomes, 9—cell with one MN.

The MP insecticide at the 1X concentration caused a high number of laggard/vagrant chromosomes and a few cells with 1 MN, and this effect is amplified at the 1.5X concentration. At 2X, the number of abnormalities slightly decreased (Figure 3). Thus, the most frequent cytogenetic abnormalities induced by the MP were the laggard/vagrant chromosomes, without a correlation between the insecticide concentration and the number of observed abnormalities. As mentioned above, MP's stimulating effect might be due to the fact that it contains three different bacterial species (*B. thuringiensis*, *L. sphaericus* and

B. subtilis) proven, in previous studies, to have bio-fertilizer potential by promoting plant growth [17,81,82].

In a very comprehensive review published in 2022, Oliveira-Filho and Grisolia showed that, in general, the *Bacillus* species commonly used in microbial insecticides have none to very low eco-toxicity and no cytogenotoxic effects on non-target organisms [83].

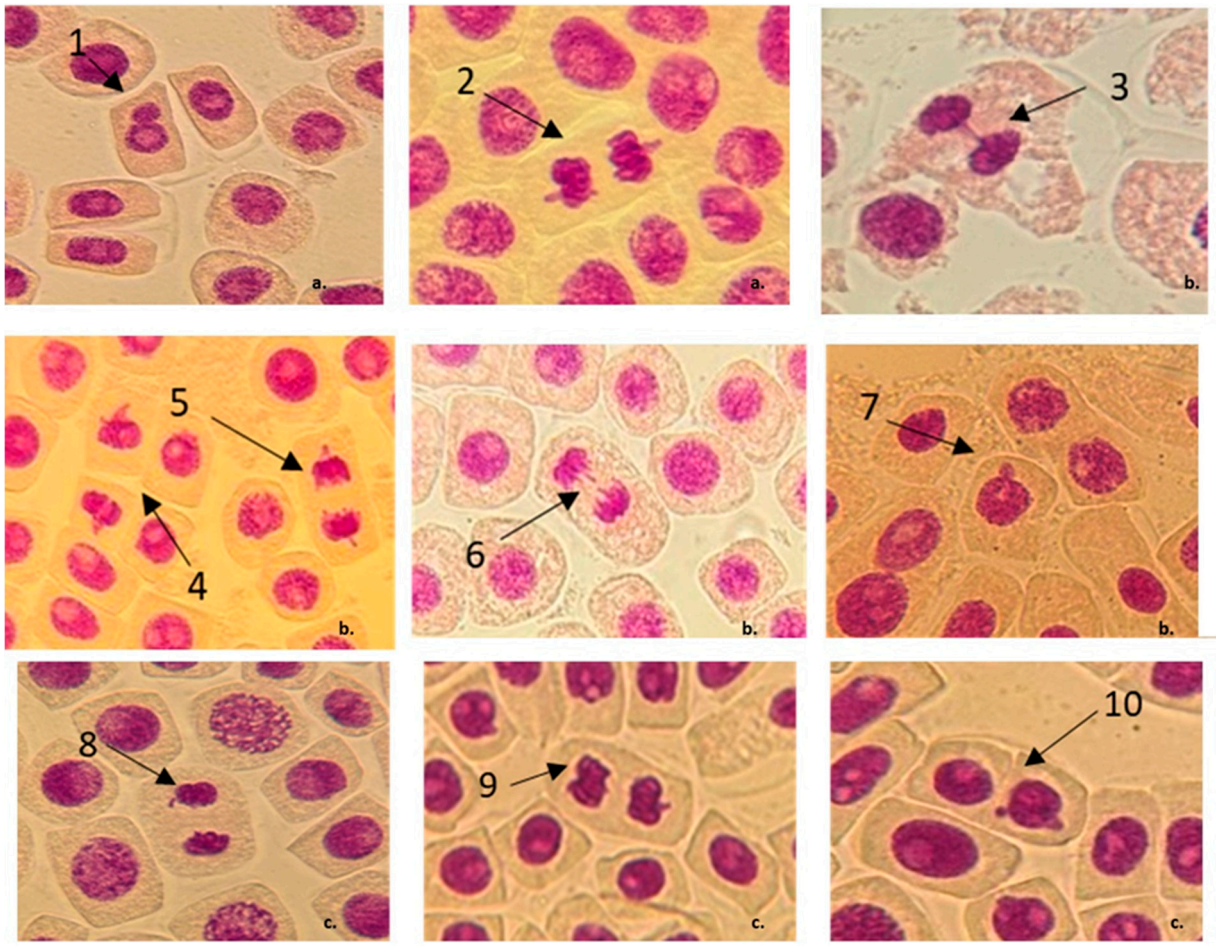

Figure 2. Chromosomal aberrations and nuclear irregularities observed in root tip cells of *A. cepa* after treatments with different concentrations of BCP insecticide. (**a**) MRFC concentration (1X concentration): 1—cell with 1 MN, 2—telophase with vagrant chromosomes, 3—telophase bridge; (**b**) 1.5X concentration: 4 and 5—telophase with vagrant chromosomes, 6—laggards, 7—cell with one MN; (**c**) 2X concentration: 8—chromosome fragment, 9—telophase with vagrant chromosomes, 10—cell with 2 MNs.

However, there are a number of studies showing that some Cry proteins (proteins that are produced by both *B. thuringiensis* and *L. sphaericus*) can induce MN formation in mice [61] and zebrafish erythrocytes [84]. Due to the fact that in our study, the MP insecticide induced the formation not only of MNs but also of other cytogenetic biomarkers (disturbed ana-telophase, chromosome laggards, stickiness, chromosomal bridges), it cannot be considered that the negative effects induced through the treatment with the MP insecticide could be due only to the substances with which the bacterial cells are associated in this commercial pesticide.

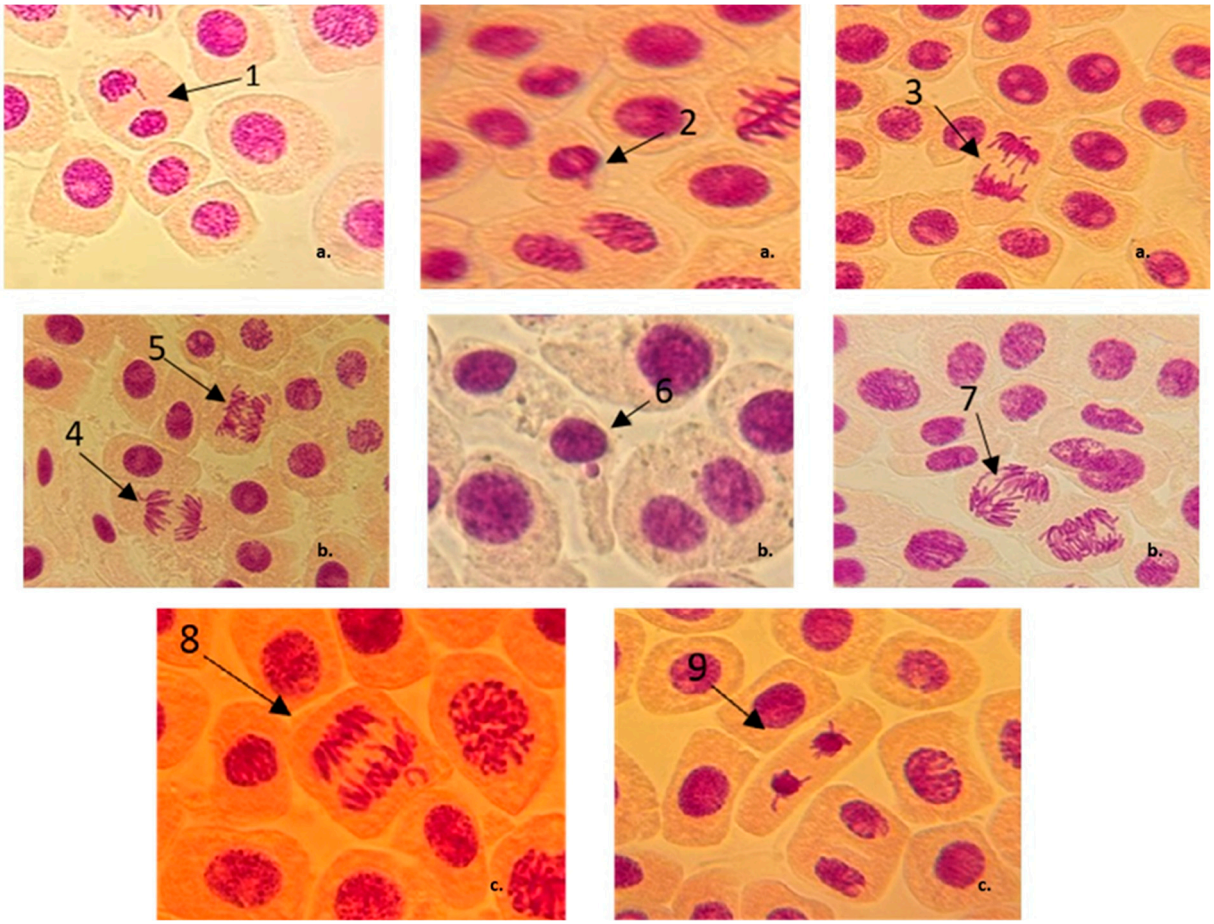

Figure 3. Chromosomal aberrations and nuclear irregularities observed in root tip cells of *A. cepa* following treatments with different concentrations of MP insecticide. (**a**) MRFC concentration (1X concentration): 1—telophase with vagrant chromosome, 2—cell with 1 MN, 3—anaphase with laggards and vagrant chromosomes; (**b**) 1.5X concentration: 4—anaphase with vagrant chromosomes, 5—anaphase with abnormal segregation, 6—cell with 1 MN, 7—anaphase bridge; (**c**) 2X concentration: 8—chromosomal fragment/vagrant chromosome, 9—telophase with laggards and vagrant chromosomes.

On the other hand, one of the main components of the MP insecticide is '*super concentrate vegetable extract*', and even though there are no clear specifications of what is the precise chemical composition of this, usually a vegetable extract consists of a mixture of terpenes, flavonoids, tannins, saponins, alkaloids, and phenols [85]. In a review research on articles from 2010 to 2024 from different databases (ScienceDirect, PubMed, Web of Science, and Scopus), Ghanya et al. [85] summarized the data from 52 studies on plant extracts genotoxicity. The analyzed papers provided a brief overview of the extracts, the primary compounds identified, the plant parts used, the extraction method, the genotoxic tests, and the phytochemicals responsible for the genotoxicity effect. Among this, a total of six plant extracts showed no genotoxic effect, another 14 showed either genotoxic or mutagenic effect, and 14 showed anti-genotoxic effect against different genotoxic-induced agents. In addition, four plant extracts showed both genotoxic and non-genotoxic effects, and six plant extracts showed both genotoxic and antigenotoxic effects. What is very important to note is that in most of the articles, even though there were a number of suggestions regarding the compounds responsible for the genotoxic effects, none of the phytocompounds were individually tested for genotoxic potential to confirm the conclusions. Moreover, the mechanisms by which most plant extracts exert their genotoxic effect remain unidentified,

and so more research is needed on the genotoxicity of plant extracts and their mechanisms of genotoxicity.

4. Conclusions

The risks of using pesticides to combat pests in agricultural crops were evaluated by applying the Allium bioassay, which proved effective in the assessment of the phyto- and cytogenotoxic effects of two insecticides recommended as relatively safe for humans and the environment. Tested insecticides are frequently used in agriculture, but, to date, there are no studies on their possible toxicity. However, there is a series of research on the clastogenic or phytostimulating effects of some of the components of the insecticides (e.g., analysis of the effect of spinosad, which is part of the composition of BCP or of the bacteria and plant extracts from MP constitution).

The tests conducted in this study showed that the microbial insecticide confers greater safety when applied even in higher doses than those recommended by the manufacturers compared with the biochemical insecticide, whose effects are similar to those induced by the chemical pesticide Deltamethrin. The obtained results suggest the clastogenic and aneugenic action of both insecticides, and, therefore, additional studies are needed to provide new information about the harmful potential of these pesticides both on the plant genome and on the environment. Moreover, the results support the idea that there is a need for prior testing of any type of pesticide before large-scale use, especially since the results of the Allium test are frequently similar to those of mammalian and human cell tests. The major problem related to insecticides is that of excessive use, without respecting the recommended concentrations and the break time between treatments.

Author Contributions: Conceptualization, G.D.-C., N.C. and A.S.-G.; investigation, G.D.-C.; methodology, M.L.D.; validation, G.D.-C.; writing—original draft, N.C. and M.-D.P.; writing—review and editing, G.D.-C. and A.S.-G. All authors have read and agreed to the published version of the manuscript.

Funding: This research received no external funding.

Institutional Review Board Statement: Not applicable.

Informed Consent Statement: Not applicable.

Data Availability Statement: The original contributions presented in this study are included in the article. Further inquiries can be directed to the corresponding author.

Conflicts of Interest: The authors declare no conflicts of interest.

References

1. Pesticides: The Basics. Available online: https://www.hse.gov.uk/pesticides/about-pesticides.htm (accessed on 23 November 2024).
2. Tudi, M.; Daniel Ruan, H.; Wang, L.; Lyu, J.; Sadler, R.; Connell, D.; Chu, C.; Phung, D.T. Agriculture development, pesticide application and its impact on the environment. *Int. J. Environ. Res. Public Health* **2021**, *18*, 1112. [CrossRef] [PubMed]
3. Carvalho, F.P. Pesticides, environment, and food safety. *Food Energy Secur.* **2017**, *6*, 48–60. [CrossRef]
4. Hayes, T.B.; Hansen, M.; Kapuscinski, A.R.; Locke, K.A.; Barnosky, A. From silent spring to silent night: Agrochemicals and the anthropocene. *Elem. Sci. Anth.* **2017**, *5*, 57. [CrossRef]
5. Bernardes, M.F.F.; Pazin, M.; Pereira, L.C.; Dorta, D.J. Impact of Pesticides on Environmental and Human Health. In *Toxicology Studies—Cells, Drugs and Environment*; Andreazza, A.C., Scola, G., Eds.; IntechOpen: London, UK, 2015; pp. 195–233.
6. Hernández, A.F.; Gil, F.; Lacasaña, M.; Rodríguez-Barranco, M.; Tsatsakis, A.M.; Requena, M.; Alarcón, R. Pesticide exposure and genetic variation in xenobiotic-metabolizing enzymes interact to induce biochemical liver damage. *Food Chem. Toxicol.* **2013**, *61*, 144–151. [CrossRef]
7. Antle, J.M.; Pingali, P.L. Pesticides, productivity, and farmer health: A Philippine case study. *Am. J. Agric. Econ.* **1994**, *76*, 418–430. [CrossRef]

8. Dasgupta, S.; Meisner, C.; Wheeler, D.; Xuyen, K.; Thi Lam, N. Pesticide poisoning of farm workers-implications of blood test results from Vietnam. *Int. J. Hyg. Environ. Health* **2007**, *210*, 121–132. [CrossRef] [PubMed]
9. Lamers, M.; Schreinemachers, P.; Ingwersen, J.; Sangchan, W.; Grovermann, C.; Berger, T. Agricultural pesticide use in mountainous areas of Thailand and Vietnam: Towards reducing exposure and rationalizing use. In *Sustainable Land Use and Rural Development in Southeast Asia: Innovations and Policies for Mountainous Areas*; Springer Environmental Science and Engineering; Fröhlich, H.L., Schreinemachers, P., Stahr, K., Clemens, C., Eds.; Springer: Heidelberg, Germany; New York, NY, USA; Dordrecht, The Netherlands; London, UK, 2013; pp. 156–180. [CrossRef]
10. Sarkar, S.; Gil, J.D.B.; Keeley, J.; Jansen, K. The use of pesticides in developing countries and their impact on health and the right to food. In *Study Retrieved by the DEVE Committee*; European Union: Brussels, Belgium, 2021; pp. 10–47. Available online: https://library.wur.nl/WebQuery/wurpubs/fulltext/548765 (accessed on 27 November 2024).
11. Teklu, B.M.; Haileslassie, A.; Mekuria, W. *Pesticides as Water Pollutants and Level of Risks to Environment and People: An Example from Central Rift Valley of Ethiopia, Environment, Development and Sustainability: A Multidisciplinary Spproach to the Theory and Practice of Sustainable Development*; Springer: Heidelberg, Germany; New York, NY, USA; Dordrecht, The Netherlands; London, UK, 2022; Volume 24, pp. 5275–5294. [CrossRef]
12. Thakur, N.; Kaur, S.; Tomar, P.; Thakur, S.; Yadav, A.N. Microbial biopesticides: Current status and advancement for sustainable agriculture and environment. In *New and Future Developments in Microbial Biotechnology and Bioengineering*; Rastegari, A.A., Yadav, A.N., Yadav, N., Eds.; Elsevier: Amsterdam, The Netherlands, 2020; pp. 243–282. [CrossRef]
13. United States Environmental Protection Agency. Biopesticides. Available online: https://www.epa.gov/pesticides/biopesticides (accessed on 23 November 2024).
14. United States Environmental Protection Agency. What are Biopesticides? Available online: https://www.epa.gov/ingredients-used-pesticide-products/what-are-biopesticides (accessed on 23 November 2024).
15. Wend, K.; Zorrilla, L.; Freimoser, F.M.; Gallet, A. Microbial pesticides—Challenges and future perspectives for testing and safety assessment with respect to human health. *Environ. Health* **2024**, *23*, 49. [CrossRef]
16. Yadav, H.; Kumar, R.; Sankhla, M.S. Residues of pesticides and heavy metals in crops resulting in toxic effects on living organism. *J. Seybold. Rep.* **2020**, *1533*, 9211. [CrossRef]
17. Kumar, S.R.; Sankhla, M.S.; Rajeev Kumar, R.; Sonone, S.S. Impact of pesticide toxicity in aquatic environment. *Biointerface Res. Appl. Chem.* **2021**, *11*, 10131–10140. Available online: https://papers.ssrn.com/sol3/papers.cfm?abstract_id=3755402 (accessed on 21 November 2024).
18. Ayoub, N.; Nawal, L.; Soumaya, R.; Nadia, I.; Amrani Souad, E. Evaluation of the phytotoxicity of a pesticide (TRACTOR 10E) based on Alpha-cypermethrin in two plant species: Lentils (*Lens culinaris*) and watercress (*Lepidium sativum*). *Pollution* **2023**, *9*, 1386–1395. [CrossRef]
19. Alves, T.A.; Roberto, C.E.O.; Pinheiro, P.F.; Alves, T.A.; Henrique, M.K.C.; Ferreira, A.; Clarindo, W.R.; Praça-Fontes, M.M. Searching an auxinic herbicide to use as positive control in toxicity assays. *An. Acad. Bras. Cienc.* **2021**, *93*, e20181262. [CrossRef] [PubMed]
20. Pinheiro, P.F.; Costa, A.V.; Alves, T.A.; Galter, I.N.; Pinheiro, C.A.; Pereira, A.F.; Oliveira, C.M.; Fontes, M.M.P. Phytotoxicity and cytotoxicity of essential oil from leaves of *Plectranthus amboinicus*, carvacrol, and thymol in plant bioassays. *J. Agric. Food Chem.* **2015**, *63*, 8981–8990. [CrossRef] [PubMed]
21. Leme, D.M.; Marin-Morales, M.A. *Allium cepa* test in environmental monitoring: A review on its application. *Mutat. Res.* **2009**, *682*, 71–81. [CrossRef]
22. Albertini, R.J.; Anderson, D.; Douglas, G.R.; Hagmar, L.; Hemmink, K.; Merlo, F.; Natarajan, A.T.; Norppa, H.; Shuker, D.E.; Tice, R.; et al. IPCS guideline for the monitoring of genotoxic effects of carcinogens in humans. *Int. Programme Chem. Saf. Mutat. Res.* **2000**, *463*, 111–172. [CrossRef] [PubMed]
23. Leme, D.M.; Angelis, D.F.; Marin-Morales, M.A. Action mechanisms of petroleum hydrocarbons present in waters impacted by an oil spill on the genetic material of *Allium cepa* root cells. *Aquat. Toxicol.* **2008**, *88*, 214–219. [CrossRef] [PubMed]
24. Fernandes, T.C.C.; Mazzeo, D.E.C.; Marin-Morales, M.A. Mechanism of micronuclei formation in polyploidizated cells of *Allium cepa* exposed to trifluralin herbicide. *Pest. Biochem. Physiol.* **2007**, *88*, 252–259. [CrossRef]
25. Ateeq, B.; Adul Farrah, M.; Ali, M.N.; Ahmad, W. Clastogenicity of pentachlorophenol, 2-4-D and butachlor evaluated by Allium rot tip test. *Mutat. Res.* **2002**, *514*, 105–113. [CrossRef] [PubMed]
26. Bolle, P.; Mastrangelo, S.; Tucci, P.; Evandri, M.G. Clastogenicity of atrazine assessed with the *Allium cepa* test. *Environ. Mol. Mutagen.* **2004**, *43*, 137–141. [CrossRef] [PubMed]
27. Haq, I.; Raj, A.; Markandeya, A.S. Biodegradation of Azure-B dye by Serratia liquefaciens and its validation by phytotoxicity, genotoxicity and cytotoxicity studies. *Chemosphere* **2018**, *196*, 58–68. [CrossRef] [PubMed]
28. Haq, I.; Kalamdhad, A.S. Phytotoxicity and cyto-genotoxicity evaluation of organic and inorganic pollutants containing petroleum refinery wastewater using plant bioassay. *Environ. Technol. Innov.* **2021**, *23*, 101651. [CrossRef]

29. Camilo-Cotrim, C.F.; Bailão, E.F.L.C.; Ondei, L.S.; Carneiro, F.M.; Almeida, L.M. What can the *Allium cepa* test say about pesticide safety? A review. *Environ. Sci. Pollut. Res.* **2022**, *29*, 48088–48104. [CrossRef] [PubMed]
30. Chauhan, L.K.S.; Saxena, P.N.; Gupta, S.K. Cytogenetic effects of cypermethrin and fenvalerate on the root meristem cells of *Allium cepa*. *Environ. Exp. Bot.* **1999**, *42*, 181–189. [CrossRef]
31. Firbas, P.; Amon, T. Chromosome damage studies in the onion plant *Allium cepa* L. *Caryologia* **2014**, *67*, 25–35. [CrossRef]
32. Fiskesjö, G. The Allium test as a standard in environmental monitoring. *Hereditas* **1985**, *102*, 99–112. [CrossRef]
33. Rank, J.; Nielsen, M.H. Evaluation of the Allium anaphase–telophase test in relation to genotoxicity screening of industrial wastewater. *Mutat. Res.* **1994**, *312*, 17–24. [CrossRef]
34. Grant, W.F. Chromosome aberration assays in Allium. *Mutat. Res.* **1982**, *99*, 273–291. [CrossRef] [PubMed]
35. European and Mediterranean Plant Protection Organization Organisation. Annual Report 2014 and Council Recommendations. *Bull. OEPP/EPPO Bull.* **2015**, *44*, 265–273. Available online: https://onlinelibrary.wiley.com/doi/epdf/10.1111/epp.12256 (accessed on 11 November 2024).
36. Fernandes, T.C.C.; Mazzeo, D.E.C.; Marin-Morales, M.A. Origin of nuclear and chromosomal alterations derived from the action of an aneugenic agent—Trifluralin herbicide. *Ecotoxicol. Environ. Saf.* **2009**, *72*, 1680–1686. [CrossRef]
37. Appendix A. Multi-Active Ingredients Product Analysis Deltamethrin. Available online: https://www3.epa.gov/pesticides/endanger/litstatus/effects/redleg-frog/2013/deltamethrin/appendix-a.pdf (accessed on 27 November 2024).
38. Almasi, A.; Sabahi, Q.; Talebi, K.; Mardani, A. Laboratory evaluation of the tox-icity of proteus, pymetrozine, deltamethrin, and pirimicarb on lady beetle *Hippodamia Variegata* (Goeze) (Col.: Coccinellidae). *J. Plant Prot. Res.* **2013**, *53*, 142–147. [CrossRef]
39. Bradberry, S.M.; Cage, S.A.; Proudfoot, A.T.; Vale, J.A. Poisoning due to pyrethroids. *Toxicol. Rev.* **2005**, *24*, 93–106. [CrossRef]
40. Das, R.; Steege, A.; Baron, S.; Beckman, J.; Harrison, R. Pesticide-related illness among migrant farm workers in the United States. *Int. J. Occup. Environ. Health* **2001**, *7*, 303–312. [CrossRef] [PubMed]
41. Tuzmen, N.; Candan, N.; Kaya, E.; Demiryas, P. Biochemical effects of chlorpyrifos and deltamethrin on altered antioxidative defense mechanisms and lipid peroxidation in rat liver. *Cell Biochem. Funct.* **2008**, *26*, 119–124. [CrossRef] [PubMed]
42. Siddiqui, Z.H.; Abbas, Z.K.; Ansari, A.A.; Khan, M.N.; Ansari, W.A. Pesticides and their effects on plants: A case study of deltamethrin. In *Agrochemicals in Soil and Environment: Impacts and Remediation*; Springer Nature Singapore: Singapore, 2022; pp. 183–193.
43. Bava, R.; Lupia, C.; Castagna, F.; Ruga, S.; Nucera, S.; Carresi, C.; Caminiti, R.; Bulotta, R.M.; Naccari, C.; Britti, D.; et al. Interaction of Flupyradifurone and Deltamethrin, two pesticides commonly used for plant pest control, in honeybees. *Animals* **2024**, *14*, 851. [CrossRef] [PubMed]
44. Zhu, Q.; Yang, Y.; Lao, Z.; Zhong, Y.; Zhang, K.; Zhao, S. Acute and chronic toxicity of deltamethrin, permethrin, and dihaloacetylated heterocyclic pyrethroids in mice. *Pest Manag. Sci.* **2020**, *76*, 4210–4221. [CrossRef] [PubMed]
45. Mustafa, K.A.; Al-Baggou, B.K. Toxicological and neurobehavioral effects of chlorpyrifos and deltamethrin insecticides in mice. *Iraqi J. Vet. Sci.* **2020**, *34*, 189–196. [CrossRef]
46. Fisa cu Date de Securitate. Available online: https://www.glissando.ro/wp-content/uploads/2021/04/LASER-240-SC-24.08.2020.pdf (accessed on 20 November 2024).
47. Vander Weele, T.J.; Mathur, M.B. Some desirable properties of the bonferroni correction: Is the bonferroni correction really so bad? *Am. J. Epidemiol.* **2019**, *188*, 617–618. [CrossRef] [PubMed]
48. Ojha, A.; Gupta, Y. Evaluation of genotoxic potential of commonly used organophosphate pesticides in peripheral blood lymphocytes of rats. *Hum. Exp. Toxicol.* **2015**, *34*, 390–400. [CrossRef]
49. Christudoss, A.C.; Kundu, R.; Dimkpa, C.O.; Mukherjee, A. Time dependent release of microplastics from disposable face masks poses cyto-genotoxic risks in *Allium cepa*. *Ecotoxicol. Environ. Saf.* **2024**, *280*, 116542. [CrossRef]
50. Ramborger, B.P.; Gomes Paz, M.E.; Cavalheiro Kieling, K.M.; Sigal Carriço, M.R.; Gollino, G.P.; Tavares Costa, M.; Bley Ribeiro, V.; Folmer, V.; Gasparotto Denardin, E.L.; Soares, J.J.; et al. Toxicological parameters of aqueous residue after using *Plectranthus neochilus* for 2,4-D phytoremediation. *Chemosphere* **2021**, *270*, 128638. [CrossRef] [PubMed]
51. Helps, J.C.; Paveley, N.D.; White, S.; van den Bosch, F. Determinants of optimal insecticide resistance management strategies. *J Theor Biol.* **2020**, *503*, 110383. [CrossRef]
52. Tekalign, K. *Phytohormone—Producing Rhizobacteria and Their Role in Plant Growth, New In-Sights into Phytohormones*; IntechOpen: London, UK, 2024. [CrossRef]
53. Ansari, M.; Devi, B.M.; Sarkar, A.; Chattopadhyay, A.; Satnami, L.; Balu, P.; Choudhary, M.; Shahid, M.A.; Jailani, A.A.K. Microbial exudates as biostimulants: Role in plant growth promotion and stress mitigation. *J. Xenobiot.* **2023**, *13*, 572–603. [CrossRef]
54. Gomis-Cebolla, J.; Berry, C. *Bacillus thuringiensis* as a biofertilizer in crops and their implications in the control of phytopathogens and insect pests. *Pest Manag. Sci.* **2023**, *79*, 2992–3001. [CrossRef] [PubMed]

55. Hajji-Hedfi, L.; Ibrahim, D.S.; Othmen, S.B.; El-Abeid, S.E.; Hlaoua, W.; Mosa, M.A.; Rhouma, A.; Riad, S.N.; Ghareeb, S.; El-Deriny, M.M.; et al. Production of microbial biostimulants as a response to the modern agricultural need for productivity and pant health. In *Microbial Biostimulants*, 1st ed.; Taylor & Francis: Oxford, NY, USA; Apple Academic Press: Palm Bay, FL, USA, 2025; pp. 31–78. [CrossRef]
56. Jensen, C.N.G.; Pang, J.K.Y.; Hahn, C.M.; Gottardi, M.; Husted, S.; Moelbak, L.; Kovács, A.T.; Fimognari, L.; Schulz, A. Differential influence of *Bacillus subtilis* strains on Arabidopsis root architecture through common and distinct plant hormonal pathways. *Plant Sci.* **2024**, *339*, 111936. [CrossRef]
57. Martínez, S.A.; Dussan-G, J. *Lysinibacillus sphaericus* plant growth promoter bacteria and lead phytoremediation enhancer with *Canavalia ensiformis*. *Environ. Prog. Sustain. Energy* **2017**, *37*, 276–282. [CrossRef]
58. Demirtaş, G.; Çavuşoğlu, K.; Aneugenic, Y.E. Clastogenic, and multi-toxic effects of diethyl phthalate exposure. *Environ. Sci. Pollut. Res.* **2020**, *27*, 5503–5510. [CrossRef] [PubMed]
59. Arni, P.; Hertner, T. Chromosomal aberrations in vitro induced by aneugens. *Mutat. Res./Fundam. Mol. Mech. Mutagen.* **1997**, *379*, 83–93. [CrossRef] [PubMed]
60. Ong, J.Y.; Torres, J.Z. Dissecting the mechanisms of cell division. *J. Biol. Chem.* **2019**, *294*, 11382–11390. [CrossRef]
61. de Souza, R.B.; de Souza, C.P.; Guimarães, J.R. Environmentally realistic concentrations of eprinomectin induce phytotoxic and genotoxic effects in *Allium cepa*. *Environ. Sci. Pollut. Res.* **2022**, *29*, 80983–80993. [CrossRef]
62. Pampalona, J.; Roscioli, E.; Silkworth, W.T.; Bowden, B.; Genescà, A.; Tusell, L.; Cimini, D. Chromosome bridges maintain kinetochore-microtubule attachment throughout mitosis and rarely break during anaphase. *PLoS ONE* **2016**, *11*, e0147420. [CrossRef] [PubMed]
63. Sabeen, M.; Mahmood, Q.; Ahmad Bhatti, Z.; Faridullah Irshad, M.; Bilal, M.; Hayat, M.T.; Irshad, U.; Ali Akbar, T.; Arslan, M.; Shahid, N. *Allium cepa* assay based comparative study of selected vegetables and the chromosomal aberrations due to heavy metal accumulation. *Saudi. J. Biol. Sci.* **2020**, *27*, 1368–1374. [CrossRef] [PubMed]
64. Poot, M. Neocentromeres to the rescue of acentric chromosome fragments. *Mol. Syndromol.* **2017**, *8*, 279–281. [CrossRef] [PubMed]
65. Magdaleno, A.; Paz, M.; Fabrizio de Iorio, A.; Weigandt, C.; Moretton, J. Micronucleus and chromosome aberration frequencies in *Allium cepa* cells exposed to coastal sediments from a polluted estuarine system. *Braz. J. Aquat. Sci. Technol.* **2021**, *25*, 8. [CrossRef]
66. Panda Brahma, B.; Mohan, M.A.V. Mitogen-activated protein kinase signal transduction and DNA repair network are involved in aluminum-induced DNA damage and adaptive response in root cells of *Allium cepa* L. *Front. Plant Sci.* **2014**, *5*, 256. [CrossRef]
67. Szurman-Zubrzycka, M.; Jędrzejek, P.; Szarejko, I. How Do Plants Cope with DNA Damage? A Concise Review on the DDR Pathway in Plants. *Int. J. Mol. Sci.* **2023**, *24*, 2404. [CrossRef]
68. Akmoutsou, P.; Mademtzoglou, D.; Nakou, I.; Onoufriadis, A.; Papadopoulou, X.; Kounatidis, I.; Frantzios, G.; Papadakis, G.; Vasiliadis, K.; Papadopoulos, N.T.; et al. Evaluation of toxicity and genotoxic effects of spinosad and deltamethrin in *Drosophila melanogaster* and *Bactrocera oleae*. *Pest Manag. Sci.* **2011**, *66*, 1534–1540. [CrossRef] [PubMed]
69. Aciole, E.H.; Guimarães, N.N.; Silva, A.S.; Amorim, E.M.; Nunomura, S.M.; Garcia, A.C.; Cunha, K.S.; Rohde, C. Genetic toxicity of dillapiol and spinosad larvicides in somatic cells of *Drosophila melanogaster*. *Pest Manag. Sci.* **2014**, *70*, 559–565. [CrossRef]
70. Pereira, B.B.; Caixeta, E.S.; Freitas, P.C.; Santos, V.S.; Limongi, J.E.; de Campos Júnior, E.O.; Campos, C.F.; Souto, H.N.; Rodrigues, T.S.; Morelli, S. Toxicological assessment of spinosad: Implications for integrated control of *Aedes aegypti* using larvicides and larvivorous fish. *J. Toxicol. Environ. Health A* **2016**, *79*, 477–481. [CrossRef] [PubMed]
71. Besard, L.; Mommaerts, V.; Abdu-Alla, G.; Smagghe, G. Lethal and sublethal side-effect assessment supports a more benign profile of spinetoram compared with spinosad in the bumblebee *Bombus terrestris*. *Pest Manag. Sci.* **2011**, *67*, 541–547. [CrossRef] [PubMed]
72. Jones, O.M.; Ottea, J. The effects of spinosad on *Culex quinquefasciatus* and three nontarget insect species. *J. Am. Mosq. Control Assoc.* **2013**, *29*, 346–351. [CrossRef]
73. Toledo-Ibarra, G.A.; Rodríguez-Sánchez, E.J.; Ventura-Ramón, H.G.; Díaz-Resendiz, K.J.G.; Girón-Pérez, M.I. Cholinergic alterations by exposure to pesticides used in control vector: Guppies fish (*Poecilia reticulta*) as biological model. *Int. J. Environ. Health Res.* **2018**, *28*, 79–89. [CrossRef]
74. Mendonça, T.P.; Davi de Aquino, J.; Junio da Silva, W.; Mendes, D.R.; Campos, C.F.; Vieira, J.S.; Barbosa, N.P.; Carvalho Naves, M.P.; Olegário de Campos Júnior, E.; Alves de Rezende, A.A.; et al. Genotoxic and mutagenic assessment of spinosad using bioassays with *Tradescantia pallida* and *Drosophila melanogaster*. *Chemosphere* **2019**, *222*, 503–510. [CrossRef] [PubMed]
75. Martelli, F.; Hernandes, N.H.; Zuo, Z.; Wang, J.; Wong, C.O.; Karagas, N.E.; Roessner, U.; Rupasinghe, T.; Robin, C.; Venkatachalam, K.; et al. Low doses of the organic insecticide spinosad trigger lysosomal defects, elevated ROS, lipid dysregulation, and neurodegeneration in flies. *eLife* **2022**, *11*, e73812. [CrossRef]
76. United States Environmental Protection Agency (EPA). *Spinosad Pesticide Fact Sheet No. HJ 501C*; Office of Pesticides and Toxic Substances: Washington, DC, USA, 1997. Available online: https://www3.epa.gov/pesticides/chem_search/reg_actions/registration/fs_PC-110003_19-Jul-99.pdf (accessed on 14 November 2024).

77. Yano, B.L.; Bond, D.M.; Novilla, M.N.; McFadden, L.G.; Reasor, M.J. Spinosad insecticide: Subchronic and chronic toxicity and lack of carcinogenicity in Fischer 344 rats. *Toxicol. Sci.* **2002**, *65*, 288–298. [CrossRef] [PubMed]
78. Stebbins, K.E. Spinosad insecticide: Subchronic and chronic toxicity and lack of carcinogenicity in CD-1 mice. *Toxicol. Sci.* **2002**, *65*, 276–287. [CrossRef]
79. Mansour, S.A.; Mossa, A.H.; Heikal, T.M. Cytogenetic and hormonal alteration in rats exposed to recommended "safe doses" of spinosad and malathion insecticides. *IJAB* **2008**, *10*, 9–14.
80. Asita, A.O.; Mohale, R.R.; Magama, S. Cytotoxicity and genotoxicity of imidacloprid, spinosad and bifenthrin—*Myclobutanil* combination to *Allium cepa* root tip meristematic cells. *Environ. Nat. Resour. Res.* **2022**, *12*, 1. [CrossRef]
81. Benaissa, A. Rhizosphere: Role of bacteria to manage plant diseases and sustainable agriculture—A review. *J. Basic Microbiol.* **2024**, *64*, 2300361. [CrossRef]
82. Mashabela, M.D.; Piater, L.A.; Dubery, I.A.; Tugizimana, F.; Mhlongo, M.I. Rhizosphere Tripartite Interactions and PGPR-Mediated Metabolic Reprogramming towards ISR and Plant Priming: A Metabolomics Review. *Biology* **2022**, *11*, 346. [CrossRef]
83. Oliveira-Filho, E.C.; Grisolia, C.K. The Ecotoxicology of microbial insecticides and their toxins in genetically modified crops: An Overview. *Int. J. Environ. Res. Public Health* **2022**, *19*, 16495. [CrossRef] [PubMed]
84. Grisolia, C.K.; Oliveira, R.; Domingues, I.; Oliveira-Filho, E.C.; Monnerat, R.G.; Soares, A.M. Genotoxic evaluation of different delta-endotoxins from *Bacillus thuringiensis* on zebrafish adults and development in early life stages. *Mutat. Res.* **2009**, *672*, 119–123. [CrossRef] [PubMed]
85. Ghanya, A.N.; Aliki, K.; Francesca, G.; Rachele, D.G.; Hellas, C. Genotoxic and antigenotoxic medicinal plant extracts and their main phytochemicals: "A review". *Front. Pharmacol.* **2024**, *15*, 1448731. [CrossRef]

Journal of *Xenobiotics*

MDPI

Article

Nanoplastic-Induced Developmental Toxicity in Ascidians: Comparative Analysis of Chorionated and Dechorionated *Phallusia mammillata* Embryos

Maria Concetta Eliso [1,2,*,†], Ilaria Corsi [1], Antonietta Spagnuolo [2,‡] and Rémi Dumollard [3,‡]

[1] Department of Physical, Earth and Environmental Sciences, University of Siena, 53100 Siena, Italy; ilaria.corsi@unisi.it
[2] Department of Biology and Evolution of Marine Organisms, Stazione Zoologica Anton Dohrn, 80121 Naples, Italy; antonietta.spagnuolo@szn.it
[3] Laboratoire de Biologie du Développement (LBDV), Institut de la Mer de Villefranche (IMEV), Sorbonne Université, Centre National de la Recherche Scientifique (CNRS), 06230 Villefranche-sur-Mer, France; remi.dumollard@imev-mer.fr
* Correspondence: mariaconcetta.eliso@szn.it
† Current address: Department of Integrative Marine Ecology, Stazione Zoologica Anton Dohrn, 80121 Naples, Italy.
‡ These authors contributed equally to this work.

Abstract: Nanoplastics pose a growing threat to marine ecosystems, particularly affecting the early developmental stages of marine organisms. This study investigates the effects of amino-modified polystyrene nanoparticles (PS-NH_2, 50 nm) on the embryonic development of *Phallusia mammillata*, a model ascidian species. Both chorionated and dechorionated embryos were exposed to increasing concentrations of PS-NH_2 so morphological alterations could be assessed with a high-content analysis of the phenotypes and genotoxicity. PS-NH_2 induced the same morphological alterations in both chorionated and dechorionated embryos, with dechorionated embryos being more sensitive (EC_{50} = 3.0 μg mL^{-1}) than chorionated ones (EC_{50} = 6.26 μg mL^{-1}). Interestingly, results from the morphological analysis showed two concentration-dependent mechanisms of action: (i) at concentrations near the EC_{50}, neurodevelopmental abnormalities resembling the ones induced by exposure to known endocrine disruptors (EDs) were observed, and (ii) at higher concentrations (15 μg mL^{-1} and 7.5 μg mL^{-1} for chorionated and dechorionated embryos, respectively), a nonspecific toxicity was evident, likely due to general oxidative stress. The phenotypes resulting from the PS-NH_2 treatment were not related to DNA damage, as revealed by a genotoxicity assay performed on neurula embryos. Our data suggest that PS-NH_2-induced toxicity is primarily mediated through oxidative stress, probably triggered by interactions between the positive charges of the PS NPs and the negative charges on the cell membranes. The lack of a protective chorion further exacerbated these effects, highlighting its role in mitigating/protecting against NP-induced damage.

Keywords: nanoplastics; polystyrene nanoparticles; PS-NH_2; *Phallusia mammillata*; embryotoxicity; oxidative stress; neurodevelopment; genotoxicity; morphometric analysis

1. Introduction

Plastic pollution is recognized to be a threat of global concern for the marine environment. Approximately 5000 tons of plastic waste was released into the environment globally in 1950–2015, and, as plastic litter ages, it breaks down, forming microplastics

(MPs, <5 mm) and nanoplastics (<100 nm), via weathering, sunlight radiation and biodegradation processes [1–6]. The formation of smaller particles leads to a modification of the physical–chemical properties, surface area and size, and, once below 1 μm in size, nanoplastics can have high reactivity and biotoxicity Although environmental concentrations of nanoplastics are still unknown, it is well accepted that they are ubiquitous, as recently found in the surface water of the North Atlantic Gyre [7] and in the West Mediterranean Sea [8]. They indeed represent a serious hazard for marine species, in particular in marine coastal areas [9–11]. On these grounds, in recent years, several studies have focused on exploring the impact of nanoplastics on marine organisms by using, among a wide variety of polymer compositions, polystyrene nanoparticles (PS NPs) as a proxy for nanoplastic [12] and references therein]. The studies showed that these small particles can affect marine phyto- and zooplankton, resulting in oxidative stress and feeding disruption, among other sub-lethal effects [13–25]. Recently, the effects of PS NPs (PS-NH_2, 50 nm) on chorionated *Ciona robusta* embryos have been investigated, revealing impairment in trunk and palps morphogenesis and oxidative stress in the larvae [18]. Furthermore, the development of an Adverse Outcome Pathway (AOP) exploiting transcriptomic data and sub-lethal endpoints suggested that a Molecular Initiating Event (MIE), the adhesion of PS NPs to the ascidian chorion, an envelope that surrounds the egg and the developing embryo until the hatching of the tadpole larva [26–29], may act as a physico-chemical barrier against pollutants [19].

Ascidians, which are abundant components in marine meso-zooplankton communities and have an invertebrate embryo that is closely related to vertebrates [30–32], represent ideal models for ecotoxicity studies aimed at exploring the effects of a large variety of physical and chemical stressors [33,34]. Here, we investigate the effect of amino-modified PS NPs (PS-NH_2, 50 nm) on the embryonic development of another ascidian species, *Phallusia mammillata*. This marine invertebrate is found exclusively in the Northeast Atlantic and the Mediterranean and it is an emerging ascidian model for developmental and molecular biology studies (e.g., live-cell imaging) since its eggs and embryos are completely transparent [35–38]. In addition, genomic and transcriptomic resources are available, thus facilitating functional gene studies (https://www.aniseed.cnrs.fr/; accessed on 20 November 2022). In the past years, *Phallusia* has been used in ecotoxicology for the testing of the embryotoxicity of several Contaminants of Emerging Concerns (CECs), at both morphological and molecular levels [39–42], and, more recently, high-content analyses of the morphological alterations of *Phallusia* larvae have been exploited to determine the phenotypic signature of different classes of chemicals such as Endocrine Disruptors (EDs), Nuclear Receptors (NRs), ligands and genotoxic and cytotoxic compounds [43]. In this work, the PS-NH_2 was tested on chorionated *Phallusia* embryos, resembling the natural exposure scenarios, and on dechorionated embryos, to evaluate the effects of direct contact with the growing embryos and unravel the potential protective/mitigation role against NP exposure. Then, high-content-based morphometric analysis of *Phallusia* larvae allowed us to quantify morphological malformations with neurodevelopmental endpoints. The morphometric analysis was coupled to a genotoxicity assay to explore the possible toxic mechanisms of action.

2. Materials and Methods

2.1. Amino-Modified PS NPs (PS-NH_2)

Unlabeled 50 nm amino-modified PS NPs (PS-NH_2, PA02N, lot: 12839) were purchased from Bangs Laboratories Inc. (Fishers, IN, USA) and received as a 100 mg mL^{-1} stock suspension in deionized water with no added surfactants, according to the manufacturer's technical sheet. After a brief sonication, as already described in the study of Eliso et al., 2020 [18], intermediate suspensions (10 mg mL^{-1}) were prepared in 0.22 μm

filtered milli-Q water (mQW) and stored in sterile vials at 4 °C until use. For the embryotoxicity assay, a PS-NH_2 working suspension (1 mg mL^{-1}) was prepared in Natural Sea Water (NSW, salinity 40‰, pH 8) collected from a clean site in the Mediterranean Sea as the exposure media without further sonication. A detailed physico-chemical characterization of PS-NH_2 behavior in mQW and NSW media is reported in the study of Eliso et al., 2020 [18]. In particular, in mQW, PS-NH_2 confirmed the primary size (50 nm), and the positive surface charge (+47.5 mV), and showed an optimal dispersion (PDI 0.175 ± 0.04) at different time points. Conversely, in NSW, PS-NH_2 was found to form large agglomerates (Z-Average of 999.7 ± 54.19 nm) with broader PDI values (>0.400), and a decrease in the ζ-potential values (+7.19 mV) showed the instability of PS NPs in this high-ionic-strength medium [18]. Details on the Fourier Transform Infrared (FTIR) analysis used to determine the structure and composition of the stock suspension are provided in the Supplementary Materials.

2.2. Animal and Gametes Collection

Adult specimens of *Phallusia mammillata* were collected in Sète (Hérault, France) and kept at 17 ± 1 °C in circulating natural seawater aquaria. Animals were kept under constant light conditions to avoid uncontrolled spawning of eggs and sperm [44]. The experimental design included two different fertilization protocols: (i) the exposure of embryos with a chorion (chorionated embryos), to mimic the natural exposure condition in the water column; (ii) exposure of embryos without a chorion (dechorionated embryos) according to a protocol already used to screen the toxic effect of several chemicals using the *Phallusia* larval teratogenic assay [42,43]. For the fertilization of chorionated eggs, eggs and sperm were collected separately by dissecting the gonoducts of several hermaphrodite adults. The sperm was stored at 4 °C until use, while oocytes were collected in tissue culture plates and rinsed twice in 0.22 µm filtered NSW, and immediately fertilized by adding diluted sperm (1:100 in NSW) to the egg suspension. After 10 min of incubation, eggs were rinsed 3 times with NSW. For the fertilization of dechorionated eggs, the protocol was the same, except for the presence of the chorion, which was removed from the eggs before fertilization. To remove the chorion, eggs were incubated in a trypsin solution for 2 h and then washed 3 times using NSW supplemented with TAPS buffer (NSW/TAPS; 0.5 mM) according to the protocol described in the study of Dumollard et al. (2017) [35].

2.3. Embryotoxicity Assay

About 1 h 30 min post-fertilization (hpf), 60 chorionated embryos (~two-cell stage) were added to 6-well plates containing PS-NH_2 suspensions in NSW (final volume 6 mL). For the exposure of dechorionated embryos, the 60 embryos were instead transferred at the zygote stage (1-cell stage, around 30 min after fertilization) to avoid the dissociation of 2-cell-stage embryos during the transfer. Both chorionated and dechorionated embryos were exposed to nominal concentrations of PS-NH_2 as follows: 2–5–7.5–10–15 µg mL^{-1} for chorionated embryos, and 2–3–3.5–5–7.5 µg mL^{-1} for the dechorionated ones. Embryos were then incubated under static conditions in the dark at 18 °C until the hatching larva stage (stage 26) was reached at about 18 hpf. After the incubation period, larvae were fixed in 4% paraformaldehyde (4% PFA, 0.5 M NaCl, PBS; Sigma, St. Louis, MO, USA), washed 3 times in Phosphate-Buffered Saline (PBS 1X) and imaged by transmitted light microscopy (Zeiss Axiovert 200, Jena, Germany) at 10× magnification for the evaluation of the percentage of normal hatched larvae and the morphometric analysis. As described by Gomes and collaborators (2019) [42], a *Phallusia* larva is considered normal when it shows a good general embryo morphology, with a proper trunk and palps formation, as well as tail elongation.

2.4. Morphometric Analysis of Larval Development

For the morphometric analysis, bright-field images (Zeiss Axiovert 200) of both chorionated and dechorionated embryos were analyzed with the in-house software Toxicosis8 (Version 1, reference IDDN.FR.001.330013.000.S.P.2018.000.10000, deposited on 13 July 2018; see full description of Toxicosis8 in the study of Gazo et al., 2021 [43]). At least 50 tadpoles were analyzed per treatment. The 5 endpoints quantified were the area of the two pigmented cells (PCs) (Oc/Ot area, μm^2), the distance between the two PCs (Oc/Ot distance, μm), the length/width ratio of the trunk, the length of the tail and the presence of well-elongated palps. The resulting data were normalized to each respective control treatment (100%) and plotted in radar charts for better comparison of phenotypes between treatments (see [43] for a full description of the morphometric analysis).

2.5. Genotoxicity Assay

Genotoxicity testing was performed only on dechorionated embryos to better visualize the fluorescent nuclei within the embryos. Embryos at the neurula stage were fixed with a fixation solution (4% paraformaldehyde, 0.5 M NaCl in PBS) for 1 h at 20 °C on a shaker. By washing them twice with PBS, the fixative was removed. After washing, the samples were incubated in PBS containing 0.1% Triton X-100 and 3% bovine serum albumin (PBSB) for 1 h at 20 °C on a shaker. The embryos were stained with 1 $\mu g\ mL^{-1}$ Hoechst in PBSB for 1–2 h at 20 °C on a shaker. Finally, the embryos were washed twice with PBSB and transferred on a glass slide. DNA-stained embryos were imaged using epifluorescence microscopy (Zeiss, Axiovert 200) with a 40×/0.8 NA water objective lens, and DNA aberrations (multinucleated cells, micronuclei or DNA bridges) were scored manually. As was performed in the study of Gazo et al., 2021 [43], the number of embryos hosting a DNA aberration was counted. The total number of embryos scored was at least 150 per condition.

2.6. Statistical Analysis

All the statistical analyses were performed using Graphpad Prism (Version 8.0.1, San Diego, CA, USA). All data are expressed as mean ± standard deviation (SD). The median effective concentration (EC_{50}), corresponding to a 50% reduction in normal hatched larvae, was calculated using a sigmoidal dose−response model according to the following equation:

$$y = b + (a - b)/1 + 10^{(LogEC50 - x)}$$

where y is the response, b is the response minimum, a is the response maximum, x is the logarithm of effect concentration and EC_{50} is the concentration of effect giving 50% of the maximum effect. Data were normalized to the control mean percentage of larval abnormality using Abbot's formula:

$$P = (Pe - Pc/100 - Pc) \times 100$$

where Pc and Pe are the control and the experimental percentages of response, respectively. For the morphometric analysis, in order to eliminate the effect of external factors, we compared and normalized each endpoint with the corresponding value in the control group obtained on the same day. The raw data (not normalized) from this assay were statistically analyzed using the Kruskal–Wallis test followed by Dunn's post hoc test.

3. Results

3.1. PS-NH_2 NPs Alter the Normal Larval Development

The results of the embryotoxicity assay were evaluated by looking at the normal larval development on both chorionated and dechorionated embryos after an exposure to PS-NH_2 lasting about 18 h (stage 26). Figure 1 shows a dose-dependent response under both tested conditions, with an increased sensitivity of the dechorionated embryos (EC_{50} = 3.0 μg mL^{-1}) compared to chorionated ones (EC_{50} = 6.26 μg mL^{-1}).

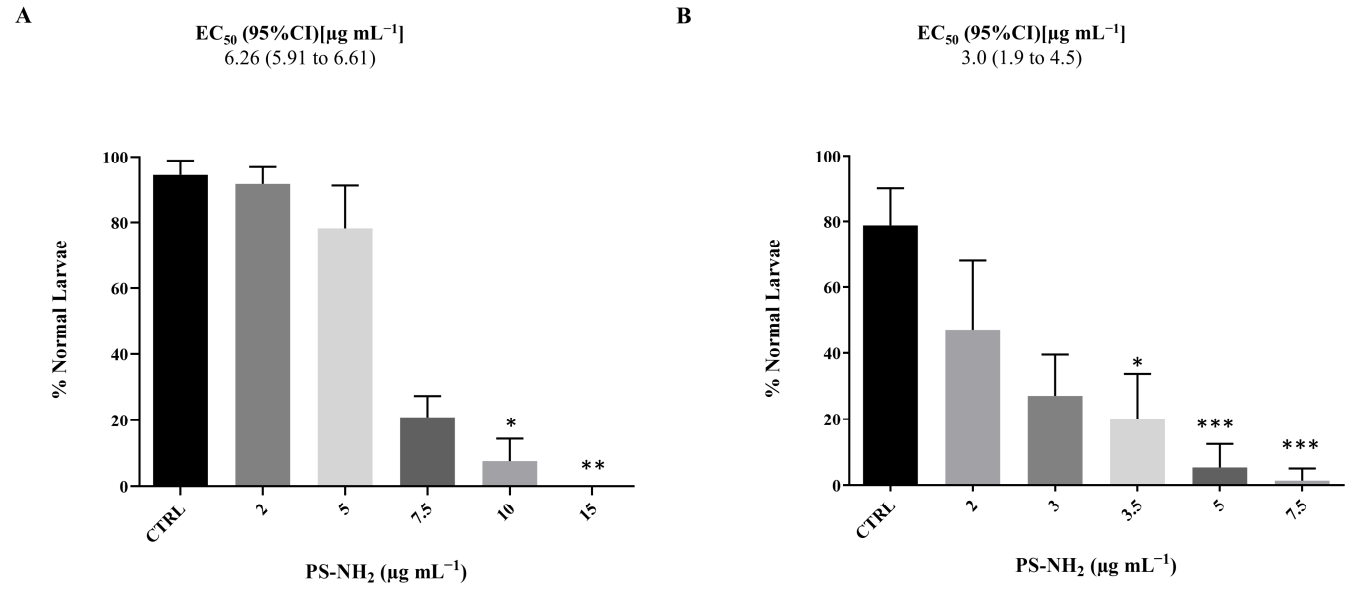

Figure 1. Percentage (%) of normal hatched larvae of *P. mammillata* upon 22 h exposure of chorionated embryos (**A**) and dechorionated embryos (**B**) to PS-NH_2 in NSW. Bars represent mean ± SD (PS-NH_2 N = 240). Asterisks indicate values that are significantly different compared to the control (Kruskal–Wallis test, Dunn's post hoc test (* $p < 0.05$, ** $p < 0.01$, *** $p < 0.001$)). EC_{50} values are shown.

3.2. Quantitative Analysis of Phenotypes

In addition to the normal larval development, we also evaluated any phenotypic alterations in developing *P. mammillata* embryos exposed to PS-NH_2 and then we quantified them using the software Toxicosis8 [43]. Observation under a light microscope indicated that the morphological defects were mainly related to the development of the trunk. As shown in Figure 2B, most chorionated embryos exposed to 5 μg mL^{-1} of PS-NH_2 showed a generally good morphology of the embryo, comparable to unexposed ones (controls only in NSW) (Figure 2A). At 7.5 μg mL^{-1}, we observed a lack of protrusion of the palps in most larvae and, upon exposure to 10 and 15 μg mL^{-1} of PS-NH_2, the embryos failed to hatch, showing malformations at both the trunk and tail levels. In fact, as shown in Figure 2D,E, the trunk became rounder and the tail shorter compared to the controls (Figure 2D,E).

The phenotypic alterations observed in the dechorionated embryos were comparable to the morphological defects detected on chorionated embryos, with an increased sensitivity at lower exposure concentrations. In fact, a rounder trunk and an inhibition of palps protrusion were already observable in larvae exposed to 2–3 μg mL^{-1} of PS-NH_2 (Figure 3A–F). Moreover, the pigmented sensory organs (PCs, composed of the otolith and ocellus) appeared to be fused already in larvae exposed to 3 μg mL^{-1} and upwards, indicating that the movement of the otolith towards the ventral side of the sensory vesicle was impaired (Figure 3C–F) [45].

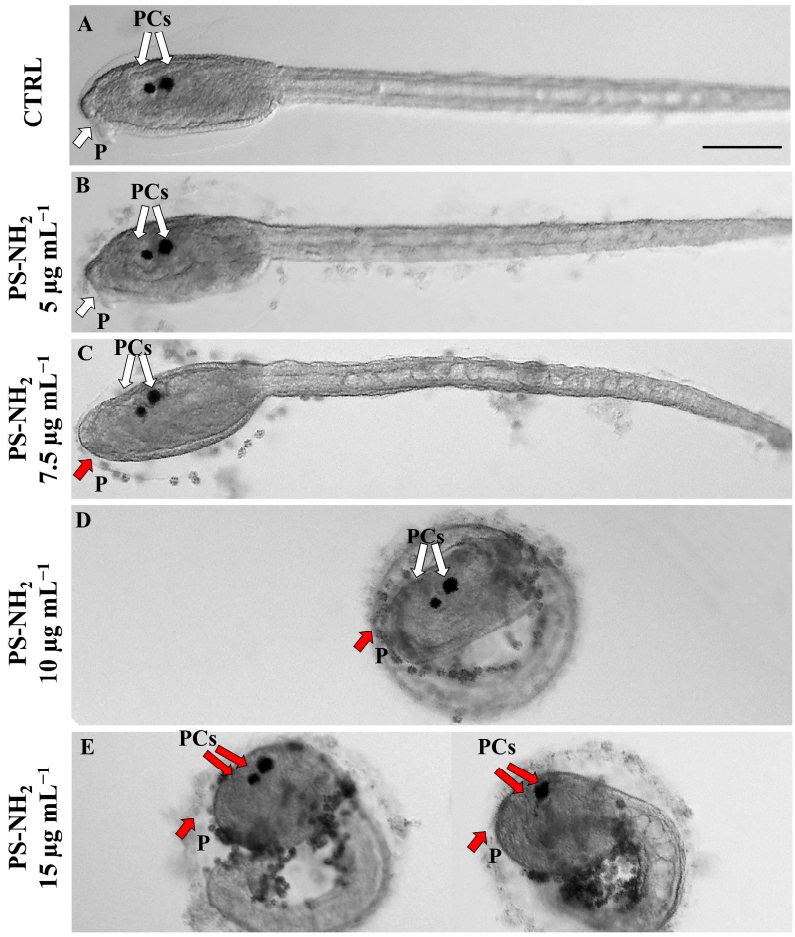

Figure 2. Light microscopy images of *P. mammillata* embryos exposed for 22 h to PS-NH_2. (**A**–**E**) represent the phenotypes for embryos developed in a chorion: (**A**) control; (**B**) 5 µg mL^{-1}; (**C**) 7.5 µg mL^{-1}; (**D**) 10 µg mL^{-1}; (**E**) 15 µg mL^{-1}. White and red arrows represent a good and wrong shape of pigmented cells (PCs) and palps (P), respectively. Scale bar: 100 µm.

Using the Toxicosis8 software, five morphometric endpoints were quantified in chorionated and dechorionated *Phallusia* embryos treated with PS-NH_2. In chorionated embryos, the most sensitive endpoint was the elongation of the palps, which gradually decreased to 1.8% in larvae exposed to 15 µg mL^{-1}, then the Ot-Oc distance (significantly reduced to 36.9%), tail length (reduced to 58.3%) and the trunk L/W ratio (reduced to 75.3%), whereas Oc-Ot area was not affected (Figure 4A, Table 1). Interestingly, dechorionated embryos displayed phenotypes similar to those of chorionated embryos, as illustrated in the radar chart, which shows almost the same order of affected endpoints: palps > Oc-Ot distance > tail > trunk (Figure 4B, Table 2). The only difference is that naked embryos were more susceptible to PS-NH_2 exposure compared to chorionated ones (compare data at 7.5 µg mL^{-1} in Tables 1 and 2).

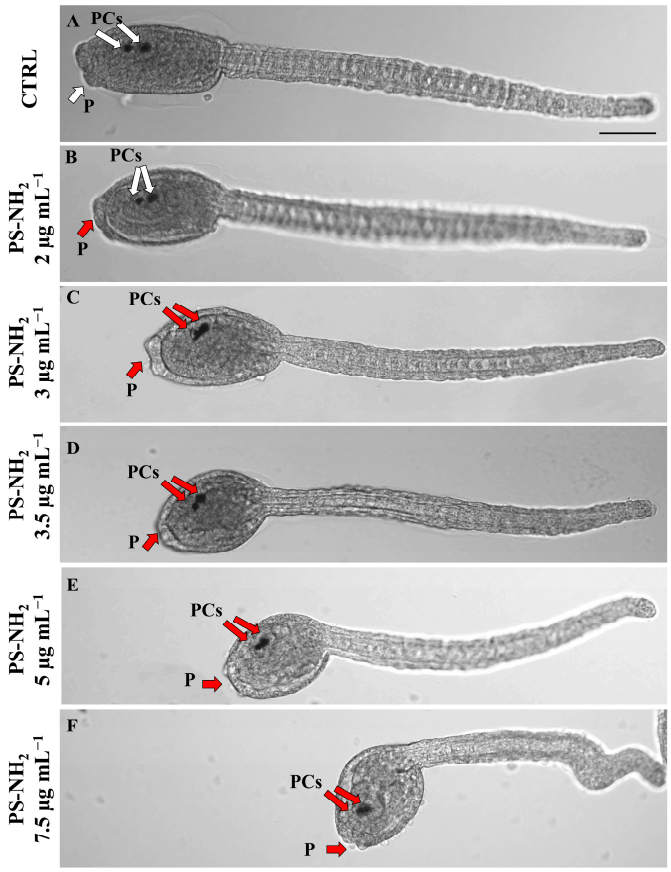

Figure 3. Light microscopy images of *P. mammillata* embryos exposed for 22 h to PS-NH_2. (**A**–**E**) represent the phenotypes for embryos developed without a chorion: (**A**) control; (**B**) 2 µg mL^{-1}; (**C**) 3 µg mL^{-1}; (**D**) 3.5 µg mL^{-1}; (**E**) 5 µg mL^{-1}; (**F**) 7.5 µg mL^{-1}. White and red arrows represent a good and wrong shape of pigmented cells (PCs) and palps (P), respectively. Scale bar: 100 µm.

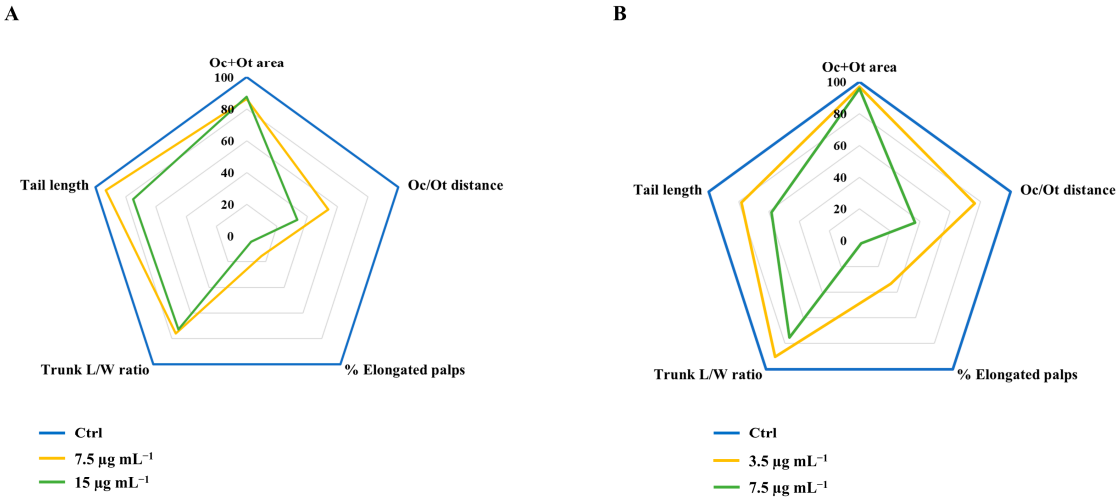

Figure 4. Morphometric analysis of phenotypes induced in *P. mammillata* embryos (**A**) with a chorion and (**B**) without a chorion exposed to PS-NH_2 (0; 7.5 and 15 µg mL^{-1} for chorionated embryos, 0; 3.5 and 7.5 µg mL^{-1} for dechorionated embryos). The radar charts summarize the following end-points: ocellus (Oc) + otolith (Ot) area (µm^2); Oc/Ot distance (µm); percentage of embryos with palps (%); trunk L/W (length/width) ratio; tail length (µm). All measurements were performed at 22 hpf. The values are normalized to the corresponding value of the same parameter in the control (stage 26) and presented as a percentage of the control value. Complete radar charts of all tested concentrations are shown in Figure S3.

Table 1. Quantitative analysis of the morphological aberrations observed after the exposure of *Phallusia mammillata* chorionated embryos to different concentrations of PS-NH_2. N represents the number of observed embryos at stage 26 (22 hpf). The endpoints analyzed were the ocellus (Oc) + otolith (Ot) area (μm^2); Oc/Ot distance (μm); percentage of embryos with palps (%); trunk L/W (length/width) ratio; tail length (μm). Data are presented as means ± S.D. and as % compared to the control. Asterisks indicate a significant difference compared to the control (Kruskal–Wallis test and Dunn's correction, * $p < 0.05$, ** $p < 0.01$, *** $p < 0.001$).

Treatment	N	Oc/Ot Area, μm^2, Mean ± S.E.	Oc/Ot Area % Compared to the Control	Oc/Ot Distance, μm, Mean ± S.E.	Oc/Ot Distance % Compared to the Control	% Elongated Palps, Means ± S.E.	Elongated Palps % Compared to the Control	Trunk L/W Ratio, Means ± S.E.	Trunk L/W % Compared to the Control	Tail Length, μm, Means ± S.E.	Tail Length % Compared to the Control
Ctrl	143	276.4 ± 60.9	-	18.8 ± 6.7	-	100.0 ± 0.0	-	1.9 ± 0.2	-	589.7 ± 98.7	-
2 $\mu g\ mL^{-1}$ PS-NH_2	85	271.0 ± 64.4	98.0	19.1 ± 6.3	101.3	86.7 ± 8.2	86.7	1.9 ± 0.2	104.1	553.5 ± 94.0	93.9
5 $\mu g\ mL^{-1}$ PS-NH_2	110	274.5± 65.0	99.3	18.3 ± 8.8	97.0	61.8 ± 17.2	61.8	2.0 ± 0.2	105.2	524.4 ± 92.6 ***	88.9
7.5 $\mu g\ mL^{-1}$ PS-NH_2	134	267.9 ± 64.6	96.9	14.4 ± 10.0 **	76.3	33.5 ± 17.9	33.5	1.7 ± 0.4 ***	90.5	461.4 ± 104.7 ***	78.2
10 $\mu g\ mL^{-1}$ PS-NH_2	105	268.8 ± 56.9	97.3	11.6 ± 10.4 ***	61.7	23.2 ± 15.9 *	23.2	1.6 ± 0.3 ***	85.8	436.6 ± 93.5 ***	74.0
15 $\mu g\ mL^{-1}$ PS-NH_2	58	264.9 ± 67.1	95.8	6.9 ± 9.5 ***	36.9	1.8 ± 3.7 ***	1.8	1.4 ± 0.3 ***	75.3	343.6 ± 120.5 ***	58.3

Table 2. Quantitative analysis of the morphological aberrations observed after the exposure of *Phallusia mammillata* dechorionated embryos to different concentrations of PS-NH_2. N represents the number of observed embryos at stage 26 (22 hpf). The endpoints analyzed were the ocellus (Oc) + otolith (Ot) area (μm^2); Oc/Ot distance (μm); percentage of embryos with palps (%); trunk L/W (length/width) ratio; tail length (μm). Data are presented as means ± S.D. and as % compared to the control. Asterisks indicate a significant difference compared to the control (Kruskal–Wallis test and Dunn's correction,* $p < 0.05$, ** $p < 0.01$, *** $p < 0.001$).

Treatment	N	Oc/Ot Area, μm^2, Mean ± S.E.	Oc/Ot Area % Compared to the Control	Oc/Ot Distance, μm, Mean ± S.E.	Oc/Ot Distance % Compared to the Control	% Elongated Palps, Means ± S.E.	Elongated Palps % Compared to the Control	Trunk L/W Ratio, Means ± S.E.	Trunk L/W % Compared to the Control	Tail Length, μm, Means ± S.E.	Tail Length % Compared to the Control
Ctrl	137	294.9.0 ± 64.0	-	23.6 ± 7.7	-	96.3 ± 3.1	-	1.8 ± 0.3	-	577.2 ± 94.6	-
2 $\mu g\ mL^{-1}$ PS-NH_2	122	256.2 ± 107.4	86.9	17.2 ± 10.5 ***	72.9	79.5 ± 19.4	82.6	1.6 ± 0.2	92.9	566.0 ± 65.2	98.1
3.5 $\mu g\ mL^{-1}$ PS-NH_2	56	254.5 ± 56.9 **	86.3	12.7 ± 9.8 ***	53.8	11.6 ± 11.5	12.0	1.3 ± 0.1 ***	76.0	537.8 ± 58.5 **	93.2
5 $\mu g\ mL^{-1}$ PS-NH_2	167	273.6 ± 83.7	92.8	8.6 ± 10.8 ***	36.4	24.7 ± 11.2	25.7	1.3 ± 0.2 ***	75.3	452.7 ± 113.4 *	78.4
7.5 $\mu g\ mL^{-1}$ PS-NH_2	141	259.0 ± 100.6	87.8	7.8 ± 9.7 ***	33.2	4.4 ± 4.3 ***	4.6	1.3 ± 0.2 ***	72.9	433.0 ± 97.0 *	75

3.3. PS-NH_2 NPs Are Not Genotoxic

Recent data on *Phallusia* embryos indicate that the alteration of palps and trunk elongation are part of the severe malformations associated with DNA damage and genotoxicity [43]. We thus sought to verify whether the phenotypes induced by PS-NH_2 treatment could also be related to DNA damage, by staining embryo DNA and scoring DNA aberrations in dechorionated embryos at the neurula stage. Figure 5 shows representative images of control and treated embryos (5 and 7.5 μg mL^{-1}). In the control cultures, almost all analyzed embryos (98.7%) showed well-aligned nuclei of constant size and tightly packed nuclear DNA without DNA aberrations (Figure 5A). The same results were obtained with treated embryos, with 98.3% and 97.5% of embryos having intact DNA at 5 and 7.5 μg mL^{-1} exposure concentrations, respectively.

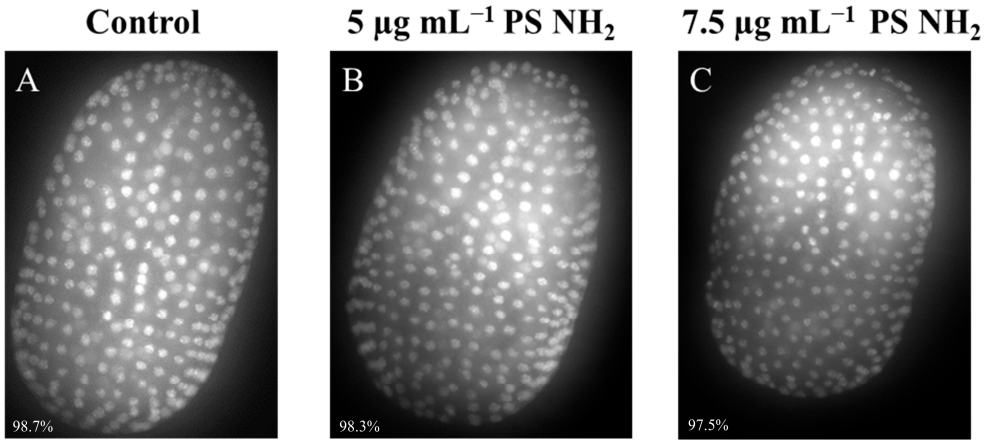

Figure 5. Genotoxicity assay performed analyzing 7 hpf embryos (neurula stage). (**A**) Control embryo (NSW), (**B**) 5 μg mL^{-1}; (**C**) 7.5 μg mL^{-1}. At the bottom of each image, the percentage of embryos not showing DNA aberrations is reported (N control = 152; 5 μg mL^{-1} = 175; 7.5 μg mL^{-1} = 160.).

4. Discussion

Early life stages of marine invertebrate and fish species are sensitive indicators of environmental pollutants including nanoplastics. Here, we investigated the effects of PS-NH_2 on the development of the ascidian *P. mammillata* by evaluating its impact on embryos, either chorionated or dechorionated, to shed some light on the potential role of the chorion in mitigating the effects of nanoplastics.

Regarding chorionated embryos, the microscopic observations showed morphological alterations mainly at the trunk level; trunks were rounded, and there was a reduction in the protrusion of the palps at exposure concentrations of up to 7.5 μg mL^{-1}. Upon exposure to 10 and 15 μg mL^{-1}, the embryos failed to hatch, showing malformations at both trunk and tail levels. This phenotype is reminiscent of that previously detected on larvae of another ascidian species, *Ciona robusta* [18], thus suggesting a similar mechanism of action of PS-NH_2 in *Ciona* and *Phallusia* embryos. Here, we also checked if the direct contact with PS-NH_2 could have different or even more devastating effects on chorion-deprived developing embryos. Our data indicate that there are no strong phenotypic differences, at the larval stage, between embryos with and without a chorion, except that dechorionated embryos are more sensitive to PS-NH_2 treatment, on the basis of EC_{50} (3.0 μg mL^{-1} compared to 6.26 μg mL^{-1}).

Through the use of the Toxicosis8 software, three neurodevelopmental endpoints (Oc/Ot area, Oc/Ot distance, % of embryos with elongated palps) and two general morphogenesis endpoints (trunk L/W ratio and tail length) were analyzed and the results were compared to previous data obtained in a toxicity screening aimed at finding phenotypic

signatures in *Phallusia* embryos associated with xenobiotics [43]. Our study indicates that PS-NH_2 was able to affect all endpoints analyzed, regardless of the presence or absence of the chorion. Furthermore, the use of this software allowed us to identify two concentration-dependent mechanisms of action: (i) at concentrations near the EC_{50}, neurodevelopmental abnormalities, resembling the ones induced by exposure to known endocrine disruptors (EDs), were observed, and (ii) at higher concentrations (15 μg mL^{-1} and 7.5 μg mL^{-1} for chorionated and dechorionated embryos, respectively), a nonspecific toxicity was evident, likely due to general oxidative stress.

Specifically, in the case of concentrations near the EC_{50} (6.26 μg mL^{-1} and 3.0 μg mL^{-1}, respectively, for embryos with and without a chorion), the significantly affected endpoints were trunk L/W ratio and tail length, which reflect the general morphology of the embryo, and Oc/Ot distance, which is a marker of the central nervous system. The mechanism of action seems similar since the endpoints were the same regardless of the presence or absence of the chorion. The higher sensitivity of non-chorionated larvae suggests a protective role of the chorion which limits the interaction of the PS-NH_2 with the embryos. Notably, the phenotypic signatures, such as the trunk L/W ratio and Oc/Ot distance at the lowest doses tested, which characterize *Phallusia* embryos exposed to PS-NH_2, were very similar to the ones caused by Rifampicin and SR12813, which are PXR agonists [43]. PXR is known to be involved in mechanisms of defense against endogenous and exogenous molecules, regulating the transcription of enzymes and transporters involved in the metabolism and elimination of potentially harmful compounds [46]. In ascidians, this receptor is expressed in the brain vesicles of embryos and larvae and exposure to its agonist induces significant changes in trunk elongation and PC formation [42]. Our findings suggest a possible interaction between PS NPs and PXRs, although we cannot rule out the possibility that the byproducts released by PS-NH_2 [19], rather than PS-NH_2, interact with PXR, resulting in the malformations during the embryonic development of ascidians. Actually, as previously shown, styrene monomers and the 2,4-Di-tert-butylphenol (DTBP), which is considered an analog of Bisphenol A (BPA), which is known to interact with PXR in the ascidian *C. robusta*, both leach from the PS-NH_2 suspension in NSW [19,47,48]. However, the phenotypic signature of PS NPs in *Phallusia* also resembles the one of ERR and RXR ligands [43] and only the measurement of the modulation of the activity of these nuclear receptors by PS-NH_2 can reveal whether nanoparticles or chemicals leaching from them can affect ascidian nuclear receptors.

On the other hand, the highest concentration of PS-NH_2 (15 μg mL^{-1} and 7.5 μg mL^{-1} for chorionated and dechorionated embryos, respectively) caused significant effects at the level of all the endpoints studied, except for the Oc/Ot area, suggesting either nonspecific toxicity or DNA damage [43]. However, our study shows that, in PS-NH_2-treated embryos, the DNA is intact, without any damage, meaning that no genotoxic effects are associated with the exposure to PS-NH_2 up to 15 μg mL^{-1}. The mechanism of toxicity induced by the highest concentration of PS-NH_2 may be due to the generation of Reactive Oxygen Species (ROS) through positive charges that interact with the negatively charged cell membranes [49]. The elevated levels of ROS may, in turn, cause significant decreases in cell viability and changes in membrane integrity [50]. This is in line with our formulated hypothesis on *Ciona* embryos exposed to PS-NH_2 [19]. In fact, the initial event leading to the above morphological changes could be the adhesion of PS-NH_2 around the chorion, potentially causing a general condition of oxidative stress. The influence of positive charge on embryonic development is highlighted in studies showing that negatively charged polystyrene nanoparticles (e.g., PS-COOH) exhibit reduced toxicity during the embryogenesis of the sea urchin *P. lividus* [8] and the ascidian *C. robusta* [21]. These nanoparticles do not affect larval phenotypes or development, likely due to their tendency for rapid

sedimentation. The similar phenotype observed in dechorionated embryos suggests that PS-NH_2 elicits comparable responses in both chorionated and dechorionated embryos, with the observed phenotype likely resulting from direct interaction of the nanoparticles with the developing larvae. From this perspective, it would be very interesting to define the Toxicosis phenotypic signature of oxidative stress and compare it with the phenotypic signature of PS-NH_2, identified in this study in *Phallusia*, in order to clarify this issue.

5. Conclusions

Using high-content analysis of embryonic phenotypes, we established the effects of PS-NH_2 on the embryogenesis of the ascidian *P. mammillata*. We compared the effects using chorionated (to reproduce the natural conditions) and dechorionated embryos (to ensure the interaction of PS NPs with the embryo), showing that the morphological alterations are the same but the dechorionated embryos have an increased sensitivity, suggesting the protective role of the chorion against PS-NH_2. The quantitative analysis revealed two different phenotypic signatures for both the conditions tested: (i) the concentrations near the EC_{50} affected trunk L/W ratio, tail length and Oc/Ot distance endpoints, as in the case of PXR agonists; (ii) the highest concentrations of PS-NH_2 affected several endpoints, suggesting a nonspecific toxicity of PS NPs probably caused by the general stress of the developing organism. Further studies are, however, fundamental to clarify if their toxic effects are due to their adhesion around the growing embryos, or to their internalization within the cells. Moreover, we cannot exclude that the toxic effects are not related to nanoparticles themselves, but to leachates from PS, like styrene monomers and the DTBP [19], which could act directly on naked embryos or by crossing the chorion.

Supplementary Materials: The following supporting information can be downloaded at https://www.mdpi.com/article/10.3390/jox15010010/s1, Figures S1 and S2: FTIR spectrum of PS-NH_2 vs. FTIR spectrum of polystyrene present in the libraries used for the match and FTIR spectrum of PS-NH_2 vs. FTIR spectrum of non-functionalized fluorescent polystyrene nanoplastics (PS-NPs, 100 nm, Polysciences Europe GmbH, Eppelheim, Germany), respectively; Figure S3: Morphometric analysis of phenotypes induced in *Phallusia mammillata* embryos (A) with a chorion and (B) without a chorion exposed to PS-NH_2. Radar charts summarize the following endpoints: ocellus (Oc) + otolith (Ot) area (μm^2); Oc/Ot distance (μm); percentage of embryos with palps (%); trunk L/W (length/width) ratio; tail length (μm). All measurements were performed at 22 hpf. The values are normalized to the corresponding value of the same parameter in the control (stage 26) and presented as a percentage of the control value; Figure S4: Genotoxicity assay performed analyzing 7 hpf embryos (neurula stage). (A) Control embryo, (B) embryo with DNA aberration.

Author Contributions: Conceptualization, R.D., I.C. and A.S.; methodology, R.D., I.C., A.S. and M.C.E.; formal analysis, M.C.E. and R.D.; investigation, M.C.E.; resources, R.D., I.C. and A.S.; data curation, M.C.E., R.D., I.C. and A.S.; writing—original draft preparation, M.C.E., A.S. and R.D.; writing—review and editing, A.S., R.D., M.C.E. and I.C.; supervision, R.D.; project administration, R.D., A.S. and I.C.; funding acquisition, M.C.E., I.C., A.S. and R.D. All authors have read and agreed to the published version of the manuscript.

Funding: This research received no external funding.

Institutional Review Board Statement: No research ethics committee approval was required to achieve the aims of this study as the experimental work was carried out on an unregulated invertebrate species.

Informed Consent Statement: Not applicable.

Data Availability Statement: Data are contained within the article and Supplementary Materials.

Acknowledgments: This study was performed within the framework of the project entitled "Ciona robusta (formerly *Ciona intestinalis* type A) as model system for ecotoxicological studies" co-funded by the University of Siena (Italy) and the Zoological Station Anton Dohrn of Naples. Maria Concetta Eliso received an EMBO Short-Term Fellowship (number 8609) to carry out research in the lab of Rémi Dumollard (Laboratoire de Biologie du Développement de Villefranche-sur-mer (LBDV), Institut de la Mer à Villefranche (IMEV), Sorbonne Universités, UPMC Univ Paris 06, Port de la Darse, 06230 Villefranche sur-mer, France). Work in the R.D. laboratory was funded by grants from the Centre National de la Recherche Scientifique DBM 2021 program and the Agence Nationale de la Recherche (ANR-21-CE34-0006-02). The authors thank Kennedi Davis for her help in the genotoxicity assays. The authors thank Carola Murano for her great help and support in the FTIR analysis.

Conflicts of Interest: The authors declare no conflicts of interest.

References

1. Andrady, A.L. Microplastics in the Marine Environment. *Mar. Pollut. Bull.* **2011**, *62*, 1596–1605. [CrossRef] [PubMed]
2. Ekvall, M.T.; Lundqvist, M.; Kelpsiene, E.; Šileikis, E.; Gunnarsson, S.B.; Cedervall, T. Nanoplastics Formed during the Mechanical Breakdown of Daily-Use Polystyrene Products. *Nanoscale Adv.* **2019**, *1*, 1055–1061. [CrossRef] [PubMed]
3. Gigault, J.; ter Halle, A.; Baudrimont, M.; Pascal, P.-Y.; Gauffre, F.; Phi, T.-L.; El Hadri, H.; Grassl, B.; Reynaud, S. Current Opinion: What Is a Nanoplastic? *Environ. Pollut.* **2018**, *235*, 1030–1034. [CrossRef] [PubMed]
4. Lambert, S.; Wagner, M. Characterisation of Nanoplastics during the Degradation of Polystyrene. *Chemosphere* **2016**, *145*, 265–268. [CrossRef] [PubMed]
5. Jahnke, A.; Arp, H.P.H.; Escher, B.I.; Gewert, B.; Gorokhova, E.; Kühnel, D.; Ogonowski, M.; Potthoff, A.; Rummel, C.; Schmitt-Jansen, M.; et al. Reducing Uncertainty and Confronting Ignorance about the Possible Impacts of Weathering Plastic in the Marine Environment. *Environ. Sci. Technol. Lett.* **2017**, *4*, 85–90. [CrossRef]
6. Cole, M.; Lindeque, P.; Halsband, C.; Galloway, T.S. Microplastics as Contaminants in the Marine Environment: A Review. *Mar. Pollut. Bull.* **2011**, *62*, 2588–2597. [CrossRef]
7. Ter Halle, A.; Jeanneau, L.; Martignac, M.; Jardé, E.; Pedrono, B.; Brach, L.; Gigault, J. Nanoplastic in the North Atlantic Subtropical Gyre. *Env. Sci Technol* **2017**, *51*, 13689–13697. [CrossRef]
8. Schirinzi, G.F.; Llorca, M.; Seró, R.; Moyano, E.; Barceló, D.; Abad, E.; Farré, M. Trace Analysis of Polystyrene Microplastics in Natural Waters. *Chemosphere* **2019**, *236*, 124321. [CrossRef] [PubMed]
9. Gonçalves, J.M.; Bebianno, M.J. Nanoplastics Impact on Marine Biota: A Review. *Environ. Pollut.* **2021**, *273*, 116426. [CrossRef]
10. Shi, C.; Liu, Z.; Yu, B.; Zhang, Y.; Yang, H.; Han, Y.; Wang, B.; Liu, Z.; Zhang, H. Emergence of Nanoplastics in the Aquatic Environment and Possible Impacts on Aquatic Organisms. *Sci. Total Environ.* **2024**, *906*, 167404. [CrossRef] [PubMed]
11. Ferreira, I.; Venâncio, C.; Lopes, I.; Oliveira, M. Nanoplastics and Marine Organisms: What Has Been Studied? *Environ. Toxicol. Pharmacol.* **2019**, *67*, 1–7. [CrossRef] [PubMed]
12. Corsi, I.; Bellingeri, A.; Eliso, M.C.; Grassi, G.; Liberatori, G.; Murano, C.; Sturba, L.; Vannuccini, M.L.; Bergami, E. Eco-Interactions of Engineered Nanomaterials in the Marine Environment: Towards an Eco-Design Framework. *Nanomaterials* **2021**, *11*, 1903. [CrossRef] [PubMed]
13. Della Torre, C.; Bergami, E.; Salvati, A.; Faleri, C.; Cirino, P.; Dawson, K.A.; Corsi, I. Accumulation and Embryotoxicity of Polystyrene Nanoparticles at Early Stage of Development of Sea Urchin Embryos *Paracentrotus lividus*. *Environ. Sci. Technol.* **2014**, *48*, 12302–12311. [CrossRef]
14. Canesi, L.; Ciacci, C.; Fabbri, R.; Balbi, T.; Salis, A.; Damonte, G.; Cortese, K.; Caratto, V.; Monopoli, M.P.; Dawson, K.; et al. Interactions of Cationic Polystyrene Nanoparticles with Marine Bivalve Hemocytes in a Physiological Environment: Role of Soluble Hemolymph Proteins. *Environ. Res.* **2016**, *150*, 73–81. [CrossRef] [PubMed]
15. Balbi, T.; Camisassi, G.; Montagna, M.; Fabbri, R.; Franzellitti, S.; Carbone, C.; Dawson, K.; Canesi, L. Impact of Cationic Polystyrene Nanoparticles (PS-NH2) on Early Embryo Development of *Mytilus galloprovincialis*: Effects on Shell Formation. *Chemosphere* **2017**, *186*, 1–9. [CrossRef]
16. Auguste, M.; Balbi, T.; Ciacci, C.; Canonico, B.; Papa, S.; Borello, A.; Vezzulli, L.; Canesi, L. Shift in Immune Parameters After Repeated Exposure to Nanoplastics in the Marine Bivalve *Mytilus*. *Front. Immunol.* **2020**, *11*, 426. [CrossRef] [PubMed]
17. Auguste, M.; Lasa, A.; Balbi, T.; Pallavicini, A.; Vezzulli, L.; Canesi, L. Impact of Nanoplastics on Hemolymph Immune Parameters and Microbiota Composition in *Mytilus galloprovincialis*. *Mar. Environ. Res.* **2020**, *159*, 105017. [CrossRef] [PubMed]
18. Eliso, M.C.; Bergami, E.; Manfra, L.; Spagnuolo, A.; Corsi, I. Toxicity of Nanoplastics during the Embryogenesis of the Ascidian *Ciona robusta* (Phylum Chordata). *Nanotoxicology* **2020**, *14*, 1415–1431. [CrossRef] [PubMed]

19. Eliso, M.C.; Bergami, E.; Bonciani, L.; Riccio, R.; Belli, G.; Belli, M.; Corsi, I.; Spagnuolo, A. Application of Transcriptome Profiling to Inquire into the Mechanism of Nanoplastics Toxicity during *Ciona robusta* Embryogenesis. *Environ. Pollut.* **2023**, *318*, 120892. [CrossRef] [PubMed]
20. Geremia, E.; Muscari Tomajoli, M.T.; Murano, C.; Petito, A.; Fasciolo, G. The Impact of Micro- and Nanoplastics on Aquatic Organisms: Mechanisms of Oxidative Stress and Implications for Human Health—A Review. *Environments* **2023**, *10*, 161. [CrossRef]
21. Liu, Z.; Li, Y.; Pérez, E.; Jiang, Q.; Chen, Q.; Jiao, Y.; Huang, Y.; Yang, Y.; Zhao, Y. Polystyrene Nanoplastic Induces Oxidative Stress, Immune Defense, and Glycometabolism Change in Daphnia Pulex: Application of Transcriptome Profiling in Risk Assessment of Nanoplastics. *J. Hazard. Mater.* **2021**, *402*, 123778. [CrossRef]
22. Contino, M.; Ferruggia, G.; Indelicato, S.; Pecoraro, R.; Scalisi, E.M.; Salvaggio, A.; Brundo, M.V. Sublethal Effects of Polystyrene Nanoplastics on the Embryonic Development of *Artemia salina* (Linnaeus, 1758). *Animals* **2023**, *13*, 3152. [CrossRef] [PubMed]
23. Wan, J.-K.; Chu, W.-L.; Kok, Y.-Y.; Lee, C.-S. Distribution of Microplastics and Nanoplastics in Aquatic Ecosystems and Their Impacts on Aquatic Organisms, with Emphasis on Microalgae. In *Reviews of Environmental Contamination and Toxicology*; De Voogt, P., Ed.; Reviews of Environmental Contamination and Toxicology; Springer International Publishing: Cham, Swizterland, 2018; Volume 246, pp. 133–158. ISBN 978-3-319-97739-3.
24. Dedman, C.J.; Christie-Oleza, J.A.; Fernández-Juárez, V.; Echeveste, P. Cell Size Matters: Nano- and Micro-Plastics Preferentially Drive Declines of Large Marine Phytoplankton Due to Co-Aggregation. *J. Hazard. Mater.* **2022**, *424*, 127488. [CrossRef] [PubMed]
25. Tallec, K.; Huvet, A.; Di Poi, C.; González-Fernández, C.; Lambert, C.; Petton, B.; Le Goïc, N.; Berchel, M.; Soudant, P.; Paul-Pont, I. Nanoplastics Impaired Oyster Free Living Stages, Gametes and Embryos. *Environ. Pollut.* **2018**, *242*, 1226–1235. [CrossRef] [PubMed]
26. De Santis, R.; Jamunno, G.; Rosati, F. A Study of the Chorion and the Follicle Cells in Relation to the Sperm-Egg Interaction in the Ascidian, *Ciona intestinalis*. *Dev. Biol.* **1980**, *74*, 490–499. [CrossRef] [PubMed]
27. Cotelli, F.; Andronico, F.; Santis, R.; Monroy, A.; Rosati, F. Differentiation of the Vitelline Coat in the ascidian*Ciona intestinalis*: An Ultrastructural Study. *Wilhelm Roux' Arch.* **1981**, *190*, 252–258. [CrossRef]
28. Sato, Y.; Morisawa, M. Loss of Test Cells Leads to the Formation of New Tunic Surface Cells and Abnormal Metamorphosis in Larvae of *Ciona intestinalis* (Chordata, Ascidiacea). *Dev. Genes Evol.* **1999**, *209*, 592–600. [CrossRef]
29. Thompson, H.; Shimeld, S.M. Transmission and Scanning Electron Microscopy of the Accessory Cells and Chorion During Development of *Ciona intestinalis* Type B Embryos and the Impact of Their Removal on Cell Morphology. *Zool. Sci.* **2015**, *32*, 217–222. [CrossRef] [PubMed]
30. Satoh, N. A Deep Dive into the Development of Sea Squirts. *Nature* **2019**, *571*, 333–334. [CrossRef] [PubMed]
31. Delsuc, F.; Brinkmann, H.; Chourrout, D.; Philippe, H. Tunicates and Not Cephalochordates Are the Closest Living Relatives of Vertebrates. *Nature* **2006**, *439*, 965–968. [CrossRef] [PubMed]
32. Ishida, T.; Satou, Y. Ascidian Embryonic Cells with Properties of Neural-Crest Cells and Neuromesodermal Progenitors of Vertebrates. *Nat. Ecol. Evol.* **2024**, *8*, 1154–1164. [CrossRef] [PubMed]
33. Rosner, A.; Rinkevich, B. Harnessing Ascidians as Model Organisms for Environmental Risk Assessment. *Environments* **2024**, *11*, 232. [CrossRef]
34. Beyer, J.; Song, Y.; Lillicrap, A.; Rodríguez-Satizábal, S.; Chatzigeorgiou, M. *Ciona* Spp. and Ascidians as Bioindicator Organisms for Evaluating Effects of Endocrine Disrupting Chemicals: A Discussion Paper. *Mar. Environ. Res.* **2023**, *191*, 106170. [CrossRef]
35. Dumollard, R.; Gazo, I.; Gomes, I.D.L.; Besnardeau, L.; McDougall, A. Ascidians: An Emerging Marine Model for Drug Discovery and Screening. *Curr. Top Med. Chem.* **2017**, *17*, 2056–2066. [CrossRef] [PubMed]
36. Sladitschek, H.L.; Fiuza, U.-M.; Pavlinic, D.; Benes, V.; Hufnagel, L.; Neveu, P.A. MorphoSeq: Full Single-Cell Transcriptome Dynamics Up to Gastrulation in a Chordate. *Cell* **2020**, *181*, 922–935.e21. [CrossRef]
37. Hotta, K.; Miyasaka, S.O.; Oka, K.; Shito, T.T. Staring into a Crystal Ball: Understanding Evolution and Development of in Vivo Aquatic Organismal Transparency. *Front. Ecol. Evol.* **2024**, *12*, 1428976. [CrossRef]
38. Yasuo, H.; McDougall, A. Practical Guide for Ascidian Microinjection: *Phallusia mammillata*. In *Transgenic Ascidians*; Sasakura, Y., Ed.; Advances in Experimental Medicine and Biology; Springer: Singapore, 2018; Volume 1029, pp. 15–24. ISBN 978-981-10-7544-5.
39. Pennati, R.; Groppelli, S.; Zega, G.; Biggiogero, M.; De Bernardi, F.; Sotgia, C. Toxic Effects of Two Pesticides, Imazalil and Triadimefon, on the Early Development of the Ascidian *Phallusia mammillata* (Chordata, Ascidiacea). *Aquat. Toxicol.* **2006**, *79*, 205–212. [CrossRef] [PubMed]
40. Messinetti, S.; Mercurio, S.; Pennati, R. Effects of Bisphenol A on the Development of Pigmented Organs in the Ascidian *Phallusia mammillata*. *Invertebr. Biol.* **2018**, *137*, 329–338. [CrossRef]
41. Groppelli, S.; Zega, G.; Biggiogero, M.; De Bernardi, F.; Sotgia, C.; Pennati, R. Fluconazole Induces Teratogenic Effects in the Tunicate *Phallusia mammillata*. *Environ. Toxicol. Pharmacol.* **2007**, *23*, 265–271. [CrossRef]

42. Gomes, I.D.L.; Gazo, I.; Besnardeau, L.; Hebras, C.; McDougall, A.; Dumollard, R. Potential Roles of Nuclear Receptors in Mediating Neurodevelopmental Toxicity of Known Endocrine-disrupting Chemicals in Ascidian Embryos. *Mol. Reprod. Dev.* **2019**, *86*, 1333–1347. [CrossRef]
43. Gazo, I.; Gomes, I.D.L.; Savy, T.; Besnardeau, L.; Hebras, C.; Benaicha, S.; Brunet, M.; Shaliutina, O.; McDougall, A.; Peyrieras, N.; et al. High-Content Analysis of Larval Phenotypes for the Screening of Xenobiotic Toxicity Using *Phallusia mammillata* Embryos. *Aquat. Toxicol.* **2021**, *232*, 105768. [CrossRef]
44. Lambert, C.C.; Brandt, C.L. The Effect Of Light On The Spawning Of *Ciona intestinalis*. *Biol Bull* **1967**, *132*, 222–228. [CrossRef]
45. Gomes, I.D.L.; Gazo, I.; Nabi, D.; Besnardeau, L.; Hebras, C.; McDougall, A.; Dumollard, R. Bisphenols Disrupt Differentiation of the Pigmented Cells during Larval Brain Formation in the Ascidian. *Aquat. Toxicol.* **2019**, *216*, 105314. [CrossRef]
46. Krasowski, M.D.; Ni, A.; Hagey, L.R.; Ekins, S. Evolution of Promiscuous Nuclear Hormone Receptors: LXR, FXR, VDR, PXR, and CAR. *Mol. Cell. Endocrinol.* **2011**, *334*, 39–48. [CrossRef] [PubMed]
47. Webster, F.; Gagné, M.; Patlewicz, G.; Pradeep, P.; Trefiak, N.; Judson, R.S.; Barton-Maclaren, T.S. Predicting Estrogen Receptor Activation by a Group of Substituted Phenols: An Integrated Approach to Testing and Assessment Case Study. *Regul. Toxicol. Pharmacol.* **2019**, *106*, 278–291. [CrossRef]
48. Richter, I.; Fidler, A.E. Tunicate Pregnane X Receptor (PXR) Orthologs: Transcript Characterization and Natural Variation. *Mar. Genom.* **2015**, *23*, 99–108. [CrossRef]
49. Sun, X.; Wang, X.; Booth, A.M.; Zhu, L.; Sui, Q.; Chen, B.; Qu, K.; Xia, B. New Insights into the Impact of Polystyrene Micro/Nanoplastics on the Nutritional Quality of Marine Jacopever (*Sebastes schlegelii*). *Sci. Total Environ.* **2023**, *903*, 166560. [CrossRef]
50. Zhang, H.; Cheng, H.; Wang, Y.; Duan, Z.; Cui, W.; Shi, Y.; Qin, L. Influence of Functional Group Modification on the Toxicity of Nanoplastics. *Front. Mar. Sci.* **2022**, *8*, 800782. [CrossRef]

Journal of *Xenobiotics*

MDPI

Article

Effects of the Interaction of Salinity and Rare Earth Elements on the Health of *Mytilus galloprovincialis*: The Case of Praseodymium and Europium

Carla Leite [1], Tania Russo [2], Gianluca Polese [2], Amadeu M. V. M. Soares [1], Carlo Pretti [3,4], Eduarda Pereira [5] and Rosa Freitas [1,*]

[1] Department of Biology & CESAM, University of Aveiro, 3810-193 Aveiro, Portugal; asoares@ua.pt (A.M.V.M.S.)
[2] Department of Biology, University of Naples Federico II, 80126 Napoli, Italy; tania.russo@unina.it (T.R.); gianluca.polese@unina.it (G.P.)
[3] Department of Veterinary Sciences, University of Pisa, San Piero a Grado, 56122 Pisa, Italy
[4] Interuniversity Consortium of Marine Biology of Leghorn "G. Bacci", 57128 Livorno, Italy
[5] Department of Chemistry & LAQV-REQUIMTE, University of Aveiro, 3810-193 Aveiro, Portugal
* Correspondence: rosafreitas@ua.pt

Abstract: The growing use of products containing rare earth elements (REEs) may lead to higher environmental emissions of these elements, which can potentially enter aquatic systems. Praseodymium (Pr) and europium (Eu) are widely used REEs with various applications. However, their ecotoxicological impacts remain largely unexplored, with poorly understood risks to wildlife. Moreover, organisms also face environmental stressors like salinity fluctuations, and the nature of the interaction between salinity variations and contaminants is not yet clear. Therefore, this study aimed to evaluate the influence of salinity shifts on the impacts of Pr and Eu on adult mussels and the sperm of the species *Mytilus galloprovincialis* after 28 days and 30 min of exposure, respectively. To do so, biochemical and histopathological alterations were evaluated in adults, while biochemical and physiological changes were analysed in sperm. Additionally, the Integrated Biological Index (IBR) was calculated to understand the overall impact of each treatment. The results showed that adult mussels were most affected when exposed to the combination of high salinity and each element, which altered the behaviour of defence mechanisms causing redox imbalance and cellular damage. On the other hand, sperm demonstrated sensitivity to specific REE-salinity combinations, particularly Pr at lower salinity and Eu at higher salinity. These specific treatments elicited changes in sperm motility and velocity: Pr 20 led to a higher production of O_2^- and a decrease in velocity, while Eu 40 resulted in reduced motility and an increase in irregular movement. At both lower and higher salinity levels, exposure to Eu caused similar sensitivities in adults and sperm, reflected by comparable IBR scores. In contrast, Pr exposure induced greater alterations in sperm than in adult mussels at lower salinity, whereas the reverse was observed at higher salinity. These findings suggest that reproductive success and population dynamics could be modulated by interactions between salinity levels and REE pollution, highlighting the need for further investigation into how REEs and environmental factors interact. This study offers valuable insights to inform policymakers about the potential risks of REE contamination, emphasising the importance of implementing environmental regulations and developing strategies to mitigate the impact of these pollutants.

Keywords: rare earth elements; salinity; biochemistry; histopathology; adult mussels; sperm

1. Introduction

Rare earth elements (REEs) have traditionally been regarded as posing minimal environmental risk due to their low solubility in water and limited (bio)availability. This is because they readily precipitate or form complexes with hydroxides, carbonates, fluorides,

phosphates, and humic and fulvic acids [1,2]. For instance, REE-phosphate products have a solubility as low as 10^{-25} mol^2/L^2 [2]. However, over the last two decades, due to their unique magnetic, optical, catalytic, and phosphorescent properties, there has been a growing demand for REEs for use in new technologies, such as in equipments in the automotive industry and in renewable energy generation systems [3–5]. Among REEs are praseodymium (Pr) and europium (Eu). Praseodymium has been used in permanent magnets to enhance magnetic strength, stability, and energy efficiency [6]; as a contrast agent in medical imaging [7]; and in alloys to improve strength and corrosion resistance [8]. Additionally, this element is used in catalysts to enhance redox reactions and oxygen storage [9] and as a coloring agent in ceramics and glass additives [10]. Despite being one of the rarest REEs, Eu plays an essential role in several industries due to its phosphorescent properties. This element is widely used in phosphors [11], optics, fluorescent lamps, displays, lasers, and light-emitting diodes [11,12]. Additionally, the ability of Eu to absorb neutrons makes it essential in control rods for nuclear reactors [13].

The intensified use of products containing REEs can lead to increasing emissions into the environment. Product manufacturing and technological processes are known to elevate environmental REEs concentrations [14,15]. These elements can reach aquatic systems through various pathways, including atmospheric deposition, surface runoff, and industrial effluents. While atmospheric deposition can occur, it has not been shown to contribute significantly to contamination outside mining regions. In contrast, industrial effluents containing REEs can be directly discharged into surface waters [16]. Praseodymium and Eu have been detected in different aquatic systems. In São Domingos Creek (Portugal), located near to a mining area, measured concentrations range from below the detection limit (<1.0 μg/L) to 51.3 μg/L for Pr and 12.7 μg/L for Eu [15]. In Ría de Huelva (Spain), the maximum concentrations reported were 5.16 μg/L for Pr and 1.48 μg/L for Eu [17]. In the Guadiamar aquifer (Spain), impacted by acid mine drainage, Olías et al. [18]) observed a maximum Pr concentration of 10.21 μg/L in July 2001 and 13.31 μg/L in July 2002. Similarly, Atinkpahoun et al. [19] recorded a maximum Eu concentration of 14.3 μg/L in urban wastewater from the city of Cotonou (Benin, West Africa). A study by Hatje et al. [20] recorded rising REE concentrations in San Francisco Bay (USA) from 1996 to 2013. For instance, Pr concentrations increased from 10.1 to 60.1 pmol/kg, and those for Eu rose from 6.45 to 16.1 pmol/kg [20].

The release of these elements into aquatic systems has led to increased wildlife exposure. However, studies regarding their toxicity in marine and coastal organisms are scarce compared to those for freshwater environments, underscoring a significant knowledge gap. Additionally, there are no specific regulatory restrictions for REEs [16], likely due to the historical perception of minimal risk and a lack of sufficient studies on their environmental impact. This highlights the need for further investigation to better understand the potential risks and ecological implications of REEs in marine ecosystems [16] and provide data for the implementation of regulatory restrictions. A study conducted by Leite et al. [21] showed that the exposure of mussels to Pr (0, 10, 20, 40, and 80 μg/L) led to an increase in metabolic activity and enhanced the activity of antioxidant and biotransformation enzymes, being insufficient to prevent cellular damage. Similarly, the same authors observed that the tested Eu concentrations (0, 10, 20, 40, and 80 μg/L) caused cellular damage in mussels, despite the increase in biotransformation enzyme activity. Histopathological analysis revealed that mussels could not recover from exposure to either element, with lower concentrations causing higher damage to digestive tubules [21]. Markich et al. [22] evaluated the chronic no (significant)-effect concentrations (N(S)ECs) and median-effect concentrations (EC_{50}s) induced by Pr and other REEs (yttrium (Y), lanthanum (La), cerium (Ce), neodymium (Nd), gadolinium (Gd), dysprosium (Dy), and lutetium (Lu)) in 30 marine species. The authors observed that for the most sensitive species (a species of sea urchin), the N(S)EC of Pr was 1.9 μg/L and the EC_{50} was 14.4 μg/L, while for the least sensitive (a cyanobacterium), the N(S)EC of Pr was 469 μg/L and the EC_{50} was 3000 μg/L. Overall, Pr, together with La, was the least toxic element among the tested REEs. Similarly, Kurvet et al. [23] reported

an EC_{50} of 12.17 mg/L for Pr in the marine bacteria *Vibrio fischeri* in terms of inhibition of luminescence. The authors observed that among the REEs tested (Pr, Ce, Gd, La, and Nd), Pr is ranked second last in terms of toxicity, with La being the least toxic. Tai et al. [24] observed that exposure of the microalgae *Skeletonema costatum* to 29.16 ± 0.61 µmol/L of Eu resulted in a 50% reduction in the growth of algae compared to the controls after 96 h (96 h-EC_{50}). Trifuoggi et al. [25] reported that all tested concentrations of Eu (15.2, 152.0, and 15,196.4 µg/L), did not cause significant developmental defects in the early life stages of the sea urchin *Sphaerechinus granularis*. However, while the lower concentrations of Eu (15.2, 152.0 µg/L) similarly did not affect the early development of the sea urchin *Arbacia lixula*, the highest concentration (15,196.4 µg/L) induced significant developmental defects.

Besides pollution, aquatic organisms also face environmental challenges related to climate change. Among the challenges, salinity is one of the key abiotic factors with the power to affect the survival and adaptability of organisms [26]. Salinity variations often result from extreme weather events, with factors like temperature rise and intensification of global rainfall and evaporation cycles contributing to salinity fluctuations in aquatic environments [27]. These changes create differences in osmotic pressure between the surrounding environment and an organism's tissue cells, leading to stress, including osmoregulation, bioenergetic, and biochemical alterations [28–30]. Salinity variations can affect aquatic species, particularly calcifying organisms such as bivalves [31], affecting shell formation, respiration rate, filtration rate, osmoregulation, metabolism, and the oxidative and immune systems [31–39]. Moreover, shifts in salinity can not only influence organisms but also alter the behaviour and toxicity of contaminants within aquatic ecosystems. Recent studies showed the influence of salinity shifts on the impacts of REEs. For instance, Andrade et al. [40] showed that lower salinity influenced the effects of La by increasing metabolism, the activity of the defence system, and lipid peroxidation. Another study demonstrated that lower salinity intensified the effects of Y on mussels by increasing their defence mechanisms and neurotoxicity [41]. Nevertheless, the data regarding the organisms' responses to the combination of REEs and salinity shifts are still scarce.

Considering that organisms in the environment are simultaneously subjected to multiple stressors, this study aimed to investigate the toxicological effects of Pr and Eu (10 µg/L) on *M. galloprovincialis* adults and sperm under varying salinity levels: low (a salinity of 20), control (a salinity of 30), and high (a salinity of 40). While recent research has already highlighted the impacts of Pr and Eu on *M. galloprovincialis*, to our knowledge, there is no available information regarding how salinity influences these effects. *M. galloprovincialis* was chosen as a model species due to its significant economic and ecological value as well as its effectiveness as a bioindicator species. Its widespread distribution, feeding habits, high stress tolerance and the ease with which it can be collected and handled make it an ideal subject for study [42].

2. Materials and Methods

2.1. Sampling and Experimental Conditions

In the present study, two experiments were performed, one with *Mytilus galloprovincialis* adult mussels that were collected in the Ria de Aveiro coastal lagoon (Portugal) in October 2021 (shell length: 64 ± 3.4 mm; width: 37 ± 2.1 mm) and the other with *M. galloprovincialis* sperm from adults collected in the Gulf of La Spezia (Italy) in May 2022 (shell length: 55 ± 5 mm; width: 28 ± 2.5 mm). While the adult mussels used in both experiments originated from two different locations, previous studies have shown that adults from these sites respond similarly under standard conditions [43,44].

In both experiments, the tested treatments were CTL 20 (non-contaminated seawater at salinity of 20 in order to simulate rainy periods); CTL 30 (non-contaminated seawater at salinity of 30, used as a control salinity); CTL 40 (non-contaminated seawater at salinity of 40 to simulate drought periods); Pr 20 (contaminated seawater with 10 µg/L of Pr at salinity of 20); Pr 30 (contaminated seawater with 10 µg/L of Pr at salinity of 30); Pr 40 (contaminated seawater with 10 µg/L of Pr at salinity of 40), Eu 20 (contaminated seawater

with 10 μg/L of Eu at salinity of 20); Eu 30 (contaminated seawater with 10 μg/L of Eu at salinity of 30); and Eu 40 (contaminated seawater with 10 μg/L of Eu at salinity of 40).

The concentration chosen was based on the values found in contaminated environments by Gomes et al. [15] (<1.0–51.3 μg/L for Pr and <1.0–12.7 μg/L for Eu), Olías et al. [18] (maximum Pr concentration of 10.24 μg/L), and Atinkpahoun et al. [19] (maximum Eu concentration of 14.3 μg/L). In addition, the Pr and Eu concentration was also selected since it was the lowest to cause negative effects in mussels within a range of 0–80 μg/L of Pr and Eu in the study by Leite et al. [21]. Given that salinity levels in Ria de Aveiro range from 5 to 15 during winter and from 36 to 37 in summer [45], salinities of 20 ± 1 and 40 ± 1 were chosen to simulate rainy and drought periods, respectively.

2.2. Adults' Exposure

After collection, mussels were transported to the laboratory, where they were held in tanks for a one-week depuration period under control conditions: temperature of 17 ± 1 °C; salinity of 30 ± 1; pH of 8.0 ± 0.1; and natural photoperiod (10 h light/14 h dark). Artificial seawater was prepared by dissolving a commercial salt (RED SEA SALT, Éilat, Israel) in deionized water, with continuous aeration and bi-daily water renewal. Following depuration, mussels were acclimated for an additional week under similar conditions, except with regard to salinity. During this week, mussels were separated into three tanks with adjusted salinity levels: in one tank, the salinity was gradually reduced to 20 at a rate of 2 units per day; in another tank, the salinity was gradually increased to 40 at a rate of 2 units per day; and in the third tank, the salinity was maintained at 30. During the acclimation phase, mussels were fed Algamac protein plus (AquaFauna Bio-Marine, Inc., Hawthorne, CA, USA) at a concentration of 150,000 cells per animal per day.

During the 28-day experiment, a total of 135 mussels were subjected to the previously mentioned treatments. The organisms were placed in different aquaria, each holding 3 L of artificial seawater, with five mussels per aquarium and three aquaria for each treatment. Mussels were fed the same diet used during acclimation three times per week. Temperature, pH, and photoperiod were kept consistent with the depuration/acclimation conditions. Water was renewed weekly, and Pr and Eu concentrations were re-established. Immediately after spiking, water samples were collected from each aquarium to verify the actual concentrations of these elements. In addition, two extra aquaria (blanks) for each contaminated treatment, without organisms, were set up to assess the stability of the elements. Water samples from these aquaria were collected at intervals (0, 72, 120, and 168 h after the spiking) during the first week.

At the end of the exposure period, three mussels were taken from each aquarium (nine per treatment) for biochemical analysis. Each mussel's tissue was homogenized with a mortar and a pestle under liquid nitrogen and then divided into five 0.5 g fresh-weight (FW) aliquots. The remaining tissue of one of these mussels per aquarium (three per treatment) was used to quantify the concentrations of both elements. In addition, one mussel was collected from each aquarium (three per treatment) for histopathological analysis. For that, each mussel's tissue was fixed in Davidson solution (a mixture of glycerol, formalin, 95% ethanol, and seawater) for a period of 24 h.

2.2.1. Praseodymium and Europium Quantification

The concentrations of Pr and Eu in water and mussels' tissues were measured using inductively coupled plasma mass spectrometry (ICP-MS). Both elements had a quantification limit (LOQ) of 0.01 μg/L. Upon collection, water samples were acidified with nitric acid (HNO_3) (65%), and before the analysis, the samples were diluted by a factor of 20 to reach salinity < 2.

Mussels' tissue samples were freeze-dried, and 0.2 g of each sample was digested with an acid mixture containing 1 mL of HNO_3 65% (v/v), 2 mL of hydrogen peroxide (30%), and 1 mL of ultrapure water (H_2O). Digestion was carried out in a CEM MARS 5 microwave, where the temperature was ramped up to 180 °C over 15 min and maintained at this level

for an additional 5 min. Following digestion, ultrapure H_2O was added to each sample to reach a final volume of 25 mL. To ensure quality control, an analysis of blank samples (with no tissue) was conducted, showing concentrations below the LOQ. The certified reference material (CRM) BCR-668 (Mussel Tissue: 12.3 ± 1.1 µg/kg Pr and 2.79 ± 0.16 µg/kg Eu) was analysed, and the percentage of recovery for Pr was 87%. The results were validated with this acceptable recovery percentage for Pr since the concentration of Eu in the CRM was below the LOQ. Differences between duplicates were <1%.

2.2.2. Biochemical Analysis

To assess the performance of the adult mussels, the biochemical parameters analysed were associated with energy balance (electron transport system (ETS) activity, total protein (PROT) and glycogen (GLY) contents); antioxidant and biotransformation defences (such as superoxide dismutase (SOD), catalase (CAT), glutathione peroxidase (GPx), carboxylesterases with *p*-nitrophenyl acetate (CbEs-*p*NPA), carboxylesterases with *p*-nitrophenyl butyrate (CbEs-*p*NPB), glutathione S-transferases (GSTs) activities); redox status and indicators of cellular damage (reduced and oxidized glutathione ratio (GSH/GSSG), lipid peroxidation (LPO), and protein carbonylation (PC) levels). Detailed procedures for the extractions and methods can be found in studies published by De Marchi et al. [43], Andrade et al. [44], and Leite et al. [46].

2.2.3. Histopathological Analysis

The histopathological alterations were evaluated in the gills and digestive tubules. After the fixation in Davidson's solution for 24 h, the mussels' tissues were transferred to 70% ethanol, and the gills and digestive gland were dissected. Dehydration and embedding procedures were then conducted according to the methods described by Leite et al. [47]. For staining, a haematoxylin solution was applied following the method described by Leite et al. [46]. Tissue alterations were observed under an optical microscope at 40× magnification, and histopathological indices (I_h) were calculated as outlined by Leite et al. [46].

2.3. Sperm Exposure

Mussels underwent a two-week depuration and acclimation process using filtered natural seawater (0.45 µm). The organisms were maintained at a temperature of 17 ± 1 °C, with a natural photoperiod. Initially, the salinity matched that at the collection site (38), and it was then gradually reduced over the first week to reach a salinity of 30. Throughout the second week, a salinity of 30 was consistently maintained as the control salinity. The seawater was aerated continuously and replaced every two days. During the second week, mussels were provided with the same diet used during the experience with the adult mussels.

The collection of the sperm was carried out by slightly cutting the mantle following the procedure outlined by Mikhailov et al. [48]. For each parameter, a sperm suspension pool from three mussels was used, with both morphology and motility checked beforehand. The concentration in each pool (cells/mL) was measured using an Olympus CH-2 optical microscope at 20× magnification and a Bürker counting chamber. After determining the initial concentration, these pools were diluted to reach the targeted concentration for each parameter. The sperm suspensions were then incubated for 30 min and subjected to the treatments mentioned before (contaminant 1:99 sperm suspension). After incubation, the suspensions were centrifuged at 3000× *g* at 4 °C for 5 min, and the resulting pellets were resuspended in filtered natural seawater at salinities of 20, 30, or 40, depending on the treatment.

Biochemical and Physiological Analysis

The quality of *M. galloprovincialis* sperm cells was assessed by analysing biochemical parameters related to the production of reactive oxygen species (ROS), specifically superox-

ide anion (O_2^-) and hydrogen peroxide (H_2O_2), as well as an indicator of cellular damage, such as LPO levels. These parameters are described in Leite et al.'s work [47].

Additionally, sperm quality was also evaluated through physiological parameters, such as the percentage of motility (% MOT), curvilinear velocity (VCL), linearity (LIN), and wobble (WOB). The methodologies for assessing these parameters are detailed in Leite et al.'s work [47].

2.4. Data Analyses

2.4.1. Bioconcentration Factor

The bioconcentration factor (BCF) was calculated following the approach by Arnot and Gobas [49]. This method can be used to calculate the ratio of the concentrations in the tissue to the concentration in the exposure medium, measured immediately after spiking.

2.4.2. Statistical Analysis

A non-parametric permutational analysis of variance (PERMANOVA + add-on in PRIMER v6) [50] was applied to examine the concentrations of Pr and Eu in the mussel tissue and several biological responses. These responses included biochemical changes in adult mussels, such as in ETS, PROT, GLY, SOD, CAT, GPx, CbEs-*p*NPA, CbEs-*p*NPB, GSTs, GSH/GSSG, LPO, and PC, as well as histopathological indices ($I_{h\ \text{Digestive tubules}}$ and $I_{h\ Gills}$). Additionally, biochemical and physiological changes in sperm were also included (ROS (O_2^-), ROS (H_2O_2), LPO, % MOT, VCL, LIN, and WOB). Pairwise comparisons were conducted when the main test showed significant differences ($p < 0.05$). The null hypotheses tested were as follows: (i) in terms of concentrations in mussel tissue, no significant differences will be observed among salinities (20, 30, 40) (in the table, significant differences are denoted by different bold and italic lowercase letters for Pr and Eu concentrations in CTL treatments, different uppercase letters for Pr concentrations in Pr treatments, and different lowercase letters for Eu concentrations in Eu treatments); (ii) in terms of concentrations in mussel tissue, no significant differences will be observed between CTL and Pr as well as CTL and Eu at each salinity (20, 30, 40) (significant differences are labelled in the table, with the *p*-value in bold); (iii) in terms of biological responses, no significant differences will be observed among salinities (20, 30, 40) in mussels and sperm (in the figures, significant differences are denoted by different bold and italic lowercase letters for CTL, different uppercase letters for Pr, and different lowercase letters for Eu); (iv) in terms of biological responses, no significant differences will be observed between CTL, Pr, and Eu at each salinity (20, 30, 40) in mussels and sperm (significant differences are labelled in the table, with the *p*-value in bold).

2.4.3. Principal Coordinates Analysis

The biological responses (biochemical and histopathological changes in adults as well as biochemical and physiological changes in sperm) were subjected to ordination analysis by Principal Coordinates (PCO) analysis to determine the relationship between treatments. The Euclidean distance similarity matrix was used to calculate the distance between centroids among the different treatments (CTL 20, 30, and 40; Pr 20, 30, and 40; and Eu 20, 30, and 40). Additionally, vectors relating to the biological descriptors were overlaid on the PCO graph using Spearman's correlation, with a correlation threshold higher than 70%.

2.4.4. Independent Action Model

The type of interaction in each biological response between the combined stressors (Pr 20, Eu 20, Pr 40, and Eu 40) was classified using the Independent Action (IA) model, as detailed by Song et al. [51]. Predicted effects for these combinations were calculated for each biological response according to the method reported by Leite et al. [52]. To confirm the additivity assumptions, observed combination responses (Pr 20, Eu 20, Pr 40, Eu 40) were compared with the IA model predictions. If the predicted values fell outside the 95%

confidence intervals (based on the t-distribution) of the observed responses, the effects were assumed to be non-additive [53]. In such cases, the type, strength, and direction of these interactions were evaluated using the methodology proposed by Piggott et al. [53] and the terminology described by Delnat et al. [54].

2.4.5. Integrated Biological Response Index

The overall response of adults and sperm to the treatments at salinities of 20 and 40 was evaluated by calculating the Integrated Biological Response Index version 2 (IBRv2), following the methods reported by Beliaeff and Burgeot [55] with adaptations by Sanchez et al. [56] and described in detail by Leite et al. [52]. Toward this end, the deviation of the stress treatments (CTL 20, Pr 20, Eu 20, CTL 40, Pr 40, and Eu 40) from the CTL treatment (CTL 30) was calculated. The IBRv2 index was determined and the final score was divided by the number of parameters for adults and sperm. The overall response provided by the IBRv2 index was discussed in terms of the generated scores, with higher IBRv2 values showing a higher degree of responsiveness by mussels/sperm.

3. Results and Discussion

This study aimed to investigate the interaction between different salinity levels and praseodymium (Pr) and europium (Eu), assessing their effects on *Mytilus galloprovincialis*. To achieve this, biochemical, histopathological, and physiological responses were evaluated in adults and sperm. Additionally, the Independent Action (IA) model was used to characterize the type of interaction for each observed effect between the elements and the different stress salinities, since it is commonly used for combinations of contaminants and natural stressors [54]. The IA model was calculated for four combinations: Pr 20, Eu 20, Pr 40, and Eu 40. The results indicated that for each treatment except for Pr 40, half of the responses were additive (Tables 1–4). This suggests that, for a significant portion of the responses, the combined effects of the elements and salinity did not significantly alter the mussels' response beyond what would be expected by summing the individual effects of each factor. Furthermore, at the lowest salinity level, Pr showed a higher synergetic potential than Eu (Tables 1 and 2), while at the highest salinity level, Pr induced the highest number of antagonistic interactions (Tables 3 and 4), suggesting that this salinity level contributed more to mitigate the effects of Pr compared to Eu. Excluding the additive responses, most of the mussels' responses to Eu were antagonistic (Tables 2 and 4), suggesting that, in general, the effects of Eu were often neutralized by salinity conditions.

Table 1. Comparison of Independent Action (IA) model predictions for the combination of praseodymium (Pr) and a salinity of 20. IA predictions not overlapping with the 95% confidence intervals of the observed results denote interactive effects. Interaction type is classified based on the magnitude of combined effects and direction of individual responses.

Endpoint	Predicted	Observed	95% CI Observed	Interaction Type (Pr 20)
ETS	0.071959	−0.09007	(−0.310–−0.130)	Additive
PROT	−0.50921	−0.38728	(−0.683–−0.092)	Additive
GLY	0.228956	−0.34281	(−0.650–−0.035)	One-directional synergism down
SOD	−0.74165	−0.6203	(−0.957–−0.283)	Additive
CAT	−0.10988	0.106398	(−0.351–0.564)	Additive
GPx	−1.24261	−0.86398	(−1.443–−0.285)	Additive
CbEs-*p*NPA	0.085179	−0.14267	(−0.276–−0.010)	Bidirectional synergism down
CbEs-*p*NPB	−0.37159	−0.09991	(−0.234–0.034)	One-directional antagonism down
GSTs	−0.62051	−0.37203	(−0.460–−0.284)	Bidirectional antagonism down
GSH/GSSG	0.436532	0.753512	(0.535–0.972)	Bidirectional synergism up
LPO adults	−1.42155	−0.51835	(−0.953–−0.083)	One-directional antagonism down
PC	−0.2615	−0.45842	(−0.622–−0.295)	One-directional synergism down
$I_{h\,G}$	−1.02073	0.092166	(−0.267–0.451)	Bidirectional antagonism up
$I_{h\,DT}$	0.630828	0.430727	(−0.137–0.998)	Additive

Table 1. *Cont.*

Endpoint	Predicted	Observed	95% CI Observed	Interaction Type (Pr 20)
O_2^-	0.580274	0.58089	(0.557–0.605)	Additive
H_2O_2	−0.01442	−0.02047	(−0.124–0.083)	Additive
LPO sperm	−0.10185	−0.09611	(−0.115–−0.077)	Additive
% MOT	−0.24752	−0.28785	(−0.611–0.035)	Additive
VCL	−0.77113	−1.17094	(−1.518–−0.825)	One-directional synergism down
LIN	−2.03888	−0.94006	(−1.626–−0.254)	One-directional antagonism down
WOB	−0.06235	0.452257	(0.003–0.902)	Bidirectional synergism up

Table 2. Comparison of Independent Action (IA) model predictions for the combination of europium (Eu) and a salinity of 20. IA predictions not overlapping with the 95% confidence intervals of the observed results denote interactive effects. Interaction type is classified based on the magnitude of combined effects and direction of individual responses.

Endpoint	Predicted	Observed	95% CI Observed	Interaction Type (Eu 20)
ETS	0.109028	−0.23344	(−0.420–−0.047)	Bidirectional synergism down
PROT	−0.40301	−0.2228	(−0.367–−0.079)	One-directional antagonism down
GLY	0.32193	−0.45303	(−0.602–−0.304)	One-directional synergism down
SOD	−2.03106	−0.14184	(−0.556–0.272)	One-directional antagonism down
CAT	0.466841	−0.02106	(−0.227–0.185)	One-directional synergism down
GPx	−0.81864	−0.45428	(−0.876–−0.032)	Additive
CbEs-*p*NPA	−0.08488	−0.20759	(−0.446–0.031)	Additive
CbEs-*p*NPB	−0.52316	−0.24514	(−0.433–−0.058)	One-directional antagonism down
GSTs	−1.46789	−0.13932	(−0.323–0.45)	One-directional antagonism down
GSH/GSSG	0.605611	0.573314	(0.291–0.855)	Additive
LPO adults	−1.00502	−0.74099	(−1.092–−0.390)	Additive
PC	−0.83813	−0.30777	(−0.504–−0.112)	One-directional antagonism down
$I_{h\,G}$	−0.77222	0.167188	(−0.253–0.587)	Bidirectional antagonism up
$I_{h\,DT}$	0.550492	0.735764	(0.632–0.840)	One-directional synergism up
O_2^-	0.525968	0.521473	(0.445–0.598)	Additive
H_2O_2	0.112305	0.019767	(−0.193–0.233)	Additive
LPO sperm	−0.08337	−0.09313	(−0.242–0.055)	Additive
% MOT	−0.40977	−0.157	(−0.308–−0.006)	One-directional antagonism down
VCL	−0.49081	−0.46957	(−0.752–−0.187)	Additive
LIN	−1.51877	−1.06139	(−1.925–−0.198)	Additive
WOB	−0.03455	0.078448	(−0.115–0.272)	Additive

Table 3. Comparison of Independent Action (IA) model predictions for the combination of praseodymium (Pr) and a salinity of 40. IA predictions not overlapping with the 95% confidence intervals of the observed results denote interactive effects. Interaction type is classified based on the magnitude of combined effects and direction of individual responses.

Endpoint	Predicted	Observed	95% CI Observed	Interaction Type (Pr 40)
ETS	−0.33829	−0.19463	(−0.438–0.049)	Additive
PROT	−0.15784	−0.01133	(−0.086–0.064)	Bidirectional antagonism down
GLY	0.509975	0.253243	(0.054–0.453)	One-directional antagonism up
SOD	−1.96644	−2.04563	(−2.535–−1.556)	Additive
CAT	0.209357	0.548691	(0.483–0.614)	Bidirectional synergism up
GPx	−0.27923	0.114762	(−0.054–0.284)	Bidirectional synergism up
CbEs-*p*NPA	−0.19717	−0.43836	(−0.511–−0.366)	One-directional synergism down
CbEs-*p*NPB	−0.9087	−0.70487	(−0.817–−0.592)	One-directional antagonism down
GSTs	−0.802	−0.58439	(−0.767–−0.402)	Bidirectional antagonism down
GSH/GSSG	−0.86958	−0.19044	(−0.656–0.275)	One-directional antagonism down
LPO adults	−0.29403	1.031288	(0.861–1.201)	Bidirectional synergism up
PC	−0.0718	−0.20163	(−0.424–0.021)	Additive
$I_{h\,G}$	−0.18414	−0.06964	(−0.184–0.044)	Bidirectional antagonism up

Table 3. *Cont.*

Endpoint	Predicted	Observed	95% CI Observed	Interaction Type (Pr 40)
$I_{h\,DT}$	0.718506	1.022093	(0.702–1.343)	Additive
O_2^-	0.18894	−0.0328	(−0.116–0.051)	One-directional synergism up
H_2O_2	−0.01296	−0.08133	(−0.386–0.224)	Additive
LPO sperm	−0.13838	−0.13397	(−0.229–−0.039)	Additive
% MOT	−0.07212	−0.14695	(−0.439–0.145)	Additive
VCL	0.101054	0.137288	(−0.060–0.334)	Additive
LIN	−2.41146	−1.11216	(−2.273–−0.049)	One-directional antagonism down
WOB	−0.33343	−0.04048	(−0.301–0.220)	One-directional antagonism down

Table 4. Comparison of Independent Action (IA) model predictions for the combination of europium (Eu) and a salinity of 40. IA predictions not overlapping with the 95% confidence intervals of the observed results denote interactive effects. Interaction type is classified based on the magnitude of combined effects and direction of individual responses.

Endpoint	Predicted	Observed	95% CI Observed	Interaction Type (Eu 40)
ETS	−0.30122	−0.18343	(−0.390–0.023)	Additive
PROT	−0.05164	0.186069	(0.090–0.282)	Bidirectional synergism up
GLY	0.602949	0.459562	(0.364–0.555)	One-directional antagonism up
SOD	−3.25585	−1.02806	(−1.498–−0.558)	One-directional antagonism down
CAT	0.786073	0.701732	(0.523–0.881)	Additive
GPx	0.144731	0.279154	(0.073–0.485)	Additive
CbEs-*p*NPA	−0.36723	−0.07788	(−0.193–0.037)	One-directional antagonism down
CbEs-*p*NPB	−1.06027	−0.47392	(−0.673–0.275)	One-directional antagonism down
GSTs	−1.64939	−0.78145	(−1.373–−0.190)	One-directional antagonism down
GSH/GSSG	−0.7005	−0.98813	(−1.298–−0.678)	Additive
LPO adults	0.122501	0.890802	(0.586–−1.195)	Bidirectional synergism up
PC	−0.64843	−0.07429	(−0.304–0.156)	Bidirectional antagonism down
$I_{h\,G}$	0.064371	0.347344	(−0.104–0.799)	Additive
$I_{h\,DT}$	0.63817	0.774256	(0.601–0.947)	Additive
O_2^-	0.134634	0.117904	(−0.021–0.257)	Additive
H_2O_2	0.11376	−0.214	(−0.604–0.176)	Additive
LPO sperm	−0.1199	−0.12805	(−0.192–−0.064)	Additive
% MOT	−0.23437	−0.8684	(−1.169–−0.568)	One-directional synergism down
VCL	0.381371	0.259969	(−0.471–0.991)	Additive
LIN	−1.89135	−0.82537	(−1.732–0.081)	One-directional antagonism down
WOB	−0.30564	0.308756	(−0.035–0.653)	One-directional synergism up

To determine the similarities and distances between the treatments, Principal Coordinates (PCO) analysis was employed. This method also enables the visualisation of the relationships and patterns between treatments, and, in the case of this study, PCO separated the salinity of 40 from the salinity of 20 (Figure 1A). This division shows the influence of salinity on the observed responses. Based on this, the following sections will focus on evaluating the influence of both salinities in the effects of Pr and Eu.

3.1. The Influence of Lower Salinity on the Elements' Effects

3.1.1. Adults' Exposure

Praseodymium and Europium Concentration in Water and Mussel Tissue

The data regarding the concentrations of both elements in water after spiking can be found in Table 5, and the concentrations over one week, regarding the stability of the elements, are presented in Table 6. The data indicate that lower salinity may have distinct influences on reductions in Pr and Eu levels. At lower salinity, the Pr levels in water decreased by 25% after one week, which is lower than 31% at the control salinity. For Eu, at lower salinity, the loss was 8%, which is higher than the loss at the control salinity (3%).

These results show the differential sensitivity of these elements to changes in salinity, likely driven by their unique chemical properties.

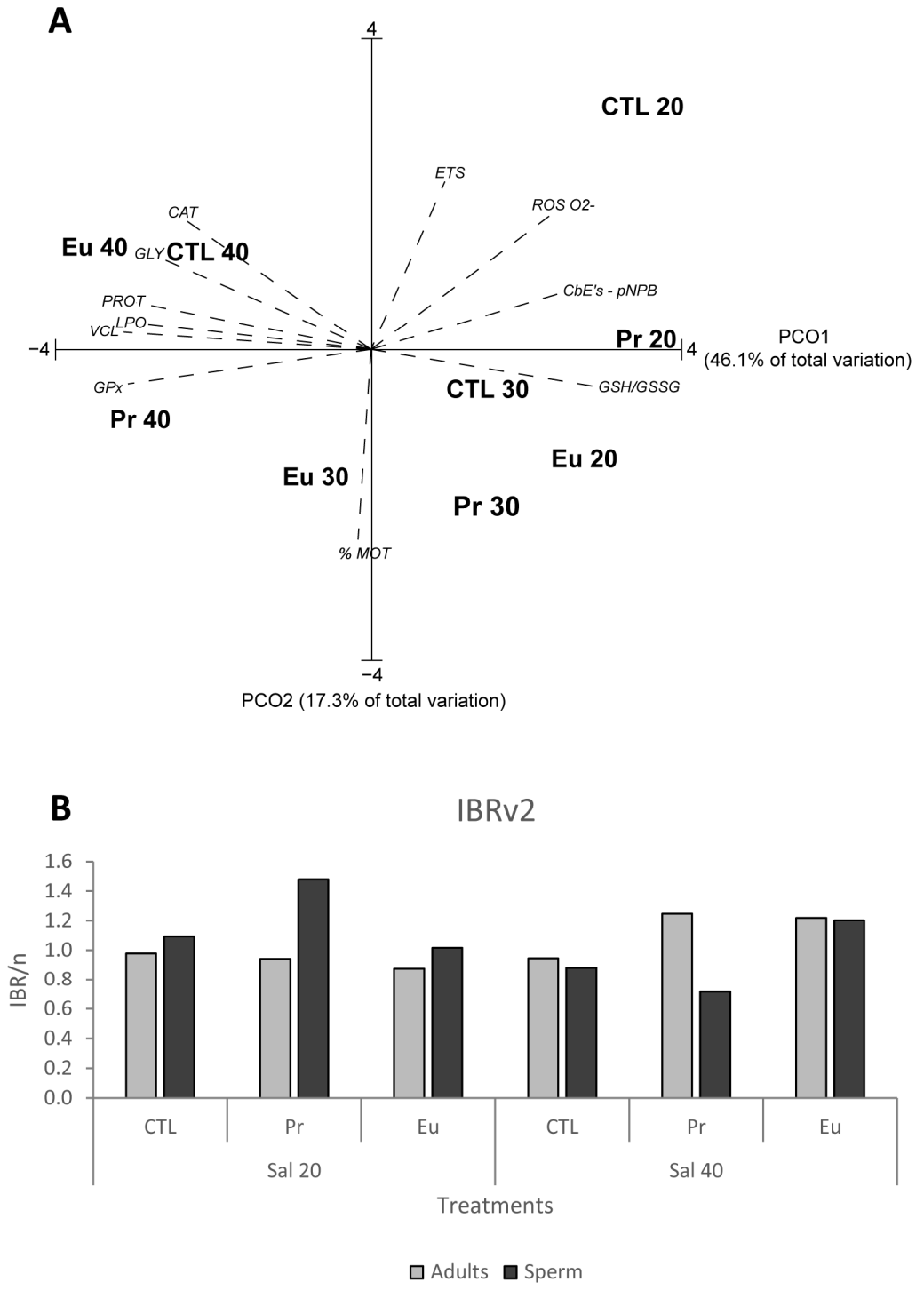

Figure 1. (**A**) Centroid ordination diagram (PCO) based on all biological responses measured in adults and sperm of *Mytilus galloprovincialis* exposed to control (CTL), praseodymium (Pr), and europium (Eu) at salinities of 20, 30, and 40. Spearman correlation vectors were superimposed as supplementary variables ($r > 0.7$): ETS, PROT, GLY, CAT, GPx, CbEs-pNPB, GSH/GSSG, LPO (adults), O_2^-, % MOT, and VCL; (**B**) Integrated Biological Response (IBRv2) score divided by the number of parameters measured in adults and sperm of *Mytilus galloprovincialis* exposed to control (CTL), praseodymium (Pr), and europium (Eu) at salinities of 20 and 40.

Table 5. Praseodymium (Pr) and europium (Eu) concentrations in water samples (µg/L) collected after spiking from exposure aquaria as well as in mussel whole soft tissue (µg/g dry weight (DW)) and BCF (L/Kg) after 28 days of exposure to CTL, Pr, and Eu at salinities of 20, 30, and 40. Results are presented as the mean ± standard deviation. Significant differences ($p < 0.05$) among salinities are denoted by different letters (bold, italic lowercase letters indicate CTL treatments; uppercase letters indicate Pr treatments; and lowercase letters indicate Eu treatments).

		Water Samples (µg/L)		**Tissue Samples (µg/g DW)**		**BCF (L/Kg)**	
		Pr	**Eu**	**Pr**	**Eu**	**Pr**	**Eu**
Sal 20	CTL	<0.01	<0.01	0.003 ± 0.001 ***a***	<0.03 ***a***	-	-
	Pr	12 ± 0.5	-	0.6 ± 0.1 ^{A}	-	49	-
	Eu	-	13 ± 0.4	-	0.2 ± 0.06 ^{a}	-	18
Sal 30	CTL	<0.01	<0.01	0.008 ± 0.004 ***ab***	<0.03 ***a***	-	-
	Pr	13 ± 0.8	-	0.3 ± 0.04 ^{B}	-	25	-
	Eu	-	14 ± 0.5	-	0.2 ± 0.02 ^{a}	-	15
Sal 40	CTL	<0.01	<0.01	0.007 ± 0.001 ***b***	<0.03 ***a***	-	-
	Pr	13 ± 0.5	-	0.2 ± 0.09 ^{B}	-	19	-
	Eu	-	14 ± 0.7	-	0.2 ± 0.07 ^{a}	-	14

Table 6. Praseodymium (Pr) and europium (Eu) concentrations (µg/L) in seawater samples collected from blanks in the first week (0, 72, 120, and 168 h after spiking) at three different salinities. Results are the mean ± standard deviation.

		Water Sample Concentrations (µg/L)			
		0 h	**72 h**	**120 h**	**168 h**
Sal 20	Pr	13 ± 0.09	11 ± 0.2	11 ± 0.04	9.4 ± 0.07
	Eu	13 ± 0.4	13 ± 0.6	12 ± 0.4	12 ± 0.9
Sal 30	Pr	13 ± 0.03	11 ± 0.3	11 ± 0.4	9.3 ± 0.3
	Eu	14 ± 0.6	12 ± 0.4	11 ± 0.07	13 ± 1.6
Sal 40	Pr	13 ± 0.3	11 ± 0.4	9.1 ± 0.3	9.9 ± 0.7
	Eu	14 ± 0.3	12 ± 0.1	11 ± 0.2	10 ± 0.3

The bioconcentration factor (BCF) showed that the accumulation of both elements by mussels was higher at a salinity of 20, despite the fact that the concentration of Eu in mussel tissue did not significantly differ from that at the other salinities (Table 5). This could be due to a reduced concentration of common ions and anions, which decreases competition for absorption and limits the formation of complexes, while increasing the bioavailability of the elements. In addition, the accumulation of Pr at a salinity of 20 was higher than that of Eu at the same salinity (Table 5). This could have occurred because, overall, Eu has a smaller ionic radius and a higher charge density than Pr due to the lanthanide contraction. Because of this, Eu can form stronger bonds, which may reduce its solubility and lead to precipitation or the formation of less soluble complexes [16]. Other rare earth elements (REEs), namely, lanthanum (La) and gadolinium (Gd), also exhibited an increased accumulation in mussels with a decrease in salinity [40,44]. In line with our findings, these studies reported that Gd, which has a smaller ionic radius and a higher charge density than La, also showed lower accumulation levels than La, highlighting the influence of ionic size and charge on metal bioavailability and uptake.

Biochemical Analyses

To assess the energy balance of the mussels, their metabolic capacity was measured through electron transport system (ETS) activity, while energy reserves were determined by analysing glycogen (GLY) and protein (PROT) contents [57–59]. The ETS activity displayed a positive correlation with CTL 20 in the PCO graph (Figure 1A), and indeed the results

indicated that low salinity alone induced a slight metabolic increase compared to the CTL 30 (Figure 2A). This increase in metabolism may be linked to an enhanced filtration rate, as salinity is an important abiotic factor influencing the filtration rate in bivalves [35]. For instance, Guzmán-Agüero et al. [33] observed that reduced salinity led to an increase in the filtration rate in the bivalve species *Crassostrea corteziensis*. The rise in metabolism could also suggest that mussels might be using the additional energy to boost their defence mechanisms. In addition, Pr seemed to consistently suppress metabolism, which was observed at the control and lower salinity (Table 7). Such a response can indicate that Pr plays a dominant role in terms of metabolic capacity, as predicted by the IA model. In the case of Eu, although no significant changes were observed in the mussels' metabolism at the control salinity, exposure to lower salinity resulted in metabolic depression (Table 7). This suppression of metabolic activity in the mussels exposed to Pr and Eu at lower salinity may suggest a potential behavioural response, such as the reduction in filtration rate caused by prolonged valve closure. This behaviour was already documented by Gosling [60] and Ortmann and Grieshaber [61] when bivalves were placed under stressful conditions. It is important to note that the slight metabolic increase observed in the mussels exposed to low salinity alone was not observed in those exposed to the elements at low salinity. This might suggest that the presence of these elements interfered with the mussels' ability to adapt to low-salinity stress. Accompanying the higher metabolic capacity of the mussels exposed to low salinity alone, lower PROT content was observed compared to CTL 30 (Figure 2B), indicating that the organisms were probably using their protein reserves to enhance their defence mechanisms under osmotic stress. In contrast, despite the metabolic suppression observed in the mussels exposed to Pr 20 and Eu 20, both groups showed a significant use of GLY content (Figure 2C and Table 7). This explains the negative correlation between these treatments and GLY in the PCO graph (Figure 1A). The organisms were likely using GLY to fuel up their defence mechanisms. The utilisation of GLY in these treatments points to a synergetic response (Tables 1 and 2), suggesting that the mussels were under significant stress and that the closure of the valves was not enough. As a result, the mussels needed additional energy to enhance the activity of their defence mechanisms. Similarly, Andrade et al. [40] showed that non-contaminated mussels at a salinity of 20 had increased metabolism and decreased PROT content compared to non-contaminated mussels at a salinity of 30. Andrade et al. [41] further demonstrated that mussels exposed to yttrium (Y) at a salinity of 20 maintained their metabolic capacity similar to those Y-exposed at a salinity of 30.

To prevent cellular damage, organisms possess defence mechanisms, which include antioxidant and biotransformation enzymes. These two types of enzymes serve distinct functions; while antioxidant enzymes help neutralize the excess of reactive oxygen species (ROS) to prevent oxidative stress, biotransformation enzymes facilitate the detoxification and excretion of pollutants from cells [62]. The data obtained demonstrated that at lower salinity, only the Eu-exposed mussels activated their antioxidant enzymes, specifically superoxide dismutase (SOD), when compared to the Eu-exposed mussels at control salinity (Figure 2D). Regarding biotransformation enzymes, carboxylesterases with *p*-nitrophenyl butyrate (CbEs-*p*NPB) exhibited a positive correlation with Pr 20 (Figure 1A) since this treatment induced a significant increase in that enzyme compared to the Pr-exposed mussels at control salinity (Figure 2H). In addition, Eu 20 induced greater glutathione S-transferases (GSTs) activity compared to that for the Eu-exposed mussels at a salinity of 30 (Figure 2I). These enzymatic activations could explain the increase in GLY consumption observed in these treatments. The activation of the mentioned antioxidant and biotransformation defences at lower salinity was enough to prevent cellular damage, as demonstrated by the lack of lipid peroxidation (LPO) and protein carbonylation (PC) (Figure 2K,L and Table 7). This explains why, in the PCO graph, LPO is positioned opposite to Pr 20 and Eu 20 (Figure 1A). In terms of redox balance assessed using the ratio of reduced to oxidized glutathione (GSH/GSSG) [62], the PCO analysis showed that this parameter has a positive correlation with Pr 20 and Eu 20 (Figure 1A), which aligns with the higher GSH/GSSG

values observed in mussels exposed to both treatments (Figure 2J). This suggests that these mussels were able to maintain redox homeostasis. The increase in GSH/GSSG showed that GSH content was being accumulated and not converted in GSSG, which can be related to the decrease in GPx and GSTs activities (Figure 2F,I) since these two enzymes are used for the conversion of GSH into GSSG.

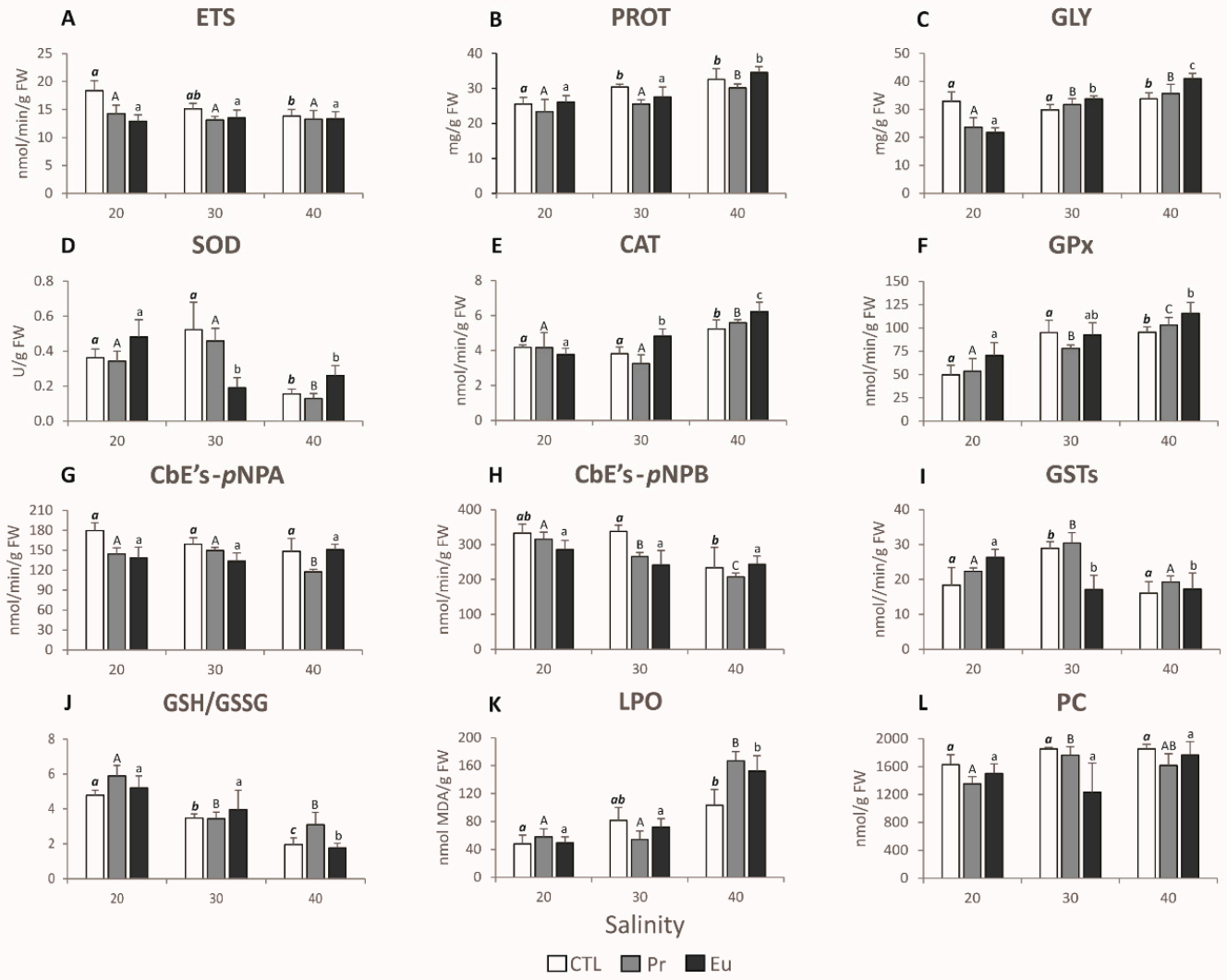

Figure 2. (**A**) Electron transport system (ETS) activity, expressed in nmol per min per g of fresh weight (FW); (**B**) protein (PROT) content, expressed in mg per g of FW; (**C**) glycogen (GLY) content, expressed in mg per g of FW; (**D**) superoxide dismutase (SOD) activity, expressed in U per g of FW, where U is a reduction of 50% in nitroblue tetrazolium (NBT) levels; (**E**) catalase (CAT) activity, expressed in nmol of formaldehyde per min per g of FW; (**F**) glutathione peroxidase (GPx) activity, expressed in nmol per min per g of FW; (**G**) carboxylesterase with *p*-nitrophenyl acetate (CbE-*p*NPA) activity, expressed in nmol per min per g of FW; (**H**) carboxylesterases with *p*-nitrophenyl butyrate (CbEs-*p*NPB), expressed in nmol per min per g of FW; (**I**) glutathione S-transferases (GSTs) activity, expressed in nmol per min per g of FW; (**J**) reduced-to-oxidized glutathione (GSH/GSSG) ratio; (**K**) lipid peroxidation (LPO) levels, expressed in nmol of malondialdehyde (MDA) per g of FW; (**L**) protein carbonylation (PC) levels, expressed in nmol per g of FW, in *Mytilus galloprovincialis* exposed to control (CTL), praseodymium (Pr), and europium (Eu) at salinities of 20, 30, and 40 for 28 days. Results are means with standard deviations. Significant differences ($p < 0.05$) among salinities are denoted by different letters (bold italic lowercase letters stand for CTL treatments, uppercase letters stand for Pr treatments, and lowercase letters stand for Eu treatments).

Table 7. Comparison among CTL, Pr, and Eu at each salinity along with the *p*-values. For each parameter/histopathological index (I_h), significant differences ($p < 0.05$) between treatments are denoted by the *p*-values in bold.

Parameter/I_h	Salinity 20			Salinity 30			Salinity 40		
	CTL vs. Pr	CTL vs. Eu	Pr vs. Eu	CTL vs. Pr	CTL vs. Eu	Pr vs. Eu	CTL vs. Pr	CTL vs. Eu	Pr vs. Eu
[Pr] tissue	**0.0004**	-	-	**0.0002**	-	-	**0.0079**	-	-
[Eu] tissue	-	**0.0025**	-	-	**0.0001**	-	-	**0.0114**	-
ETS	**0.040**	**0.013**	0.29	**0.045**	0.18	0.69	0.66	0.68	0.95
GLY	**0.025**	**0.0068**	0.43	0.31	**0.033**	0.21	0.14	0.55	0.074
PROT	0.40	0.72	0.30	**0.0057**	0.17	0.32	0.28	0.37	**0.017**
SOD	0.68	0.14	0.11	0.55	**0.030**	**0.0080**	0.32	0.46	**0.023**
CAT	0.99	0.14	0.50	0.20	**0.037**	**0.015**	0.33	0.088	0.13
GPx	0.71	0.11	0.21	0.10	0.53	0.14	0.25	0.053	0.20
CbEs-*p*NPA	**0.014**	**0.026**	0.62	0.20	0.051	0.11	0.053	0.85	**0.0047**
CbEs-*p*NPB	0.42	0.095	0.20	**0.0047**	**0.023**	0.39	0.47	0.80	0.068
GSTs	0.25	0.077	0.56	0.51	**0.011**	**0.010**	0.20	0.73	0.50
GSH/GGSG	**0.049**	0.38	0.26	0.90	0.50	0.50	0.067	0.52	**0.034**
LPO adults	0.38	0.87	0.38	0.10	0.50	0.15	**0.015**	0.053	0.38
PC	0.055	0.32	0.22	0.29	0.062	0.11	0.083	0.49	0.37
I_h Gills	**0.024**	**0.022**	0.74	0.75	0.25	0.28	**0.016**	**0.047**	0.11
I_h Digestive tubules	0.30	0.059	0.25	**0.024**	**0.025**	0.56	**0.0079**	**0.0045**	0.19
O_2^-	**0.046**	0.36	0.14	0.42	0.45	**0.043**	0.056	0.62	0.091
H_2O_2	*	*	*	*	*	*	*	*	*
LPO sperm	0.58	0.87	0.93	0.23	0.86	0.43	0.69	0.70	0.92
% MOT	0.85	0.16	0.44	0.44	0.36	0.16	0.96	**0.0057**	**0.014**
VCL	**0.016**	0.55	**0.018**	0.68	0.70	0.51	0.29	0.97	0.59
LIN	*	*	*	*	*	*	*	*	*
WOB	0.16	0.97	0.16	0.24	0.61	0.80	0.26	**0.036**	0.11

* Main test > 0.05.

Histopathological Analyses

The gills and digestive gland are critical organs for assessing the health statuses of mussels when exposed to stressors. The gills serve as the initial interface with the surrounding water, filtrating the water before it reaches other internal organs [63,64]. On the other hand, the digestive gland plays a central role in the biotransformation of xenobiotics, functioning as the primary site for detoxification and metabolic processing [65]. This makes both organs highly sensitive indicators of environmental changes and contaminant exposure. The data regarding the histopathological alterations showed that the index (I_h) in the gills of mussels exposed to Pr and Eu at lower salinity was similar to that for those exposed to Pr 30 and Eu 30 (Figure 3A). However, in the presence of these contaminants at a salinity of 20, the I_h was significantly higher compared to that for CTL 20 (Table 7), with higher haemocyte infiltration, as well as an increased number of enlarged vessels (Figure 4A). This shows that the contaminants impacted gills, and it can explain why mussels likely close their valves. The haemocyte infiltration and enlarged vessels can be linked with inflammatory processes [66–68]. Concerning the digestive tubules, Pr 20 and Eu 20 showed similar I_h to Pr 30 and Eu 30 (Figure 3B), with the latter displaying significantly higher I_h than CTL 30 (Table 7), characterized by an increase in the number of atrophied tubules and the appearance of necrosis (Figure 4B). This type of injury is associated with inflammatory processes [69] and may contribute to physiological impairments, such as inefficient nutrient absorption [70]. This suggests that these elements induced consistent histopathological injuries, regardless of the salinity level. Furthermore, the absence of significant differences between CTL 20 and CTL 30, combined with the similar I_h values between Pr 20 and Eu 20 to their respective salinity 30 counterparts (Figure 3A,B), indicates that the observed effects are primarily due to the elements rather than salinity stress. Also, Coppola et al. [71] showed that mussels exposed for 28 days to 50 µg/L of mercury (Hg) at a salinity of 20 presented significantly higher I_h in their gills compared to those exposed to CTL at a salinity of 20.

3.1.2. Sperm Exposure

The sperm under low-salinity conditions showed a significant increase in the production of superoxide anion (O_2^-) compared to the sperm at the control salinity (Figure 5A).

This can indicate that salinity played a more significant role than the elements in inducing ROS production. In addition, Pr 20 induced the highest amount of O_2^- production among the treatments at the same salinity (Figure 5A and Table 7). This elevated O_2^- production at lower salinity can indicate that the sperm were under osmotic stress. However, despite this, no increase in H2O2 production was observed, nor was there any LPO (Figure 5B,C and Table 7), which can suggest that the defence mechanisms were activated and sufficient to prevent cell damage. Regarding the motility of the sperm, lower salinity by itself seemed to be prejudicial to the motility of the sperm, as there was a decrease in the percentage of motility at CTL 20 compared to the sperm at CTL 30 (Figure 5D). However, the combination of lower salinity and Pr or Eu did not induce significant differences compared to their counterparts at control salinity (Figure 5D). This may suggest that these elements have a neutralizing effect on the stress response, preventing further motility decline compared to CTL 20. On the other hand, the velocity of the sperm exposed to the treatments at lower salinity was significantly lower than that for the sperm at control salinity (Figure 5E), which explains the opposite position of the velocity from Pr 20 and Eu 20 in the PCO (Figure 1A). Furthermore, the lowest velocity was observed for the Pr-exposed sperm (Figure 5E and Table 7). This behaviour is likely due to the increase in O_2^- production observed in that treatment, since it may affect mitochondrial function and, subsequently, sperm function [72]. Furthermore, despite there being no significant differences (Figure 5F), it seemed that linearity (LIN) decreased in sperm exposed to the treatments at lower salinity compared to that for the sperm at CTL30 (Figure 5F). In addition, a more pronounced irregular movement (WOB) was observed in sperm exposed to Pr 20 (with no significant difference) than in the sperm exposed to CTL and Pr 30 (Figure 5G). Trifuoggi et al. [25] demonstrated that when sperm of two sea urchin species (*Paracentrotus lividus* and *Sphaerechinus granularis*) were exposed to 10^{-4} M and 10^{-5} M of Eu, the offspring of the sperm exposed to 10^{-5} M did not present developmental defects. In contrast, the offspring from the sperm exposed to 10^{-4} M were severely affected, with significant developmental defects. Furthermore, Cuccaro et al. [73] observed that the sperm of *Ficopomatus enigmaticus* exposed to cadmium (Cd), arsenic (As), and zinc (Zn) at a salinity of 20 did not exhibit higher LPO levels than the sperm exposed at a salinity of 30.

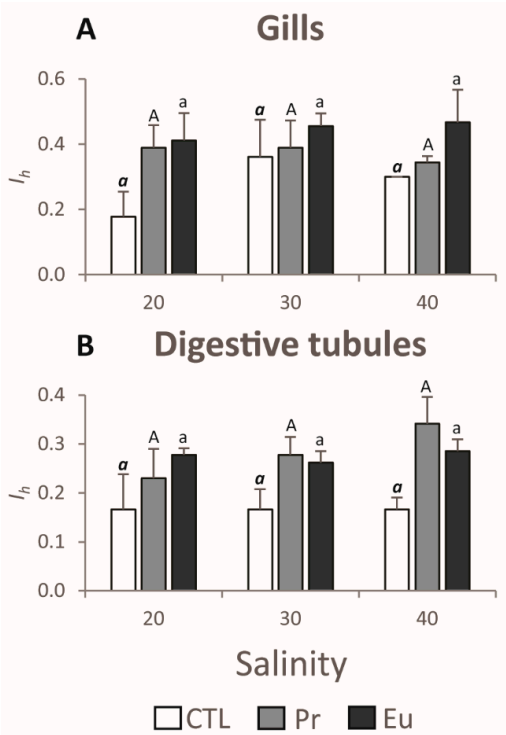

Figure 3. Histopathological index (Ih) in (**A**) gills; (**B**) digestive tubules of *Mytilus galloprovincialis* exposed to control (CTL), praseodymium (Pr), and europium (Eu) at salinities of 20, 30, and 40 for

28 days. Results are means with standard deviations. Significant differences ($p < 0.05$) among salinities are denoted by different letters (bold italic lowercase letters stand for CTL treatments, uppercase letters stand for Pr treatments, and lowercase letters stand for Eu treatments).

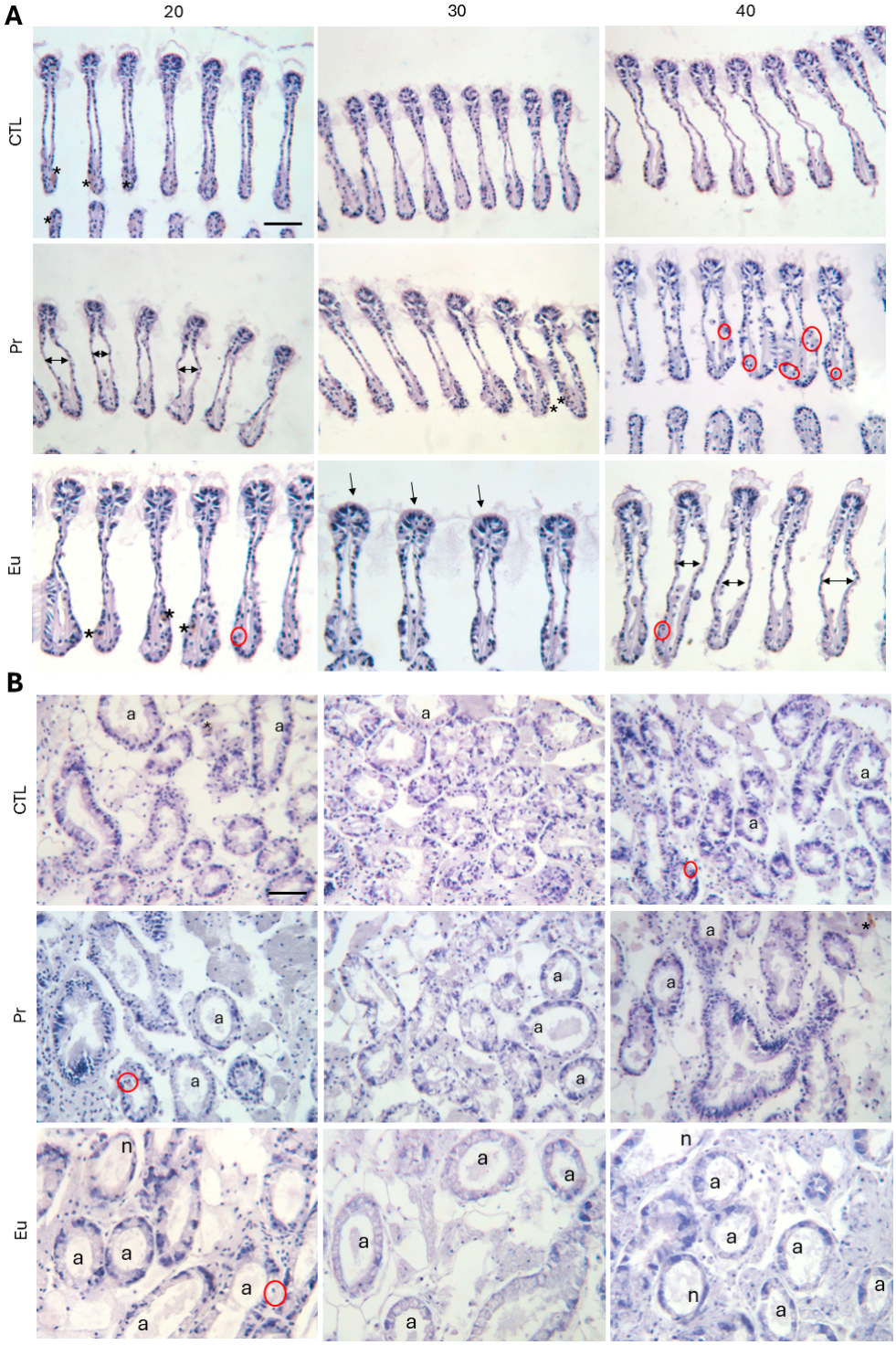

Figure 4. Representative micrographs of the histopathological alterations observed in (**A**) gills and (**B**) digestive tubules of *Mytilus galloprovincialis* exposed to control (CTL), praseodymium (Pr), and europium (Eu) at salinities of 20, 30, and 40 for 28 days and stained with haematoxylin. Alterations: lipofuscin aggregates (*); enlargement of the central vessel (double-headed arrow); haemocyte infiltration (red circle); loss of cilia (single arrow) atrophy (a); necrosis (n). Scale bar: 50 μm.

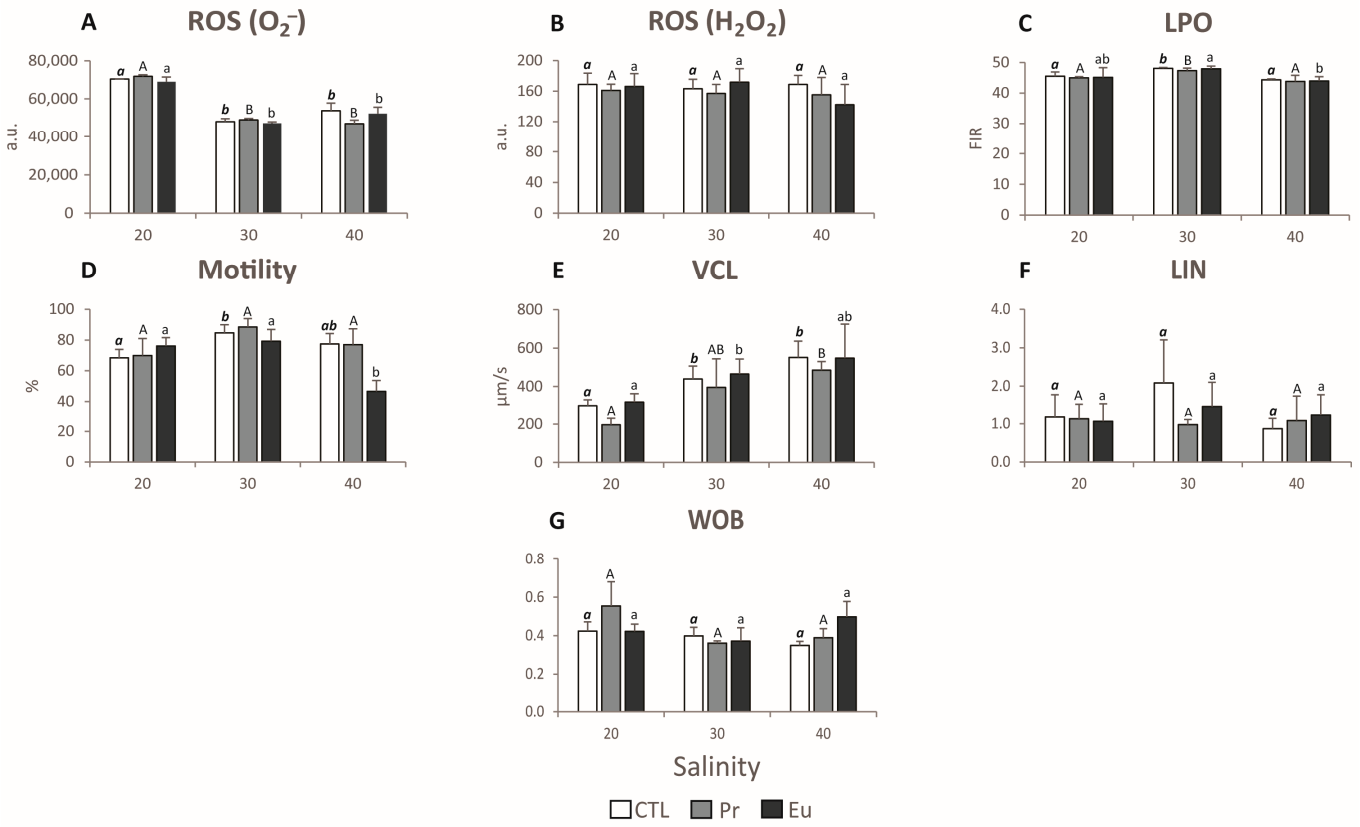

Figure 5. (**A**) Superoxide-anion-derived reactive oxygen species (ROS (O_2^-)) production, expressed in arbitrary units of fluorescence intensity (a.u.); (**B**) hydrogen-peroxide-derived reactive oxygen species (ROS (H_2O_2)) production, expressed in a.u.; (**C**) lipid peroxidation (LPO) levels, expressed as the fluorescence intensity ratio (FIR); (**D**) motility, expressed as percentage (%) of motility; (**E**) curvilinear velocity (VLC), expressed in µm per s; (**F**) linearity (LIN); and (**G**) wobble (WOB) in sperm of the species *Mytilus galloprovincialis* exposed to control (CTL), praseodymium (Pr), and europium (Eu) at salinities of 20, 30, and 40 for 30 min. Results are means with standard deviations. Significant differences ($p < 0.05$) among salinities are denoted by different letters (bold italic lowercase letters stand for CTL treatments, uppercase letters stand for Pr treatments, and lowercase letters stand for Eu treatments).

3.2. The Influence of Higher Salinity on the Elements' Effects

3.2.1. Adult Exposure

Praseodymium and Europium Concentrations in Mussel Tissue

Higher salinity had contrasting effects on Pr and Eu when compared to the control salinity. While Pr loss decreased slightly at a salinity of 40 (amounting to 25% at a salinity of 40 and 31% at a salinity of 30), Eu loss increased dramatically (28% at a salinity of 40 and 3% at a salinity of 30). These findings emphasise the differential behaviour of these elements in saline environments, driven by their distinct chemical properties, such as solubility and interactions with other ions in the system.

The accumulation of Pr at higher salinity was lower than the accumulation of Pr in mussels exposed to control salinity, while the accumulation of Eu remained similar (Table 5). This is likely because Pr has a higher ionic radius and may experience more ion competition under high-salinity conditions. On the other hand, Eu may form stronger complexes and have more stable bioavailability, explaining the more consistent accumulation across salinities. Despite this, the concentrations of the elements in the mussels' tissues were more similar at a salinity of 40 compared to a salinity of 30 (Table 5). Similarly, Freitas et al. [74] observed that the concentrations of lead (Pb) in mussels' tissues were similar at the higher salinity (35) and control salinity (30).

Biochemical Analyses

Unlike the mussels at CTL 20, those at CTL 40 slightly decreased their metabolic capacity (Figure 2A), suggesting that they were attempting to reduce filtration by closing their valves to minimize stress. On the other hand, the mussels exposed to Pr and Eu at higher salinity did not significantly change their metabolic capacity compared to those exposed to Pr and Eu at control salinity (Figure 2A). This suggests that these elements could have neutralized the need to close the valves imposed by the higher salinity. Regarding the energy reserves, along with the limited changes in their metabolic capacity, the mussels kept at higher salinity increased their PROT and GLY content compared to those at control salinity (Figure 2B,C), revealing that the mussels were able to avoid energy reserve expenditure under this condition. This explains the association in the PCO graph between the energy reserves and the treatments at a salinity of 40 (Figure 1A). Similarly, Freitas et al. [31] observed that when exposed to a higher salinity (35), this species reduced its metabolism and increased GLY and PROT content compared to those under the control salinity (28). De Marchi et al. [43] also noted a trend of reduced metabolism in mussels at a salinity of 37 compared to those at 28. However, the author also found no changes in the metabolism between mussels exposed to carbon nanotubes at a higher salinity than those also exposed but at the control salinity.

Concerning antioxidant enzymes, the mussels exposed to the highest salinity had higher CAT activity than their counterparts at a salinity of 30 (Figure 2E), which justifies the strong correlation observed in the PCO analysis between this parameter and CTL 40 and Eu 40 (Figure 1A). Mussels exposed to Pr 40 also activated GPx (Figure 2F) to eliminate the excess of ROS, explaining the association observed in the PCO graph between the treatment and this parameter (Figure 1A). Regarding the biotransformation enzymes, the mussels did not activate these defences when they were kept under high salinity (Figure 2G–I and Table 7). It seems that Pr 40 induced the inhibition of these enzymes since the activity decreased compared to that at a salinity of 30 (Figure 2G–I). Nevertheless, the activation of antioxidant enzymes was enough to avoid PC (Figure 2L) but not sufficient to prevent LPO (Figure 2K), justifying the positive association between the treatments at a salinity of 40 and LPO (Figure 1A). Similarly, a study conducted by Andrade et al. [44] noted that mussels exposed to Gd at a salinity of 40 presented significantly more LPO than those exposed to Gd at a salinity of 30. The present study, further demonstrates that the mussels subjected to high salinity were under redox imbalance (Figure 2J). The results revealed that in the PCO graph, GSH/GSSG was in the opposite position from CTL 40 and Eu 40 (Figure 1A), and this is because mussels under these treatments presented the lowest values of GSH/GSSG (Figure 2J). This indicates that these mussels were using more GSH to neutralize ROS and convert GSH to GSSG, likely using GPx activity since the activity of this enzyme increased at this salinity (Figure 2F).

Histopathological Analyses

The histopathological data indicated that salinity did not have much influence on the alterations observed in gills and digestive tubules. The I_h in gills and digestive tubules showed no significant differences between the mussels at control salinity and those kept under higher salinity (Figure 3A,B). On the other hand, at a salinity of 40, the mussels exposed to Pr and Eu presented a significantly higher I_h compared to those exposed to CTL (Table 7). In the case of the gills, the mussels exposed to Pr 40 showed higher haemocyte infiltration, while those exposed to Eu presented an increase in lipofuscin aggregates and enlarged central vessels (Figure 4A). In terms of digestive tubules, the Pr-exposed mussels presented more lipofuscin aggregates and an increased number of atrophied tubules, while the Eu-exposed mussels only presented more necrotic tubules (Figure 4B). Like the mussels kept under low salinity, those under high salinity were also under stress since the inflammatory system was likely activated due to haemocyte infiltration in the gills and atrophied digestive tubules. Additionally, lipofuscin aggregates showed that under this salinity, cellular damage was present both in the gills and digestive tubules [75]. Similarly,

Coppola et al. [71] observed that after 28 days of exposure to Hg (50 µg/L), mussels of *M. galloprovincialis* kept at a salinity of 40 presented significantly higher I_h in their gills and digestive tubules compared to those at CTL 40. Also, Pagano et al. (2016b) observed histological alterations in the gills and digestive system of *M. galloprovincialis* when exposed to quaternium-15 under high salinity (37) in comparison to non-contaminated mussels at the same salinity.

3.2.2. Sperm Exposure

In the case of the sperm, it seemed that they were not under oxidative stress when exposed to higher salinity, as there was no increase in ROS production compared to the sperm kept under the control salinity, nor was any LPO observed (Figure 5A–C and Table 7). This could have happened because the ROS were being neutralized by the defence mechanisms or because these treatments did not induce sufficient stress to induce oxidative stress. In terms of motility, compared to the sperm at control salinity, the percentage of motile sperm was slightly lower in the non-contaminated sperm at higher salinity and significantly lower in the Eu-exposed sperm (Figure 5D). In addition, at higher salinitya salinity of 40, the Eu-exposed sperm presented a significantly lower percentage than the CTL and Pr-exposed ones at the same salinity (Table 7). This might suggest that Eu may exacerbate the effects of high salinity, as this combination is detrimental to the motility of sperm. On the other hand, the velocity of the sperm at a salinity of 40 was not reduced when compared to that for the sperm kept at a salinity of 30 (Figure 5E). This may suggest that the sperm could be consuming more oxygen to maintain their velocity, as suggested by Rahi et al. [76]. This could compensate for the loss of sperm motility and thus help ensure fertilisation success. Similar to the observations at lower salinity, although no significant differences were observed (Figure 5F), the LIN appeared to decrease in sperm at higher salinity compared to that for non-contaminated sperm at control salinity (Figure 5F), potentially impairing fertilisation. Additionally, Eu 40 induced significantly more irregular sperm movement compared to that for the sperm at CTL 20 (Table 7), which can also impair fertilisation. Pagano et al. [77] found that in the sperm of *P. lividus*, 10^{-5} M of Eu did not induce any change in the success of fertilisation and the percentage of developmental defects in the offspring. On the other hand, 10^{-4} M of Eu caused a reduction in fertilisation success and an increase in the percentage of developmental defects. Cuccaro et al. [73] observed that the exposure of *F. enigmaticus* sperm to Cd and copper at a salinity of 40 did not induce any change in the production of ROS nor cause an increase in LPO levels in comparison to sperm kept at a salinity of 30.

3.3. Salinity of 20 vs. Salinity of 40

To compare the overall impacts of each treatment at salinities of 20 and 40 and identify the worst treatments for both adults and sperm, the Integrated Biological Index (IBR) was employed. This index is considered one of the most commonly used among similar indices developed in recent years, as noted by Catteau et al. [78]. Its wide applicability is demonstrated by its use by several authors, including Khan et al. [79] and Andrade et al. [41].

According to the IBR index, both elements combined with a salinity of 40 constituted the treatments that induced the most alterations in adult mussels (Figure 1B). Mussels exposed to these treatments exhibited inhibited SOD activity and increased CAT and GPx activities. Additionally, these mussels were under oxidative stress indicated by redox imbalance and higher LPO levels. For sperm, specific treatments also induced higher alterations. Pr 20 and Eu 40 induced the potential increase in the irregular movement of sperm. In addition, Eu 40 led to a reduction in motile sperm, while the sperm exposed to Pr 20 exhibited the lowest velocity and higher production of O_2^-. These alterations yielded the highest IBR scores for Pr 20 and Eu 40 in sperm, identifying them as the treatments most detrimental to sperm function in mussels (Figure 1B). Furthermore, comparing the IBR scores for adults and sperm provided insights into differential sensitivity. At lower salinity, the IBR scores for adults and sperm exposed to CTL and Eu were similar (Figure 1B),

suggesting comparable sensitivity to these treatments. However, Pr at lower salinity seemed to induce higher alterations in sperm than in adults (Figure 1B), which could indicate a higher sensitivity of sperm to this treatment. Similar to the results for lower salinity, adults and sperm at higher salinity showed similar IBR scores when exposed to the CTL and Eu treatments (Figure 1B). On the other hand, contrary to what was observed at lower salinity, adult mussels exposed to Pr at higher salinity showed higher responsiveness than sperm, with a higher IBR score (Figure 1B). These findings highlight the complex interactions between environmental stressors like salinity and exposure to REEs, with salinity modulating the biological impacts of REEs on different life stages in mussels. The different sensitivities of adults and sperm to the tested stressors suggests that environments contaminated with REEs and subjected to fluctuating salinity could induce distinct ecological impacts on population dynamics and reproductive health.

These findings provide essential insights into how REEs and salinity shifts can impact aquatic ecosystems. These biochemical and histopathological alterations observed in mussels can impair cellular and physiological functions, energy allocation, and homeostasis, affecting their health, growth, and reproductive capacities. The observed effects on sperm further emphasise potential reductions in reproductive success, which could lead to a decline in mussel populations. A diminished mussel population could disrupt mussels' ecological roles, such as maintaining trophic balance and supporting biodiversity. Additionally, it could reduce the critical ecosystem services provided by mussels, including water filtration and nutrient cycling, ultimately affecting the health and stability of the aquatic environment.

4. Conclusions

The present study demonstrated that shifts in salinity could modulate the effects of both Pr and Eu in different life stages of *Mytilus galloprovincialis*. High salinity combined with both elements induced the most alterations in adult mussels, including changes in defence mechanisms, causing redox imbalance and cellular damage. On the other hand, sperm showed particular sensitivity to specific REE–salinity combinations, with the most changes in motility and velocity observed when exposed to Pr at low salinity and Eu at higher salinity. Interestingly, while adults and sperm exhibited similar responses to Eu across salinities, Pr exposure revealed distinct vulnerabilities, with sperm being more affected at low salinity and adults being more affected at high salinity. These findings highlight the ecological risks posed by REE pollution, particularly under varying environmental salinities, which could influence mussel reproductive success and population dynamics. Such changes may impact ecosystems, affecting biodiversity and ecosystem services, including water filtration and nutrient cycling. This study emphasises the need for further research, incorporating additional REEs, species, and environmental stressors like temperature fluctuations or pH variations. Developing predictive models for REE toxicity under dynamic environmental scenarios is crucial for better risk assessment and mitigation strategies in coastal ecosystems prone to REE contamination. However, caution must be exercised when utilizing such models due to the complexity of REE-salinity interactions. This study highlights the need to validate models with observed data since half of the parameters were not additive for most treatments, and for one treatment in particular, neither half was additive. Additionally, this research provides some data that can help to predict potential ecological impacts induced by REEs–salinity interactions, helping to guide regulations aimed at protecting aquatic ecosystems and ensuring the sustainability of services provided by bivalves like mussels.

Author Contributions: Conceptualisation, C.P., E.P. and R.F.; formal analysis, C.L.; funding acquisition, A.M.V.M.S., C.P., E.P. and R.F.; investigation, C.L., T.R. and G.P.; methodology, C.L.; resources, C.P., E.P. and R.F.; supervision, C.P., E.P. and R.F.; writing—original draft, C.L.; writing—review and editing, C.P., E.P. and R.F. All authors have read and agreed to the published version of the manuscript.

Funding: Thanks are due for financial support provided via REQUIMTE (UIDB/50006/2020) and CESAM (UIDP/50017/2020 + UIDB/50017/2020 + LA/P/0094/2020). Carla Leite acknowledges her Ph.D. grant (2020.05296. BD) from the National Funds through the Portuguese Science Foundation (Fundação para a Ciência e a Tecnologia; FCT).

Institutional Review Board Statement: Not applicable.

Informed Consent Statement: Not applicable.

Data Availability Statement: The data presented in this study are available on request from the corresponding author. (as authors wish to be informed of their use).

Conflicts of Interest: The authors declare no conflicts of interest.

References

1. Arienzo, M.; Ferrara, L.; Trifuoggi, M.; Toscanesi, M. Advances in the Fate of Rare Earth Elements, REE, in Transitional Environments: Coasts and Estuaries. *Water* **2022**, *14*, 401. [CrossRef]
2. Sneller, F.E.C.; Kalf, D.F.; Weltje, L.; Van Wezel, A.P. *Maximum Permissible Concentrations and Negligible Concentrations for Rare Earth Elements (REEs)*; RIVM Repport 601501011; RIVM: Bilthoven, The Netherlands, 2000; Volume 601, 66p.
3. Balaram, V. Rare earth elements: A review of applications, occurrence, exploration, analysis, recycling, and environmental impact. *Geosci. Front.* **2019**, *10*, 1285–1303. [CrossRef]
4. Gwenzi, W.; Mangori, L.; Danha, C.; Chaukura, N.; Dunjana, N.; Sanganyado, E. Sources, behaviour, and environmental and human health risks of high-technology rare earth elements as emerging contaminants. *Sci. Total Environ.* **2018**, *636*, 299–313. [CrossRef] [PubMed]
5. Rim, K.T.; Koo, K.H.; Park, J.S. Toxicological Evaluations of Rare Earths and Their Health Impacts to Workers: A Literature Review. *Saf. Health Work* **2013**, *4*, 12–26. [CrossRef]
6. Rho, B.-J.; Sun, P.-P.; Cho, S.-Y. Recovery of neodymium and praseodymium from nitrate-based leachate of permanent magnet by solvent extraction with trioctylphosphine oxide. *Sep. Purif. Technol.* **2020**, *238*, 116429. [CrossRef]
7. Shirotani, I.; Hayashi, J.; Yamanashi, K.; Hirano, K.; Adachi, T.; Ishimatsu, N.; Shimomura, O.; Kikegawa, T. X-ray study with synchrotron radiation of cerium and praseodymium monopnictides with the NaCl-type structure at high pressures. *Phys. B Condens. Matter* **2003**, *334*, 167–174. [CrossRef]
8. Melchakov, S.Y.; Yamshchikov, L.F.; Ivanov, V.A.; Volkovich, V.A.; Raspopin, S.P.; Osipenko, A.G. Thermodynamic properties of alloys of praseodymium with the gallium-indium eutectic melt. Russ. *J. Non-Ferr. Met.* **2014**, *55*, 550–553. [CrossRef]
9. Fahed, S.; Pointecouteau, R.; Aouine, M.; Bor'eave, A.; Gil, S.; Meille, V.; Bazin, P.; Toulemonde, O.; Demourgues, A.; Daturi, M.; et al. Pr-rich ceriumzirconium-praseodymium mixed oxides for automotive exhaust emission control. *Appl. Catal. A Gen.* **2022**, *644*, 118800. [CrossRef]
10. Naranjo, L.P.; Oliveira, N.T.C.; Kassab, L.R.P.; de Araújo, C.B. Optical properties of B_2O_3–CaF_2 glass-ceramics doped with silver nanoparticles and praseodymium ions. *J. Lumin.* **2021**, *238*, 118225. [CrossRef]
11. Wang, C.; Li, Y.; Chen, S.; Li, Y.; Lv, Q.; Shao, B.; Zhu, G.; Zhao, L. A novel high efficiency and ultra-stable red emitting europium doped pyrophosphate phosphor for multifunctional applications. *Inorg. Chem. Front.* **2021**, *8*, 3984–3997. [CrossRef]
12. Malhotra, N.; Hsu, H.S.; Liang, S.T.; Roldan, M.J.M.; Lee, J.S.; Ger, T.R.; Hsiao, C. An updated review of toxicity effect of the rare earth elements (REEs) on aquatic organisms. *Animals* **2020**, *10*, 1663. [CrossRef] [PubMed]
13. Klochkov, E.P.; Risovany, V.D. Utilization of europium-containing control rods by development of gamma-europium sources. In *Analysis of Risks Associated with Nuclear Submarine Decommissioning, Dismantling and Disposal*; Sarkisov, A.A., du Clos, A.T., Eds.; NATO Science Series; Springer: Dordrecht, The Netherlands, 1999; Volume 24, pp. 425–432. [CrossRef]
14. Figueiredo, C.; Oliveira, R.; Lopes, C.; Brito, P.; Caetano, M.; Raimundo, J. Rare earth elements biomonitoring using the mussel *Mytilus galloprovincialis* in the Portuguese coast: Seasonal variations. *Mar. Pollut. Bull.* **2022**, *175*, 113335. [CrossRef] [PubMed]
15. Gomes, P.; Valente, T.; Marques, R.; Prudêncio, M.I.; Pamplona, J. Rare earth elements—Source and evolution in an aquatic system dominated by mine-Influenced waters. *J. Environ. Manag.* **2022**, *322*, 116125. [CrossRef] [PubMed]
16. Revel, M.; van Drimmelen, C.K.E.; Weltje, L.; Hursthouse, A.; Heise, S. Effects of rare earth elements in the aquatic environment: Implications for ecotoxicological testing. *Critic. Rev. Environ. Sci. Technol.* **2024**, 1–42. [CrossRef]
17. Gutiérrez-León, J.; Millán-Becerro, R.; Carrero, S.; Pérez-López, R.; Ceballos, E.; Freydier, R.; Soler, J.M.; Cama, J. Distribution of trace and rare earth elements in the estuary of Ría de Huelva (SW Spain): Field data and geochemical modeling. *Chem. Geol.* **2024**, *662*, 122208. [CrossRef]
18. Olías, M.; Cerón, J.C.; Fernández, I.; De la Rosa, J. Distribution of rare earth elements in an alluvial aquifer affected by acid mine drainage: The Guadiamar aquifer (SW Spain). *Environ. Pollut.* **2005**, *135*, 53–64. [CrossRef]
19. Atinkpahoun, C.N.H.; Pons, M.N.; Louis, P.; Leclerc, J.P.; Soclo, H.H. Rare earth elements (REE) in the urban wastewater of Cotonou (Benin, West Africa). *Chemosphere* **2020**, *251*, 126398. [CrossRef]
20. Hatje, V.; Bruland, K.W.; Flegal, A.R. Increases in Anthropogenic Gadolinium Anomalies and Rare Earth Element Concentrations in San Francisco Bay over a 20 Year Record. *Environ. Sci. Technol.* **2016**, *50*, 4159–4168. [CrossRef]

21. Leite, C.; Russo, T.; Pinto, J.; Polese, G.; Soares, A.M.V.M.; Pretti, C.; Pereira, E.; Freitas, R. From the cellular to tissue alterations induced by two rare earth elements in the mussel species *Mytilus galloprovincialis*: Comparison between exposure and recovery periods. *Sci. Total Environ.* **2024**, *915*, 169754. [CrossRef]
22. Markich, S.J.; Hall, J.P.; Dorsman, J.M.; Brown, P.L. Toxicity of rare earth elements (REEs) to marine organisms: Using species sensitivity distributions to establish water quality guidelines for protecting marine life. *Environ. Res.* **2024**, *261*, 119708. [CrossRef]
23. Kurvet, I.; Juganson, K.; Vija, H.; Sihtmäe, M.; Blinova, I.; Syvertsen-Wiig, G.; Kahru, A. Toxicity of nine (doped) rare earth metal oxides and respective individual metals to aquatic microorganisms *Vibrio fischeri* and *Tetrahymena thermophila*. *Materials* **2017**, *10*, 754. [CrossRef] [PubMed]
24. Tai, P.; Zhao, Q.; Su, D.; Li, P.; Stagnitti, F. Biological toxicity of lanthanide elements on algae. *Chemosphere* **2010**, *80*, 1031–1035. [CrossRef] [PubMed]
25. Trifuoggi, M.; Pagano, G.; Guida, M.; Palumbo, A.; Siciliano, A.; Gravina, M.; Lyons, D.M.; Burić, P.; Levak, M.; Thomas, P.J.; et al. Comparative toxicity of seven rare earth elements in sea urchin early life stages. *Environ. Sci. Pollut. Res.* **2017**, *24*, 20803–20810. [CrossRef] [PubMed]
26. Tan, K.; Yan, X.; Julian, R.; Lim, L.; Peng, X.; Fazhan, H.; Kwan, K.Y. Effects of climate change induced hyposalinity stress on marine bivalves. *Estuar. Coast. Shelf Sci.* **2023**, *294*, 108539. [CrossRef]
27. Durack, P. Ocean salinity and the global water cycle. *Oceanography* **2015**, *28*, 20–31. [CrossRef]
28. Bal, A.; Panda, F.; Pati, S.G.; Das, K.; Agrawal, P.K.; Paital, B. Modulation of physiological oxidative stress and antioxidant status by abiotic factors especially salinity in aquatic organisms. *Comp. Biochem. Physiol. Part C Toxicol. Pharmacol.* **2021**, *241*, 108971. [CrossRef]
29. Gonçalves, A.M.M.; Barroso, D.V.; Serafim, T.L.; Verdelhos, T.; Marques, J.C.; Gonçalves, F. The biochemical response of two commercial bivalve species to exposure to strong salinity changes illustrated by selected biomarkers. *Ecol. Indic.* **2017**, *76*, 59–66. [CrossRef]
30. Rivera-Ingraham, G.A.; Lignot, J.H. Osmoregulation, bioenergetics and oxidative stress in coastal marine invertebrates: Raising the questions for future research. *J. Exp. Biol.* **2017**, *220*, 1749–1760. [CrossRef]
31. Freitas, R.; De Marchi, L.; Bastos, M.; Moreira, A.; Velez, C.; Chiesa, S.; Wrona, F.J.; Figueira, E.; Soares, A.M.V.M. Effects of seawater acidification and salinity alterations on metabolic, osmoregulation and oxidative stress markers in *Mytilus galloprovincialis*. *Ecol. Indic.* **2017**, *79*, 54–62. [CrossRef]
32. Coughlan, B.M.; Moroney, G.A.; Pelt, F.N.A.M.; van O'Brien, N.M.; Davenport, J.; O'Halloran, J. The effects of salinity on the Manila clam (*Ruditapes philippinarum*) using the neutral red retention assay with adapted physiological saline solutions. *Mar. Pollut. Bull.* **2009**, *58*, 1680–1684. [CrossRef]
33. Guzmán-Agüero, J.E.; Nieves-Soto, M.; Hurtado, M.Á.; Piña-Valdez, P.; Garza-Aguirre, M.D.C. Feeding physiology and scope for growth of the oyster *Crassostrea corteziensis* (Hertlein, 1951) acclimated to different conditions of temperature and salinity. *Aquac. Int.* **2013**, *21*, 283–297. [CrossRef]
34. Ivanina, A.V.; Jarrett, A.; Bell, T.; Rimkevicius, T.; Beniash, E.; Sokolova, I.M. Effects of seawater salinity and pH on cellular metabolism and enzyme activities in biomineralizing tissues of marine bivalves. *Comp. Biochem. Physiol. Part A Mol. Integr. Physiol.* **2020**, *248*, 110748. [CrossRef] [PubMed]
35. Pourmozaffar, S.; Tamadoni Jahromi, S.; Rameshi, H.; Sadeghi, A.; Bagheri, T.; Behzadi, S.; Gozari, M.; Zahedi, M.R.; Abrari Lazarjani, S. The role of salinity in physiological responses of bivalves. *Rev. Aquac.* **2020**, *12*, 1548–1566. [CrossRef]
36. Riisgård, H.U.; Lüskow, F.; Pleissner, D.; Lundgreen, K.; López, M.Á.P. Effect of salinity on filtration rates of mussels *Mytilus edulis* with special emphasis on dwarfed mussels from the low-saline Central Baltic Sea. *Helgol. Mar. Res.* **2013**, *67*, 591–598. [CrossRef]
37. Xie, Z.; Wei, S.; Dong, H.; Chen, H.; Zhang, Q.; Liu, W.; Peng, J.; Sokolova, I.M.; Hu, M.; Wang, Y. Hemocyte Responses of the Oyster *Crassostrea hongkongensis* Exposed to Diel-Cycling Hypoxia and Salinity Change. *Front. Mar. Sci.* **2021**, *8*, 749623. [CrossRef]
38. Xie, Z.; Shi, J.; Shi, Y.; Tu, Z.; Hu, M.; Yang, C.; Deng, Y.; Dupont, S.; Xu, Z.; Wang, Y. Physiological responses to salinity change and diel-cycling hypoxia in gills of Hong Kong oyster *Crassostrea hongkongensis*. *Aquaculture* **2023**, *570*, 739443. [CrossRef]
39. Zhou, C.; Song, H.; Feng, J.; Hu, Z.; Yang, M.J.; Shi, P.; Li, Y.R.; Guo, Y.J.; Li, H.Z.; Zhang, T. Metabolomics and biochemical assays reveal the metabolic responses to hypo-salinity stress and osmoregulatory role of cAMP-PKA pathway in *Mercenaria mercenaria*. *Comput. Struct. Biotechnol. J.* **2022**, *20*, 4110–4121. [CrossRef]
40. Andrade, M.; Soares, A.M.V.M.; Solé, M.; Pereira, E.; Freitas, R. Salinity influences on the response of *Mytilus galloprovincialis* to the rare-earth element lanthanum. *Sci. Total Environ.* **2021**, *794*, 148512. [CrossRef]
41. Andrade, M.; Pinto, J.; Soares, A.M.V.M.; Solé, M.; Pereira, E.; Freitas, R. Yttrium effects on the Mediterranean mussel under a scenario of salinity shifts and increased temperature. *Mar. Environ. Res.* **2024**, *195*, 106365. [CrossRef]
42. Curpan, A.-S.; Impellitteri, F.; Plavan, G.; Ciobica, A.; Faggio, C. Review: *Mytilus galloprovincialis*: An essential, low-cost model organism for the impact of xenobiotics on oxidative stress and public health. *Comp. Biochem. Physiol. Part C Toxicol. Pharmacol.* **2022**, *256*, 109302. [CrossRef]
43. De Marchi, L.; Freitas, R.; Oliva, M.; Cuccaro, A.; Manzini, C.; Tardelli, F.; Andrade, M.; Costa, M.; Leite, C.; Morelli, A.; et al. Does salinity variation increase synergistic effects of triclosan and carbon nanotubes on *Mytilus galloprovincialis*? Responses on adult tissues and sperms. *Sci. Total Environ.* **2020**, *734*, 138837. [CrossRef] [PubMed]

44. Andrade, M.; Soares, A.M.V.M.; Solé, M.; Pereira, E.; Freitas, R. Will climate changes enhance the impacts of e-waste in aquatic systems? *Chemosphere* **2022**, *288*, 132264. [CrossRef] [PubMed]
45. Lopes, J.F.; Dias, J.M.; Cardoso, A.C.; Silva, C.I.V. The water quality of the Ria de Aveiro lagoon, Portugal: From the observations to the implementation of a numerical model. *Mar. Environ. Res.* **2005**, *60*, 594–628. [CrossRef] [PubMed]
46. Leite, C.; Coppola, F.; Monteiro, R.; Russo, T.; Polese, G.; Lourenço, M.A.O.; Silva, M.R.F.; Ferreira, P.; Soares, A.M.V.M.; Freitas, R.; et al. Biochemical and histopathological impacts of rutile and anatase (TiO_2 forms) in *Mytilus galloprovincialis*. *Sci. Total Environ.* **2020**, *719*, 134886. [CrossRef]
47. Leite, C.; Russo, T.; Cuccaro, A.; Pinto, J.; Polese, G.; Soares, A.M.V.M.; Pretti, C.; Pereira, E.; Freitas, R. The role of warming in modulating neodymium effects on adults and sperm of *Mytilus galloprovincialis*. *J. Environ. Manag.* **2024**, *358*, 120854. [CrossRef]
48. Mikhailov, A.T.; Torrado, M.; Korochkin, L.I.; Kopantzeva, M.A.; Méndez, J. Male predominant carboxylesterase expression in the reproductive system of molluscs and insects: Immunochemical and biochemical similarity between *Mytilus* male associated polypeptide (MAP) and Drosophila sex-specific esterase S. *Comp. Biochem. Physiol. Part B Biochem. Mol. Biol.* **1997**, *118*, 197–208. [CrossRef]
49. Arnot, J.A.; Gobas, F.A. A review of bioconcentration factor (BCF) and bioaccumulation factor (BAF) assessments for organic chemicals in aquatic organisms. *Environ. Rev.* **2006**, *14*, 257–297. [CrossRef]
50. Anderson, M.J.; Gorley, R.N.; Clarke, K.R. *PERMANOVA+ for PRIMER: Guide to Software and Statistical Methods*; PRIMER-E: Plymouth, UK, 2008.
51. Song, Y.; Asselman, J.; de Schamphelaere, K.A.C.; Salbu, B.; Tollefsen, K.E. Deciphering the combined effects of environmental stressors on gene transcription: A conceptua approach. *Environ. Sci. Technol.* **2018**, *52*, 5479–5489. [CrossRef]
52. Leite, C.; Andrade, M.; Pinto, J.; Soares, A.M.V.M.; Solé, M.; Pereira, E.; Freitas, R. Complex interactions of rare earth elements in aquatic systems: Comparing observed and predicted cellular responses on *Mytilus galloprovincialis*. *Sci. Total Environ.* **2024**, *955*, 176608. [CrossRef]
53. Piggott, J.J.; Townsend, C.R.; Matthaei, C.D. Reconceptualizing synergism and antagonism among multiple stressors. *Ecol. Evol.* **2015**, *5*, 1538–1547. [CrossRef]
54. Delnat, V.; Swaegers, J.; Asselman, J.; Stoks, R. Reduced stress defence responses contribute to the higher toxicity of a pesticide under warming. *Mol. Ecol.* **2020**, *29*, 4735–4748. [CrossRef] [PubMed]
55. Beliaeff, B.; Burgeot, T. Integrated biomarker response: A useful tool for ecological risk assessment. *Environ. Toxicol. Chem.* **2002**, *21*, 1316–1322. [CrossRef] [PubMed]
56. Sanchez, W.; Burgeot, T.; Porcher, J.-M. A novel "Integrated Biomarker Response" calculation based on reference deviation concept. *Environ. Sci. Pollut. Res.* **2013**, *20*, 2721–2725. [CrossRef]
57. Ansaldo, M.; Nahabedian, D.E.; Holmes-Brown, E.; Agote, M.; Ansay, C.V.; Guerrero, N.R.V.; Wider, E.A. Potential use of glycogen level as biomarker of chemical stress in *Biomphalaria glabrata*. *Toxicology* **2006**, *224*, 119–127. [CrossRef] [PubMed]
58. Cammen, L.M.; Corwin, S.; Christensen, J.P. Electron transport system (ETS) activity as a measure of benthic macrofaunal metabolism. *Mar. Ecol. Prog. Ser.* **1990**, *65*, 171–182. [CrossRef]
59. Vasseur, P.; Cossu-Leguille, C. Biomarkers and community indices as complementary tools for environmental safety. *Environ. Int.* **2003**, *28*, 711–717. [CrossRef]
60. Gosling, E. Circulation, respiration, excretion and osmoregulation. In *Bivalve Molluscs: Biology, Ecology and Culture*; Blackwell Publishing: Hoboken, NJ, USA, 2003; pp. 201–225. [CrossRef]
61. Ortmann, C.; Grieshaber, M.K. Energy metabolism and valve closure behaviour in the Asian clam *Corbicula fluminea*. *J. Exp. Biol.* **2003**, *206*, 4167–4178. [CrossRef]
62. Regoli, F.; Giuliani, M.E. Oxidative pathways of chemical toxicity and oxidative stress biomarkers in marine organisms. *Mar. Environ. Res.* **2014**, *93*, 106–117. [CrossRef]
63. Au, D.W.T. The application of histo-cytopathological biomarkers in marine pollution monitoring: A review. *Mar. Pollut. Bull.* **2004**, *48*, 817–834. [CrossRef]
64. Rajalakshmi, S.; Mohandas, A. Copper-induced changes in tissue enzyme activity in a freshwater mussel. *Ecotoxicol. Environ. Saf.* **2005**, *62*, 140–143. [CrossRef]
65. Faggio, C.; Tsarpali, V.; Dailianis, S. Mussel digestive gland as a model tissue for assessing xenobiotics: An overview. *Sci. Total Environ.* **2018**, *636*, 220–229. [CrossRef] [PubMed]
66. Costa, P.M.; Carreira, S.; Costa, M.H.; Caeiro, S. Development of histopathological indices in a commercial marine bivalve (*Ruditapes decussatus*) to determine environmental quality. *Aquat. Toxicol.* **2013**, *126*, 442–454. [CrossRef] [PubMed]
67. Pagano, M.; Capillo, G.; Sanfilippo, M.; Palato, S.; Trischitta, F.; Manganaro, A.; Faggio, C. Evaluation of functionality and biological responses of *Mytilus galloprovincialis* after exposure to quaternium-15 (Methenamine 3-Chloroallylochloride). *Molecules* **2016**, *21*, 144. [CrossRef]
68. Sunila, I. Acute histological responses of the gill of the mussel, *Mytilus edulis*, to exposure by environmental pollutants. *J. Invertebr. Pathol.* **1988**, *52*, 137–141. [CrossRef]
69. Cuevas, N.; Zorita, I.; Costa, P.M.; Franco, J.; Larreta, J. Development of histopathological indices in the digestive gland and gonad of mussels: Integration with contamination levels and effects of confounding factors. *Aquat. Toxicol.* **2015**, *162*, 152–164. [CrossRef]

70. Świacka, K.; Smolarz, K.; Maculewicz, J.; Caban, M. Effects of environmentally relevant concentrations of diclofenac in *Mytilus trossulus*. *Sci. Total Environ.* **2020**, *737*, 139797. [CrossRef]
71. Coppola, F.; Russo, T.; Soares, A.M.V.M.; Marques, P.A.A.P.; Polese, G.; Pereira, E.; Freitas, R. The influence of salinity on the toxicity of remediated seawater. *Environ. Sci. Pollut. Res.* **2022**, *29*, 32967–32987. [CrossRef]
72. Agarwal, A.; Virk, G.; Ong, C.; du Plessis, S.S. Effect of Oxidative Stress on Male Reproduction. *World J. Men's Health* **2014**, *32*, 1–17. [CrossRef]
73. Cuccaro, A.; de Marchi, L.; Oliva, M.; Sanches, M.V.; Freitas, R.; Casu, V.; Monni, G.; Miragliotta, V.; Pretti, C. Sperm quality assessment in *Ficopomatus enigmaticus* (Fauvel, 1923): Effects of selected organic and inorganic chemicals across salinity levels. *Ecotoxicol. Environ. Saf.* **2021**, *207*, 111219. [CrossRef]
74. Freitas, R.; Leite, C.; Pinto, J.; Costa, M.; Monteiro, R.; Henriques, B.; di Martino, F.; Coppola, F.; Soares, A.M.V.M.; Solé, M.; et al. The influence of temperature and salinity on the impacts of lead in *Mytilus galloprovincialis*. *Chemosphere* **2019**, *235*, 403–412. [CrossRef]
75. Viarengo, A.; Canesi, L.; Pertica, M.; Poli, G.; Moore, M.N.; Orunesu, M. Heavy metal effects on lipid peroxidation in the tissues of *mytilus gallopro vincialis* lam. *Comp. Biochem. Physiol. Part C Comp. Pharmacol.* **1990**, *97*, 37–42. [CrossRef]
76. Rahi, D.; Dzyuba, B.; Policar, T.; Malinovskyi, O.; Rodina, M.; Dzyuba, V. Bioenergetic pathways in the sperm of an under-ice spawning fish, burbot (*Lota lota*): The role of mitochondrial respiration in a varying thermal environment. *Biology* **2021**, *10*, 739. [CrossRef] [PubMed]
77. Pagano, G.; Guida, M.; Siciliano, A.; Oral, R.; Koçbaş, F.; Palumbo, A.; Castellano, I.; Migliaccio, O.; Thomas, P.J.; Trifuoggi, M. Comparative toxicities of selected rare earth elements: Sea urchin embryogenesis and fertilization damage with redox and cytogenetic effects. *Environ. Res.* **2016**, *147*, 453–460. [CrossRef]
78. Catteau, A.; Le-Guernic, A.; Palos-Ladeiro, M.; Dedourge-Geffard, O.; Bonnard, M.; Bonnard, I.; Delahaut, L.; Bado-Nilles, A.; Porcher, J.M.; Lopes, C.; et al. Integrative biomarker response—*Threshold* (IBR-T): Refinement of IBRv2 to consider the reference and threshold values of biomarkers. *J. Environ. Manag.* **2023**, *341*, 118049. [CrossRef]
79. Khan, F.U.; Chen, H.; Gu, H.; Wang, T.; Dupont, S.; Kong, H.; Shang, Y.; Wang, X.; Lu, W.; Hu, M.; et al. Antioxidant responses of the mussel *Mytilus coruscus* coexpose to ocean acidification, hypoxia and warming. *Mar. Pollut. Bull.* **2021**, *162*, 111869. [CrossRef]

Journal of *Xenobiotics*

MDPI

Article

Single but Not Combined In Vitro Exposure to Bisphenol A and Nanoplastics Affects the Cholinergic Function of the Ascidian *Ciona robusta*

Safa Melki [1,†], Emma Ferrari [2,3,*,†], Raja Ben Ahmed [1], Antonietta Spagnuolo [3] and Ilaria Corsi [2]

[1] Department of Biology, Laboratory of Ecology, Biology and Physiology of Aquatic Organisms LR18ES41, Faculty of Sciences of Tunis, University of Tunis El Manar, Tunis 2092, Tunisia; safa.melki@etudiant-fst.utm.tn (S.M.); raja.benahmed@fst.utm.tn (R.B.A.)
[2] Department of Physical, Earth and Environmental Sciences, University of Siena, 53100 Siena, Italy; ilaria.corsi@unisi.it
[3] Department of Biology and Evolution of Marine Organisms, Stazione Zoologica Anton Dohrn, 80121 Naples, Italy; niettaspagnuolo1@gmail.com
* Correspondence: emma.ferrari@student.unisi.it
† These authors contributed equally to this work.

Abstract: Nanoplastics are known to represent a threat to marine ecosystems. Their combination with other contaminants of emerging concerns (CECs) may amplify ecotoxic effects, with unknown impacts on marine biodiversity. This study investigates the effects, single and combined, of bisphenol A (BPA)—one of the most hazardous CECs—and polystyrene nanoparticles (PS NPs)—as a proxy for nanoplastics, being among the most commonly found asmarine debris—on cholinesterase (ChE) activities of the ascidian *Ciona robusta*. ChE activity was first measured in the siphons, tunic, and viscera of wild-caught adult specimens and exposed in vitro to BPA (0.01, 0.21, 0.69 mM) and PS NPs (0.0096–0.096 mM; 8.096×10^9–10^{10} particles, respectively) alone and combined for 15 min of incubation. PS NPs' behavior in milliQ water and in the ChE assay reaction buffer was characterized alone, combined with BPA, and analyzed through ζ-potential measurements via Dynamic Light Scattering. The results revealed that ChE activity was predominant in the viscera and siphons of *C. robusta*; PS NPs did not affect the ChE activity alone or combined, while BPA caused a concentration-dependent inhibition of ChE activity in the viscera. No changes in ζ-potential were observed for PS NPs alone or combined with BPA in the ChE buffer, suggesting no interaction. Further investigations are needed to understand the potential neurotoxic consequences for *C. robusta* and ecological risk scenarios due to exposure to BPA and nanoplastics in marine coastal waters.

Keywords: ecotoxicology; cholinesterases; ascidians; emerging contaminants; mixture toxicity; polystyrene nanoparticles

1. Introduction

Cholinesterases (ChE), and in particular acetylcholinesterase activity (AChE), are widely used as biomarkers of neurotoxicity in marine pollution monitoring and assessment due to their conservative role in hydrolyzing the neurotransmitter acetylcholine in the peripheral and central nervous systems of many organisms [1]. Studies have demonstrated that exposure to certain compounds, including industrial chemicals and plastic additives, causes AChE inhibition in marine species, highlighting the sensitivity of this biomarker also for monitoring the effects of contaminants of emerging concern (CECs) [2,3]. A wide range of toxic chemicals can potentially inhibit AChE activity across diverse species, from invertebrates to mammals, thus impairing neurotransmission and embryo development [4,5]. Bisphenol A (BPA) is among the most hazardous CECs associated with domestic sewage effluents and it is widely used in the production of epoxy resins and polycarbonate plastics [6]. BPA is nearly ubiquitous in aquatic environments, with a strong association

with plastic waste [7]. Data on the environmental fate of BPA—as well as its levels in environmental matrices—are scarce as compared to data on its biological effects, which include a broad range of biological functions, such as phenotypic abnormalities, altered behavior and disruption in the cardiovascular and reproductive system, with consequences on development, growth, and survival of marine species [8–10]. The biological effects of BPA are most likely mediated by its endocrine-disrupting action—particularly as an estrogen-mimic—thus impacting development, metabolism, and the reproductive system, but also affecting the central nervous system (CNS) [11]. Recent findings on BPA as a neurotoxicant revealed that the bioaccumulation in the zebrafish brain causes overexpression of myelin (MBP), with significant inhibition of AChE activity [3]. Therefore, AChE is a target of BPA also in *Ciona* and merits further investigation also in realistic exposure scenarios when mixtures of CECs are present and affect biological responses as well as pathways of ecotoxicity. Nanoplastics are listed among CECs and being abundant in the marine coastal waters of the Mediterranean Sea, they can interact with other micropollutants released into wastewater treatment plants' effluents, including plastic additives such as BPA. As such, nanoplastics and BPA can interact, leading to synergistic, antagonistic, or additive effects and thus affecting several biological functions of marine species [12–14]. Current evidence suggests that plastics, regardless of whether they are micro or nano size, play a substantial role in exposing marine organisms to complex mixtures of chemical contaminants [15–17]. The neurotoxicity of nanoplastics and BPA single and/or combined has been overlooked in marine species, although exposure to them occurs in marine coastal areas. We recently demonstrated the absence of interaction between BPA and nanoplastics (polystyrene nanoparticles, PSNPs) in natural seawater, using as an end point the development of *Ciona robusta* embryos. While BPA alone caused a reduced pigmentation of sensory organs (4.5 μM and 10 μM), in agreement with previous findings [18–20], no effect was observed by PS NPs at the range of tested concentrations (1 and 10 g/mL) either alone or combined with BPA [21]. The ability of salts and natural organic matter (NOM) present in natural seawater (NSW) were considered responsible for limiting BPA adsorption onto PS NPs, as also demonstrated by the significant changes observed in the ζ-potential, which was far less negative upon incubation with NSW. Indeed, the ζ-potential is a measure of the electrical potential at the boundary between the particle and the water suspension; therefore, it represents a crucial indicator of the stability of colloidal dispersions, here applied to PS NPs in NSW.

The ascidian *Ciona* spp.—at the embryo, juvenile, and adult stages—is increasingly used in ecotoxicological studies, thanks to its phylogenetic position as a sister group of vertebrates [22]. Adults have been used to monitor anthropogenic stressors such as heavy metals, MPs, phthalate acid esters, and pharmaceutically active compounds [23,24] while embryos and juveniles have been instrumental in addressing nanoplastic ecotoxicity [19,25]. A remarkable increase in AChE activity has been detected after the exposure of unfertilized eggs, embryos, and juveniles of *Ciona* to tributyltin—a toxic organotin compound used primarily as an antifouling agent—suggesting that this enzyme is targeted by it [26,27].

Our study aims to characterize ChEs' activity across different tissues of *Ciona robusta* and assess the in vitro effects of BPA and PS NPs, single and combined. An in vitro study was performed using a range of concentrations (0.01–0.21–0.69 mM for BPA and 0.0096–0.096 mM for PS NPs) resembling realistic and acute exposure scenarios and to align with previous investigations on embryotoxicity [21].

2. Materials and Methods

2.1. Materials

Unfunctionalized 20 nm PS NPs were purchased from Bangs Laboratories Inc. (Fishers, IN, USA) and received as stock suspensions (100 mg/L) in deionized water. To resemble realistic exposure scenarios to PS NPs in the marine environment, an unfunctionalized batch was tested here. A brief 15 min bath sonication at 70% power was performed on the stock suspensions to ensure optimal dispersion and prevent aggregation. Subsequently,

working suspensions of PS NPs were prepared at concentrations of 1 mg/L and 10 mg/L in MilliQ water (mQW) and stored in sterile vials at 4 °C until use. PS NPs' stock characterization in mQW was performed by Dynamic Light Scattering (DLS) and already reported by Ferrari et al. [21] (ζ-Average (nm) 22.8 ± 0.3 nm, PDI 0.35 ± 0.4, ζ-Potential (mV) 51 ± 5 mV). Here, the ζ-potential (mV) of PS NPs aliquot alone and combined with BPA in mQW and in the ChE reaction buffer (0.1 M Na_2PO_4, pH 7.2, Ellman et al. [28]) used for in vitro ChE analysis was measured to infer potential interaction between particles and BPA in the exposure media. The measurements were carried out using 50 µg/mL of PS NP and 0.69 mM of BPA using a Zetasizer Nano ZS90 (Malvern, Malvern, UK) equipped with the Zetasizer Nano Series software (Version 7.02). BPA was purchased from Merck (CAS Nr. 80-05-7) and dissolved in mQW after a bath sonication (10 min, 70% power) at 50 mg/L, 100 mg/L, and 300 mg/L stock solutions. A standardization of units for BPA and PS NPs was conducted using molarity based on their respective molecular weights (BPA: 228.29 g/mol, Styrene: 104.15 g/mol) and the number of NPs/mL has been calculated for both concentrations of PS NPs (see Appendix A—Supplementary information). So, the BPA range of tested concentration was: 0.01–0.21–0.69 mM; PS NP 0.0096–0.096 mM and 8.096×10^9–8.096×10^{10} particles. Acetylthiocholine (iodide) (ASCh), 5,5′-Dithio-bis-(2-nitrobenzoic Acid) (DTNB), and selective inhibitor of AChE 1,5-Bis(4-allyldimethylammoniumphenyl) pentan-3-one dibromide (BW284c51) (Sigma, St. Louis, MO, USA).

2.2. Ciona robusta

Adult specimens of ascidian *Ciona robusta* were collected in the Gulf of Taranto (Italy) by local fishermen between March and June 2023 and immediately shipped in cool boxes to the University of Siena (Italy). Animals were kept in the aquarium for 1 week in NSW collected from the Tuscany coast of the Mediterranean Sea (18 ± 1 °C, salinity 40 ± 1‰, dissolved O_2 7 mg/L, pH 8.1), specimens were kept under constant aeration and photoperiod (16:8, light/dark).

2.3. AChE Activity Characterization

Three types of tissues as inner body organs (branchial sac, heart, viscera and gonads (V), tunic (T), and siphons (S)) of 51 adult specimens were carefully dissected and stored separately in 1.5 mL Eppendorf for ChE activities characterization. Tissues (V, S, T) were finely cut with scissors while kept on ice and homogenization buffer (Low Salt Triton, 20 mM Tris, 5 mM $MgCl_2$, 0.1 mg/mL Bacitracin, 8×10^{-3} TIU/mL Aprotinin, 1% Triton X-100, pH = 7.4) was added in weight/volume (w/v) ratios as 1:5: 0.1 g: 0.5 mL. Samples were homogenized using a Potter–Elvehjem and centrifuged at 8400× g and 4 °C for 20 min. The pellet was then discarded, and the supernatant obtained from V, S, and T was used for the measurement of ChE activities; preferably fresh or upon storage at −80 °C. The AChE activity was assayed by the method of Ellman et al. [28], modified for a microplate reader.

ASCh was selected as a preferential substrate to determine the optimum concentration for the measurement of true-AChE activity. Initial assay conditions in the reaction mixture (final volume 300 µL) were as follows: 0.1 M ChE reaction buffer (0.1 M Na_2PO_4 pH 7.2), supernatant (V, S, and T), DTNB (1 mM), and ASCh substrate (1 mM). Each sample was evaluated in three replicates. The reaction starts when the substrate is added and read for 5 min. The amount of supernatant and ASCh was changed to obtain a better linearity of the reaction curve as follows: four different amounts of supernatant (40, 60, 80, and 100 µL) and three amounts of ASCh (10, 15, and 20 µL) were tested. Reaction rates were measured using a BIO-RAD max tunable microplate reader (Model550) (BioRad Laboratories, 2000 Alfred Nobel Drive, Hercules, CA) which measured the rate of change of absorbance at 405 nm for 5 min after the addition of substrate at 20 °C. ChE vs. ASCh activities were initially expressed as Δ absorbance units/min, converted to nmoles hydrolyzed substrate/min and normalized by tissue total protein content (mg).

2.4. Acetylcholinesterases Activity In Vitro Study

The inhibition studies were carried out by incubating for 15 min the reaction mixture (as a modification of the Ellmann method [28]) (supernatant V, S, and T; ASCh, DTNB) with BPA and PS NPs single and in combination at the following concentrations: BPA 0.01 mM, 0.21 mM, and 0.69 mM, PS NPs 1–10 mg/L (respectively, 0.0096 mM and 0.096 mM and 8.096×10^9–8.096×10^{10} particles), PS NPs (0.096 mM) combined with BPA (0.69 mM). BW24C51 was used to confirm true-AChE activity as a selective inhibitor of pure AChE by adding 20 µL (1 µM final reaction concentration) to the reaction mixture and incubating for 15 min.

To determine the inhibition of BPA, the stock solutions were diluted in the reaction buffer to reach the respective concentrations (0.01–0.21–0.69 mM) and added to the mixture as follows: 160 µL 0.1 M Reaction buffer (pH 7.2) and BPA, supernatant 100 µL, 20 µL DTNB (1 mM), and 20 µL of ASCh substrate (1 mM); incubating for 15 min. The same procedure was carried out for PS NPs (0.0096–0.096 mM). To carry out the combined exposure in vitro, PS NPs (0.096 mM) and BPA (0.69 mM) were diluted in the same vial with reaction buffer and then added to the mixture, following the same process as described earlier. Each sample was analyzed in three replicates and, subsequently, the mean was calculated among samples subjected to the same treatment to obtain a representative value for each treatment. The total protein concentration of extracts of *Ciona* tissues (T, S, and V) was measured following the method of Bradford [29] using bovine serum albumin as standard; values are expressed in mg total protein per ml supernatant.

2.5. Statistical Analysis

Data are shown as mean ± standard deviation. Statistical analysis was performed using GraphPad Prism software (Version 8.0.1, San Diego, CA, USA) using 2-way ANOVA with a Tukey multiple comparisons test with significance indicated in the figures as * $p < 0.0001$ and Unpaired *t*-test, significance as * $p < 0.01$. A Pearson correlation test was used to analyze concentration-dependent variables in the Ellman assay.

3. Results

3.1. Behavior of PS NPs in mQW and Combined with BPA in ChE Reaction Buffer

DLS analysis on the ζ-potential of PS NPs was performed on NPs alone in mQW and combined with BPA in ChE reaction buffer solution at time 0 and after 15 min, to resemble the in vitro incubation media and time (Table 1). PS NPs showed a negative surface charge in mQW (-51 ± 5 mV) (Table 1) and similar values were also measured in those suspended in ChE reaction buffer either alone (-49.1 ± 1.78 mV) and with BPA at T_0 (-50.8 ± 1.72 mV) and after 15 min of incubation T_{15} (-47.3 ± 1.57 mV).

Table 1. ζ-potential measured by Dynamic Light Scattering (DLS) of non-functionalized PS NPs (50 µg/mL) alone in mQW and combined with BPA (0.69 mM) in ChE reaction buffer, at time 0 (T_0) and after 15 min of incubation (T_{15}). Values are shown as mean ± standard deviation.

	ζ-Potential (mV)
mQW	-51 ± 5
ChE reaction buffer	-49.1 ± 1.78
ChE reaction buffer + BPA (T_0)	-50.8 ± 1.72
ChE reaction buffer + BPA (T_{15})	-47.3 ± 1.57

3.2. Characterization of ChE Activity in Ciona Tissues

As a first step, ChE vs. ASCh activities on viscera (V), tunic (T), and siphon (S) were assessed. The findings indicate that the viscera (V) of *Ciona* exhibited the highest ChE activity vs. ASCh compared to tunic (T) and siphon (S) (Figure 1) (* *p*-value < 0.0001). Only in V and S, variations in substrate ASCh concentration (0.24 mM to 0.48 mM) and the amount of tissue extract (40 µL–100 µL) significantly affected ChE activities with a

similar pattern (Table 2); however, activities of T extract did not vary (Table 3). Moreover, by increasing the amounts of the samples of V extracts (ranging from 40 to 100 µL) and substrate (0.24 and 0.48 mM), ChE vs. ASCh significantly increased. The Pearson correlation coefficient "r" was 0.94 and 0.99, respectively, indicating a clear and proportional correlation (Table 3). The use of the selective inhibitor BW284C51 reveals that ChE vs. ASCh activities in V were mostly of AChE, since the inhibition observed was 84.36% of the total activity measured without the inhibitor (Table 2).

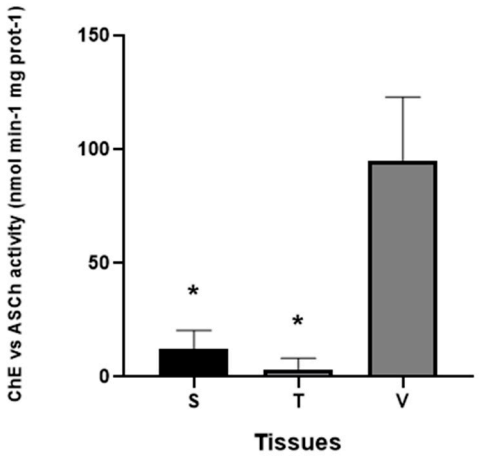

Figure 1. ChE vs. ASCh activity (nmol/min/mg prot) in the three tissues of Ciona as siphons (S), tunic (T), and viscera (V). Values are shown as mean ± standard deviation. Asterisks denote significant differences compared to (V) group. A 2-way ANOVA with a Tukey multiple comparisons test was performed.

Table 2. Optimization of ChE vs. ASCh in viscera (V) and sensitivity towards the selected AChE inhibitor BW. ChE activities are expressed as nmol/min/mg proteins and shown as mean ± standard deviation.

Viscera (V)			
Extract (µL)	**Substrate ASCh (mM)**	**ChE**	
40	0.24	58.2 ± 21.6	
60		76.8 ± 7.8	
80		81.8 ± 3.2	
100		126 ± 8.7	
Extract (µL)	**Substrate ASCh (mM)**	**ChE**	
100	0.24	90.3 ± 16.2	
	0.36	136.6 ± 26.2	
	0.48	201.7 ± 14.8	
Extract (µL)	**Substrate ASCh (mM)**	**ChE**	**BW284C51 (1 µM) residual activity**
100	0.48	95.1 ± 8.6	10.8 ± 2.4

Table 3. Optimization of ASCh vs. ChE in siphons (S) and tunic (T) of Ciona. ChE vs. ASCh activities are expressed as nmol/min/mg proteins and shown as mean ± standard deviation.

Siphons (S)			Tunic (T)
Extract (µL)	**Substrate ASCh (mM)**	**ChE**	**ChE**
40	0.24	58.2 ± 21.6	1.04 ± 0.7
60		76.8 ± 7.8	0.18 ± 0.6
80		81.8 ± 3.2	11.6 ± 2.2
100		126 ± 8.7	0.18 ± 0.6
Extract (µL)	**Substrate ASCh (mM)**	**ChE**	**ChE**
100	0.48	9.13	3.78

3.3. In Vitro BPA and PS NP Exposure Study

Figure 2A shows the inhibition of ChE vs. ASCh activity caused by BPA in viscera (V) extracts of *Ciona*. A clear concentration-dependent inhibitory effect was observed, with a significant decrease in ChE vs. ASCh activity as the BPA concentration increased. This decrease is already observable at the lowest BPA concentration (−30%; 0.01 mM) compared to the control group. All tested concentrations significantly decreased ChE vs. ASCh activity in V extracts compared to the control (* $p < 0.0001$), with an inhibition percentage of approximately 50% for 0.21 mM and 0.69 mM BPA. Conversely, exposure to PS NPs at both molarities (0.0096 and 0.096 mM) did not cause any inhibition in ChE vs. ASCh activity (Figure 2B) with values such as unexposed tissue extracts. Combined exposure to PS NPs and BPA, both administered at their highest doses (0.096 mM and 0.69 mM, respectively), caused a significant inhibition (* $p < 0.01$) compared to control (Figure 2C). This inhibition was notably like the effect observed with BPA alone at the intermediate and the highest concentration tested (Figure 2A). Table 4 presents the percentage of inhibition for each concentration tested on ChE vs. ASCh activity.

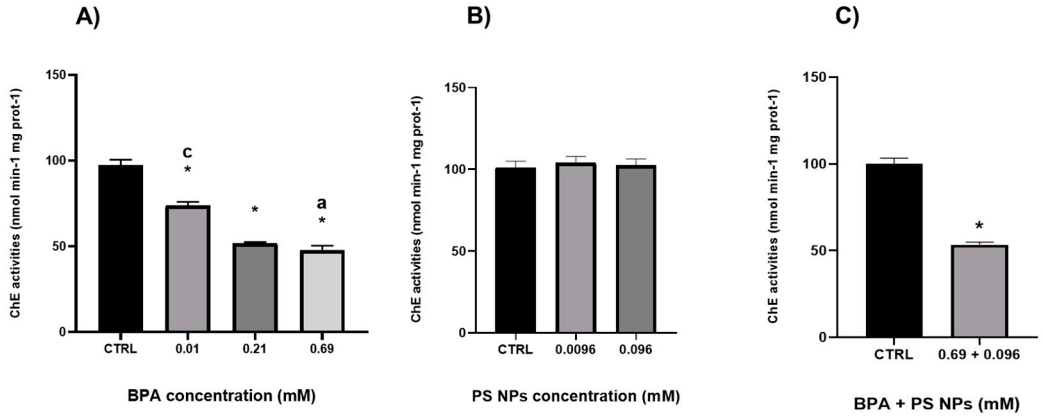

Figure 2. ChE vs. ASCh activity (**A**) = BPA alone, (**B**) = PS NPs alone, (**C**) = PS NPs + BPA combined) in the viscera of Ciona in vitro exposed to BPA (0.01–0.21–0.69 mM), PS NPs (0.0096–0.096 mM) and combined (0.096 mM PS NPs and 0.69 mM BPA). Values are shown as mean ± standard deviation. Asterisks denote significant differences compared to control groups and letters between treatment groups (a = 0.01 mM, c = 0.69 mM). Two-way ANOVA with a Tukey multiple comparisons test and anUnpaired *t*-test were performed.

Table 4. Percentage of ChE vs. ASCh activities inhibition vs. controls (Ctrl).

BPA Alone (mM)	%ChE Inhibition
Ctrl	0
0.01	26.8
0.2	48.42
0.69	50.86
PS NPs Alone (mM)	**%ChE Inhibition**
Ctrl	0
0.0096	0
0.096	0
BPA + PS NPs (mM)	**%ChE Inhibition**
Ctrl	0
0.69 + 0.096	46.34

4. Discussion

This study aims to characterize for the first time the ChE vs. ASCh activity in different tissues of *Ciona* and investigate the in vitro sensitivity towards BPA and PS NPs alone and in combination. ChE vs. ASCh activities were mainly identified in viscera and siphons, while the tunic exhibited bare activity close to the detection limit. The almost complete inhibition of ChE vs. ASCh activity upon incubation with the selective AChE inhibitor (BW284C51) revealed the presence of true-AChE activity in both viscera and siphons of adults of *Ciona*. Our findings are consistent with the knowledge that AChE in ascidians has a pivotal role in neuromuscular synapses but is also found on the external surfaces of cells and in various cytoplasmic regions [30]. At the embryonic stages, AChE is involved in labeling embryonic muscle cells [31] and larval adhesive papillae, playing a crucial role in the development of various tissues, while in adults its main role is in regulating muscle and ciliary activities [30,32]. The study by Arkett et al. [32] indicated that ChE activity in the adult and juvenile stages of ascidians is primarily situated in the innervation of the branchial basket and is not restricted to synaptic sites but is distributed throughout the neurons. Recently, AChE histochemical reactions, on fresh preparations of adult pharyngeal gills of *Ciona*, revealed strong signals on the laterodistal ciliated cells of stigmata, referred to as trapezial cells. The direct administration of ACh and other agonists of nicotinic ACh receptors (nAChRs) onto ciliated cells reliably evoked ciliary arrest that persisted for seconds in a dose-dependent manner. Furthermore, the authors provided evidence to show that a nicotinic ACh receptor, A7/8-1 nAChR, expressed in *Ciona* stigmata, mediates neuro-ciliary transmission to elicit ciliary arrest [33]. This is consistent with our findings, showing AChE activity in the viscera including the large branchial sac. Furthermore, Zaniolo et al. [34] confirmed the presence of numerous free nerve endings in the oral siphon tentacles, while describing the development of the nervous system in ascidians. Moreover, the study reported no innervation running through the tunic, supporting our findings, as no activity was detected in the tunic extracts. ChE vs. ASCh activities increased proportionally with the amount of siphon extracts while keeping constant substrate molarity (0.24 mM). In contrast, tunic extracts showed a certain variability, with a significant increase of ChE vs. ASCh activities from 40 to 80 µL (11.6 $\pm$ 2.2) but a decrease at 100 µL (0.18 $\pm$ 0.6). This variability makes uncertain the hydrolysis of ChE vs. ASCh in the tunic extracts played by the only AChE enzyme (Table 3). More recently, the entire neural network of *Ciona* has been visualized in adult transgenic animals harboring a reporter gene construct driven by the pan-neuronal PC2 promoter [35]. The data clearly showed that eight main anterior nerves and ten main posterior nerves, leading from the cerebral ganglion, head toward the oral siphon and atrial siphon, and periphery branch into thin nerves that reach the edge of the siphon lobes. Thus, the innervation surrounding the siphons is complex; however, as the authors point out, further studies will allow us to identify the neuropeptides and neurotransmitters that are likely to regulate the functions of

these nerves. Our findings further support such hypotheses, as indicated by lower cholinergic activity in the siphons compared to the viscera, suggesting variations in neural activity based on anatomical regions and peptidergic regulatory networks. BPA was revealed to be a concentration-dependent inhibitor of ChE vs. ASCh activity in *Ciona* viscera and in a concentration-dependent manner. At environmentally realistic concentrations, BPA has already been reported to affect the embryo development of aquatic species, including invertebrates [7,19,36]. Regarding ascidians, BPA is probably the individual chemical that has been most addressed in emerging contaminants' ecotoxicological studies. Messinetti et al. [18] reported that larvae of *Ciona* and *Phallusia mammillata* exposed to BPA, showed short and kinked tails, impaired neural development and malformations of pigmented organs (otolith and ocellus). Moreover, Gomes et al. [19] reported that micromolar doses of BPA inhibited otolith movement within the sensory vesicle and that BPA may target ERRs (Estrogen-Related Receptors) during otolith movement in *P. mammillata*. Together, these observations suggest that BPA may affect ascidian otolith differentiation by altering ERR activity, whereas otolith pigmentation defects might be due to the known inhibitory effect of bisphenols on tyrosinase enzymatic activity. Similarly, BPA can cause decreased pigmentation in zebrafish embryos (5.0 mgL^{-1}) by downregulating the melanin synthases and reducing the melanin content. The role of BPA as a ligand of the zebrafish tyrosinase (Tyr) family of proteins has been hypothesized, thus causing skin pigmentation interference [20]. These studies align with our previous findings, confirm that one of the most reproducible phenotypes of BPA in ascidian larvae is the disruption of the pigmented cells [21]. The results presented here reveal that BPA can affect not only the most vulnerable stages of *Ciona*, such as embryo or larvae, but also the neurotransmission system of the adult stage, impairing cholinergic activity. These findings are consistent with those obtained recently on zebrafish and mussels; zebrafish exposed to BPA for 96 h at environmentally relevant concentrations (220, 1180, and 1500 ng/L) showed an increased production of reactive oxygen species (ROS) and a significant reduction in AChE activity [11]. Chronic exposure to BPA (0.25, 1, 2, and 5 µg/L, 28d) caused concentration-dependent inhibition of AChE in the date mussel, *Lithophaga lithophaga* [37]. One can envisage that in *Ciona*, as in the other species examined so far, AChE inhibition may cause the persistence of neurotransmitters in the neuronal cleft, which in turn can induce an altered pathway of branchial sac contraction in response to different stimuli, thus influencing an organism's behavior. From this perspective, further studies are fundamental to link the disruption/inhibition of ChE vs. ASCh activity caused by BPA to predict behavioral endpoints. We found that BPA inhibits ChE and ASCh activity in the V, T, and S, while PS NPs had no effect on ChE enzyme activity alone or in combination with BPA. This is consistent with previous studies on *Ciona* larvae, in which no effect of amino-modified PS NPs (PS-NH_2) was observed upon in vivo exposure up to µg/mL (22 h post-fertilization) [27]. Co-exposure to PS NPs and BPA resulted in a 50% inhibition of ChE activity compared to ASCh, consistent with the effect of BPA alone (Table 2). DLS analysis of the ζ-potential showed no significant changes between PS NPs alone in mQW and combined with BPA in the ChE reaction buffer after 15 min of incubation (Table 1), thus indicating no interaction between PS NPs and BPA within this timeframe. The short incubation time (15 min) may not have allowed sufficient interactions between BPA and the PS NPs to induce notable changes in surface charge. Studies have shown that interaction time plays a key role in surface modifications, and longer exposure periods could potentially lead to different outcomes [38]. Additionally, the buffer's composition itself can stabilize the NPs by creating an ionic environment that shields surface interactions, explaining the lack of variation in the ζ-potential. The presence of ions in the buffer can also enhance colloidal stability, reducing electrostatic interactions between BPA and PS NPs. This was similarly observed in studies examining NPs' interactions in complex media, where surface charge often remains stable in short-term exposures despite the presence of other compounds [38,39]. Therefore, it is plausible that under different timeframes or conditions, BPA could influence PS NPs more significantly, warranting further investigation. On the other hand, in vivo exposure studies, such as the one by Chen

et al. [3], showed that combined exposure to PS NPs and BPA led to a significant uptake of BPA in the head and viscera of zebrafish, along with significant inhibition of AChE activity. Therefore, waterborne exposure lasting for 3 days is enough for BPA and PS NPs' ability to interact, leading to synergistic effects. However, such interaction could be strongly abolished by the presence of seawater, as shown in our recent study in which the effects on pigmentation in *Ciona* larvae were visually the same upon exposure to BPA alone or in combination with PS NPs. This suggested that no interaction was taking place between BPA and PS NPs in the seawater media, unlike in freshwater media where a carrier role of PS NPs towards BPA has been hypothesized [3]. The absence of an interactive effect of PS NPs towards BPA in seawater, compared to freshwater, was attributed to the high ionic strength of seawater, which can trigger the sorption surface properties of PS NPs as confirmed by the significant changes in the NPs' surface charges shown by ζ-potential values. Thus, a further important variable factor concerns the media used for the experiments [21,38].

5. Conclusions

To the best of our knowledge, our study provides the first evidence of ChE vs. ASCh activities in the tissues (V, T, and S) of adults of *Ciona*. Sensitivity towards BPA was confirmed as an inhibitor of ChE vs. ASCh activities, while no effects have been observed for PS NPs alone or combined with BPA. Therefore, when combined as in a realistic exposure scenario, BPA neurotoxicity is occurring regardless of the presence of PS NP. The concentration-dependent inhibition of ChE vs. ASCh activity by BPA underscores its potential neurotoxic effects on ascidians at the adult stage, as already observed at the embryonic stage with depigmentation and abnormal development [21].

Overall, this study contributes to the understanding of BPA neurotoxicity in ascidian by targeting ChE vs. ASCh activities in several organs and no further effects from the synergistic exposure to nanoplastics is expected. Indeed, nanoplastic–molecule interactions must be considered as case-by-case studies, as well as the need to perform in vivo studies for setting more realistic scenarios in which interactions could occur at levels other than the AChE binding site.

Author Contributions: S.M.: formal analysis, writing—original draft, writing—review and editing; E.F.: conceptualization, methodology, data curation, investigation, formal analysis, visualization, writing—original draft, writing—review and editing; R.B.A.: writing—review and editing; A.S.: conceptualization, investigation, writing—original draft, writing—review and editing; I.C.: conceptualization, methodology, data curation, investigation, formal analysis, visualization, writing—original draft, writing—review and editing. All authors have read and agreed to the published version of the manuscript.

Funding: Project funded under the National Recovery and Resilience Plan (NRRP), Mission 4 Component 2 Investment 1.4—Call for tender No.3138 of 16 December 2021, rectified by Decree n.3175 of 18 December 2021 of Italian Ministry of University and Research funded by the European Union—NextGenerationEU; Award Number: Project code CN_00000033, Concession Decree No. 1034 of 17 June 2022 adopted by the Italian Ministry of University and Research, CUP B63C22000650007, Project Title "National Biodiversity Future Center—NBFC".

Institutional Review Board Statement: No approval of research ethics committees was required to accomplish the goals of this study because experimental work was conducted with an unregulated invertebrate species.

Informed Consent Statement: Not applicable.

Data Availability Statement: The data presented in this study are available in this article.

Acknowledgments: Graphical abstract: the image of *Ciona* modified from Jeffery et al. (2015) [40]. We thank Arianna Bellingeri for support in the DLS measurements.

Conflicts of Interest: The authors declare that the research was conducted in the absence of any commercial or financial relationships that could be construed as a potential conflict of interest.

Appendix A

Supplementary informations—Method used to calculate the number of PS NP per mL

Nanoparticle diameter (from TEM image) = 33 nm
Radius = 16.5 nm
Polystyrene density = 1.05 g/cm^3
The surface area of a single particle: $4\pi r^2 \rightarrow 4 \times \pi \times 16.5^2 = 3419.46$ nm^2
The volume of a single particle: $4/3\pi r^3 \rightarrow 4/3 \times \pi \times 16.5^3 = 18{,}816.56$ nm^3
Weight of a single particle (convert 18,816.56 nm^3 to cm^3):
Density*number of particles $\rightarrow 1.05 \times 1.88 \times 10^{-17} = 1.974 \times 10^{-17}$ g
Number of particles/mL (convert particle concentration to g/mL and divide by the weight of a single particle):
1 μg/mL $\rightarrow 1 \times 10^{-6}$ g/mL $\rightarrow (1 \times 10^{-6})/(1.974 \times 10^{-17}) = 0.506 \times 10^{11}$ particles/mL
10 μg/mL $\rightarrow 1 \times 10^{-5}$ g/mL $\rightarrow (1 \times 10^{-5})/(1.974 \times 10^{-17}) = 0.506 \times 10^{12}$ particles/mL
Calculation of number of particles in 160 μL used for the in vitro study:
1 μg/mL $\rightarrow 8.096 \times 10^9$ particles
10 μg/mL $\rightarrow 8.096 \times 10^{10}$ particles

References

1. Barboza, L.G.A.; Lopes, C.; Oliveira, P.; Bessa, F.; Otero, V.; Henriques, B.; Raimundo, J.; Caetano, M.; Vale, C.; Guilhermino, L. Microplastics in wild fish from North East Atlantic Ocean and its potential for causing neurotoxic effects, lipid oxidative damage, and human health risks associated with ingestion exposure. *Sci. Total Environ.* **2020**, *717*, 134625. [CrossRef] [PubMed]
2. Solé, M.; Shaw, J.P.; Frickers, P.E.; Readman, J.W.; Hutchinson, T.H. Effects on feeding rate and biomarker responses of marine mussels experimentally exposed to propranolol and acetaminophen. Effects on feeding rate and biomarker responses of marine mussels experimentally exposed to propranolol and acetaminophen. *Anal. Bioanal. Chem.* **2010**, *396*, 649–656. [CrossRef] [PubMed]
3. Chen, Q.; Yin, D.; Jia, Y.; Schiwy, S.; Legradi, J.; Yang, S.; Hollert, H. Enhanced uptake of BPA in the presence of nanoplastics can lead to neurotoxic effects in adult zebrafish. *Sci. Total Environ.* **2017**, *609*, 1312–1321. [CrossRef] [PubMed]
4. Lionetto, M.G.; Caricato, R.; Calisi, A.; Schettino, T. Acetylcholinesterase inhibition as a relevant biomarker in environmental biomonitoring: New insights and perspectives. *Biomed. Res. Int.* **2013**, *2013*, 321213. [CrossRef] [PubMed]
5. Fu, H.; Xia, Y.; Chen, Y.; Xu, T.; Xu, L.; Guo, Z.; Xu, H.; Xie, H.Q.; Zhao, B. Acetylcholinesterase is a potential biomarker for a broad spectrum of organic environmental pollutants. *Environ. Sci. Technol.* **2018**, *52*, 8065–8074. [CrossRef] [PubMed]
6. National Center for Biotechnology Information. PubChem Compound Summary for CID 6623, Bisphenol A. 2024. Available online: https://pubchem.ncbi.nlm.nih.gov/compound/Bisphenol-A (accessed on 2 October 2024).
7. Wu, N.C.; Seebacher, F. Effect of the plastic pollutant bisphenol A on the biology of aquatic organisms: A meta-analysis. *Glob. Chang. Biol.* **2020**, *26*, 3821–3833. [CrossRef]
8. Flint, S.; Markle, T.; Thompson, S.; Wallace, E. Bisphenol A exposure, effects, and policy: A wildlife perspective. *J. Environ. Manag.* **2012**, *104*, 19–34. [CrossRef]
9. Lin, Z.; Wang, L.; Jia, Y.; Zhang, Y.; Dong, Q.; Huang, C. A study on environmental bisphenol A pollution in plastics industry areas. *Water Air Soil Pollut.* **2017**, *228*, 98. [CrossRef]
10. Ozhan, K.; Kocaman, E. Temporal and spatial distributions of bisphenol A in marine and freshwaters in Turkey. *Arch. Environ. Contam. Toxicol.* **2019**, *76*, 246–254. [CrossRef]
11. Heredia-García, G.; Elizalde-Velázquez, G.A.; Gómez-Oliván, L.M.; Islas-Flores, H.; García-Medina, S.; Galar-Martínez, M.; Dublán-García, O. Realistic concentrations of Bisphenol-A trigger a neurotoxic response in the brain of zebrafish: Oxidative stress, behavioral impairment, acetylcholinesterase inhibition, and gene expression disruption. *Chemosphere* **2023**, *330*, 138729. [CrossRef]
12. Llorca, M.; Vega-Herrera, A.; Schirinzi, G.; Savva, K.; Abad, E.; Farré, M. Screening of suspected micro(nano)plastics in the Ebro Delta (Mediterranean Sea). *J. Hazard. Mater.* **2021**, *404*, 124022. [CrossRef] [PubMed]
13. Bhagat, J.; Nishimura, N.; Shimada, Y. Toxicological interactions of microplastics/nanoplastics and environmental contaminants: Current knowledge and future perspectives. *J. Hazard. Mater.* **2021**, *405*, 123913. [CrossRef] [PubMed]
14. Corsi, I.; Bellingeri, A.; Bergami, E. Progress in selecting marine bioindicators for nanoplastics ecological risk assessment. *Ecol. Indic.* **2023**, *154*, 110836. [CrossRef]
15. Hermabessiere, L.; Dehaut, A.; Paul-Pont, I.; Lacroix, C.; Jezequel, R.; Soudant, P.; Duflos, G. Occurrence and effects of plastic additives on marine environments and organisms: A review. *Chemosphere* **2017**, *182*, 781–793. [CrossRef] [PubMed]
16. Gallo, F.; Fossi, C.; Weber, R.; Santillo, D.; Sousa, J.; Ingram, I.; Nadal, A.; Romano, D. Marine litter plastics and microplastics and their toxic chemicals components: The need for urgent preventive measures. *Environ. Sci. Eur.* **2018**, *30*, 13. [CrossRef]

17. Fauser, P.; Vorkamp, K.; Strand, J. Residual additives in marine microplastics and their risk assessment—A critical review. *Mar. Pollut. Bull.* **2022**, *177*, 113467. [CrossRef]
18. Messinetti, S.; Mercurio, S.; Pennati, R. Bisphenol A affects neural development of the ascidian *Ciona robusta*. *J. Exp. Zool. Part A Ecol. Integr. Physiol.* **2019**, *331*, 5–16. [CrossRef]
19. Gomes, I.D.; Gazo, I.; Nabi, D.; Besnardeau, L.; Hebras, C.; Mcdougall, A.; Dumollard, R. Bisphenols disrupt differentiation of the pigmented cells during larval brain formation in the ascidian. *Aquat. Toxicol.* **2019**, *216*, 105314. [CrossRef]
20. Mu, X.; Liu, J.; Yuan, L.; Huang, Y.; Qian, L.; Wang, C. The pigmentation interference of bisphenol F and bisphenol A. *Environ. Pollut.* **2020**, *266*, 115139. [CrossRef]
21. Ferrari, E.; Eliso, M.C.; Bellingeri, A.; Corsi, I.; Spagnuolo, A. Short-Term Exposure to Nanoplastics Does Not Affect Bisphenol A Embryotoxicity to Marine Ascidian *Ciona robusta*. *Biomolecules* **2022**, *12*, 1661. [CrossRef]
22. Delsuc, F.; Brinkmann, H.; Chourrout, D.; Philippe, H. Tunicates and not cephalochordates are the closest living relatives of vertebrates. *Nature* **2006**, *439*, 965–968. [CrossRef] [PubMed]
23. Vered, G.; Kaplan, A.; Avisar, D.; Shenkar, N. Using solitary ascidians to assess microplastic and phthalate plasticizers pollution among marine biota: A case study of the Eastern Mediterranean and Red Sea. *Mar. Pollut. Bull.* **2019**, *138*, 618–625. [CrossRef] [PubMed]
24. Tzafriri-Milo, R.; Benaltabet, T.; Torfstein, A.; Shenkar, N. The Potential Use of Invasive Ascidians for Biomonitoring Heavy Metal Pollution. *Front. Mar. Sci.* **2019**, *6*, 611. [CrossRef]
25. Eliso, M.C.; Bergami, E.; Manfra, L.; Spagnuolo, A.; Corsi, I. Toxicity of nanoplastics during the embryogenesis of the ascidian *Ciona robusta* (Phylum Chordata). *Nanotoxicology* **2020**, *14*, 1415–1431. [CrossRef] [PubMed]
26. Cangialosi, M.V.; Puccia, E.; Mazzola, A.; Mansueto, V.; Arukwe, A. Screening of ovarian steroidogenic pathway in *Ciona intestinalis* and its modulation after tributyltin exposure. *Toxicol. Appl. Pharmacol.* **2010**, *245*, 124–133. [CrossRef]
27. Mansueto, V.; Cangialosi, M.V.; Arukwe, A. Acetylcholinesterase activity in juvenile *Ciona intestinalis* (Ascidiacea, Urochordata) after exposure to tributyltin. *Caryologia* **2012**, *65*, 18–26. [CrossRef]
28. Ellman, G.L.; Courtney, K.D.; Andres Jr, V.; Featherstone, R.M. A new and rapid colorimetric determination of acetylcholinesterase activity. *Biochem. Pharmacol.* **1961**, *7*, 88–95. [CrossRef]
29. Bradford, M.M. A rapid and sensitive method for the quantitation of microgram quantities of protein utilizing the principle of protein-dye binding. *Anal. Biochem.* **1976**, *72*, 248–254. [CrossRef]
30. Burighel, P.; Sorrentino, M.; Zaniolo, G.; Thorndyke, M.C.; Manni, L. The peripheral nervous system of an ascidian, *Botryllus schlosseri*, as revealed by cholinesterase activity. *Invertebr. Biol.* **2001**, *120*, 185–198. [CrossRef]
31. Whittaker, J.R. Acetylcholinesterase development in extra cells caused by changing the distribution of myoplasm in ascidian embryos. *J. Embryol. Exp. Morphol.* **1980**, *55*, 343–354. [CrossRef] [PubMed]
32. Arkett, S.A.; Mackie, G.O.; Singla, C.L. Neuronal organization of the ascidian (Urochordata) branchial basket revealed by cholinesterase activity. *Cell Tissue Res.* **1989**, *257*, 285–294. [CrossRef]
33. Jokura, K.; Nishino, J.M.; Ogasawara, M.; Nishino, A. An α7-related nicotinic acetylcholine receptor mediates the ciliary arrest response in pharyngeal gill slits of *Ciona*. *J. Exp. Biol.* **2020**, *223*, jeb209320. [CrossRef] [PubMed]
34. Zaniolo, G.; Lane, N.J.; Burighel, P.; Tiozzo, S. Development and distribution of acetylcholinesterase in the nervous system of a colonial ascidian during blastogenesis. *J. Comp. Neurol.* **2002**, *121*, 189–201. [CrossRef]
35. Osugi, T.; Sasakura, Y.; Satake, H. The nervous system of the adult ascidian *Ciona intestinalis* Type A (*Ciona robusta*): Insights from transgenic animal models. *PLoS ONE* **2017**, *12*, e0180227. [CrossRef] [PubMed]
36. Canesi, L.; Fabbri, E. Environmental effects of BPA: Focus on aquatic species. *Dose-Response* **2015**, *13*, 1559325815598304. [CrossRef]
37. Abd Elkader, H.-T.A.E.; Al-Shami, A.S. Chronic exposure to bisphenol A induces behavioural, neurochemical, histological, and ultrastructural alterations in the ganglia tissue of the date mussels *Lithophaga lithophaga*. *Environ. Sci. Pollut. Res.* **2023**, *30*, 109041–109062. [CrossRef]
38. Li, W.; Zu, B.; Yang, Q.; An, J.; Li, J. Nanoplastic adsorption characteristics of bisphenol A: The roles of pH, metal ions, and suspended sediments. *Mar. Pollut. Bull.* **2022**, *178*, 113602. [CrossRef]
39. Cortés-Arriagada, D. Elucidating the co-transport of bisphenol A with polyethylene terephthalate (PET) nanoplastics: A theoretical study of the adsorption mechanism. *Environ. Pollut.* **2021**, *270*, 116192. [CrossRef]
40. Jeffery, W.R. The tunicate *Ciona*: A model system for understanding the relationship between regeneration and aging. *Invertebr. Reprod. Dev.* **2015**, *59* (Suppl. S1), 17–22. [CrossRef]

Journal of *Xenobiotics*

MDPI

Article

Oxidative Stress in Mussel *Mytilus trossulus* Induced by Different-Sized Plastics

Nadezhda Vladimirovna Dovzhenko , Valentina Vladimirovna Slobodskova , Andrey Alexandrovich Mazur *, Sergey Petrovich Kukla, Aleksandra Anatolyevna Istomina , Victor Pavlovich Chelomin and Dmitriy Denisovich Beskhmelnov

Il'ichev Pacific Oceanological Institute, Far Eastern Branch, Russian Academy of Sciences, 690041 Vladivostok, Russia

* Correspondence: mazur.aa@poi.dvo.ru

Abstract: Polyethylene and polystyrene are massively used around the world in various applications and are the most abundant plastic waste. Once in the marine environment, under the influence of physical and chemical factors, plastic products degrade, changing from the size category of macroplastics to microplastics. In order to study the effect of plastic on marine organisms, we modeled the conditions of environmental pollution with different-sized plastic—polystyrene microparticles of 0.9 μm and macro-sized polyethylene fragments of 10 cm—and compared their effect on biochemical parameters in the tissues of the bivalve mollusk *Mytilus trossulus*. Using biomarkers, it was found that regardless of the size and type of polymer, polystyrene microparticles and polyethylene macrofragments induced the development of oxidative stress in mussels. A significant decrease in the level of lysosomal stability in mussel hemocytes was observed. Increases in the level of DNA damage and the concentration of malonic dialdehyde in the cells of gills and the digestive gland were also shown. The level of total antiradical activity in cells varied and had a tissue-specific character. It was shown that both ingested polystyrene particles and leachable chemical compounds from polyethylene are toxic for mussels.

Keywords: polyethylene; polystyrene; lysosome membrane stability; DNA damage; ecotoxicology; antiradical activity

1. Introduction

Plastic fragments and microparticles account for about 60–90% of ocean debris on the planet, significantly affecting the quality of the aquatic environment and the hydrobionts that inhabit it, and plastic entering the environment is becoming an integral component of global pollution [1,2]. Due to ocean currents, plastics have spread to all regions of the world's oceans, forming large-scale debris accumulations and migrating at the surface and in the water column [2]. Another problem of plastic debris in the marine environment is its constant defragmentation. Under the influence of ultraviolet light, friction, and other physical and chemical factors, plastic products break down into smaller fragments, resulting in the formation of micro- and nanoparticles [3]. To date, the level of microparticles in water in littoral zones and open sea waters of different regions of the world ranges from 0.001 to 140 particles/m^3, and in bottom sediments, from 0.2 to 8766 particles/m^3 [4]. Therefore, addressing the problem of plastic pollution due to its ubiquity in the ocean is considered one of the most important challenges today [5,6].

In the presence of plastic waste, aquatic organisms are negatively exposed both physically and chemically. Fragments of plastic objects can damage the cover of hydrobionts, be mistaken for food, and mechanically restrict movements [4]. By penetrating into marine organisms, plastic can damage the mucous membranes of organs and tissues, as well as accumulate in the gastrointestinal tract. This can result in serious damage to biochemical

and physiological processes [7–10]. The presence of plastic in the environment also poses a threat of chemical exposure, as its production is based on mixing a base polymer with various additive components that impart certain properties to the final plastic product in order to reach performance standards [11]. According to various estimates, polymers include from 300 to 400 constituent components, among which there are hazardous monomers, low-molecular-weight oligomer fragments, synthetic stabilizers, catalysts, and various chemical additives, most of which are not covalently bonded to the polymer, dyes containing metal ions, plasticizers, phthalates, bisphenol-a, polychlorinated biphenyls, etc. [12,13]. Through interaction with the environment, these additives can actively leach into the water and become bioavailable to living organisms. Because of interaction with the environment, these additives actively leached into the water. Through the toxic effects of leaching chemical constituents into water, among which the most toxic are hydrophobic organic compounds and metals, the bioavailability of plastic to living organisms is observed. Leached chemical compounds trigger mechanisms of oxyradical generation in cells, leading to the development of oxidative stress, DNA molecule damage, and irreversible pathological processes, posing a life threat to aquatic organisms [14–16]. The degree of leaching of additives from polymers and leachate composition is influenced by the properties of compounds, the degree of amorphous or crystalline structure of the polymer, and the persistence of chemical bonds between additives and the polymer [17].

There are now several studies on the toxicity of individual additives migrating from plastic materials into the water, causing acute toxicity in hydrobionts [16,18,19]. It has been shown in different studies that marine organisms are prone to ingest plastic particles [20,21], but very few studies have investigated the toxicity of polymers to hydrobionts surrounded by plastic fragments not consumed by them [22].

In addition to releasing toxic substances into the environment, multi-sized plastics, mainly micro- and nanoplastics, actively penetrate trophic chains since marine inhabitants feeding on plastic particles mistake them for food objects [21,23]. Swallowed plastic particles damage internal organs; have a negative impact on the nervous, reproductive, and immune systems; and stop cell growth and reproduction by releasing chemicals inside the body [24–26]. At the biochemical level, active generation of free radicals and changes in metabolic processes are observed in cells. Thus, polymers pose a serious threat to marine organisms, being a multiple stressor due to their negative properties. Various studies at the molecular level have shown that plastics disrupt the redox balance in cells of living organisms, described in the literature as oxidative stress [27–29]. Molecular markers (biomarkers) of oxidative stress—the earliest indicators of environmental pollution—are used to diagnose such changes at different stages. As a rule, the use of these markers in ecotoxicological monitoring assumes a reliable correlation between the activity of metabolic processes and the level of environmental pollution [13,29,30].

Fragments of products made from polyethylene and polystyrene are the most common in plastic pollution both on land and in the ocean. These polymers are massively used around the world in applications ranging from light industry to medicine [31,32]. Moreover, the most commonly used items made from these types of plastic are disposable items [2,6]. In recent decades, the level of plastic waste pollution, dominated by polystyrene and polyethylene, has been increasing in the coastal zones of the Asia–Pacific region due to the increase in population density in the region and the associated increasing of economic activity in the region [33,34]. In order to understand the effects of this pollution, it is necessary to study the responses of hydrobionts to different types of plastics and their additives that are leached into the marine environment.

Therefore, the aim of this study was to evaluate the effects of polyethylene macrofragments and polystyrene microparticles on the Pacific mussel *Mytilus trossulus* and to carry out a comparative assessment of the toxicity of certain types of plastic on filter-feeding mollusks. To evaluate the toxic effect of polymers on living organisms, markers of oxidative stress were used: stability of lysosome membranes, DNA molecule damage, changes in the

level of lipid peroxidation products, and integrated assessment of the level of antioxidant system activity.

2. Materials and Methods

2.1. Site of Bivalves Collection

Adults *M. trossulus* of equal age and size (6.1 ± 0.9 cm) were collected in the marine experimental station "Popov Island" of the Alekseev Bay in the Sea of Japan (42°59′ N; 131°43′ E). Mollusks were acclimated for 168 h in laboratory conditions in glass tanks in natural seawater. The water temperature in the tanks was +16 °C and salinity was 32.6‰. Water and air temperature were recorded every 12 h. During the period of acclimation and experiment, the mollusks where not fed.

2.2. Description of the Experiments

Two experiments were carried out. Experiment 1 (with HDPE fragments) was conducted for 72 h in two tanks—"control" (without exposure) and "experiment". The volume of water in each tank was 25 L. There was 0.5 L of water for each mollusk. HDPE fragments were placed in the experimental tank with mussels. As HDPE fragments in the work, we used the film (produced in Russia, State Standard for HDPE film (16338-85)). The area of one fragment was 0.01 m^2, the total area of fragments per experimental tank was 1 m^2 (0.04 m^2/L). The aeration of water in the tanks was carried out with the help of compressors, which, at the same time, created intensive wave flows of water, contributing to the washing out of intrinsic organic substances of the polyethylene film. During the experiment the filtration system was switched off, the water in the tanks with HDPE fragments and control did not change.

Experiment 2 (with polystyrene microspheres—μPS) lasted 72 h. Mussels were placed in the "control" (without exposure) and "experimental" tanks, with the rate of 0.5 L of water per one mussel. The volume of water in each tank was 25 L. The water and air temperature during the experiment was stable (+16 °C). Water and air temperatures were recorded every 12 h. μPS solution was added to the experimental tank with mollusks at a concentration of 10^5 pcs/L. A standard solution of μPS (Cat. №6-1-0090, Tianjin BaseLine ChromTech Research Centre, China) was used to prepare a working solution of "microplastic". The diameter of the microspheres was 0.9 μm. Water aeration in the tanks was carried out using compressors, which simultaneously created intense wave water flows, allowing the microspheres to remain in the water column and not settle to the bottom of the tank, as well as washing out their own persistent organic matter. Water changes in the control tank and with μPS were performed every 24 h. During the experiment, the filtration system was switched off; the water in the tanks with microspheres PS and control was not changed.

No mortality of *M. trossulus* was observed during both experiments. At the end of the exposure time in both experiments, 20 *M. trossulus* individuals from the control and experimental groups were used to determine the stability of the lysosomal membrane, 15 were used to determine % DNA damage, and 10 were used to prepare homogenates for the determination of MDA content and an index of antiradical activity.

All procedures in the present work, as well as the mollusks disposal methods, were approved by the Commission on Bioethics at the V.I. Il'ichev Pacific Oceanological Institute, Far Eastern Branch of Russian Academy of Science (protocol №16 and date of approval 15 April 2021), Vladivostok, Russia.

2.3. Cytochemical Methods

The level of DNA damage was determined using the alkaline comet assay, which is adapted to marine organisms [35]. Mollusks gills and the digestive gland were removed and gently cut in isotonic solution; then, gel slides were prepared (an amount of 50 μL of cell suspension was mixed with low gelling temperature agarose (100 μL), cell–agarose suspension was stirred and transferred to a slide containing normal gelling temperature agarose and covered with a coverslip), and the slide was then incubated in the lysis

solution for 1 h in a light-protected place at 4 °C. After this, the slides were incubated in electrophoresis buffer (pH > 13) for 40 min. This was followed by electrophoresis for 15 min. After neutralization, the slides were stained with SYBR Green. The DNA comets were visualized and registered using a scanning fluorescence microscope (Carl Zeiss, AxioImager A1) equipped with a digital camera AxioCam MRc. The mollusks in the control and experimental groups were analyzed with 15 slides per group (1 slide = 1 mussel). Each slide contained no less than 50 comets. The program Casp 1.2.2 software (CASPlab, Wroclaw, Poland) was used to process digital images.

Lysosome membrane stability (LMS) in mollusk hemolymph was assessed using a cytochemical method based on the capture of a dye by lysosomes, the retention time of which shows the degree of damage to the membranes of the organelle [36]. Hemolymph from the mollusk closure muscle was sampled using a 1 mL hypodermic syringe. A total of 0.1 mL of hemolymph was taken from each individual. The incubation time of samples with the dye was 15 min. The stained samples were viewed under a microscope for 90 min at 15 min intervals.

2.4. Biochemical Methods

For determination of integral antiradical activity (IAA) and malonic dialdehyde (MDA) content, digestive gland and gill tissues were homogenized in chilled phosphate buffer (+4 °C) at a ratio of 1:10 g/mL (0.1 M, pH 7.0). Homogenates were centrifuged at 10,000 rpm for 40 min at +4 °C. Integral antiradical activity in tissue supernatant was determined by a method based on the ability of the antioxidant system of cells to reduce the radical cation ABTS+ [37]. Determination of the content of lipid peroxidation product-malonic dialdehyde in cells was carried out according to the colorimetric method [38].

2.5. Statistical Analysis

Statistical processing of the obtained results was performed using statistical tools MS Office Excel and Statistica 10 (StatSoft, Tulsa, OK, USA) program package: the arithmetic mean and standard deviation were calculated. The assumptions of normality and homogeneity were assessed using the Levene and Shapiro–Wilk tests, respectively. Normality was not observed, and nonparametric Mann–Whitney U-tests were performed. Differences were considered statistically significant at $p < 0.05$.

3. Results

During short-term exposure of *M. trossulus* to polymers of different types and sizes, we revealed visible changes in biochemical parameters in mollusk tissues, indicating the development of oxidative stress and destructive processes in the cellular apparatus of the cell. Exposure of mollusks to polyethylene resulted in a 2.7-fold decrease in lysosome membrane stability (LMS) of hemocytes relative to the control. In the control group, the ability of lysosome membrane to retain dye was 58 ± 4.91 min, and under PE exposure, 21.5 ± 6.5 min. In the presence of μPS in mollusk hemocytes, the NR dye retention time was also found to decrease to 65 ± 4.24 min in comparison with the control (76.14 ± 3.05 min). (Figure 1).

The results of the comet assay showed that the effects of both polyethylene and polysterol caused a significant increase in the DNA damage in the gills and digestive gland of *M. trossulus*. In the experiment on exposure to polyethylene, it was 3.4 ± 0.7 and 4.95 ± 0.68% of DNA in the tail, compared to 7.89 ± 1.01 and 8.23 ± 0.93 in the control group for the gills and digestive gland, respectively. In the presence of μPS, these values were 5.6 ± 0.36 and 3.29 ± 0.35 compared to 2.17 ± 032 and 1.43 ± 0.34% of DNA in the tail for the gills and digestive gland, respectively (Figure 2).

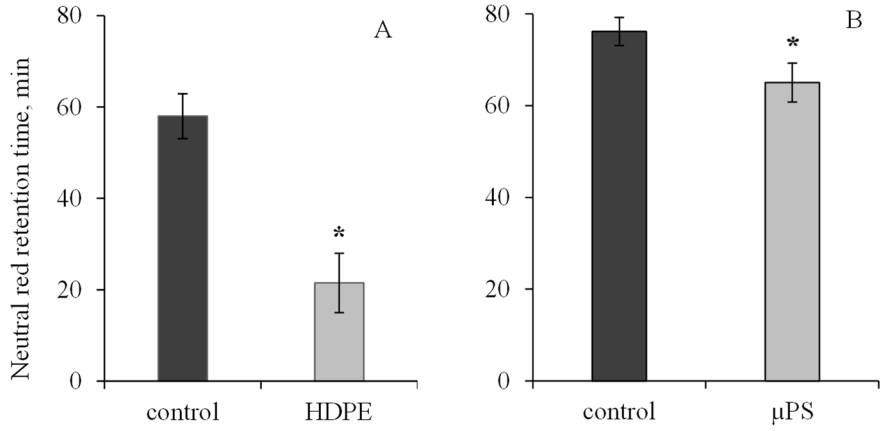

Figure 1. Changes in the lysosome membranes stability in *M. trossulus* hemolymph under the influence of different types of plastic ((**A**) high-density polyethylene fragments; (**B**) polystyrene microspheres) (mean ± standard deviation; $n = 20$). * Difference from control is significant at $p < 0.05$.

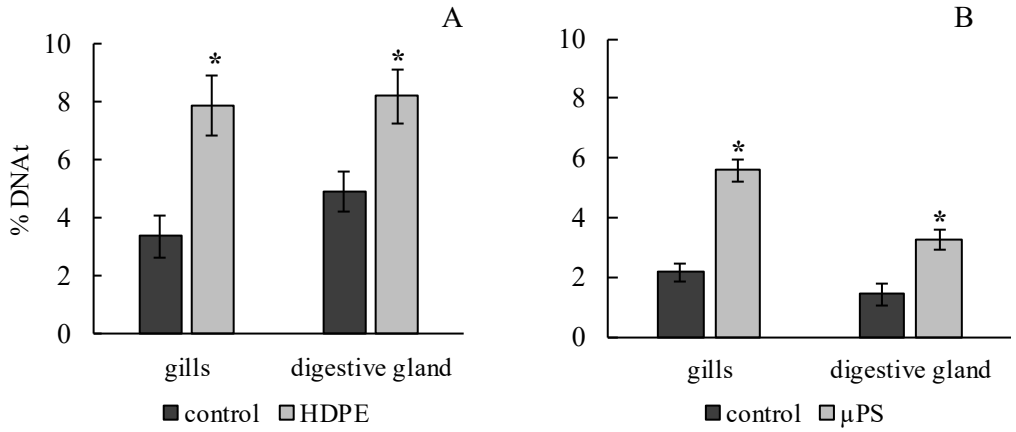

Figure 2. Damage of DNA molecule in cells of gills and digestive gland of *M. trossulus* under the influence of different types of plastic ((**A**) high-density polyethylene fragments; (**B**) polystyrene microspheres) (mean ± standard deviation; $n = 15$). * Difference from control is significant at $p < 0.05$.

The presence of PE fragments and PS microparticles in mussel tanks caused the development of lipid peroxidation processes, which led to a significant increase in MDA concentration in gill and digestive gland cells. Under the influence of PE, the MDA concentration in gills increased to 3.25 ± 0.05 mmol/g wet weight compared to the control (2.39 ± 0.09 mmol/g wet weight). In the presence of μPS in water, MDA level in gill cells also increased to 26.34 ± 2.22 mmol/g wet weight compared to control 19.2 ± 1.32 mmol/g wet weight. In digestive gland cells under PE exposure, MDA level increased to 4.34 ± 0.09 mmol/g wet weight compared to control 3.5 ± 0.073 mmol/g wet weight, with μPS increased to 47.01 ± 1.97 mmol/g wet weight against control 38.94 ± 1.69 mmol/g wet weight (Figure 3).

According to the results, the presence of plastic in tanks caused a tissue-specific reaction of the antioxidant system of mollusks. Under exposure to polyethylene and μPS, the level of integrated antiradical activity (IAA) in the gills of mollusks did not change significantly and was 11.11 ± 0.65 nmol/g wet weight 2.9 ± 0.09 nmol/g wet weight for polyethylene and μPS fragments and at control values of 15.76 ± 0.91 nmol/g wet weight and 3.34 ± 1.05 nmol/g wet weight, respectively, while in digestive gland cells, there was a significant decrease in IAA under the influence of μPS from control values of 22.87 ± 1.24 nmol/g wet weight to 19.55 ± 0.2 nmol/g wet weight. However, the effect of polyethylene caused an increase in the IAA level in digestive gland cells

to 80.61 ± 1.22 nmol/g wet weight compared to control 61.13 ± 1.9 nmol/g wet weight (Figure 4).

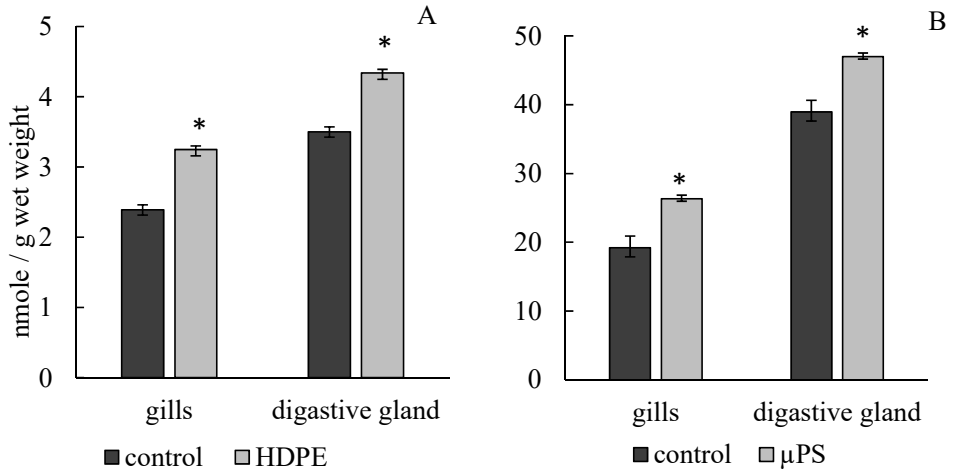

Figure 3. Changes in malonic dialdehyde content in cells of gills and digestive gland of *M. trossulus* under the influence of different types of plastic ((**A**) high-density polyethylene fragments; (**B**) polystyrene microspheres) (mean ± standard deviation; n = 10). * Difference from control is significant at $p < 0.05$.

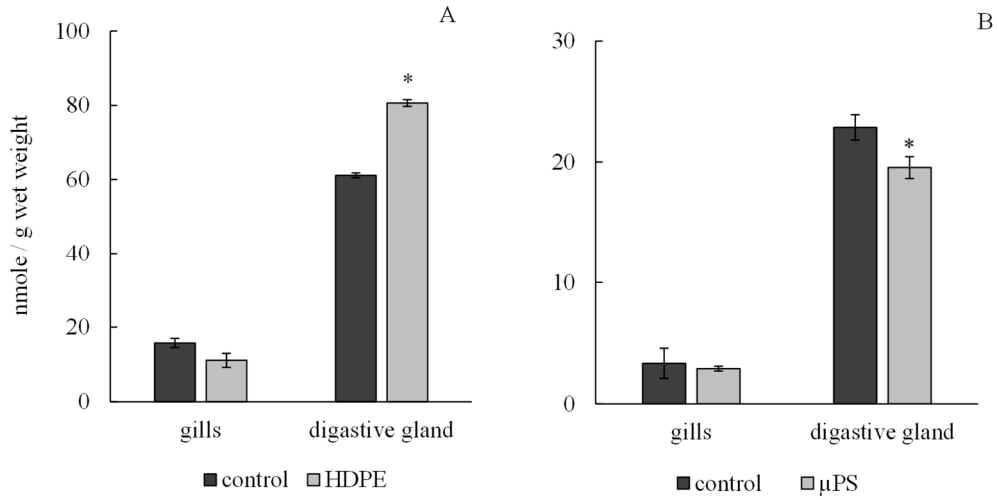

Figure 4. Changes in integral antiradical activity in cells of gills and digestive gland of *M. trossulus* under the influence of different types of plastic ((**A**) high-density polyethylene fragments; (**B**) polystyrene microspheres) (mean ± standard deviation; n = 10) * Difference from control is significant at $p < 0.05$.

4. Discussion

In this work, a short-term experimental model of 72 h was used, assuming that under these conditions, the time would be sufficient to leach some concentration of chemical additives in PE and PS [13,39–41]. Despite the short time period, the results obtained revealed significant changes in biochemical parameters in mussel tissues.

In Experiment 1, the mussels had no direct contact with HDPE. All polymer fragments were on the surface and in the water column, while the mollusks were distributed on the bottom of the aquarium and attached to it by byssus threads. In earlier studies on *Daphnia magna*, it was shown that the leaching of additives from polymers, particularly HDPE, occurs in a very short time (48 h) [12,42]. At the outcome of our short-term experiment (72 h), biomarkers indicated the toxic effects of the leached substances from HDPE and the active development of oxidative stress in mollusk tissues, which was indicated by an

increase in MDA content and a differential antioxidant system response (IAA) in mollusk tissues. The results of our studies also showed the bioavailability and toxicity of short-term effects of leachable substances from HDPE fragments on the lysosomal apparatus of mussels; in the hemolymph of experimental mollusks, the LMS decreased two-fold. Some authors have shown that a complex mixture of additives is leached from polymers into water, accumulates in the organism, and causes various processes such as lysosomal disorders, DNA molecule destruction, and, as a consequence, the development of oxidative stress [11,43–45]. In addition, studies have clearly demonstrated that the greatest toxic effect on *Mytilus galloprovincialis* mollusks is exerted by leached hydrophobic organic compounds, which activate the process of generating reactive oxygen species [45].

Microplastic particles also release endogenous substances both into the water and within the living organism. Therefore, in this case, the toxic effect of microplastics would be achieved by both mechanical and chemical damage. In the experiment with polystyrene, microparticles actively interacted with mussels by penetrating inside the mollusk with water. In our work, we used PS microspheres with a diameter of 0.9 μm, considering that particles of this size would be absorbed by mussels on par with their usual food. In bivalves, microplastic penetration has several possible pathways. Microplastics, in interaction with the gills surface, can be deposited on the gill mucus and gill epithelium or enter the mouth and then the digestive system of mollusks. But not every particle captured by the gills is ingested, as the mussels' selectivity allows them to sort out inedible or large particles like pseudofeces. However, particles that are smaller in size than their normal food are freely ingested and more easily digested by the mollusks [39,46]. Early studies have already shown the ability of mussels to absorb polystyrene microspheres ranging in size from 3 to 10 μm and transport them into the circulatory system [13,47]. Penetration of microplastics of different sizes into organs and tissues of mollusks favors their active accumulation in the gut. Microspheres of different polymers, ranging in size from 0.1 to 90 μm, have been shown to concentrate within hours in the digestive organs and other tissues of *Mytilus* sp. and to remain there for a long time [39]. Larger particles (>20 μm) are removed from the body first, whereas smaller particles are still present in the gut and hemolymph after their three-day purification and can migrate into the bloodstream, persisting there for up to 48 days [39,48]. Subsequent uptake of the polymeric microspheres by the surface of the gastrointestinal tract occurs by endocytosis and by granulocytes. Then, the microspheres are transported to lysosomes, hemolymph, and other organs [39,40,49,50]. This indicates the direct contact of polymer microparticles with cell organelles.

According to these studies, the 0.9 μm μPS used in our work could actively settle on the gills, penetrate the digestive tract, and hemolymph, affecting each tissue directly. Intensive accumulation of lipid oxidation products and decreased antioxidant activity in the cells of the organs studied also indicated the toxic effect of μPS and the development of oxidative stress in the mollusk organism. It was shown that even short-term exposures of polymers' microparticles to the hydrobionts organs and tissues cells resulted in the formation of oxyradicals and stress proteins, changes in the activity of anti-radical enzymes and the anti-radical system, the accumulation of lipid oxidation products, the destabilization of lysosome membranes, DNA molecule damage, and histological changes and inflammatory reactions with the formation of granulocytes [13,41,51]. At the cellular level, this is shown by the disruption of the DNA molecule structure, the destabilization of lysosomal membranes, and lysosomal compartmentalization, with the effects increasing with chronic exposure [27,47,52]. In mussel gill and digestive gland cells exposed to μPS, we observed the highest rates of DNA damage compared to exposure to HDPE fragments. Comet assay and LMS determination allowed us to efficiently assess short-term exposure to microplastics, and this proved to be one of the sensitive methods in our experiment. Compared to HDPE fragments, the bioavailability of which is related only to washed out additives, μPS possess several mechanisms of effect on the organism that act at once—the release of their own toxic compounds, mechanical damage during their penetration into mollusk organs and tissues, and the generation of oxyradicals.

5. Conclusions

Despite the toxicity of both types of polymers, the bioavailability of microplastics to filter-feeding mollusks is higher and more dangerous compared to mesoplastics. The investigated polymers cause a serious threat to the biological system of filter feeding mollusks, irrespective of size and species. The toxic effects of polymers are shown at the genetic and biochemical level; therefore, analyzing the effects of different types of plastics from macro- to micro-size is important in environmental and organismal risk assessment.

Author Contributions: Conceptualization, N.V.D., V.V.S. and V.P.C.; methodology, N.V.D., V.V.S., and A.A.I.; software, S.P.K.; validation, N.V.D., V.V.S. and V.P.C.; formal analysis, N.V.D., S.P.K., A.A.M., A.A.I. and D.D.B.; investigation, N.V.D., V.V.S., S.P.K. and A.A.M.; resources, N.V.D. and V.P.C.; data curation, N.V.D.; writing—original draft preparation, N.V.D.; writing—review and editing, N.V.D., V.V.S. and S.P.K.; visualization, S.P.K. and A.A.M.; supervision, N.V.D., V.V.S. and V.P.C.; project administration, V.P.C.; funding acquisition, N.V.D. All authors have read and agreed to the published version of the manuscript.

Funding: The study was supported by a grant from the Russian Science Foundation, № 23-27-00361 (https://rscf.ru/en/project/23-27-00361/) (accessed on 16 April 2024).

Institutional Review Board Statement: Not applicable.

Informed Consent Statement: Not applicable.

Data Availability Statement: Dataset available on request from the authors.

Conflicts of Interest: The authors declare no conflicts of interest.

References

1. Kibria, M.G.; Masuk, N.I.; Safayet, R.; Nguyen, H.Q.; Mourshed, M. Plastic Waste: Challenges and Opportunities to Mitigate Pollution and Efective Management. *Int. J. Environ. Res.* **2023**, *17*, 20. [CrossRef] [PubMed]
2. Feldman, M.; Cowger, W.; Erdle, L.M.; Coffin, S.; Villarrubia-Gómez, P.; Moore, C.J.; Carpenter, E.J.; Day, R.H.; Thiel, M.; Wilcox, C. A growing plastic smog, now estimated to be over 170 trillion plastic particles afloat in the world's oceans—Urgent solutions required. *PLoS ONE* **2023**, *18*, e0281596. [CrossRef]
3. Bandow, N.; Will, V.; Wachtendorf, V.; Simon, F.G. Contaminant release from aged microplastic. *Environ. Chem.* **2017**, *14*, 394–405. [CrossRef]
4. Thushari, G.G.N.; Senevirathna, J.D.M. Plastic pollution in the marine environment. *Heliyon* **2020**, *6*, e04709. [CrossRef] [PubMed]
5. Kako, S.; Isobe, A.; Kataoka, T.; Hinata, H. A decadal prediction of the quantity of plastic marine debris littered on beaches of the East Asian marginal seas. *Mar. Pollut. Bull.* **2014**, *81*, 174–184. [CrossRef]
6. Jang, Y.; Kim, K.N.; Woo, J.R. Post-consumer plastic packaging waste from online food delivery services in South Korea. *Waste Manage* **2023**, *156*, 177–186. [CrossRef]
7. Dimitriadi, A.; Papaefthimiou, C.; Genizegkini, E.; Sampsonidis, I.; Kalogiannis, S.; Feidantsis, K.; Bobori, D.C.; Kastrinaki, G.; Koumoundouros, G.; Lambropoulou, D.A.; et al. Adverse effects polystyrene microplastics exert on zebrafish heart—Molecular to individual level. *J. Hazard. Mater.* **2021**, *416*, 125969. [CrossRef]
8. He, S.; Wang, J.; Zhou, L.; Mao, Z.; Zhang, X.; Cai, J.; Huang, P. Enhanced hepatic metabolic perturbation of polystyrene nanoplastics by UV irradiation-induced hydroxyl radical generation. *J. Environ. Sci.* **2024**, *142*, 259–268. [CrossRef]
9. Trifuoggi, M.; Pagano, G.; Oral, R.; Hamer, D.; Burić, P.; Kovačić, I.; Siciliano, A.; Toscanesi, M.; Thomas, P.J.; Paduano, L.; et al. Microplastic-induced damage in early embryonal development of sea urchin Sphaerechinus granularis. *Environ. Res.* **2019**, *179*, 108815. [CrossRef]
10. Silva, M.S.S.; Pires, A.; Vethaak, D.; Martínez-G'omez, C.; Almeida, M.; Pinto, R.; Figueira, E.; Oliveira, M. Effects of polymethylmethacrylate nanoplastics on the polychaete Hediste diversicolor: Behavioural, regenerative, and biochemical responses. *Aquat. Toxicol.* **2023**, *265*, 106743. [CrossRef]
11. Capolupo, M.; Sørensen, L.; Jayasena, K.D.R.; Booth, A.M.; Fabbri, E. Chemical composition and ecotoxicity of plastic and car tire rubber leachates to aquatic organisms. *Water Res.* **2020**, *69*, 115270. [CrossRef] [PubMed]
12. Lithner, D.; Damberg, J.; Dave, G.; Larsson, Å. Leachates from plastic consumer products—Screening for toxicity with *Daphnia magna*. *Chemosphere* **2009**, *74*, 1195–1200. [CrossRef]
13. Revel, M.; Yakovenko, N.; Caley, T.; Guillet, C.; Chatel, A.; Mouneyrac, C. Accumulation and immunotoxicity of microplastics in the estuarine worm Hediste diversicolor in environmentally relevant conditions of exposure. *Environ. Sci. Pollut. Res.* **2018**, *27*, 3574–3583. [CrossRef] [PubMed]

14. Teuten, E.L.; Saquing, J.M.; Knappe, D.R.U.; Barlaz, M.A.; Jonsson, S.; Bjorn, A.; Rowland, S.J.; Thompson, R.C.; Galloway, T.S.; Yamashita, R.; et al. Transport and release of chemicals from plastics to the environment and to wildlife. *Philos. Trans. R. Soc.* **2009**, *364*, 2027–2045. [CrossRef]
15. Mato, Y.; Isobe, T.; Takada, H.; Kanehiro, H.; Ohtake, C.; Kaminuma, T. Plastic resin pellets as a transport medium for toxic chemicals in the marine environment. *Environ. Sci. Technol.* **2001**, *35*, 318–324. [CrossRef]
16. Lithner, D.; Larsson, A.; Dave, G. Environmental and health hazard ranking and assessment of plastic polymers based on chemical composition. *Sci. Total Environ.* **2011**, *409*, 3309–3324. [CrossRef]
17. Bejgarn, S.; MacLeod, M.; Bogdal, C.; Breitholtz, M. Toxicity of leachate from weathering plastics: An exploratory screening study with *Nitocra spinipes*. *Chemosphere* **2015**, *132*, 114–119. [CrossRef] [PubMed]
18. Lambert, S.; Wagner, M. Characterisation of nanoplastics during the degradation of polystyrene. *Chemosphere* **2016**, *145*, 265–268. [CrossRef]
19. Menéndez-Pedriza, A.; Jaumot, J. Interaction of environmental pollutants with microplastics: A critical review of sorption factors, bioaccumulation and ecotoxicological effects. *Toxics* **2020**, *8*, 40. [CrossRef]
20. Galloway, T.S.; Cole, M.; Lewis, C. Interactions of microplastic debris throughout the marine ecosystem. *Nat. Ecol. Evol.* **2017**, *1*, 116. [CrossRef]
21. Santana, M.F.M.; Moreira, F.T.; Turra, A. Trophic transference of microplastics under a low exposure scenario: Insights on the likelihood of particle cascading along marine food-webs. *Mar. Pollut. Bull.* **2017**, *121*, 154–159. [CrossRef] [PubMed]
22. Hermabessiere, L.; Dehaut, A.; Paul-Pont, I.; Lacroix, C.; Jezequel, R.; Soudant, P.; Duflos, G. Occurrence and effects of plastic additives on marine environments and organisms: A review. *Chemosphere* **2017**, *182*, 781–793. [CrossRef] [PubMed]
23. Carbery, M.; O'Connor, W.; Palanisami, T. Trophic transfer of microplastics and mixed contaminants in the marine food web and implications for human health. *Environ Int.* **2018**, *115*, 400–409. [CrossRef] [PubMed]
24. Nobre, C.R.; Santana, M.F.M.; Maluf, A.; Cortez, F.S.; Cesar, A.; Pereira, C.D.; Turra, A. Assessment of microplastic toxicity to embryonic development of the sea urchin *Lytechinus variegatus* (Echinodermata: Echinoidea). *Mar. Pollut. Bull.* **2015**, *92*, 99–104. [CrossRef]
25. Foley, C.J.; Feiner, Z.S.; Malinich, T.D.; Höök, T.O. A meta-analysis of the effects of exposure to microplastics on fish and aquatic invertebrates. *Sci. Total Environ.* **2018**, *631–632*, 550–559. [CrossRef]
26. Varo, I.; Perini, A.; Torreblanca, A.; Garcia, Y.; Bergami, E.; Vannuccini, M.L.; Corsi, I. Time-dependent effects of polystyrene nanoparticles in brine shrimp *Artemia franciscana* at physiological, biochemical and molecular levels. *Sci. Total Environ.* **2019**, *675*, 570–580. [CrossRef]
27. Avio, C.G.; Gorbi, S.; Milan, M.; Benedetti, M.; Fattorini, D.; D'Errico, G.; Pauletto, M.; Bargelloni, L.; Regoli, F. Pollutants bioavailability and toxicological risk from microplastics to marine mussels. *Environ. Pollut.* **2015**, *198*, 211–222. [CrossRef]
28. Gambardella, C.; Morgana, S.; Bari, G.D.; Ramoino, P.; Bramini, M.; Diaspro, A.; Falugi, C.; Faimali, M. Multidisciplinary screening of toxicity induced by silica nanoparticles during sea urchin development. *Chemosphere* **2015**, *139*, 486–495. [CrossRef] [PubMed]
29. Gonzalez-Soto, N.; Hatfield, J.; Katsumiti, A.; Duroudier, N.; Lacave, J.M.; Bilbao, E.; Orbea, A.; Navarro, E.; Cajaraville, M.P. Impacts of dietary exposure to different sized polystyrene microplastics alone and with sorbed benzo[a]pyrene on biomarkers and whole organism responses in mussels *Mytilus galloprovincialis*. *Sci. Total. Environ.* **2019**, *684*, 548–566. [CrossRef]
30. Istomina, A.; Chelomin, V.; Kukla, S.; Zvyagintsev, A.; Karpenko, A.; Slinko, E.; Dovzhenko, N.; Slobodskova, V.; Kolosova, L. Copper effect on the biomarker state of the Mizhuhopecten yessoensis tissues in the the prespawning period. *Environ. Toxicol. Pharm.* **2019**, *70*, 103189. [CrossRef]
31. Hong, S.; Lee, J.; Kang, D.; Choi, H.W.; Ko, S.H. Quantities, composition, and sources of beach debris in Korea from the results of nationwide monitoring. *Mar. Pollut. Bull.* **2014**, *84*, 27–34. [CrossRef] [PubMed]
32. Turner, A. Foamed polystyrene in the marine environment: Sources, additives, transport, behavior, and impacts. *Environ. Sci. Technol.* **2020**, *54*, 10411–10420. [CrossRef] [PubMed]
33. Jang, Y.C.; Lee, J.; Hong, S.; Mok, J.Y.; Kim, K.S.; Lee, Y.J. Estimation of the annual flow and stock of marine debris in South Korea for management purposes. *Mar. Pollut. Bull.* **2014**, *86*, 505–511. [CrossRef] [PubMed]
34. Lee, J.; Hong, S.; Song, Y.K.; Hong, S.H.; Jang, Y.C.; Jang, M.; Heo, N.W.; Han, G.M.; Lee, M.J.; Kang, D.; et al. Relationships among the abundances of plastic debris in different size classes on beaches in South Korea. *Mar. Pollut. Bull.* **2013**, *77*, 349–354. [CrossRef]
35. Kukla, S.P.; Slobodskova, V.V.; Zhuravel, E.V.; Mazur, A.A.; Chelomin, V.P. Exposure of adult sand dollars (*Scaphechinus mirabilis*) (Agassiz, 1864) to copper oxide nanoparticles induces gamete DNA damage. *Environ. Sci. Pollut. Res.* **2022**, *29*, 39451–39460. [CrossRef]
36. Martinez-Gomez, C.; Bignell, J.; Lowe, D. Lysosoma membrane stability in mussels. *ICES Tech. Mar. Environ. Sci.* **2015**, *56*, 41. [CrossRef]
37. Bartosz, G.; Janaszewska, A.; Ertel, D.; Bartosz, M. Simple determination of peroxyl radical-trapping capacity. *Biochem. Mol. Biol. Int.* **1998**, *46*, 519–528. [CrossRef]
38. Buege, J.A.; Aust, S.D. Microsomal lipid peroxidation. *Methods Enzymol.* **1978**, *52*, 302–310. [CrossRef]
39. Li, J.; Lusher, A.L.; Rotchell, J.M.; Deudero, S.; Turra, A.; Bråte, I.L.N.; Sun, C.; Hossain, M.; Li, Q.; Kolandhasamy, P.; et al. Using mussel as a global bioindicator of coastal microplastic pollution. *Environ. Pollut.* **2019**, *244*, 522–533. [CrossRef]

40. Wang, S.; Hu, M.; Zheng, J.; Huang, W.; Shang, Y.; Fang, J.K.-H.; Shi, H.; Wang, Y. Ingestion of nano/micro plastic particles by the mussel *Mytilus coruscus* is size dependent. *Chemosphere* **2021**, *263*, 127957. [CrossRef]
41. Paul-Pont, I.; Lacroix, C.; Fernandez, C.G.; Hegaret, H.; Lambert, C.; Le Goic, N.; Frere, L.; Cassone, A.L.; Sussarellu, R.; Fabioux, C.; et al. Exposure of marine mussels *Mytilus* spp. to polystyrene microplastics: Toxicity and influence on fluoranthene bioaccumulation. *Environ. Pollut.* **2016**, *216*, 724–737. [CrossRef] [PubMed]
42. Lithner, D.; Nordensvan, I.; Dave, G. Comparative acute toxicity of leachates from plastic products made of polypropylene, polyethylene, PVC, acrylonitrile–butadiene–styrene, and epoxy to *Daphnia magna*. *Environ. Sci. Pollut. Res.* **2012**, *19*, 1763–1772. [CrossRef] [PubMed]
43. Kwon, B.G.; Amamiya, K.; Sato, H.; Chung, S.Y.; Kodera, Y.; Kim, S.K.; Lee, E.J.; Saido, K. Monitoring of styrene oligomers as indicators of polystyrene plastic pollution in the North-West Pacific Ocean. *Chemosphere* **2017**, *180*, 500–505. [CrossRef] [PubMed]
44. Lee, S.; Alam, M.B.; Lee, S.H.; Jung, M.J.; Shim, W.J.; Kim, S. Identification and quantification of photodegradation products of disposed expanded polystyrene buoy used in aquaculture. *Mar. Pollut. Bull.* **2023**, *192*, 114998. [CrossRef] [PubMed]
45. Vilke, J.M.; Fonseca, T.G.; Alkimin, G.D.; Gonçalves, J.M.; Edo, C.; Errico, G.; Seilitz, F.S.; Rotander, A.; Benedetti, M.; Regoli, F.; et al. Looking beyond the obvious: The ecotoxicological impact of the leachate from fishing nets and cables in the marine mussel Mytilus galloprovincialis. *J. Hazard. Mater.* **2024**, *473*, 134479. [CrossRef]
46. Anbumani, S.; Kakkar, P. Ecotoxicological effects of microplastics on biota: A review. *Environ. Sci. Pollut. Res.* **2018**, *25*, 14373–14396. [CrossRef]
47. Von Moos, N.; Burkhardt-Holm, P.; Köhler, A. Uptake and effects of microplastics on cells and tissue of the blue mussel *Mytilus edulis* L. after an experimental exposure. *Environ. Sci. Technol.* **2012**, *46*, 11327–11335. [CrossRef]
48. Browne, M.A.; Dissanayake, A.; Galloway, T.S.; Lowe, D.M.; Thompson, R.C. Ingested microscopic plastic translocates to the circulatory system of the mussel, *Mytilus edulis* (L). *Environ. Sci. Technol.* **2008**, *42*, 5026–5031. [CrossRef]
49. Kolandhasamy, P.; Su, L.; Li, J.; Qul, X.; Jabeen, K.; Shi, H. Adherence of microplastics to soft tissue of mussels: A novel way to uptake microplastics beyond ingestion. *Sci. Total Environ.* **2018**, *610–611*, 635–640. [CrossRef]
50. Sıkdokur, E.; Belivermisë, M.; Sezer, N.; Pekmez, M.; Bulan, O.K.; Kılıc, O. Effects of microplastics and mercury on manila clam *Ruditapes philippinarum*: Feeding rate, immunomodulation, histopathology and oxidative stress. *Environ. Pollut.* **2020**, *262*, 114247. [CrossRef]
51. Liu, P.; Qian, L.; Wang, H.; Zhan, X.; Lu, K.; Gu, C.; Gao, S. New insights into the aging behavior of microplastics accelerated by advanced oxidation processes. *Environ. Sci. Technol.* **2019**, *53*, 3579–3588. [CrossRef] [PubMed]
52. Bråte, L.N.; Hurley, R.; Iversen, K.; Beyer, J.; Thomas, K.V.; Steindal, C.C.; Green, N.W.; Olsen, M.; Lusher, A. *Mytilus* spp. as sentinels for monitoring microplastic pollution in Norwegian coastal waters: A qualitative and quantitative study. *Environ. Pollut.* **2018**, *243*, 383–393. [CrossRef] [PubMed]

Journal of *Xenobiotics*

MDPI

Article

Impact of Legacy Perfluorooctane Sulfonate (PFOS) and Perfluorooctanoate (PFOA) on GABA Receptor-Mediated Currents in Neuron-Like Neuroblastoma Cells: Insights into Neurotoxic Mechanisms and Health Implications

Laura Lagostena [1,*], Davide Rotondo [2], Davide Gualandris [2], Antonio Calisi [2], Candida Lorusso [2], Valeria Magnelli [2] and Francesco Dondero [2,*]

[1] IBF-CNR, 16149 Genova, Italy
[2] Department of Science and Technological Innovation, Università del Piemonte Orientale, 15121 Alessandria, Italy; davide.rotondo@uniupo.it (D.R.); davide.gualandris@uniupo.it (D.G.); antonio.calisi@uniupo.it (A.C.); candida.lorusso@uniupo.it (C.L.); valeria.magnelli@uniupo.it (V.M.)
* Correspondence: laura.lagostena@ibf.cnr.it (L.L.); francesco.dondero@uniupo.it (F.D.)

Abstract: Perfluorooctane sulfonate (PFOS) and perfluorooctanoic acid (PFOA) are persistent environmental pollutants, raising concerns due to their widespread presence and disruptive biological effects. These compounds are highly stable, allowing them to bioaccumulate in the environment and living organisms, potentially impacting critical physiological functions such as hormonal balance, immune response, and increasing cancer risk. Despite regulatory restrictions, their pervasive nature necessitates further research into their potential effects on cellular and neuronal function. This study first evaluated the cytotoxic effects of PFOS and PFOA on S1 neuroblastoma cells; a dose-dependent reduction in cell viability was revealed for PFOS, while PFOA exhibited minimal toxicity until millimolar concentrations. We further investigated their potential to modulate GABAergic neurotransmission using patch-clamp electrophysiology. Both PFOS and PFOA caused a significant but reversible reduction in GABA receptor-mediated currents following one-minute pre-treatment. These findings suggest that PFOS and PFOA can interfere with both cellular viability and GABAergic signaling, providing critical insights into their functional impacts and highlighting the need for further investigation into the long-term consequences of PFAS exposure on nervous system health.

Keywords: electrophysiology; GABAergic signaling; neurotoxicity; PFAS; persistence; toxicology

1. Introduction

Perfluorooctane sulfonate (PFOS) and perfluorooctanoate (PFOA) are notorious environmental contaminants that fall under the extensive category of per- and polyfluoroalkyl substances (PFAS). Renowned for their multiple industrial applications such as aqueous film forming foams (AFFFs), fluoropolymer resins, water- and stain-resistant additives, these chemicals have sparked growing alarm due to their extraordinary persistence in the environment, their ability to bioaccumulate in living organisms, and their potential for long term toxicity including cancer [1]. Of particular concern is the impact of PFOS and PFOA on the nervous system, which is especially susceptible to damage. These compounds can penetrate the blood–brain barrier [2] and accumulate within the brain, in which emerging research indicates they may interfere with normal neuronal function and contribute to neurotoxicity [3]. Although regulatory measures have phased out the production of PFOS and PFOA in many regions, these legacy PFAS compounds remain highly relevant due to their environmental persistence and bioaccumulation potential. While next-generation PFAS compounds are under investigation, these legacy compounds continue to serve as essential models for understanding the persistent impacts of PFAS on human health. Studies across various species, including humans, fish, and polar bears, have documented PFAS

accumulation in specific brain regions. Recent findings suggest that PFAS, particularly PFOS, concentrate disproportionately in protein-rich regions of the brain, such as the hypothalamus [4], which is critical for neuroendocrine regulation. This selective accumulation implies that even low environmental exposures may lead to significant buildup in key neuroendocrine centers, potentially disrupting GABAergic signaling and other essential physiological processes.

Furthermore, recent studies have detected relatively high concentrations of PFOA and total PFAS in the brains of potentially exposed individuals [5], indicating that chronic, low-dose environmental exposures can result in meaningful accumulation over time. Given this context, our study used controlled, elevated doses of PFAS to elucidate potential acute effects on GABAergic signaling, providing a mechanistic foundation that could relate to cumulative impacts in chronic exposure scenarios.

One crucial aspect of neuronal function involves gamma-aminobutyric acid (GABA) receptors, which play a pivotal role in maintaining the excitatory–inhibitory balance in the brain. GABA receptors, particularly the $GABA_A$ subtype, mediate inhibitory synaptic transmission and are essential for various neurological processes, including anxiety modulation, muscle relaxation, and seizure prevention. Disruption of $GABA_A$ receptor-mediated currents can, therefore, have profound implications for brain function and overall health. $GABA_A$ receptors are crucial components of the nervous system, functioning as ligand-gated chloride channels that play a key role in inhibitory neurotransmission. These receptors are composed of five subunits arranged in a pentameric structure, with each subunit drawn from a diverse set of possibilities. In humans, researchers have identified 19 distinct genes that encode the subunits of $GABA_A$ receptors. These include six α (1–6), three β (1–3), three γ (1–3), three ρ (1–3), and one each for δ, ε, π, and θ subunits [6,7]. The vast diversity observed in $GABA_A$ receptors stems from the multiple ways these subunits can combine, which is further enhanced by the alternative splicing of several genes. This alternative splicing process allows a single gene to produce multiple different subunit variants, thereby significantly expanding the potential combinations and functional diversity of the receptors. This diversity is critical, as it enables $GABA_A$ receptors to fulfill a wide range of functions in various regions of the brain and to modulate neuronal activity in response to different physiological, and pharmacological stimuli [8–10]. The $\alpha1\beta2\gamma2$ subtype is the predominant form in the mammalian nervous system, representing a significant majority. It is estimated that this specific configuration may constitute as much as 60% of all $GABA_A$ receptors [9], highlighting its crucial role in functioning and regulation of neural activity [11]. $GABA_A$ receptors are ligand-gated chloride channels, made by pentameric combination of different subunits. $GABA_A$ receptor subunits share a common structure. Each mature subunit consists of approximately 450 amino acid residues and includes several key regions: an N-terminal region, a large hydrophilic extracellular domain (ECD), and four hydrophobic transmembrane domains (TMD: TM1–TM4). The TM2 domain is thought to form the pore of the chloride channel, while an intracellular domain (ICD) located between TM3 and TM4 serves as a critical site for protein interactions and post-translational modifications that regulate receptor activity [12,13]. The neurotransmitter GABA, along with psychotropic drugs like benzodiazepines (BZDs), binds to the N-terminal at the α–β and α–γ interfaces, respectively. Additionally, neurosteroids and anesthetics such as barbiturates interact within the TMD of the α and β subunits [14,15]. Several GABAergic insecticides, despite their diverse chemical structures, act as noncompetitive antagonists by binding to the same GABA receptor site located in the TM2 domain. Compounds such as β-endosulfan, lindane, and fipronil, along with botanical agents like picrotoxinin, target the chloride channel pore of the GABA receptor, blocking ion flow and leading to neural hyperexcitation, which is critical for insecticidal action and human neurotoxicity [16].

This study aimed to investigate the impact of PFOS and PFOA on GABA receptor-mediated currents in neuron-like neuroblastoma cells, providing insights into the neurotoxic mechanisms of these pollutants. For this purpose, we utilized the S1 neuroblastoma cell line, a specialized derivative of the SK-N-BE(2) cell line, specifically developed to

express functional $GABA_A$ receptors. Unlike standard SH-SY5Y cells, which do not exhibit GABA-evoked responses [17], the S1 line is especially suited for examining PFAS effects on GABAergic signaling, offering a controlled study model for preliminary toxicology assessment [18]. This research directly reveals how legacy PFAS affect neuron-like cells, representing a major advancement in our understanding. By examining the interactions between PFOS, PFOA, and $GABA_A$ receptors, we seek to uncover how these interactions may disrupt neuronal activity. This knowledge will help elucidate the broader health implications of exposure to these widespread environmental contaminants. The study not only deepens our understanding of PFAS-induced neurotoxicity but also highlights the urgent need for stringent regulatory measures to limit exposure and protect public health. The findings are expected to prompt policy changes and interventions aimed at reducing the prevalence of these harmful substances, thereby safeguarding both human health and environmental integrity.

2. Materials and Methods

2.1. Cell Culture

S1 neuroblastoma cells were maintained as reported in [18]. Briefly, cells were grown in RPMI 1640 medium supplied with 10% FBS, 2 mM L-Glu, 100 μg/mL penicillin–streptomycin, 200 μg/mL geneticin sulfate (G418), and kept at 37 °C in a 5% CO_2 incubator. All chemicals were purchased from Merck (Sigma-Aldrich, Milan, Italy).

2.2. Cytotoxicity Assay

Cells were seeded in 96 multiwell plates (Greiner) at a density of 5×10^3 cells per well in complete medium as described in Section 2.1. Once settled, the medium was removed and replaced with fresh medium containing varying concentrations of PFOA and PFOS to assess their impact on cell viability. The plates were incubated for 72 h at 37 °C in a 5% CO_2 atmosphere to allow for cell adhesion, proliferation, and PFAS exposure. Following this incubation, resazurin was added to each well at a concentration of 0.1 mg/mL. The plates were further incubated for 2 h under the same conditions, after which fluorescence was measured using a Tecan Infinite 200 Pro fluorimeter (Tecan Group Ltd., Männedorf, Switzerland) (excitation 535 nm, emission 590 nm) to quantify the reduction of resazurin to resorufin, indicating cell viability [19] For statistics, data were evaluated for normality and homoscedasticity and analyzed using one-way analysis of variance (ANOVA), followed by Holm–Sidak's multiple comparisons test using GraphPad Prism™ 9 (GraphPad Software, San Diego, CA, USA).

2.3. Electrophysiological Recordings

S1 neuroblastoma cells were plated in 3.5 cm Petri dishes and submerged in a bath of extracellular solution containing the following (in mM): 140 NaCl, 5.4 KCl, 2 $CaCl_2$, 1 $MgCl_2$, 10 HEPES, and 10 glucose (pH adjusted to 7.4 with NaOH). Observations were performed under an inverted microscope (IMT-2, Olympus Life Science, Milan, Italy) using a 40× objective. Whole-cell patch-clamp recordings were conducted at room temperature (22–25 °C) using an Axopatch 200A amplifier (Molecular Devices, San Jose, CA, USA). Patch pipettes were fabricated from borosilicate glass capillaries (Hilgenberg, Malsfeld, Germany), pulled using a vertical pipette puller (PIP6, HEKA, Lambrecht, Germany), and filled with internal solution containing the following (in mM): 142 KCl, 2 $MgCl_2$, 2 EGTA, and 10 HEPES (pH adjusted to 7.3 with KOH). Final pipette resistance ranged from 3–5 MΩ.

After establishing a stable whole-cell configuration, cells were clamped at a holding potential (Vh) of −80 mV. Voltage-gated currents were elicited by applying voltage pulses ranging from −100 mV to +100 mV in 20 mV increments, each lasting for 20 s. GABA-evoked currents were activated by brief agonist application via a gravity-driven perfusion system localized near the patched cell. Recordings were acquired using a custom program, GePulse (http://users.ge.ibf.cnr.it/pusch/programs-mik.htm) (accessed

on 10 September 2024) on, and whole-cell currents were low-pass filtered at 2 kHz and digitized at 20 kHz.

GABA stock solution (in distilled water), picrotoxin (PTX, in DMSO), and PFOS or PFOA (in DMSO or isopropanol, respectively) were freshly prepared and added to the saline solution, ensuring the final concentration of DMSO or isopropanol remained at 0.02% (v/v) prior to each experiment. This careful preparation maintained the integrity and consistency of the experimental conditions. GABA, PTX, and PFAS were rapidly applied to patched cells using the gravity-driven perfusion system, followed by a 1 min washout period between applications to allow for receptor recovery and minimize desensitization effects. To prevent cross-contamination, PFOS and PFOA were tested on different S1 cells from separate Petri dishes.

Acquired data were analyzed offline using Clampfit 10.7 (Molecular Devices, USA) and SigmaPlot (Systat Software Inc., San Jose, CA, USA). Data are expressed as mean ± standard error, and statistical significance was determined using a paired *t*-test.

3. Results

3.1. Acute Toxicity of PFAS in S1 Cells

This study assessed the cytotoxic effects of PFOA and PFOS across a range of PFAS concentrations (Figure 1) in neuron-like S1 neuroblastoma cells. PFOA displayed a threshold response, with minimal toxicity observed until millimolar concentrations. A stimulatory effect was noted at 229 μM, followed by a sharp drop in viability only at 1.69 mM, suggesting that acute toxicity for PFOA is virtually absent at lower doses. In contrast, PFOS exhibited a dose-dependent cytotoxic response. A Weibull regression analysis for PFOS indicated a significant reduction in cell viability across a broader concentration range, with an estimated EC50 of 230.01 ± 26.31 μM, highlighting its higher acute toxicity compared to PFOA.

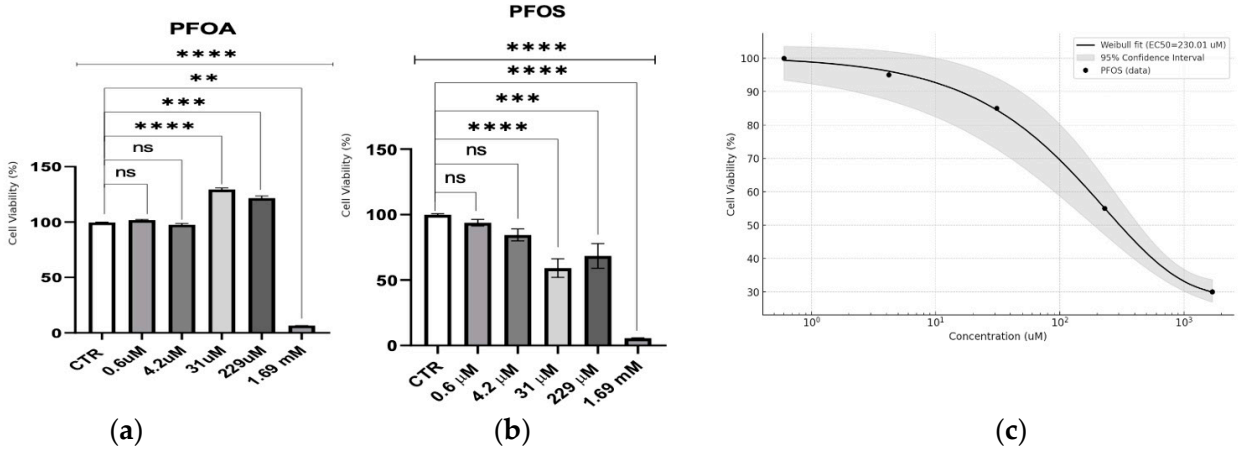

Figure 1. Cytotoxicity assessment using the Alamar Blue test on S1 neuroblastoma cells. (**a**) Dose-dependent effects of PFOA on cell viability, expressed as a percentage relative to the control (CTR). (**b**) Dose-dependent effects of PFOS on cell viability, expressed as a percentage relative to the control (CTR). The upper line represents the outcome of the statistical test, where the control group (CTR) was compared to all treated samples, regardless of concentration level. Statistical significance is indicated as follows: ns, not significant ($p > 0.05$), ** $p < 0.01$, *** $p < 0.001$, **** $p < 0.0001$. (**c**) Weibull dose-response curve for PFOS, showing the fit (solid black line) with an estimated EC50 of 230.01 μM. The 95% confidence intervals (shaded gray area) are shown, along with the averaged data points (black circles).

3.2. Electrophysiological Characterization of S1 Neuron-Like Neuroblastoma Cells

After verifying the effect of PFAS on the survival of neuron-like cells, we investigated whether these substances could exert an effect on synaptic transmission on GABA receptors.

First, to confirm the neuron-like differentiation of S1 neuroblastoma cells, we investigated the presence of voltage-dependent currents. Voltage steps of 20 mV were applied every 20 s, ranging from −100 mV to +100 mV, starting from a holding potential (Vh) of −80 mV (Figure 2a, top). This protocol revealed both inward and outward currents (Figure 2a, bottom) in all patched cells (330/330, 100%). The inward currents are indicative of Na^+-channel activity, demonstrating a typical voltage-dependent activation and inactivation pattern (Figure 2b), while the outward currents suggest K^+-channel activity, characterized by a voltage-dependent activation that is sustained over the voltage steps (Figure 2c).

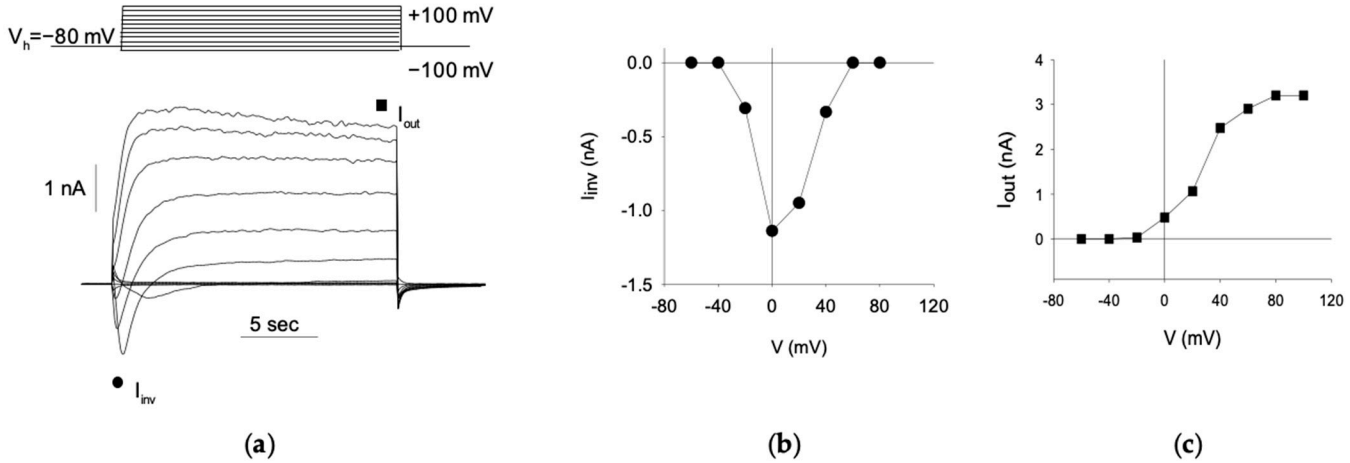

Figure 2. Voltage-activated currents in differentiated S1 neuroblastoma cells. (**a**) Representative current responses (**bottom**) evoked by the voltage protocol (illustrated in the top panel) applied to a patched S1 cell. (**b**) current–voltage (I–V) relationship of the inward currents (value taken at the peak value, •) recorded from the cell shown in A. (**c**) I–V relationship of the outward currents (at the steady-state level, ■) for the same cell.

Since an exhaustive characterization of voltage-gated currents in S1 cells has been provided by Gavazzo et al. [18], further investigation was not pursued. These findings confirm that S1 neuroblastoma cells have differentiated into an excitatory neuron-like phenotype.

To assess the presence of functional GABAergic receptors in S1 cells, rapid application of 100 μM GABA to patched cells, held at −80 mV, elicited an inward current carried by Cl^- ions following the electrochemical gradient. The mean current amplitude was 249 ± 29.5 pA (ranging from 23 to 1314 pA), which aligns well with previous findings [18]. However, only 27% (89/330) of the cells responded to GABA, suggesting a significant reduction in the proportion of S1 cells expressing functional $GABA_A$ receptors. Despite this, in cells that did respond, the GABA-evoked current was reproducible and stable across multiple stimulations (Figure 3a). This indicates the reliability of GABA-induced responses in cells expressing functional $GABA_A$ receptors. Additionally, picrotoxin (PTX, 100 μM), a known $GABA_A$ receptor antagonist, significantly and reversibly inhibited the GABA-evoked currents (control, 372 ± 139 pA; PTX, 28.17 ± 12.1 pA; recovery, 302.5 ± 78.36, n = 6, Figure 3b), confirming that the observed inward currents were indeed mediated by $GABA_A$ receptors, as previously reported [18].

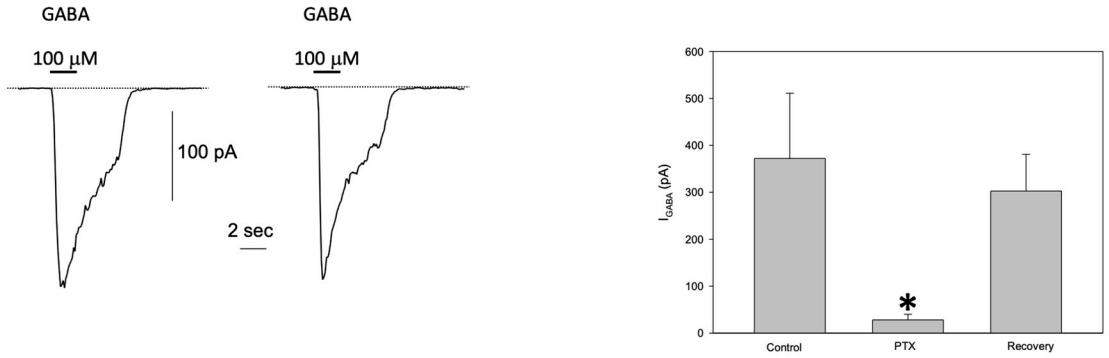

(**a**) (**b**)

Figure 3. $GABA_A$ activated currents in differentiated S1 neuroblastoma cells. (**a**) Two successive applications of 100 µM GABA, administered 1 min apart to a patched S1 cell, elicited stable and repetitive inward current responses. (**b**) Bath application of PTX significantly and reversibly reduced the GABA-evoked currents (* $p < 0.05$).

3.3. Effect of PFOS and PFOA on GABA-Evoked Currents in Neuron-Like S1 Neuroblastoma Cells

To determine whether the two PFAS compounds influence baseline current in neuron-like cells, a localized application of sublethal PFOS or PFOA concentrations—10 µM—was administered to patched S1 cells. The results showed that neither compound induced any detectable currents, nor were there any observable effects on the baseline current (data not shown), consistent with findings reported by Tukker et al. [20]. This lack of response strongly suggests that PFOS and PFOA, when applied alone at this concentration, do not have an immediate or direct impact on the baseline electrical activity of these cells.

In order to investigate if PFOS is able to modulate GABA-evoked currents, we co-applied GABA with PFOS at 10 µM, a concentration previously shown to be effective in injected oocytes [20]. In GABA-responding S1 cell, brief co-application of PFOS showed no significant effect on GABA-evoked current (Figure 4a •). However, when S1 cell was pretreated with PFOS for 1 min, current amplitude was almost completely suppressed (Figure 4a ■). After a 1 min washout, the current recovered, indicating that PFOS block on GABA-dependent current is reversible. Similar results were observed in $n = 5$ cells. To reduce data variability due to scattering of GABA-evoked current amplitude, responses in the presence of PFOS were normalized to responses recorded without it (no treatment: 0.88 ± 0.12; pre-treatment: $6.8 \times 10^{-5} \pm 5.12 \times 10^{-5}$, see plot on Figure 4b).

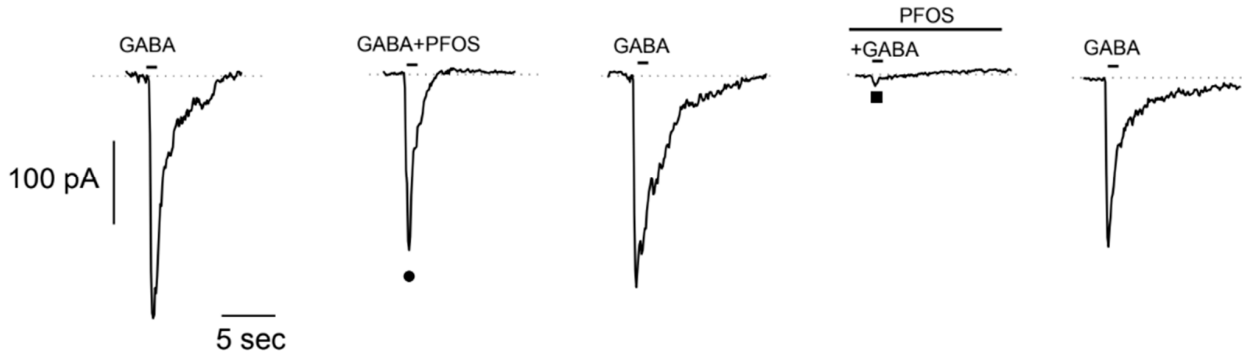

(**a**)

Figure 4. *Cont.*

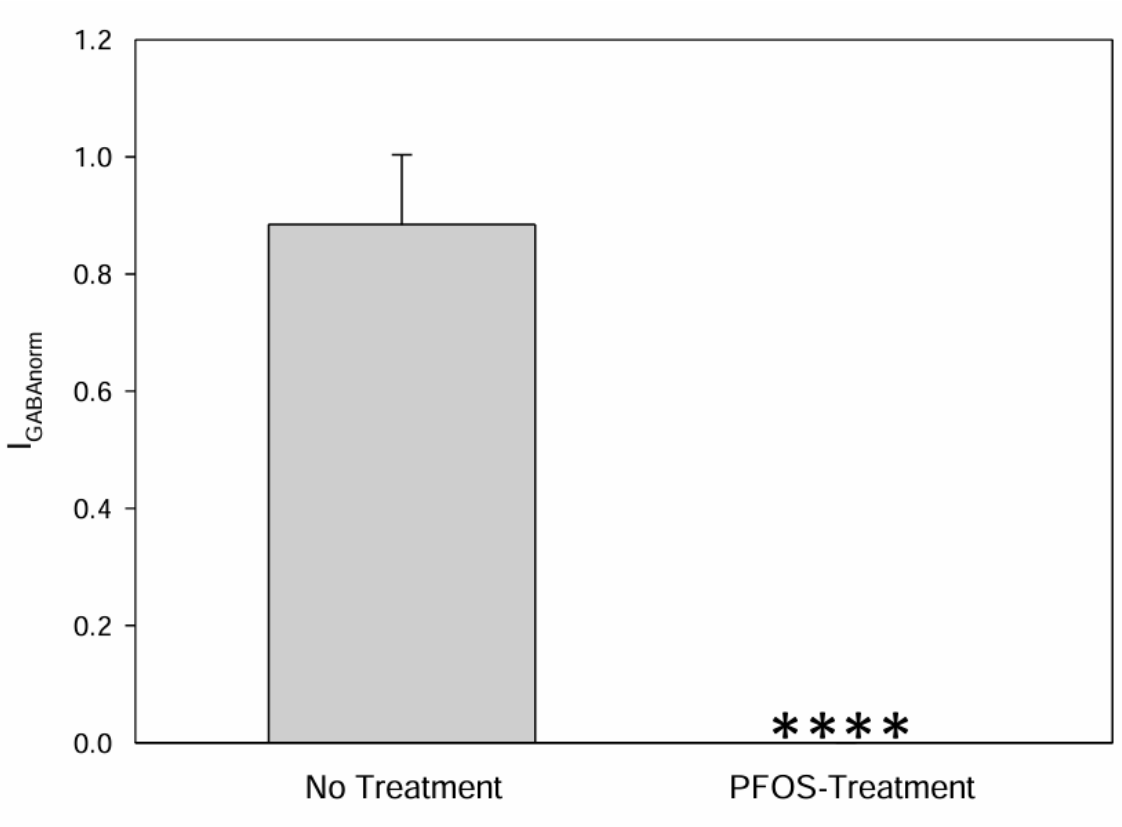

(**b**)

Figure 4. Effect of PFOS on GABA-activated currents in differentiated S1 neuroblastoma cells. (**a**) Representative effect of PFOS-modulation on GABA-current with (■) or without (●) PFOS-pretreatment from the same patched cell. Reversible almost complete current reduction was observed when S1 cells were previously exposed to PFOS. (**b**) Effect of PFOS on normalized GABA-amplitude (mean ± SE, n = 5) showing significant inhibition (**** $p < 0.0001$) when cells were pre-treated with PFOS.

The same experimental protocol was applied to GABA-responsive cells to investigate the effects of PFOA. Like PFOS, PFOA reduced the GABA-evoked current amplitude only when S1 cells were pretreated (Figure 5a). Although the block of GABA-dependent current was less pronounced (no treatment normalized current: 1.05 ± 0.23, n = 5; pre-treatment: 0.6 ± 0.14, n = 6, Figure 5b), it was still significant, and reversible as seen for the PFOS.

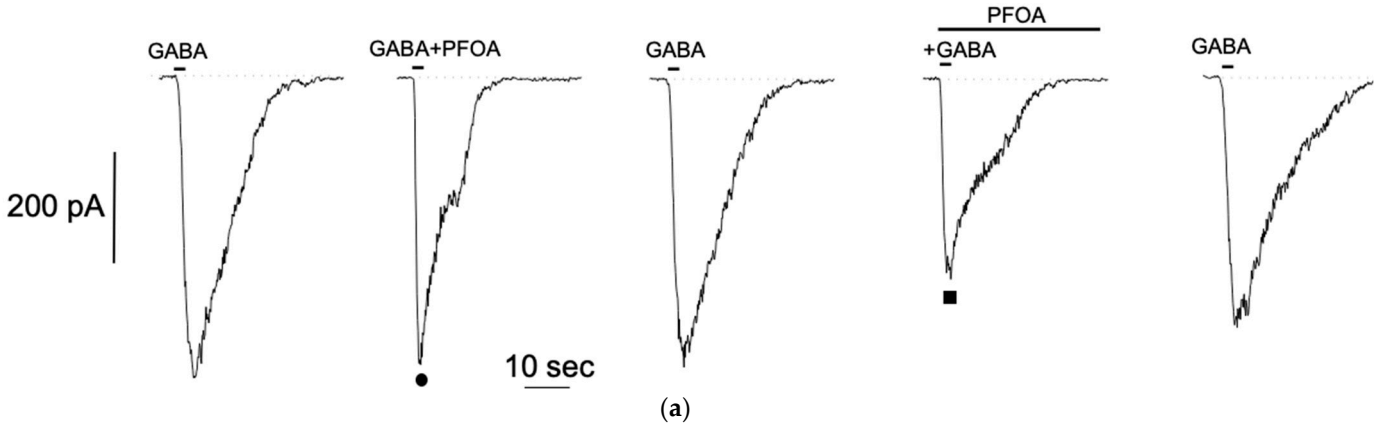

(**a**)

Figure 5. *Cont*.

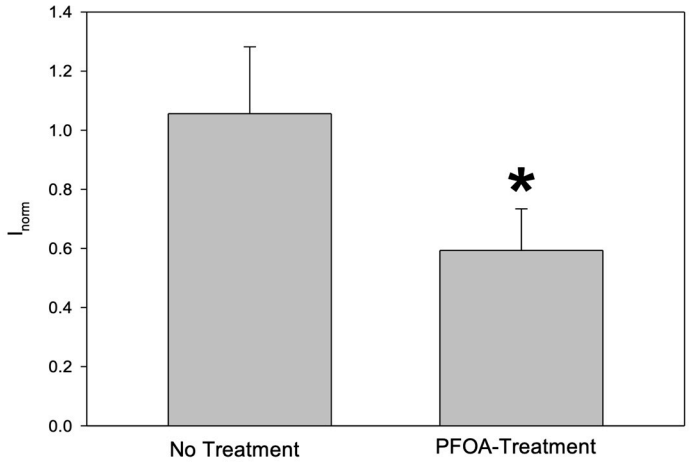

(**b**)

Figure 5. Effect of PFOA on GABA-activated currents in differentiated S1 neuroblastoma cells. (**a**) Representative effect of PFOA-modulation on GABA-current with (■) or without (●) PFOA-pretreatment from the same patched cell. Reversible current reduction was observed when S1 cells were previously exposed to PFOA. (**b**) Effect of PFOA on normalized GABA-amplitude (mean ± SE) showing significant inhibition (* $p < 0.05$) when cells were pre-treated.

4. Discussion

The results of this study provide compelling evidence that both PFOS and PFOA significantly alter GABAA receptor-mediated currents in neuron-like neuroblastoma S1 cells, revealing important insights into the neurotoxic mechanisms of these persistent pollutants. The choice to utilize the S1 neuroblastoma cell line for this study is grounded in the principles of non-animal testing models, which align with the 3Rs framework (Replacement, Reduction, and Refinement) aimed at minimizing reliance on animal experimentation. Neuroblastoma cells provide a relevant platform for studying the neurotoxic effects of PFAS compounds, as they retain key neuronal characteristics and exhibit similar physiological responses to excitatory and inhibitory signaling. Moreover, traditional methods relying on animal testing are being replaced by 3R principle-based alternatives, emphasizing in vitro test methods that consider broader chemical–biological interactions. Recent advances, as discussed by Giusy del Giudice et al. [21], highlight the importance of leveraging multiple informational levels to strengthen the understanding of biological responses, ultimately enhancing the predictive capacity of in vitro methods. By utilizing the S1 neuroblastoma cell line, we can effectively explore the mechanisms of PFAS-induced neurotoxicity while adhering to ethical considerations and improving the reliability of our findings.

The reduction in GABA-evoked currents following pre-treatment with PFOS and PFOA highlights a potentially critical pathway by which these compounds exert their neurotoxic effects, specifically through the modulation of inhibitory neurotransmission.

While the 10 μM concentration used in this study may appear elevated compared to typical environmental exposures, data from both community and occupational studies strongly support its relevance. Evidence suggests that PFAS accumulation in the brain could approach levels observed in our findings, especially under chronic environmental conditions. Recent analyses have reported average PFOA concentrations close to 160 ng/g in the hypothalamus of deceased individuals from areas near contamination sources, with variability indicating that brain levels may reach two to three times higher in certain individuals [5].

Remarkably, a nearly 1:1 brain-to-blood concentration ratio observed in some cases suggests a direct proportionality in PFAS retention between serum and brain tissue [4,5]. In communities near contamination sites, mean serum PFOA levels of approximately 1 μM (423 ng/mL) have been reported among residents, with even higher levels observed in

children aged 2–5 approaching 1 ppm as maximum value [22]. These findings underscore that even non-occupationally exposed individuals in highly contaminated areas can experience elevated serum PFOA concentrations. In occupational settings, exposure levels are even significantly higher. Median serum PFOA levels of up to 2.88 ppm have been documented among workers in specific roles within fluoropolymer manufacturing plants, with maximum values reaching 59.4 ppm (148.5 μM) [23]. Additionally, historical data indicate that serum PFOA levels could reach up to 92 ppm (230 μM) in highly exposed industrial workers, reflecting cumulative exposure over extended periods due to direct handling of PFAS-containing materials [24].

These data illustrate a continuum of exposure, from elevated community levels to extreme concentrations in occupational settings, supporting the relevance of our chosen 10 μM concentration. By using this level in vitro, we simulate acute effects that provide insights into potential neurotoxic mechanisms of PFOA and PFOS. This concentration models effects likely present in occupationally exposed individuals and provides a mechanistic basis for understanding cumulative impacts from long-term, low-dose exposure in the general population. Thus, our experimental approach serves as a valuable model for investigating PFAS-induced neurotoxicity in both environmental and occupational contexts.

First, it must be pointed out that, due to the GABA amplitude scattering and a limited number of GABA-expressing cells, we used GABA at a very high concentration (100 μM) to increase the probability of finding responsive cells. We are aware that this concentration is saturating, that some other effects of PFAS could be masked, and that it is necessary to conduct experiments with lower doses in a more suitable cellular model to better understand PFAS effects. Nevertheless, our results are in good agreement with Tukker's data [20], showing a PFOS/PFOA-dependent reduction of current in GABA-expressing oocytes. Moreover, they claim that both PFAS are non-competitive GABA antagonists. Similarly, our findings indicate that PFOS and PFOA do not directly induce currents or alter baseline electrical activity in the S1 neuroblastoma cells when applied alone. This suggests that their neurotoxic effects may not stem from direct interaction with the $GABA_A$ receptor in the absence of the neurotransmitter, supporting the hypothesis of an indirect effect on the receptor. However, the significant reduction in GABA-evoked currents following pre-exposure to these PFAS compounds suggests that PFOS and PFOA may interfere with the receptor's ability to respond to GABA, potentially by altering receptor conformation, hindering receptor function, or affecting the receptor's interaction with modulatory binding sites known to be present in the GABAA receptors. There is compelling evidence suggesting that the neurotoxic effects of PFAS may result from their accumulation in cell membranes [25], as these compounds tend to integrate into cell membranes and other lipid bilayers due to their lipophilic nature [3,26–28]. Moreover, PFAS can alter plasma membrane potential and intracellular pH level [29]. However, the effects observed in our study are unlikely to be exclusively attributed to these mechanisms. We observed no significant impact on baseline current, and the relative brief 1 min exposure followed by rapid washout makes membrane accumulation an improbable cause for the observed outcomes. The effect on membrane potentials seems unlikely, as adding just 10 micromolar of negative charge on the extracellular side would not be sufficient to cause a complete block or even a 60% reduction of GABA-induced current. Furthermore, if the effect were purely charge-dependent, both PFOS and PFOA would produce identical outcomes due to their shared negative charge. Additionally, there was no observed impact on the baseline current. However, the potential impact of PFAS on cell membranes cannot be definitively excluded. While our findings suggest that membrane accumulation may not be the primary mechanism, especially given the brief exposure and rapid washout, it remains a possibility that warrants further investigation

In our neuron-like S1 cells, both PFAS effects were reversible within seconds upon washout. However, in GABA-expressing oocytes, PFOS-induced inhibition was poorly reversible, suggesting a stronger and more persistent interaction with the receptor in this model [20]. This discrepancy could be ascribed to differences in biological systems,

as oocytes express recombinant $GABA_A$ receptors with controlled subunit composition, which may lack the accessory proteins or native conditions present in neuronal cells [20]. Additionally, the subunit composition of $GABA_A$ receptors can vary significantly between models, potentially affecting PFAS binding affinity and reversibility. Nonetheless, the reversibility of PFAS-dependent inhibition suggests that the interaction between PFOS or PFOA and $GABA_A$ receptors is not permanently damaging but rather a temporary interference, particularly when PFAS exposure is brief and localized. This reversible nature also raises concerns about the potential for chronic exposure to cause cumulative neurotoxic effects, where repeated or prolonged exposure might lead to lasting disruptions in inhibitory signaling.

$GABA_A$ receptors play a crucial role in maintaining the excitatory–inhibitory balance in the central nervous system. Disruptions to this balance, such as those caused by PFOS and PFOA, can have far-reaching consequences, potentially leading to increased neuronal excitability, impaired neural circuits, and the onset of neurological disorders. The fact that PFOS and PFOA can suppress GABA-evoked currents suggests that their presence could contribute to altered neural excitability and function, particularly under conditions of prolonged exposure where recovery between exposures may be incomplete. These findings are particularly concerning given the widespread and persistent nature of PFOS and PFOA in the environment and their ability to bioaccumulate in human tissues, including the brain.

Evidence from animal models further underscores the relevance of our in vitro exposure levels. For example, PFOS has been shown to accumulate to concentrations as high as 17 μM in the hippocampus of mice following sub-chronic exposure [30]. Such accumulation in the hippocampus, a brain region crucial for memory and learning, suggests that our chosen in vitro concentration mirrors real-world levels that PFOS can achieve in specific neural structures. This accumulation aligns with our findings on GABAergic suppression, indicating that PFOS can disrupt normal neurotransmission at concentrations observable in vivo. Additionally, research in hippocampal neurons [31] demonstrates that PFOS can enhance excitatory signaling by increasing the frequency and amplitude of excitatory miniature postsynaptic currents and amplifying field excitatory postsynaptic potentials. The combination of increased excitatory drive and suppressed inhibitory control suggests a potential shift toward hyperexcitability in hippocampal circuits, a change that could impair synaptic plasticity mechanisms essential for cognitive function, such as long-term potentiation and long-term depression. This pro-excitatory state may lead to excitotoxicity under prolonged exposure, aligning with epidemiological evidence linking PFAS exposure to cognitive deficits, developmental delays, and other neurological conditions [3,32,33]. Collectively, these findings support the neurotoxic potential of PFOS and reinforce the need for examining its effects on GABAergic and excitatory systems in the context of environmental exposure.

The study underscores the broader health implications of exposure to PFOS and PFOA, particularly regarding their potential to disrupt critical neurobiological processes. The observed effects on $GABA_A$ receptor-mediated currents provide a mechanistic link between PFAS exposure and neurotoxic outcomes, supporting the hypothesis that these compounds could contribute to the development of neurological disorders.

This research highlights the need for further studies to explore the long-term effects of chronic PFAS exposure on GABAergic neurotransmission and overall brain health. Moreover, the findings call attention to the urgent need for stringent regulatory measures to limit PFAS exposure. The potential for these compounds to interfere with key neurotransmitter systems suggests that current exposure levels, even if deemed safe by existing standards, could pose significant risks to public health, particularly for vulnerable populations such as children and individuals with pre-existing neurological conditions.

5. Perspectives

Looking forward, it is essential to deepen our understanding of the mechanisms underlying PFAS-induced inhibition of $GABA_A$ receptor function. Future studies should

aim to identify the specific sites of interaction between PFOS/PFOA and the $GABA_A$ receptor. Conducting molecular docking studies could provide valuable insights into how these compounds interact at the molecular level with the receptor's binding sites or transmembrane regions. Such computational approaches can predict potential binding sites and modes, guiding experimental efforts to confirm these interactions.

Additionally, exploring the effects of a broader range of PFAS compounds on $GABA_A$ receptor function is crucial. Given the structural diversity within the PFAS family, including congeners and classes that are not yet restricted or banned, testing other PFAS could reveal whether the inhibitory effects observed with PFOS and PFOA are common to other related compounds or are specific legacy ones. This would enhance our understanding of the structure–activity relationships governing PFAS interactions with $GABA_A$ receptors and identify potential risks associated with other PFAS substances that are currently in use.

From a public health perspective, our findings highlight the importance of revisiting safety standards and regulatory policies concerning PFAS exposure. Considering their persistent nature and bioaccumulative properties, even low-level exposure could have significant health implications over time. Collaborative efforts between scientists, policymakers, and industry stakeholders are necessary to develop strategies for reducing PFAS emissions, remediating contaminated environments, and limiting human exposure.

Finally, investigating potential therapeutic interventions to mitigate PFAS-induced neurotoxicity is an important area for future research. Identifying compounds or treatments that can counteract the inhibitory effects of PFAS on $GABA_A$ receptors may offer protective strategies for individuals at risk of exposure.

6. Conclusions

This study demonstrates that PFOS and PFOA significantly inhibit $GABA_A$ receptor-mediated currents in neuron-like neuroblastoma S1 cells. These findings suggest that PFAS compounds can disrupt inhibitory neurotransmission, potentially shifting the excitatory–inhibitory balance in the brain and increasing the risk of neurological disorders associated with excitotoxicity and cognitive deficits. The relevance of our findings is further underscored by reports of legacy PFAS accumulation in brain regions like the hippocampus at levels comparable to those used in our experiments. Given the widespread presence of these bioaccumulative compounds in the environment, there is an urgent need to reassess safety standards and minimize human exposure to PFAS to protect neurological health.

Author Contributions: L.L., Conceptualization, Methodology, Investigation, Formal Analysis, Data Curation, Statistical Analysis, Software, Writing—Original Draft, Review, Editing, Visualization. D.R., Methodology, Investigation, Formal Analysis, Data Curation, Statistical Analysis, Software, Writing—Original Draft, Review, Editing, Visualization. D.G., Formal Analysis, Statistical Analysis, Visualization. A.C., Review. C.L., Review, Visualization. V.M., Conceptualization, Methodology, Investigation, Review, Editing, Visualization. F.D., Conceptualization, Methodology, Investigation, Validation, Formal Analysis, Data Curation, Statistical Analysis, Writing—Original Draft, Review, Editing, Visualization, Project administration, Funding acquisition. All authors have read and agreed to the published version of the manuscript.

Funding: This project has received funding from the European Union's Horizon 2020 research and innovation programme under grant agreement No 101037509 (SCENARIOS project).

Institutional Review Board Statement: Not applicable.

Informed Consent Statement: Not applicable.

Data Availability Statement: The original contributions presented in the study are included in the article, further inquiries can be directed to the corresponding authors.

Acknowledgments: S1 neuroblastoma cells were kindly provided to L.L. by Aldo Pagano and Paola Gavazzo. L.L. also thanks Michele Fiore for technical support.

Conflicts of Interest: The authors declare no conflicts of interest.

References

1. Zahm, S.; Bonde, J.P.; Chiu, W.A.; Hoppin, J.; Kanno, J.; Abdallah, M.; Blystone, C.R.; Calkins, M.M.; Dong, G.H.; Dorman, D.C.; et al. Carcinogenicity of perfluorooctanoic acid and perfluorooctanesulfonic acid. *Lancet Oncol.* **2024**, *25*, 16–17. [CrossRef] [PubMed]
2. Yu, Y.; Wang, C.; Zhang, X.; Zhu, J.; Wang, L.; Ji, M.; Zhang, Z.; Ji, X.M.; Wang, S.L. Perfluorooctane sulfonate disrupts the blood brain barrier through the crosstalk between endothelial cells and astrocytes in mice. *Environ. Pollut.* **2020**, *256*, 113429. [CrossRef] [PubMed]
3. Brown-Leung, J.M.; Cannon, J.R. Neurotransmission Targets of Per- and Polyfluoroalkyl Substance Neurotoxicity: Mechanisms and Potential Implications for Adverse Neurological Outcomes. *Chem. Res. Toxicol.* **2022**, *35*, 1312–1333. [CrossRef] [PubMed]
4. Starnes, H.M.; Rock, K.D.; Jackson, T.W.; Belcher, S.M. A critical review and meta-analysis of impacts of per-and polyfluorinated substances on the brain and behavior. *Front. Toxicol.* **2022**, *4*, 881584. [CrossRef] [PubMed]
5. Di Nisio, A.; De Toni, L.; Sabovic, I.; Guidolin, D.; Dall'Acqua, S.; Sfriso, M.M.; Rocca, M.S.; De Filippis, V.; Foresta, C.; Garolla, A. Impairment of human dopaminergic neurons at different developmental stages by perfluoro-octanoic acid (PFOA) and differential human brain areas accumulation of perfluoroalkyl chemicals. *Environ. Res.* **2021**, *197*, 111152. [CrossRef]
6. Sieghart, W.; Fuchs, K.; Tretter, V.; Ebert, V.; Jechlinger, M.; Hoger, H.; Adamiker, D. Structure and subunit composition of GABA(A) receptors. *Neurochem. Int.* **1999**, *34*, 379–385. [CrossRef]
7. Steiger, J.L.; Russek, S.J. GABAA receptors: Building the bridge between subunit mRNAs, their promoters, and cognate transcription factors. *Pharmacol. Ther.* **2004**, *101*, 259–281. [CrossRef]
8. Ghit, A.; Assal, D.; Al-Shami, A.S.; Hussein, D.E.E. GABA(A) receptors: Structure, function, pharmacology, and related disorders. *J. Genet. Eng. Biotechnol.* **2021**, *19*, 123. [CrossRef]
9. Rudolph, U.; Knoflach, F. Beyond classical benzodiazepines: Novel therapeutic potential of GABAA receptor subtypes. *Nat. Rev. Drug Discov.* **2011**, *10*, 685–697. [CrossRef]
10. Sigel, E.; Baur, R.; Trube, G.; Mohler, H.; Malherbe, P. The effect of subunit composition of rat brain GABAA receptors on channel function. *Neuron* **1990**, *5*, 703–711. [CrossRef]
11. Sallard, E.; Letourneur, D.; Legendre, P. Electrophysiology of ionotropic GABA receptors. *Cell Mol. Life Sci.* **2021**, *78*, 5341–5370. [CrossRef] [PubMed]
12. Chen, Z.W.; Olsen, R.W. GABAA receptor associated proteins: A key factor regulating GABAA receptor function. *J. Neurochem.* **2007**, *100*, 279–294. [CrossRef] [PubMed]
13. Jacob, T.C.; Moss, S.J.; Jurd, R. GABA(A) receptor trafficking and its role in the dynamic modulation of neuronal inhibition. *Nat. Rev. Neurosci.* **2008**, *9*, 331–343. [CrossRef]
14. Sigel, E.; Luscher, B.P. A closer look at the high affinity benzodiazepine binding site on GABAA receptors. *Curr. Top Med. Chem.* **2011**, *11*, 241–246. [CrossRef]
15. Wang, M. Neurosteroids and GABA-A Receptor Function. *Front. Endocrinol.* **2011**, *2*, 44. [CrossRef] [PubMed]
16. Chen, L.; Durkin, K.A.; Casida, J.E. Structural model for γ-aminobutyric acid receptor noncompetitive antagonist binding: Widely diverse structures fit the same site. *Proc. Natl. Acad. Sci. USA* **2006**, *103*, 5185–5190. [CrossRef]
17. Nikonorov, I.M.; Blanck, T.J.; Recio-Pinto, E. G-protein Activation Decreases Isoflurane Inhibition of N-type Ba^{2+} Currents. *Anesthesiology* **2003**, *99*, 392–399. [CrossRef]
18. Gavazzo, P.; Vella, S.; Marchetti, C.; Nizzari, M.; Cancedda, R.; Pagano, A. Acquisition of neuron-like electrophysiological properties in neuroblastoma cells by controlled expression of NDM29 ncRNA. *J. Neurochem.* **2011**, *119*, 989–1001. [CrossRef]
19. Rampersad, S.N. Multiple applications of Alamar Blue as an indicator of metabolic function and cellular health in cell viability bioassays. *Sensors* **2012**, *12*, 12347–12360. [CrossRef]
20. Tukker, A.M.; Bouwman LM, S.; van Kleef, R.; Hendriks, H.S.; Legler, J.; Westerink, R.H.S. Perfluorooctane sulfonate (PFOS) and perfluorooctanoate (PFOA) acutely affect human alpha(1)beta(2)gamma(2L) GABA(A) receptor and spontaneous neuronal network function in vitro. *Sci. Rep.* **2020**, *10*, 5311. [CrossRef]
21. Del Giudice, G.; Migliaccio, G.; D'Alessandro, N.; Saarimäki, L.A.; Torres Maia, M.; Annala, M.E.; Leppänen, J.; Möbus, L.; Pavel, A.; Vaani, M.; et al. Advancing chemical safety assessment through an omics-based characterization of the test system-chemical interaction. *Front. Toxicol.* **2023**, *5*, 1294780. [CrossRef] [PubMed]
22. Emmett, E.A.; Shofer, F.S.; Zhang, H.; Freeman, D.; Desai, C.; Shaw, L.M. Community exposure to perfluorooctanoate: Relationships between serum concentrations and exposure sources. *J. Occup. Environ. Med.* **2006**, *48*, 759–770. [CrossRef] [PubMed]
23. Woskie, S.R.; Gore, R.; Steenland, K. Retrospective exposure assessment of perfluorooctanoic acid serum concentrations at a fluoropolymer manufacturing plant. *Ann. Occup. Hyg.* **2012**, *56*, 1025–1037.
24. Olsen, G.W.; Burris, J.M.; Ehresman, D.J.; Froehlich, J.W.; Seacat, A.M.; Butenhoff, J.L.; Zobel, L.R. Half-life of serum elimination of perfluorooctanesulfonate, perfluorohexanesulfonate, and perfluorooctanoate in retired fluorochemical production workers. *Environ. Health Perspect.* **2007**, *115*, 1298–1305. [CrossRef]
25. Zhao, L.; Teng, M.; Zhao, X.; Li, Y.; Sun, J.; Zhao, W.; Ruan, Y.; Leung KM, Y.; Wu, F. Insight into the binding model of per- and polyfluoroalkyl substances to proteins and membranes. *Environ. Int.* **2023**, *175*, 107951.
26. Cao, Y.; Ng, C. Absorption, distribution, and toxicity of per- and polyfluoroalkyl substances (PFAS) in the brain: A review. *Environ. Sci. Process. Impacts* **2021**, *23*, 1623–1640. [CrossRef]

27. Harada, K.H.; Ishii, T.M.; Takatsuka, K.; Koizumi, A.; Ohmori, H. Effects of perfluorooctane sulfonate on action potentials and currents in cultured rat cerebellar Purkinje cells. *Biochem. Biophys. Res. Commun.* **2006**, *351*, 240–245. [CrossRef]
28. Naumann, A.; Alesio, J.; Poonia, M.; Bothun, G.D. PFAS fluidize synthetic and bacterial lipid monolayers based on hydrophobicity and lipid charge. *J. Environ. Chem. Eng.* **2022**, *10*, 107351. [CrossRef] [PubMed]
29. Kleszczynski, K.; Skladanowski, A.C. Mechanism of cytotoxic action of perfluorinated acids. I. alteration in plasma membrane potential and intracellular pH level. *Toxicol. Appl. Pharmacol.* **2009**, *234*, 300–305. [CrossRef]
30. Austin, M.E.; Kasturi, B.S.; Barber, M.; Kannan, K.; MohanKumar, P.S.; MohanKumar, S.M. Neuroendocrine effects of perfluorooctane sulfonate in rats. *Environ. Health Perspect.* **2003**, *111*, 1485–1489. [CrossRef]
31. Liao, C.Y.; Li, X.Y.; Wu, B.; Duan, S.M.; Jiang, G.B. Acute enhancement of synaptic transmission and chronic inhibition of synaptogenesis induced by perfluorooctane sulfonate through mediation of voltage-dependent calcium channel. *Environ. Sci. Technol.* **2008**, *42*, 5335–5341. [CrossRef] [PubMed]
32. Panieri, E.; Baralic, K.; Djukic-Cosic, D.; Buha Djordjevic, A.; Saso, L. PFAS Molecules: A Major Concern for the Human Health and the Environment. *Toxics* **2022**, *10*, 44. [CrossRef] [PubMed]
33. Reardon, A.J.F.; Hajihosseini, M.; Dinu, I.; Field, C.J.; Kinniburgh, D.W.; MacDonald, A.M.; Dewey, D.; England-Mason, G.; Martin, J.W.; APrON Study. Maternal co-exposure to mercury and perfluoroalkyl acid isomers and their associations with child neurodevelopment in a Canadian birth cohort. *Environ. Int.* **2023**, *178*, 108087. [CrossRef] [PubMed]

Journal of
Xenobiotics

MDPI

Article

Assessing the Effects of a Diet of BPA Analogue-Exposed Microalgae in the Clam *Ruditapes philippinarum*

Jacopo Fabrello [1,*], Michela Dalla Fontana [1], Noemi Gaiani [1], Maria Ciscato [1], Marco Roverso [2], Sara Bogialli [2] and Valerio Matozzo [1,*]

[1] Department of Biology, University of Padova, Via Bassi 58/B, 35131 Padova, Italy; michela.dallafontana@studenti.unipd.it (M.D.F.); noemi.gaiani@studenti.unipd.it (N.G.); mariaciscato95@gmail.com (M.C.)
[2] Department of Chemical Sciences, University of Padova, Via Marzolo 1, 35131 Padova, Italy; marco.roverso@unipd.it (M.R.); sara.bogialli@unipd.it (S.B.)
* Correspondence: jacopofabrello@gmail.com (J.F.); valerio.matozzo@unipd.it (V.M.)

Abstract: In our previous study, we demonstrated that the microalgae *Phaeodactylum tricornutum* can bioaccumulate bisphenol A analogues. Since this microalgae species is part of the diet of marine filter-feeding organisms, such as bivalves, in this study we tested the hypothesis that a diet based on exposed microalgae can exert negative effects on the clam *Ruditapes philippinarum*. Microalgae were exposed for 7 days to 300 ng/L of bisphenol AF (BPAF), bisphenol F (BPF), and bisphenol S (BPS), alone or as a mixture (MIX), to allow bioaccumulation. Microalgae were then supplied as food to bivalves. After 7 and 14 days of diet, the effects of exposed microalgae were evaluated on a battery of biomarkers measured in haemolymph/haemocytes, gills and digestive glands of clams. In addition, bioaccumulation of the three bisphenols was investigated in clams by UHPLC-HRMS. The results obtained demonstrated that total haemocyte count (THC) increased in clams following ingestion for 7 days of BPAF- and BPF-exposed microalgae, while BPS-exposed microalgae significantly reduced THC after 14 days of diet. MIX- and BPS-exposed microalgae increased haemocyte proliferation. The diet of exposed microalgae affected acid and alkaline phosphatase activity in clams, with an opposite response between haemolymph and haemocytes. Regarding antioxidants, an increase in catalase activity was observed in clams after ingestion of BPA analogue-exposed microalgae. The results also demonstrated marked oxidative stress in gills, the first tissue playing an important role in the feeding process. Oxidative damage was recorded in both the gills and digestive glands of clams fed BPA analogue-exposed microalgae. Alterations in epigenetic-involved enzyme activity were also found, demonstrating for the first time that BPA analogue-exposed food can alter epigenetic mechanisms in marine invertebrates. No bioaccumulation of BPA analogues was detected in clam soft tissues. Overall, this study demonstrated that a diet of BPA analogue-exposed microalgae can induce significant alterations of some important biological responses of *R. philippinarum*. To our knowledge, this is the first study demonstrating the effects of ingestion of BPA analogue-exposed microalgae in the clam *R. philippinarum*, suggesting a potential ecotoxicological risk for the marine food chain, at least at the first levels.

Keywords: bisphenol A analogues; microalgae; clams; dietary exposure; biomarkers; bioaccumulation; antioxidants

1. Introduction

Bisphenol A (BPA) is the most used bisphenol worldwide, with production still growing [1]. BPA is mainly used in polycarbonate plastic production [2]. However, the increasing evidence on the estrogenic activity of BPA also in aquatic species [3] has led to some limitations in its uses. Consequently, the replacement of BPA with other similar compounds—named BPA analogues—has begun. At least 17 different native bisphenols and another 131 chemicals derived from them have been synthesised.

Three of the most known BPA analogues are bisphenol AF (BPAF), bisphenol F (BPF) and bisphenol S (BPS), being largely used to produce polycarbonate copolymers, epoxy resins, liners, water pipes, toys, adhesives, food packaging and thermal paper [4]. The increasing use of such BPA analogues led to a consequent release of detectable concentrations into ecosystems, including freshwater and seawater. Generally, environmental concentrations of BPA analogues range from few ng/L up to hundreds of ng/L in both freshwater and seawater [5]. For example, a concentration of up to 140 ng/L of BPAF was recorded in Taihu Lake in China [6]. Moreover, BPF reached an environmental concentration of up to 2850 ng/L in the Tamagawa River in Japan [7]. High levels of BPS (up to 65,600 ng/L) were recorded in rivers of China [8]. As for the marine coastal environment, the concentrations of BPA analogues are generally lower than those recorded in freshwater [5]. However, concentrations of 282 ng/L and 1470 ng/L of BPF were detected in seawater in South China and Tokyo Bay, respectively [7,9]. Furthermore, BPA was detected at a mean concentration of 13 ng/g dw (dry weight) in marine sediments from coastal areas of Zhejiang in East China [10]. In the same area, BPF, BPAF and BPS reached concentrations of 1.6 ng/g dw, 0.53 ng/g dw and 0.69 ng/g dw, respectively [10]. In that study, all seawater samples contained measurable concentrations of BPA (mean 23 ng/L, range 2.7–52 ng/L), BPS (2.2 ng/L, 0.15–12 ng/L), and BPAF (0.34 ng/L, 0.12–0.91 ng/L), while BPF was only detectable in some seawater samples at concentrations lower than 1.0 ng/L [10]. BPA was also predominant in surface seawater and sediment samples from the Beibu Gulf, South China Sea, with concentrations ranging from 5.26 to 12.04 ng/L in seawater and from 0.56 to 5.22 ng/g dw in sediment samples, followed by BPAF (0.44–0.60 ng/L in seawater and 0.08–0.66 ng/g dw in sediments, respectively) and BPS (0.07–0.63 ng/L in seawater and up to 0.19 ng/g dw in sediments, respectively) [11]. The predicted no-effect concentrations (PNECs) in freshwater and seawater for the three compounds are, respectively, 1.02 µg/L and 100 ng/L for BPAF, 5.44 µg/L and 540 ng/L for BPF, and 12.9 µg/L and 27 µg/L for BPS [12]. However, the only adopted PNEC with legislative relevance is the BPA PNEC, which was settled at 1500 ng/L for freshwater and 150 ng/L in seawater by the European Union [13].

In a recent study, we demonstrated that exposure to BPAF, BPF and BPS induced oxidative stress and ultrastructural changes in the microalgae *Phaeodactylum tricornutum* [14]. In that study, bioaccumulation of the three BPA analogues in microalgae was also assessed, and the results obtained demonstrated that BPAF and BPS were bioaccumulated in microalgae. In another study, we evaluated the effects and bioaccumulation of the same BPA analogues (at the same concentrations) in the clam *Ruditapes philippinarum* [15]. However, information regarding the toxicity of these compounds in aquatic organisms, whether exposed to water or subjected to a diet of pre-exposed food, is rather scarce. The present study tries to fill this knowledge gap. Consequently, we evaluated for the first time the effects of food-borne exposure to BPAF, BPF, and BPS—alone or as a mixture—on some important biomarkers in the clam *Ruditapes philippinarum*. The aim of this study was to compare the effects caused by the ingestion of BPA analogue-exposed microalgae to the effects observed in a recent study in which bivalves were exposed to the same contaminants dissolved in seawater [15].

2. Materials and Methods

2.1. Microalgae Culture and Exposure

P. tricornutum was purchased from the Culture Collection of Algae at Göttingen University (SAG). Microalgae were grown for 10 days in F/2 medium [16] prepared in 0.45 µm filtered seawater at 16 °C, with a light intensity corresponding to 40.5 µmol photons $m^{-2}s^{-1}$, and a photoperiod of 12:12 light/dark. BPAF and BPF stock solutions (1 mg/L) were prepared in methanol, while the BPS solution (1 mg/L) was prepared in distilled water. Five experimental conditions, namely control, BPAF, BPF, BPS and their mixture (MIX), were prepared in Erlenmeyer flasks with an F/2 volume of 600 mL at an initial concentration of microalgae of 5×10^5 cells/mL (*inoculum*). BPA analogues were added

in the corresponding experimental condition at a final concentration of 300 ng/L. As for the mixture, microalgae were exposed to 100 ng/L of each compound. We chose these concentrations because they are in the same order of magnitude as the BPA analogue concentrations recorded in marine coastal areas.

Microalgae were treated for 7 days to allow them to bioaccumulate BPA analogues [14]. A solvent control was not performed because we previously observed that methanol does not cause negative effects on microalgae [14]. In addition, it has been demonstrated that methanol can cause toxic effects at very high concentrations in aquatic species (tens and hundreds of mg/L), including marine microalgae [17,18].

2.2. Clam Acclimation and Treatment

R. philippinarum specimens were sampled in February 2023 from a licenced fishing area in the Lagoon of Venice (Italy). Then, molluscs were acclimated in large aquaria filled with aerated seawater (salinity of 35 ± 1, temperature of 11 ± 0.5 °C) and a sandy bottom for 7 days. After acclimation, 80 clams (mean length: 36.7 mm) were randomly divided into 10 experimental tanks without sand (30-litre capacity, 2 tanks per experimental condition, 40 clams per tank). Every two days, seawater was renewed, and 200 mL of control or exposed microalgae suspensions were added. To allow clams to take up contaminants only from the microalgae and not from the medium in which they grew, all microalgae suspensions (both control and treated groups) were centrifuged at $4000\times$ *g* rpm at room temperature for 10 min using an ultracentrifuge Avant-J-25. The supernatant (=BPA analogue-exposed medium) was discharged, and microalgae were then carefully re-suspended in 0.45 mm filtered seawater. Clam tissues were collected after 7 and 14 days of diet with control or exposed microalgae.

2.3. Tissue Collection

A 1 mL syringe was used to collect the haemolymph from the anterior adductor muscle of clams. We prepared 5 pools of haemolymph (from six clams each) for each experimental condition at each tissue sampling time (7 and 14 days). After sampling, total haemocyte count (THC), haemocyte diameter and volume, lactate dehydrogenase (LDH) activity and haemocyte proliferation (XTT assay) were measured. To obtain cell-free haemolymph (CFH) and haemocyte lysate (HL), pooled haemolymph was centrifuged at $780\times$ *g* for 10 min, the pellets (=haemocytes) were then re-suspended in distilled water to obtain HL, whereas supernatants (CFH) were collected and stored on ice. Both CFH and HL samples were frozen in liquid nitrogen and stored at -80 °C until analyses. After haemolymph sampling, gills and digestive glands were excised and pooled (five pools of six clams each). Aliquots of each pooled tissue were then frozen in liquid nitrogen and stored at -80 °C until analyses.

2.4. Haemolymph and Haemocyte Biomarkers

A Scepter™ 2.0 Automated Cell Counter (Millipore, FL, USA) was used to determine the THC, as well as the haemocyte diameter and volume. In detail, 20 µL of haemolymph was diluted into 2 mL of Coulter Isoton II diluent. THC was expressed as the number of haemocytes (10^5)/mL of haemolymph, while haemocyte diameter and volume were expressed in µm and picolitres (pL), respectively.

Cell-free haemolymph (CFH) LDH activity was measured using the commercial kit *Cytotoxicity Detection* Kit (Roche). Briefly, after centrifugation ($780\times$ *g* for 10 min), 500 µL of CFH was mixed with an equal volume of reagent provided with the kit. After 30 min, we measured the absorbance, and the results were expressed as optical density (OD) at 490 nm.

To evaluate haemocyte proliferation, we used the *Cell proliferation* Kit II. In detail, a volume of the reagent mixture (provided with the kit) was added to two volumes of pooled haemolymph and incubated for 4 h at room temperature. Then, we measured the

absorbance at 450 nm and the results were normalised to THC values of each sample and expressed as optical density (OD) at 450 nm.

Lysozyme activity was measured in haemocyte lysate (HL) by mixing 50 µL of HL with 950 µL of a 0.15% suspension of *Micrococcus lysodeikticus* (Sigma) phosphate buffer (pH 6.2). The decrease in absorbance was recorded for 3 min at 450 nm at room temperature. Results were expressed as µg lysozyme/mg of proteins.

The arylsulfatase activity was measured in HL samples measuring the production of p-nitrocatechol after 1 h at 515 nm [19] and then calculated using the formula proposed by Baum et al. [20]. Results are expressed as µg of p-nitrocatechol produced per hour/mg of proteins.

The acid phosphatase and alkaline phosphatase activity were measured both in HL and CFH. The acid phosphatase hydrolysed the substrate 4-nitrophenyl phosphate during the incubation at 37 °C and the absorbance was measured at 405 nm using a microplate reader. Results were expressed as U/mg of proteins. Similarly, the alkaline phosphatase hydrolysed the same substrate in an alkaline buffer, and after the incubation at 30 °C, the absorbance was recorded at 405 nm [21].

Lastly, the total antioxidant capacity of haemolymph was assessed following the cupric reducing antioxidant capacity (CUPRAC) method [22]. In detail, the cupric ions produced a coloured complex with neocuproine. Then, the absorbance was measured at 450 nm using a microplate reader. Results are reported as mM of Trolox equivalents/mg of proteins.

2.5. Gill and Digestive Gland Biomarkers

Gills and digestive gland samples were homogenised using the TissueLyser LT (Qiagen). In detail, samples were homogenised in four volumes of 10 mM Tris-HCl buffer, pH 7.5, containing 0.15 M KCl, 0.5 M sucrose, 1 mM EDTA and protease inhibitor cocktail (1:10 v/v) (Merck, Milano, Italy) at 50 oscillations per second for 5 min at 4 °C. The samples were centrifuged at 12,000× g for 30 min at 4 °C and supernatants (SNs) were collected for analyses. All analyses were performed in triplicate.

Like haemolymph, a CUPRAC assay was performed in SNs of both gills and digestive glands according to the CUPRAC method [22]. The results were expressed as mM of Trolox equivalents/mg of proteins.

Total superoxide dismutase (SOD) activity was measured following the xanthine oxidase/cytochrome *c* method in both gill and digestive gland SNs [23]. Enzyme activity was expressed as U/mg proteins, and one unit of SOD has been defined as the amount of sample causing 50% inhibition under the assay conditions.

Catalase (CAT) activity was measured in gill and digestive gland SNs by recording the absorbance at 240 nm. Results were expressed as U/mg proteins [24]. One unit of CAT was defined as the amount of enzyme that catalysed the dismutation of 1 µmol of H_2O_2/min.

Acetylcholinesterase (AChE) activity was measured only in gills following the colorimetric reaction between acetylthiocholine and the reagent dithiobisnitrobenzoate [25]. The increase in absorbance at 405 nm was recorded for 5 min using a microplate reader at room temperature. Results are expressed as nmol/min/mg of protein. Similarly, the butyrylcholinesterase (BChE) activity was measured using butyrylthiocholine as a substrate and the absorbance was quantified at 405 nm [26]. The enzymatic activity is expressed as nmol/min/mg proteins.

Glutathione reductase (GR) activity was measured in both gill and digestive gland SNs following the method proposed by Smith et al. [27]. In detail, we quantified the amount of 5-thio (2-nitrobenzoic acid) produced at 412 nm. Results are expressed as U/mg proteins.

Glutathione S-transferase (GST) activity was evaluated only in the digestive gland SN using 1-chloro-2,4-dinitrobenzene (CDNB) and reduced glutathione (GSH) as substrates [28]. GST activity was expressed as nmol/min/mg proteins.

The protein carbonyl content (PCC) and lipid peroxidation (LPO) were measured as oxidative damage biomarkers. Briefly, PCC was measured using the method of Mecocci et al. [29]. This spectrophotometric method is based on the reaction of carbonyl groups with 2,4-

dinitrophenylhydrazine (DNPH). Results were expressed as nmol carbonyl group/mg of proteins.

LPO was quantified according to the method of Buege and Aust [30]. The method is based on the quantification of malondialdehyde (MDA) at 532 nm and the results were expressed as nmoles of thiobarbituric reactive substances (TBARSs)/mg of proteins. TBARSs, considered as "MDA-like peroxide products", were quantified by reference to MDA absorbance ($\varepsilon = 156 \times 10^3$ M^{-1} cm^{-1}) [31].

Total protein concentration in SN samples was quantified according to Bradford et al. [32].

2.6. Epigenetic Biomarkers

The histone N-terminal acetyltransferases (HATs) and histone deacetylases activities (HDACs) were evaluated in gills and digestive glands. The HAT activity was measured at 412 nm [33]. In detail, SN samples were prepared as described above, followed by a sonication step. Then, we used the histone extracted from the calf thymus (Sigma Aldrich, Milan, Italy) as an acetyl acceptor and acetyl-CoA as an acetyl group donator. The resulting free thiol group was quantified using 5,5′-dithiobis-(2-nitrobenzoic acid) at 412 nm in a microplate. Results are expressed as μM of 5-thio-2-nitrobenzoic acid (TNB^-)/mg of proteins. The HDAC activity of class I and II was quantified following the spectrophotometric method proposed by Yuan et al. [34]. Briefly, SN samples reacted with the synthetic substrate Boc-Lys(Ac)-pNA, removing the acetyl group from the lysine. This reaction led to the formation of a chromogen compound that was quantified at 405 nm in a microplate. Results are expressed as OD at 405 nm/mg of proteins.

2.7. Bioaccumulation

Methanol, acetonitrile, ammonium acetate, BPAF, BPF, BPS and bisphenol A d-16, used as internal standard, were purchased from Merck (Milan, Italy), while the ultrapure-grade water was produced with a Pure-Lab Option Q apparatus (Elga Lab Water, High Wycombe, UK). Bioaccumulation of BPs was evaluated in five organisms collected after 7 and 14 days of diet with BPA analogue-exposed microalgae. Each sample was accurately weighed and homogenised (Homogeniser SHM1, Avantor, VWR International Srl, Milano, Italia) after the addition of 1 mL of ultrapure water. The homogenate was treated with cold acetonitrile (7 mL) containing the internal standard at 500 μg/L, vortexed for 3 min, and centrifuged at 5000× *g* rpm for 5 min. After a further centrifugation step (13,000× *g* rpm, 10 min, 4 °C), 20 μL of the supernatant was analysed by UHPLC-HRMS. The system was equipped with an Agilent 1260 Infinity II LC chromatographer coupled to an Agilent 6545 LC/Q-TOF mass analyser (Agilent Technologies, Palo Alto, Santa Clara, CA, USA). The analytical column was a Kinetex 2.6 μm C18 Polar, 100 A, 100 × 2.1 mm (Phenomenex, Bologna, Italy), at 25 °C. Mobile phases A and B were water and acetonitrile, respectively, both containing 10 mM ammonium acetate, and the eluent flow rate was 0.30 mL/min. The mobile-phase gradient profile was as follows (t in min): t0–4 0% B; t4–22 0–100% B, t22–25 100% B; t25–32 0% B. The MS conditions were electrospray (ESI) ionisation in negative mode, gas temperature of 320 °C, drying gas at 12 L/min, nebulizer at 35 psi, sheath gas temperature of 350 °C, sheath gas flow of 11 L/min, VCap at 5000 V, nozzle voltage of 0 V, and fragmentor at 150 V. Centroid full-scan mass spectra were recorded in the range 100–1000 m/z with a scan rate of 2 spectra/s. The QTOF calibration was performed daily with the manufacturer's solution in this mass range. The Mass Hunter Qualitative Analysis software (Agilent Technologies, Palo Alto, Santa Clara, CA, USA) was used to analyse the MS.

Homogenates from untreated organisms were used to build a matrix-matched seven-point external calibration curve, in the range 0.1–100 μg/L (corresponding to 0.8–800 ng/g in the initial animal tissues). Linearity was evaluated by least squares regression and $R^2 > 0.998$ was obtained for all the analytes. LODs were 40 ng/g for BPF, 2 ng/g for BPS

and 1 ng/g for BPAF. Each treated organism was analysed separately, and results are reported as mean and standard deviation.

2.8. Statistical Analysis

The normal distribution of data (Shapiro–Wilk's test) and the homogeneity of the variances (Bartlett's test) were assessed. The results obtained were compared by performing the two-way ANOVA analysis, using "exposure time", "treatment" (=diet) and "exposure time–treatment interaction" as independent factors. Pairwise comparisons among experimental conditions were performed using Fisher's LSD post hoc test. The significant difference was set at $p < 0.05$. All results are expressed as means ± standard deviation (SD), n = 5. The software package Origin 2023 (Origin Lab, Northampton, MA, USA) was used for statistical analyses.

3. Results

3.1. Haemolymph and Haemocyte Biomarkers

The two-way ANOVA analysis demonstrated that the factors "exposure time" (two-way ANOVA: $p < 0.01$), "treatment" (two-way ANOVA: $p < 0.001$) and "exposure time–treatment interaction" (two-way ANOVA: $p < 0.001$) significantly affected THC in clams. The post hoc test revealed a significant increase in THC values in clams fed for 7 days with BPAF- and BPF-treated microalgae (Figure 1A). Moreover, clams fed with BPS-exposed microalgae showed a significant reduction in THC at 14 days when compared to the related control (Figure 1A).

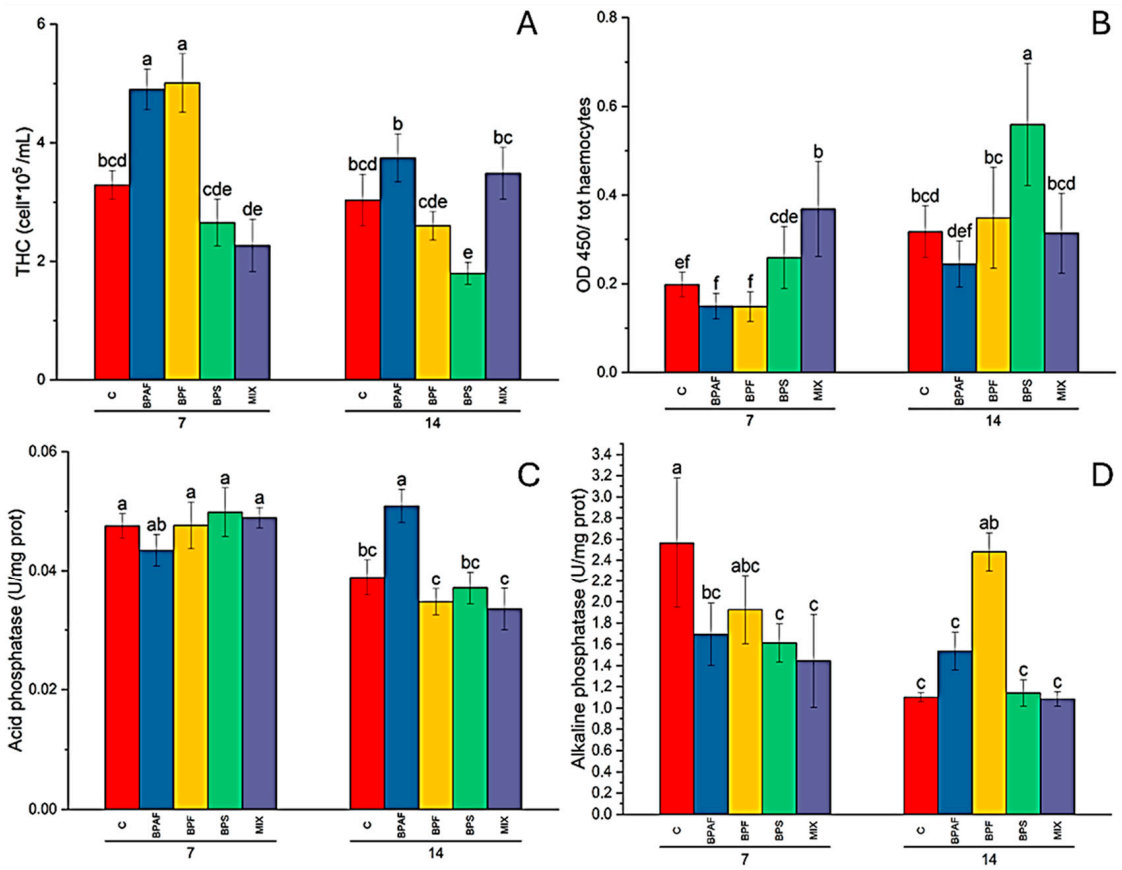

Figure 1. Total haemocyte count (THC), expressed as n° haemocytes (10^5)/mL haemolymph (**A**); haemocyte proliferation, expressed as OD450 (**B**); acid phosphatase activity in CFH, expressed as U/mg proteins (**C**); and alkaline phosphatase activity in HL, expressed as U/mg proteins (**D**), in clams fed with bisphenol-exposed microalgae. Different letters indicate significant differences among all treatments. N = 5.

No significant alterations in both the diameter and volume of haemocytes were observed (Figure S1 and Figure S2 in Supplementary Material, respectively).

Similarly, ingestion of BPA analogue-exposed microalgae did not induce cytotoxicity (LDH assay) in clam haemocytes (Figure S3).

On the contrary, cell proliferation was significantly affected by all the independent factors (two-way ANOVA: $p < 0.001$). Pairwise comparisons revealed a significant increase in haemocyte proliferation in clams fed for 7 days with MIX-exposed microalgae and in those fed for 14 days with BPS-treated microalgae, with respect to the related controls (Figure 1B).

Regarding immune-related enzyme activity, only a significant (two-way ANOVA: $p < 0.05$) effect of the factor "exposure time" on both lysozyme and arylsulfatase activity was observed (Figure S4 and Figure S5, respectively). As for acid phosphatase and alkaline phosphatase activity, a different response of HL and CFH was recorded. Indeed, HL acid phosphatase activity was influenced only by the factor "exposure time" (two-way ANOVA: $p < 0.05$) (Figure S6), while the factors "exposure time" (two-way ANOVA: $p < 0.001$) and its interaction with treatment (two-way ANOVA: $p < 0.01$) had a significant effect in CFH enzyme activity. A post hoc test revealed a significant increase in CFH acid phosphatase activity in clams fed for 14 days with BPAF-exposed microalgae, when compared to the related control (Figure 1C). As for alkaline phosphatase activity, no significant alteration was found in CFH (Figure S7), while all the independent factors affected (two-way ANOVA: $p < 0.05$) enzyme activity. In the latter case, the pairwise comparisons revealed a significant reduction in enzyme activity in clams fed for 7 days with microalgae treated with BPAF, BPS and MIX, whereas significantly increased enzyme activity was observed in clams fed with BPF-treated microalgae, with respect to the related controls (Figure 1D).

Lastly, no significant effects of exposed microalgae on the total antioxidant capacity of haemolymph (assessed using CUPRAC assay) were observed (Figure S8).

3.2. Gill and Digestive Gland Biomarkers

In gills, the factor "treatment" significantly altered (two-way ANOVA: $p < 0.01$) the CUPRAC levels, and the post hoc test revealed significantly increased CUPRAC levels in clams fed for 7 and 14 days with microalgae treated with MIX (Figure 2A). On the contrary, digestive gland CUPRAC levels were altered by the factor "exposure time" (two-way ANOVA: $p < 0.001$) (Figure S9).

Total SOD activity was influenced by the factor "exposure time" (two-way ANOVA: $p < 0.01$) in gills (Figure S10), while the factors "exposure time" (two-way ANOVA: $p < 0.001$) and its interaction with treatment (two-way ANOVA: $p < 0.05$) influenced SOD activity in digestive glands significantly, even if the post hoc test did not reveal significant differences among experimental conditions (Figure 2B).

Two-way ANOVA revealed that the factors "exposure time" ($p < 0.001$) and "treatment" ($p < 0.05$) affected CAT activity in gills, with a significant increase in enzyme activity recorded in clams fed for 7 days with microalgae treated with BPS and in those fed for 14 days with BPF-treated microalgae (Figure 2C). Only the factor "exposure time" had a significant effect (two-way ANOVA: $p < 0.01$) on CAT activity in the digestive gland (Figure S11).

As for GR activity, two-way ANOVA demonstrated that all the independent factors affected enzyme activity in both gills (two-way ANOVA: $p < 0.001$, for the factors exposure time and treatment; $p < 0.01$ for the factor exposure time–treatment interaction) and digestive glands (two-way ANOVA: $p < 0.001$, for the factor exposure time; $p < 0.01$ for the factors treatment and exposure time–treatment interaction). The post hoc test revealed a significant decrease in GR activity in digestive glands in clams fed for 7 days with MIX-treated microalgae, when compared to the related control (Figure 2D). Significantly increased GR activity was observed in gills of clams fed for 7 days with MIX-exposed microalgae, with respect to the related control (Figure 2E).

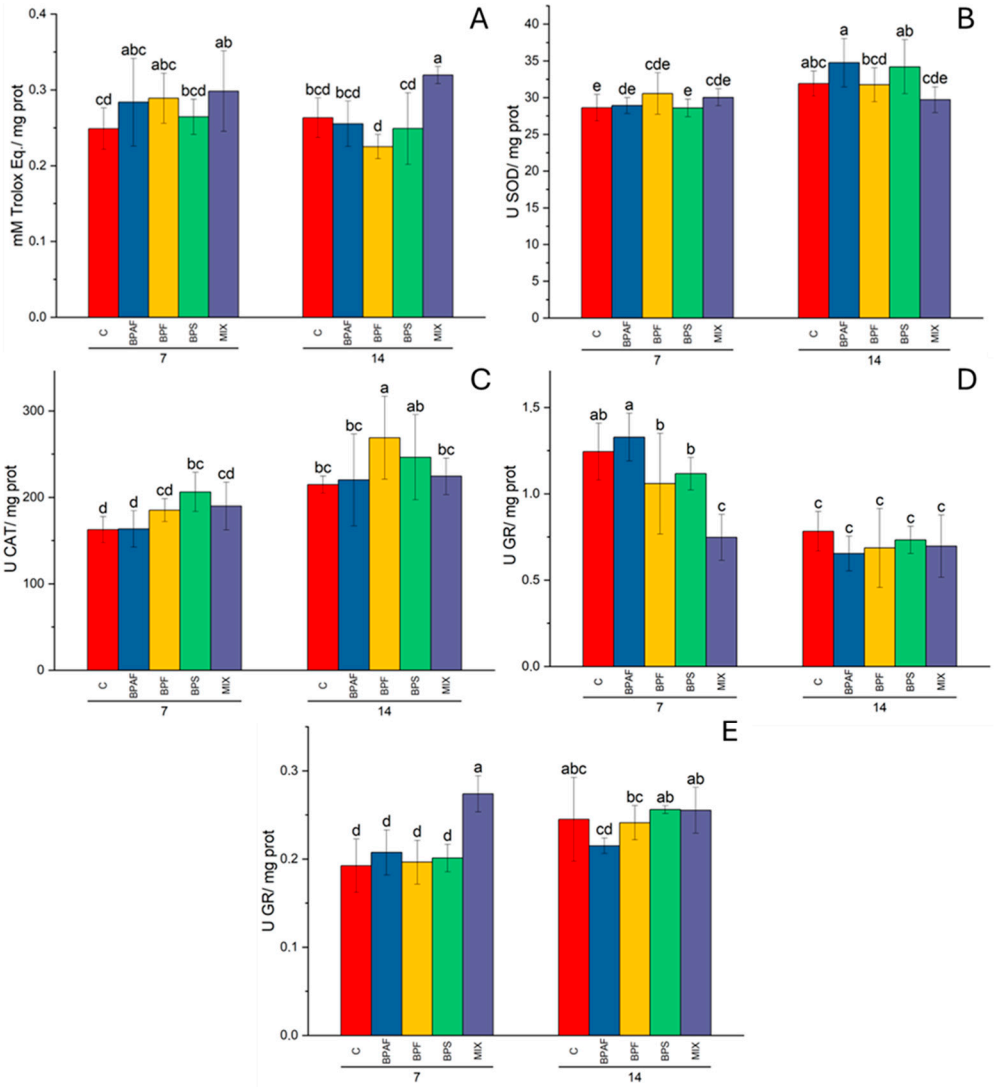

Figure 2. Gill CUPRAC (**A**), expressed as mM of Trolox equivalents/mg proteins; digestive gland SOD activity (**B**), expressed as U/mg proteins; gill CAT activity (**C**), expressed as U/mg proteins; and GR activity in digestive glands (**D**) and gills (**E**), expressed as U/mg proteins, in clams fed with bisphenol-exposed microalgae. Different letters indicate significant differences among all treatments. N = 5.

Only the factor "exposure time" significantly affected digestive gland GST activity (two-way ANOVA: $p < 0.05$) (Figure S12).

As for oxidative damage biomarkers, namely PCC and LPO levels, significant effects of experimental conditions were observed. The PCC level was influenced by the factors "exposure time" in gills (two-way ANOVA: $p < 0.001$) (Figure S13) and "treatment" (two-way ANOVA: $p < 0.01$) in the digestive gland. In the latter tissue, significantly increased PCC levels were observed in clams fed for 14 days with BPS-treated microalgae (Figure 3A). In the digestive gland, LPO levels were influenced by the factors "treatment" and its interaction with exposure time (two-way ANOVA: $p < 0.05$), and the post hoc test highlighted a significant increase in LPO in clams fed for 14 days with MIX- treated microalgae (Figure 3B). In gills, LPO values were influenced by the factors "exposure time" and "exposure time–treatment interaction" (two-way ANOVA: $p < 0.05$). The post hoc test demonstrated that BPS-exposed microalgae caused an increase in LPO levels in the clams fed for 14 days (Figure 3C).

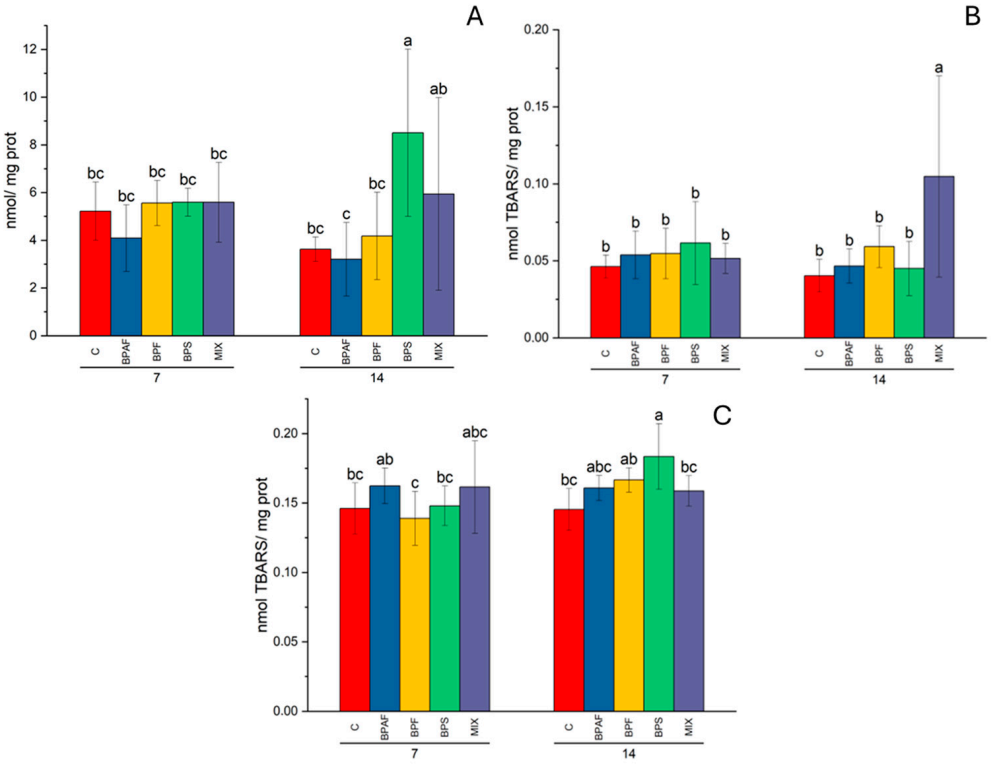

Figure 3. PCC levels in digestive gland (**A**), expressed as nmol/mg proteins, and LPO levels in digestive gland (**B**) and in gills (**C**), expressed as nmol TBARS/mg proteins, in clams fed with bisphenol-exposed microalgae. Different letters indicate significant differences among all treatments. N = 5.

Regarding neurotoxicity biomarkers, only the factor "exposure time" affected gill AChE activity (two-way ANOVA: $p < 0.01$), while all the independent factors did not affect gill BChE activity (Figure S14 and Figure S15, respectively).

3.3. Epigenetic Biomarkers

The HAT activity was measured in clam gills and digestive glands. In the first tissue, independent factors did not affect HAT according to the two-way ANOVA analysis (Figure S16), while in the digestive glands, the factor "exposure time*treatment interaction" significantly affected this epigenetic-involved enzyme activity ($p < 0.05$). The post hoc test showed that clams fed for 14 days with microalgae exposed to MIX had significantly reduced HAT activity (Figure 4A). Regarding the HDAC activity, the factor "treatment" significantly altered enzyme activity in gills ($p < 0.05$). Interestingly, the post hoc test indicated that all clams fed with exposed microalgae had significantly reduced enzyme activity after 7 days of diet (Figure 4B). As for the digestive gland, HDAC activity was altered by the factors "exposure time" ($p < 0.001$) and "treatment" ($p < 0.05$). In particular, clams fed MIX-exposed microalgae showed significantly increased HDAC activity after 7 days (Figure 4C).

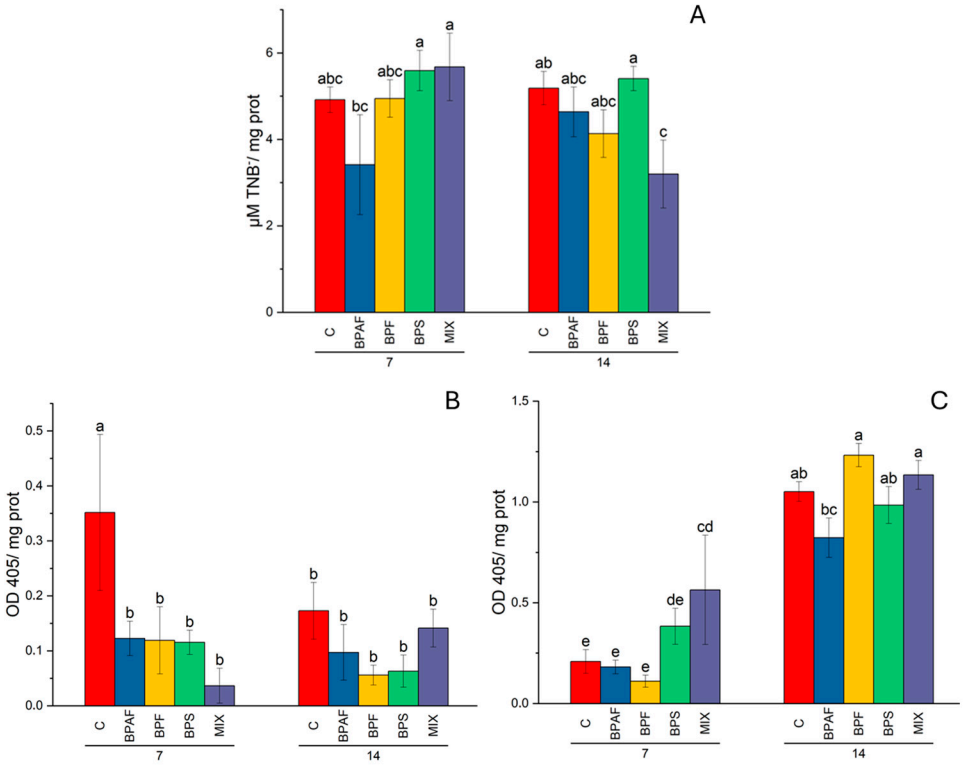

Figure 4. Histone acetyltransferase in digestive glands (**A**), expressed as µmol TNB^-/mg proteins, and histone deacetylase in gills (**B**) and in digestive glands (**C**), expressed as OD405/ mg proteins. Different letters indicate significant differences among all treatments. N = 5.

3.4. Bioaccumulation

Chemical analyses have shown that clams fed for 7 or 14 days with exposed microalgae did not bioaccumulate the three bisphenols. Indeed, measured concentrations were always <LOD for all the samples analysed.

4. Discussion

To the best of our knowledge, this is the first study demonstrating the effects of a diet of BPA analogue-exposed microalgae in the clam *R. philippinarum*. Consequently, the comparison of our results with those of the literature is limited and often refers to data obtained in aquatic organisms exposed to water contaminated by BPA and its analogues or by other contaminants supplied through food.

At the cellular level, we observed increased THC values in clams fed for 7 days with BPAF- and BPF-exposed microalgae, whereas THC was reduced in clams fed for 14 days with BPS-exposed microalgae. Cell proliferation significantly increased in clams fed for 7 days with MIX-exposed microalgae and in those fed for 14 days with BPS-exposed microalgae. Our results highlighted a negative relationship between THC and cell proliferation, both after 7 and 14 days of clam diet (Pearson correlation coefficient: −0.808, $p < 0.001$), with increased THC values generally corresponding to reduced haemocyte proliferation, and vice versa. We hypothesised that the increase in cell proliferation was, at least in part, an attempt of clams to cope with the reduction in THC values, as in the cases of clams fed for 7 days with MIX-exposed microalgae and in those fed for 14 days with BPS-treated microalgae. In contrast, there was no increase in cell proliferation in clams where there were high levels of THC, as in the case of clams fed with BPAF- and BPF-treated microalgae. In our previous study, no significant alterations in THC were observed in clams exposed to the three bisphenols dissolved in water at the same concentrations used in this study, whereas there was a general reduction in both the diameter and volume of haemocytes [15]. In that study, a significant increase in cell proliferation was recorded in

clams exposed for 7 and 14 days to the bisphenol mixture. An impairment of THC was also reported by Tang et al. [35] in the clam *Tegillarca granosa* exposed to BPA. Indeed, the authors reported that THC was reduced after 2 weeks of exposure to 10 and 100 ng/L of BPA, with a decreased percentage of red granulocytes and an increased percentage of both basophil granulocytes and hyalinocytes [35]. BPA was also able to reduce THC values in the crab *Charybdis japonica* exposed for 1, 3, and 6 days to 1 mg/L of BPA [36]. In a recent study, the marine bivalve *Lithophaga lithophaga* was exposed for 28 days to 0.25, 1, 2, and 5 μg/L BPA [37]. In that study, the authors observed an increase in THC value in mussels exposed to 0.25, 2 and 5 μg/L. Interestingly, they also observed a reduction in both mean haemocyte diameter and haemocyte nucleus diameter in all the treatments and all the haemocyte cell types (agranulocytes, hyalinocytes, and granulocytes) [37].

Our findings indicate that BPA analogues can affect THC in clams fed with exposed microalgae, like what was observed for BPA in different model species and experimental designs.

Based on the results of the LDH assay, in the present study, we can state that BPA analogues were not able to cause cytotoxic effects in clams fed with exposed microalgae, similar to what was observed in our previous survey with clams exposed via seawater to the same contaminants [15]. However, it has been demonstrated that higher concentrations of both BPF and BPS than those tested in our studies (0, 15.63, 31.25, 62.50, 125, 250, and 500 μM) can cause cytotoxic effects in hepatocytes of the rainbow trout *Oncorhyncus mykiss* after 24 h of treatment [38,39]. As for hydrolytic enzymes, CFH acid phosphatase activity was significantly increased in clams fed for 14 days with BPAF-exposed microalgae, while HL alkaline phosphatase was reduced in clams fed for 7 days with BPAF, BPS and MIX-exposed microalgae and increased in clams after 14-day diet with BPF-exposed microalgae. These results contrast with the findings obtained in clams exposed to BPA analogue-exposed seawater. Indeed, in that case, acid phosphatase activity decreased significantly in CFH after 7 days of exposure of clams to BPAF, BPF and BPS, and after 14 days in BPF-, BPS- and MIX-exposed clams [15]. Moreover, it has recently been demonstrated that BPA can alter both acid phosphatase and lysozyme activity in the marine worm *Urechis unicinctus* exposed for 15 days to 0.07, 7 and 700 μg/L [40]. In detail, that study reported that the acid phosphatase activity of the experimental group exposed to the highest concentration initially increased and then decreased. Moreover, the acid phosphatase activity of BPA-exposed groups was significantly higher than that of the control group on days 5 and 15. Regarding the lysozyme activity, it was significantly decreased in the worms exposed to 0.07 μg/L after 0.5, 1, 3 and 5 days, while it was significantly increased after 10 and 15 days [40]. On the contrary, the exposure to both 7 and 700 μg/L caused a significant decrease in lysozyme activity in all the sampling times [40].

Overall, it seems that BPA analogues can exert different effects on clam haemocytes, depending on exposure modality, via seawater or contaminated diet. However, it is difficult to state which of the two modalities is more dangerous for *R. philippinarum* haemocytes because both (the one adopted in this study and that of the study by Fabrello et al. [15]) caused effects on haemocyte parameters. Moreover, in the present study, phosphatases showed an opposite pattern of variation between HL and CFH, suggesting a release of enzymes from haemocytes into CFH. Indeed, an increase in enzyme activity was generally observed in CFH, whereas a decrease was observed in HL samples of clams during the first week.

The BPA analogue-exposed diet was able to alter the total antioxidant capacity in clam gills, where CUPRAC levels increased in bivalves fed for 7 and 14 days with MIX-exposed microalgae. Moreover, gill CAT activity significantly increased in clams fed for 7 and 14 days with microalgae exposed to BPS and BPF. Interestingly, no significant alterations of the cupric reducing antioxidant capacity (=CUPRAC) were recorded in the digestive gland, suggesting that the main diet-mediated toxic effects occurred in gills during the first part of the feeding process. These findings also suggest that BPA analogue-exposed microalgae caused an increase in hydrogen peroxide, inducing a response of CAT in gills. At the same time, no induction of SOD activity was recorded, suggesting the absence of

superoxide anion production. However, further studies are necessary to better elucidate the involvement of bisphenols in ROS production.

This evidence is in accordance with our previous results obtained in clams exposed to contaminated seawater [15]. Indeed, in that study, no significant alterations of CUPRAC levels were observed in digestive glans, whereas there was a significant reduction in the total antioxidant capability in gills from clams exposed for 14 days to BPS and MIX. In addition, gill SOD activity increased significantly in animals exposed to BPS (after 14 days) and MIX (after 7 and 14 days), while CAT activity increased following exposure for 7 and 14 days to MIX [15].

The glutathione cycle plays a pivotal role in both restoring the oxidative status inside the cells and detoxifying xenobiotics. Two of the main glutathione cycle-involved enzymes are GR and GST. In the present study, the first one was significantly affected by the ingestion of exposed microalgae in both the gills and digestive glands of clams. Indeed, GR activity was significantly increased in the gills of clams fed for 7 days with MIX-exposed microalgae, while a reduction in GR activity was found in the digestive gland. The increased activity of GR in gills indicates that the glutathione level (GSH) needed to be restored, probably because it was reduced during antioxidant response. In accordance, the CUPRAC results in gills highlighted an increased antioxidant level in the gills of clams exposed to MIX-treated microalgae. Recently, the effects of BPA on a simplified food chain were investigated by Esperanza et al. [41] in which the clams *Corbicula fluminea* were exposed for 30 days to BPA-exposed microalgae, BPA-exposed water or BPA in both microalgae and water. For the preparation of BPA-exposed microalgae, they exposed *Chlamydomonas reinhardtii* cultures for 24 h at 30 mg/L of BPA, while the tested BPA concentration in water was 7.5 mg/L. Like our study, Esperanza et al. [41] measured several biomarkers in clams. CAT, selenium-dependent glutathione peroxidase (GPX) and total GPX activities were significantly increased in the whole tissues, whereas GR activity increased at all the exposure conditions, even if the exposure to exposed microalgae only caused the lowest GR increase. Contrary to what was observed in our study concerning GST results, which did not reveal any alteration, Esperanza et al. [41] observed a significant inhibition of GST activity after exposure to both BPA-exposed water and microalgae. Regarding BPA analogues, very few studies have been conducted on a simplified marine food chain. In *Chlamys farreri*, the effects of exposure via microalgae alone or microalgae + water contaminated with the BPA analogue tetrabromobisphenol A (TBBPA) were assessed [42]. Firstly, the authors exposed the microalgae *Nitzschia closterium f. minutissima* to 400 μg/L of TBBPA for 24 h and then they provided the microalgae to scallops for 10 days. After 0.5, 1, 3, 6 and 10 days of diet, GST activity, as well as glutathione levels, was significantly increased by experimental conditions in both gills and digestive glands. The authors reported that TBBPA also increased SOD activity at almost all the conditions tested, concluding that TBBPA was able to cause oxidative stress in clams [42]. They also reported a significant reduction in microsomal cytochrome P450 in the gills and digestive gland. Similarly, cytochrome b5 values were significantly reduced by all treatments, even if 3 days of water+food-borne exposure caused a significant increase in gills [42].

As for the results of previous studies on the effects of food contaminated by other contaminants, Iummato et al. [43] analysed the biochemical alterations in the golden mussel *Limnoperna fortunei* under dietary glyphosate exposure. Briefly, the green algae *Scenedesmus vacuolatus* was previously exposed to a mixture of commercial formulation of glyphosate (6 mg/L active principle) with the addition of alkyl aryl polyglycol ether surfactant. Then, the algae were used as food for mussels for 4 weeks and the authors measured the activity of SOD, CAT, GST, and alkaline phosphatase, as well as the glutathione (GSH) content after 1, 7, 14, 21 and 28 days of dietary exposure of mussels. They found that mussels fed on glyphosate-exposed microalgae for 28 days showed increased GST activity, whereas alkaline phosphatase activity was significantly increased at 21 and 28 days of dietary exposure. On the contrary, GSH content and CAT and SOD activities did not show significant differences between treated and untreated bivalves [43]. A similar experimental plan was adopted

to assess the effect and transfer of other compounds, such as heavy metals, nanoparticles and hydrocarbons [44–47]. For instance, the effects of benzo(α)pyrene and 7,12-dimethyl benz(α)anthracene on a marine food chain were evaluated at a concentration of 5 ng/L each on the mussels *Mytilus galloprovincialis* that were directly exposed to contaminated seawater and in fishes *Dicentrarchus labrax* that were exposed to contaminated seawater or fed with exposed mussels for 75 days. Benzo(α)pyrene-monooxygenase activity increased in treated shellfish, while ethoxyresorufin-O-deethylase (EROD) activity increased after 20 days in fishes exposed to contaminated seawater or fed with exposed mussels [44]. More recently, Wang et al. [47] assessed the trophic transfer and effects of titanium dioxide nanoparticles (TiO_2 NPs) from the marine microalga *Nitzschia closterium* to the scallop *Chlamys farreri*. In detail, they exposed the scallop through aqueous exposure or dietary exposure, and they found increased lysosomal membrane permeability, DNA damage, and histopathological effects induced by TiO_2 NPs, mainly in scallops after aqueous exposure rather than dietary exposure [47]. In another study, the effects of silver nanoparticles (Ag NPs) (soluble or as lactate Ag NPs) at low concentrations (10 µg/L) were evaluated in the bivalve *Scrobicularia plana* exposed for 14 days directly (water) or via the diet (microalgae) [48]. Interestingly, the authors highlighted that the response of oxidative stress biomarkers (CAT, GST, SOD) in the whole soft tissues of bivalves was more important after dietary than water-borne exposure to Ag. In detail, CAT activity significantly increased by both water and dietary Ag, whereas an Ag-contaminated diet caused significantly increased activity of both SOD and GST [48].

We have also evaluated oxidative damage to both lipids and proteins in clams fed with BPA analogue-exposed microalgae. As a result, oxidative damage to proteins (PCC levels) increased significantly only in the digestive gland of clams fed for 14 days with BPS-exposed microalgae. Moreover, LPO increased in clam gills following a diet of 14 days with BPS-exposed microalgae, while in the digestive gland, LPO levels increased significantly after 14 days in clams fed with MIX-exposed microalgae. The finding that BPS- and MIX-exposed microalgae were able to increase oxidative damage in clams suggested that BPS, if provided via food, both alone or in a mixture, can be considered the most harmful BPA analogue among the three tested.

Esperanza et al. [41] reported an increased LPO level in the clams *Corbicula fluminea* exposed for 30 days to BPA-exposed water or BPA-exposed microalgae and water. Overall, the results obtained in this study indicated that BPA analogues can alter the antioxidant system and cause oxidative damage in clams.

Previous studies indicated that bisphenols can cause neurotoxic effects [49,50]. However, we did not observe neurotoxicity in both the present and the previous study [15]. Therefore, we can exclude that BPA analogues are neurotoxic to clams, at least under the experimental conditions tested.

The effects of a contaminated diet on the activity of enzymes involved in epigenetic mechanisms were also evaluated for the first time in clams. We measured the activity of enzymes involved in the addition and remotion of acetyl groups from the histones, which is a well-known histone post-translational modification that can change the regulation of gene expression [51]. Regarding ecotoxicological studies, it has been demonstrated that exposure to chemical compounds can alter epigenetic mechanisms, as reported in zebrafish exposed to several compounds, such as benzo-α pyrene, heavy metals, PFASs and BPA [52–56]. In particular, it has been demonstrated that exposure to BPA induced global transcriptomic changes in zebrafish embryos and larvae with an alteration in the gene expression of histone deacetylases and DNA methyltransferases [57]. Similarly, Gonzalez-Rojo et al. [58] reported that BPA significantly altered the gene expression of histone acetylation-related genes. In detail, they observed that zebrafish males exposed to 2 mg/L of BPA showed alterations in the expression of two histone deacetylase genes in the testes after 21 days of exposure. There was a decrease in gene expression of the *kat6a* gene and, at the same time, an increase in the *hdac4* gene expression level. Interestingly, they also observed that the global H3 histone acetylation in the testes increased after exposure to both 0.1 mg/L and

2 mg/L, while HAT activity in testes nuclear extracts significantly increased after exposure for 21 days to 2 mg/L of BPA. Our results indicated that BPA analogues provided through food can also alter the enzyme activity of both HAT and HDAC. In particular, clams fed for 14 days with MIX-treated microalgae had significantly reduced HAT activity in the digestive gland. In the same tissue, HDAC activity was significantly increased by the same treatment, but after 7 days of diet. Altered enzyme activities could have caused a reduction in the global histone acetylation level in the digestive gland of clams. On the contrary, gill HDAC activity significantly decreased after 7 days under all the treatments, in comparison to the related control, suggesting an increased histone acetylation level. However, the global histone acetylation level was not evaluated in this study.

Regarding bioaccumulation, no detectable concentrations of bisphenols were found in clams after ingestion of exposed microalgae. However, it is reported that diet can be a vehicle for bisphenols between different food chain levels. Indeed, Hu et al. [42] reported that TBBPA was significantly bioaccumulated after both food-borne and water+food-borne exposure to the mollusc *Clamys farreri*. Interestingly, bioaccumulation was observed in gills, digestive glands, muscles and soft tissues after 0.5, 1, 3 and 6 days of exposure. However, the dietary uptake was lower than the direct TBBPA uptake from water [42]. A similar result was reported in *Scrobicularia plana* for both soluble and lactate Ag NPs, in which bioaccumulation was higher after 14 days of water-borne than dietary exposure [48]. Similar conclusions (greater bioaccumulation in clams exposed to seawater compared to those fed contaminated food) can be formulated for this study because in the previous one, we demonstrated that clams exposed to bisphenols through seawater can accumulate such contaminants [15].

In conclusion, our results suggest that a diet of BPA analogue-exposed microalgae can affect important biomarkers in different clam tissues. Indeed, THC, haemocyte proliferation and two important hydrolytic enzymes, acid and alkaline phosphatases, were affected by exposed microalgae, revealing that BPA analogues can alter some immune responses if provided via food. We also observed an increase in CAT activity, suggesting that a BPA analogue-exposed diet exerted toxic effects, mainly in gills, which is the first organ of the feeding process. Nevertheless, GR activity increased in gills and decreased in digestive glands. Oxidative damage was found in both gills and digestive glands, suggesting that BPA analogues can affect important macromolecules when provided to clams through diet. Lastly, our study demonstrated for the first time that BPA analogue-exposed microalgae can alter epigenetic mechanisms in marine invertebrates. No bioaccumulation of BPA analogues was detected in clam soft tissues. Overall, this study demonstrated that a diet of BPA analogue-exposed microalgae can induce significant alterations of some important biological responses of *R. philippinarum*. To the best of our knowledge, this is the first study demonstrating the effects of ingestion of exposed microalgae in the clam *R. philippinarum*, suggesting a potential ecotoxicological risk for the marine food chain, at least at the first levels.

Supplementary Materials: The following supporting information can be downloaded at: https://www.mdpi.com/article/10.3390/jox14030069/s1, Figure S1: haemocyte diameter, expressed as µm. Different letters indicate significant differences among all treatments. N = 5; Figure S2: haemocyte volume, expressed as pL. Different letters indicate significant differences among all treatments. N = 5; Figure S3: LDH activity expressed, as OD490 nm. Different letters indicate significant differences among all treatments. N = 5; Figure S4: lysozyme activity in HL, expressed as µg lysozyme/mg proteins. Different letters indicate significant differences among all treatments. N = 5; Figure S5: arylsulfatase activity in HL, expressed as µg p-nitrocatechol/h/mg proteins. Different letters indicate significant differences among all treatments. N = 5; Figure S6: acid phosphatase activity in HL, expressed as U/mg proteins. Different letters indicate significant differences among all treatments. N = 5; Figure S7: alkaline phosphatase activity in CFH, expressed as U/mg proteins. Different letters indicate significant differences among all treatments. N = 5; Figure S8: CUPRAC levels in haemolymph, expressed as mM Trolox Eq/mg proteins. Different letters indicate significant differences among all treatments. N = 5; Figure S9: CUPRAC levels in digestive gland, expressed as

mM Trolox Eq/mg proteins. Different letters indicate significant differences among all treatments. N = 5; Figure S10: SOD activity in gills, expressed as U SOD/mg proteins. Different letters indicate significant differences among all treatments. N = 5; Figure S11: CAT activity in the digestive gland, expressed as U CAT/mg proteins. Different letters indicate significant differences among all treatments. N = 5; Figure S12: GST activity in the digestive gland, expressed as nmol/min/mg proteins. Different letters indicate significant differences among all treatments. N = 5; Figure S13: PCC levels in gills expressed as nmol/mg proteins. Different letters indicate significant differences among all treatments. N = 5; Figure S14: AChE activity in gills, expressed as nmol/min/mg proteins. Different letters indicate significant differences among all treatments. N = 5; Figure S15: BChE activity in gills, expressed as nmol/min/mg proteins. Different letters indicate significant differences among all treatments. N = 5; Figure S16: HAT activity in gills, expressed as µmol TNB-/mg proteins. Different letters indicate significant differences among all treatments. N = 5.

Author Contributions: Conceptualization, J.F., M.R., S.B. and V.M.; methodology, J.F., M.D.F., N.G. and M.C.; formal analysis, J.F. and M.R.; writing—original draft preparation, J.F., M.R., S.B. and V.M.; supervision, V.M. All authors have read and agreed to the published version of the manuscript.

Funding: This research received no external funding.

Institutional Review Board Statement: Not applicable.

Informed Consent Statement: Not applicable.

Data Availability Statement: The data presented are available in this article.

Conflicts of Interest: The authors declare no conflicts of interest.

References

1. Almeida, S.; Raposo, A.; Almeida-González, M.; Carrascosa, C. Bisphenol A: Food Exposure and Impact on Human Health. *Compr. Rev. Food Sci. Food Saf.* **2018**, *17*, 1503–1517. [CrossRef] [PubMed]
2. Vandenberg, L.N.; Hauser, R.; Marcus, M.; Olea, N.; Welshons, W.V. Human Exposure to Bisphenol A (BPA). *Reprod. Toxicol.* **2007**, *24*, 139–177. [CrossRef] [PubMed]
3. Bhandari, R.K.; Deem, S.L.; Holliday, D.K.; Jandegian, C.M.; Kassotis, C.D.; Nagel, S.C.; Tillitt, D.E.; Vom Saal, F.S.; Rosenfeld, C.S. Effects of the Environmental Estrogenic Contaminants Bisphenol A and 17α-Ethinyl Estradiol on Sexual Development and Adult Behaviors in Aquatic Wildlife Species. *Gen. Comp. Endocrinol.* **2015**, *214*, 195–219. [CrossRef] [PubMed]
4. Chen, D.; Kannan, K.; Tan, H.; Zheng, Z.; Feng, Y.-L.; Wu, Y.; Widelka, M. Bisphenol Analogues Other Than BPA: Environmental Occurrence, Human Exposure, and Toxicity—A Review. *Environ. Sci. Technol.* **2016**, *50*, 5438–5453. [CrossRef] [PubMed]
5. Fabrello, J.; Matozzo, V. Bisphenol Analogs in Aquatic Environments and Their Effects on Marine Species—A Review. *J. Mar. Sci. Eng.* **2022**, *10*, 1271. [CrossRef]
6. Wang, Q.; Chen, M.; Shan, G.; Chen, P.; Cui, S.; Yi, S.; Zhu, L. Bioaccumulation and Biomagnification of Emerging Bisphenol Analogues in Aquatic Organisms from Taihu Lake, China. *Sci. Total Environ.* **2017**, *598*, 814–820. [CrossRef] [PubMed]
7. Yamazaki, E.; Yamashita, N.; Taniyasu, S.; Lam, J.; Lam, P.K.S.; Moon, H.-B.; Jeong, Y.; Kannan, P.; Achyuthan, H.; Munuswamy, N.; et al. Bisphenol A and Other Bisphenol Analogues Including BPS and BPF in Surface Water Samples from Japan, China, Korea and India. *Ecotoxicol. Environ. Saf.* **2015**, *122*, 565–572. [CrossRef]
8. Huang, C.; Wu, L.-H.; Liu, G.-Q.; Shi, L.; Guo, Y. Occurrence and Ecological Risk Assessment of Eight Endocrine-Disrupting Chemicals in Urban River Water and Sediments of South China. *Arch. Environ. Contam. Toxicol.* **2018**, *75*, 224–235. [CrossRef]
9. Zhao, X.; Qiu, W.; Zheng, Y.; Xiong, J.; Gao, C.; Hu, S. Occurrence, Distribution, Bioaccumulation, and Ecological Risk of Bisphenol Analogues, Parabens and Their Metabolites in the Pearl River Estuary, South China. *Ecotoxicol. Environ. Saf.* **2019**, *180*, 43–52. [CrossRef]
10. Xie, J.; Zhao, N.; Zhang, Y.; Hu, H.; Zhao, M.; Jin, H. Occurrence and Partitioning of Bisphenol Analogues, Triclocarban, and Triclosan in Seawater and Sediment from East China Sea. *Chemosphere* **2022**, *287*, 132218. [CrossRef]
11. Gao, Y.; Xiao, S.-K.; Wu, Q.; Pan, C.-G. Bisphenol Analogues in Water and Sediment from the Beibu Gulf, South China Sea: Occurrence, Partitioning and Risk Assessment. *Sci. Total Environ.* **2023**, *857*, 159445. [CrossRef] [PubMed]
12. NORMAN Ecotoxicology Database. Available online: https://www.norman-network.com/nds/ecotox/lowestPnecsIndex.php (accessed on 6 June 2024).
13. European Commission; Joint Research Centre. Institute for Health and Consumer Protection. In *Updated European Union Risk Assessment Report: 4,4'-Isopropylidenediphenol (Bisphenol-A): Environment Addendum of February 2008*; Office for Official Publications of the European Communities: Luxembourg, 2010.
14. Fabrello, J.; Guidorizzi, S.; Ciscato, M.; Battistuzzi, M.; Moschin, E.; Dalla Vecchia, F.; Moro, I.; Roverso, M.; Bogialli, S.; Matozzo, V. Ultrastructural Changes, Pigment Responses and Bioaccumulation in the Microalga *Phaeodactylum tricornutum* Bohlin Exposed to BPA Analogues. *Aquat. Toxicol.* **2024**, *272*, 106970. [CrossRef]

15. Fabrello, J.; Ciscato, M.; Munari, M.; Vecchiatti, A.; Roverso, M.; Bogialli, S.; Matozzo, V. Ecotoxicological Effects and Bioaccumulation of BPA Analogues and Their Mixture in the Clam *Ruditapes philippinarum*. *Mar. Environ. Res.* **2023**, *192*, 106228. [CrossRef] [PubMed]
16. Guillard, R.R.L. Culture of Phytoplankton for Feeding Marine Invertebrates. In *Culture of Marine Invertebrate Animals: Proceedings—1st Conference on Culture of Marine Invertebrate Animals Greenport*; Smith, W.L., Chanley, M.H., Eds.; Springer: Boston, MA, USA, 1975; pp. 29–60, ISBN 978-1-4615-8714-9.
17. Hutchinson, T.H.; Shillabeer, N.; Winter, M.J.; Pickford, D.B. Acute and Chronic Effects of Carrier Solvents in Aquatic Organisms: A Critical Review. *Aquat. Toxicol.* **2006**, *76*, 69–92. [CrossRef] [PubMed]
18. Kaviraj, A.; Bhunia, F.; Saha, N.C. Toxicity of Methanol to Fish, Crustacean, Oligochaete Worm, and Aquatic Ecosystem. *Int. J. Toxicol.* **2004**, *23*, 55–63. [CrossRef]
19. Zucker-Franklin, D.; Grusky, G.; Yang, J.S. Arylsulfatase in Natural Killer Cells: Its Possible Role in Cytotoxicity. *Proc. Natl. Acad. Sci. USA* **1983**, *80*, 6977–6981. [CrossRef]
20. Baum, H.; Dodgson, K.S.; Spencer, B. The Assay of Arylsulphatases A and B in Human Urine. *Clin. Chim. Acta* **1959**, *4*, 453–455. [CrossRef]
21. Ross, N.W.; Firth, K.J.; Wang, A.; Burka, J.F.; Johnson, S.C. Changes in Hydrolytic Enzyme Activities of Naïve Atlantic Salmon *Salmo salar* Skin Mucus Due to Infection with the Salmon Louse *Lepeophtheirus salmonis* and Cortisol Implantation. *Dis. Aquat. Org.* **2000**, *41*, 43–51. [CrossRef]
22. Apak, R.; Güçlü, K.; Özyürek, M.; Karademir, S.E. Novel Total Antioxidant Capacity Index for Dietary Polyphenols and Vitamins C and E, Using Their Cupric Ion Reducing Capability in the Presence of Neocuproine: CUPRAC Method. *J. Agric. Food Chem.* **2004**, *52*, 7970–7981. [CrossRef]
23. Crapo, J.D.; McCord, J.M.; Fridovich, I. [41] Preparation and Assay of Superioxide Dismutases. In *Methods in Enzymology*; Fleischer, S., Packer, L., Eds.; Biomembranes—Part D: Biological Oxidations; Academic Press: Cambridge, MA, USA, 1978; Volume 53, pp. 382–393.
24. Aebi, H. Catalase In Vitro. In *Methods in Enzymology*; Oxygen Radicals in Biological Systems; Academic Press: Cambridge, MA, USA, 1984; Volume 105, pp. 121–126.
25. Ellman, G.L.; Courtney, K.D.; Andres, V.; Featherstone, R.M. A New and Rapid Colorimetric Determination of Acetylcholinesterase Activity. *Biochem. Pharmacol.* **1961**, *7*, 88–95. [CrossRef]
26. Escartín, E.; Porte, C. The Use of Cholinesterase and Carboxylesterase Activities from *Mytilus galloprovincialis* in Pollution Monitoring. *Environ. Toxicol. Chem.* **1997**, *16*, 2090–2095. [CrossRef]
27. Smith, I.K.; Vierheller, T.L.; Thorne, C.A. Assay of Glutathione Reductase in Crude Tissue Homogenates Using 5,5′-Dithiobis(2-Nitrobenzoic Acid). *Anal. Biochem.* **1988**, *175*, 408–413. [CrossRef] [PubMed]
28. Habig, W.H.; Pabst, M.J.; Jakoby, W.B. Glutathione S Transferases. The First Enzymatic Step in Mercapturic Acid Formation. *J. Biol. Chem.* **1974**, *249*, 7130–7139. [CrossRef]
29. Mecocci, P.; Fanó, G.; Fulle, S.; MacGarvey, U.; Shinobu, L.; Polidori, M.C.; Cherubini, A.; Vecchiet, J.; Senin, U.; Beal, M.F. Age-Dependent Increases in Oxidative Damage to DNA, Lipids, and Proteins in Human Skeletal Muscle. *Free Radic. Biol. Med.* **1999**, *26*, 303–308. [CrossRef]
30. Buege, J.A.; Aust, S.D. Microsomal Lipid Peroxidation. *Methods Enzymol.* **1978**, *52*, 302–310. [CrossRef] [PubMed]
31. Damiens, G.; Gnassia-Barelli, M.; Loquès, F.; Roméo, M.; Salbert, V. Integrated Biomarker Response Index as a Useful Tool for Environmental Assessment Evaluated Using Transplanted Mussels. *Chemosphere* **2007**, *66*, 574–583. [CrossRef]
32. Bradford, M.M. A Rapid and Sensitive Method for the Quantitation of Microgram Quantities of Protein Utilizing the Principle of Protein-Dye Binding. *Anal. Biochem.* **1976**, *72*, 248–254. [CrossRef] [PubMed]
33. Foyn, H.; Thompson, P.R.; Arnesen, T. DTNB-Based Quantification of In Vitro Enzymatic N-Terminal Acetyltransferase Activity. *Methods Mol. Biol.* **2017**, *1574*, 9–15. [CrossRef]
34. Yuan, Z.; Rezai-Zadeh, N.; Zhang, X.; Seto, E. Histone Deacetylase Activity Assay. *Methods Mol. Biol.* **2009**, *523*, 279–293. [CrossRef]
35. Tang, Y.; Zhou, W.; Sun, S.; Du, X.; Han, Y.; Shi, W.; Liu, G. Immunotoxicity and Neurotoxicity of Bisphenol A and Microplastics Alone or in Combination to a Bivalve Species, *Tegillarca granosa*. *Environ. Pollut.* **2020**, *265*, 115115. [CrossRef]
36. Peng, Y.Q.; Wang, M.J.; Chen, H.G.; Chen, J.H.; Gao, H.; Huang, H.H. Immunological Responses in Haemolymph and Histologic Changes in the Hepatopancreas of *Charybdis japonica* (A. Milne-Edwards, 1861) (Decapoda: Brachyura: Portunidae) Exposed to Bisphenol A. *J. Crustac. Biol.* **2018**, *38*, 489–496. [CrossRef]
37. Abd Elkader, H.-T.A.E.; Al-Shami, A.S. Chronic Exposure to Bisphenol A Induces Behavioural, Neurochemical, Histological, and Ultrastructural Alterations in the Ganglia Tissue of the Date Mussels *Lithophaga lithophaga*. *Environ. Sci. Pollut. Res. Int.* **2023**, *30*, 109041–109062. [CrossRef]
38. Aykut, H.; Kaptaner, B. In Vitro Effects of Bisphenol F on Antioxidant System Indicators in the Isolated Hepatocytes of Rainbow Trout (*Oncorhyncus mykiss*). *Mol. Biol. Rep.* **2021**, *48*, 2591–2599. [CrossRef]
39. Kaptaner, B.; Yılmaz, C.; Aykut, H.; Doğan, E.; Fidan, C.; Bostancı, M.; Yıldız, F. Bisphenol S Leads to Cytotoxicity-Induced Antioxidant Responses and Oxidative Stress in Isolated Rainbow Trout (*Oncorhyncus mykiss*) Hepatocytes. *Mol. Biol. Rep.* **2021**, *48*, 7657–7666. [CrossRef]

40. Ranđelović, D.; Gajić, G.; Mutić, J.; Pavlović, P.; Mihailović, N.; Jovanović, S. Nonspecific Immune, Histology and Accumulation of Marine Worm, *Urechis unicinctus* in Response to Bisphenol A (BPA). *Ecotoxicol. Environ. Saf.* **2024**, *271*, 115993. [CrossRef]
41. Esperanza, M.; Seoane, M.; Servia, M.J.; Cid, Á. Effects of Bisphenol A on the Microalga *Chlamydomonas reinhardtii* and the Clam Corbicula Fluminea. *Ecotoxicol. Environ. Saf.* **2020**, *197*, 110609. [CrossRef] [PubMed]
42. Hu, F.; Pan, L.; Xiu, M.; Liu, D. Dietary Accumulation of Tetrabromobisphenol A and Its Effects on the Scallop *Chlamys farreri*. *Comp. Biochem. Physiol. Part C Toxicol. Pharmacol.* **2015**, *167*, 7–14. [CrossRef] [PubMed]
43. Iummato, M.M.; Sabatini, S.E.; Cacciatore, L.C.; Cochón, A.C.; Cataldo, D.; de Molina, M.D.C.R.; Juárez, Á.B. Biochemical Responses of the Golden Mussel *Limnoperna fortunei* under Dietary Glyphosate Exposure. *Ecotoxicol. Environ. Saf.* **2018**, *163*, 69–75. [CrossRef]
44. D'adamo, R.; Pelosi, S.; Trotta, P.; Sansone, G. Bioaccumulation and Biomagnification of Polycyclic Aromatic Hydrocarbons in Aquatic Organisms. *Mar. Chem.* **1997**, *56*, 45–49. [CrossRef]
45. Wikfors, G.H.; Twarog, J.W.; Ferris, G.E.; Smith, B.C.; Ukeles, R. Survival and Growth of Post-Set Oysters and Clams on Diets of Cadmium-Contaminated Microalgal Cultures. *Mar. Environ. Res.* **1994**, *37*, 257–281. [CrossRef]
46. Ettajani, B.; Berthet, J.C.; Amiard, H. Determination of Cadmium Partitioning in Microalgae and Oysters: Contribution to the Assessment of Trophic Transfer. *Arch. Environ. Contam. Toxicol.* **2001**, *40*, 209–221. [CrossRef]
47. Wang, Z.; Xia, B.; Chen, B.; Sun, X.; Zhu, L.; Zhao, J.; Du, P.; Xing, B. Trophic Transfer of TiO2 Nanoparticles from Marine Microalga (*Nitzschia closterium*) to Scallop (*Chlamys farreri*) and Related Toxicity. *Environ. Sci. Nano* **2017**, *4*, 415–424. [CrossRef]
48. Buffet, P.E.; Pan, J.F.; Poirier, L.; Amiard-Triquet, C.; Amiard, J.C.; Gaudin, P.; Risso-de Faverney, C.; Guibbolini, M.; Gilliland, D.; Valsami-Jones, E.; et al. Biochemical and Behavioural Responses of the Endobenthic Bivalve *Scrobicularia plana* to Silver Nanoparticles in Seawater and Microalgal Food. *Ecotoxicol. Environ. Saf.* **2013**, *89*, 117–124. [CrossRef]
49. Jenzri, M.; Gharred, C.; Bouraoui, Z.; Guerbej, H.; Jebali, J.; Gharred, T. Assessment of Single and Combined Effects of Bisphenol-A and Its Analogue Bisphenol-S on Biochemical and Histopathological Responses of Sea Cucumber *Holothuria poli*. *Mar. Environ. Res.* **2023**, *188*, 106032. [CrossRef] [PubMed]
50. Minier, C.; Forget-Leray, J.; Bjørnstad, A.; Camus, L. Multixenobiotic Resistance, Acetyl-Choline Esterase Activity and Total Oxyradical Scavenging Capacity of the Arctic Spider Crab, *Hyas Araneus*, following Exposure to Bisphenol A, Tetra Bromo Diphenyl Ether and Diallyl Phthalate. *Mar. Pollut. Bull.* **2008**, *56*, 1410–1415. [CrossRef] [PubMed]
51. Kouzarides, T. Chromatin Modifications and Their Function. *Cell* **2007**, *128*, 693–705. [CrossRef]
52. Bouwmeester, M.C.; Ruiter, S.; Lommelaars, T.; Sippel, J.; Hodemaekers, H.M.; van den Brandhof, E.J.; Pennings, J.L.; Kamstra, J.H.; Jelinek, J.; Issa, J.P.J.; et al. Zebrafish Embryos as a Screen for DNA Methylation Modifications after Compound Exposure. *Toxicol. Appl. Pharmacol.* **2016**, *291*, 84–96. [CrossRef]
53. Laing, L.V.; Viana, J.; Dempster, E.L.; Trznadel, M.; Trunkfield, L.A.; Webster, T.M.U.; van Aerle, R.; Paull, G.C.; Wilson, R.J.; Mill, J.; et al. Bisphenol A Causes Reproductive Toxicity, Decreases Dnmt1 Transcription, and Reduces Global DNA Methylation in Breeding Zebrafish (*Danio rerio*). *Epigenetics* **2016**, *11*, 526–538. [CrossRef] [PubMed]
54. Corrales, J.; Fang, X.; Thornton, C.; Mei, W.; Barbazuk, W.B.; Duke, M.; Scheffler, B.E.; Willett, K.L. Effects on Specific Promoter DNA Methylation in Zebrafish Embryos and Larvae following Benzo[a]Pyrene Exposure. *Comp. Biochem. Physiol. Part C Toxicol. Pharmacol.* **2014**, *163*, 37–46. [CrossRef]
55. Meyer, D.N.; Crofts, E.J.; Akemann, C.; Gurdziel, K.; Farr, R.; Baker, B.B.; Weber, D.; Baker, T.R. Developmental Exposure to Pb^{2+} Induces Transgenerational Changes to Zebrafish Brain Transcriptome. *Chemosphere* **2020**, *244*, 125527. [CrossRef]
56. Khazaee, M.; Guardian, M.G.E.; Aga, D.S.; Ng, C.A. Impacts of Sex and Exposure Duration on Gene Expression in Zebrafish following Perfluorooctane Sulfonate Exposure. *Environ. Toxicol. Chem.* **2020**, *39*, 437–449. [CrossRef] [PubMed]
57. Huang, W.; Zheng, S.; Wang, X.; Cai, Z.; Xiao, J.; Liu, C.; Wu, K.A. Transcriptomics-Based Analysis of Toxicity Mechanisms of Zebrafish Embryos and Larvae following Parental Bisphenol A Exposure. *Ecotoxicol. Environ. Saf.* **2020**, *205*, 111165. [CrossRef] [PubMed]
58. González-Rojo, S.; Lombó, M.; Fernández-Díez, C.; Herráez, M.P. Male Exposure to Bisphenol a Impairs Spermatogenesis and Triggers Histone Hyperacetylation in Zebrafish Testes. *Environ. Pollut.* **2019**, *248*, 368–379. [CrossRef] [PubMed]

Journal of
Xenobiotics

MDPI

Article

Estrogenic Responsiveness of Brown Trout Primary Hepatocyte Spheroids to Environmental Levels of 17α-Ethinylestradiol

Rodrigo F. Alves [1,2], Célia Lopes [1,2], Eduardo Rocha [1,2,†] and Tânia Vieira Madureira [1,2,*,†]

[1] Team of Animal Morphology and Toxicology, Interdisciplinary Centre of Marine and Environmental Research (CIIMAR/CIMAR), University of Porto (U.Porto), Terminal de Cruzeiros do Porto de Leixões, Av. General Norton de Matos s/n, 4450-208 Matosinhos, Portugal; rodrigo.r.f.alves@hotmail.com (R.F.A.); cclopes@icbas.up.pt (C.L.); erocha@icbas.up.pt (E.R.)
[2] Laboratory of Histology and Embryology, Department of Microscopy, ICBAS—School of Medicine and Biomedical Sciences, University of Porto (U.Porto), Rua Jorge Viterbo Ferreira 228, 4050-313 Porto, Portugal
* Correspondence: tvmadureira@icbas.up.pt
† Joint senior authors.

Abstract: Three-dimensional (3D) fish hepatocyte cultures are promising alternative models for replicating in vivo data. Few studies have attempted to characterise the structure and function of fish 3D liver models and illustrate their applicability. This study aimed to further characterise a previously established spheroid model obtained from juvenile brown trout (*Salmo trutta*) primary hepatocytes under estrogenic stimulation. The spheroids were exposed for six days to environmentally relevant concentrations of 17α-ethinylestradiol—EE2 (1–100 ng/L). The mRNA levels of peroxisome (*catalase—Cat* and *urate oxidase—Uox*), lipid metabolism (*acyl-CoA long chain synthetase 1—Acsl1*, *apolipoprotein AI—ApoAI*, and *fatty acid binding protein 1—Fabp1*), and estrogen-related (*estrogen receptor α—ERα*, *estrogen receptor β—ERβ*, *vitellogenin A—VtgA*, *zona pellucida glycoprotein 2.5—ZP2.5*, and *zona pellucida glycoprotein 3a.2—ZP3a.2*) target genes were evaluated by quantitative real-time polymerase chain reaction. Immunohistochemistry was used to assess Vtg and ZP protein expressions. At the highest EE2 concentration, *VtgA* and *ZP2.5* genes were significantly upregulated. The remaining target genes were not significantly altered by EE2. Vtg and ZP immunostaining was consistently increased in spheroids exposed to 50 and 100 ng/L of EE2, whereas lower EE2 levels resulted in a weaker signal. EE2 did not induce significant changes in the spheroids' viability and morphological parameters. This study identified EE2 effects at environmentally relevant doses in trout liver spheroids, indicating its usefulness as a proxy for in vivo impacts of xenoestrogens.

Keywords: brown trout; primary hepatocytes spheroids; environmental concentrations; 17α-ethinylestradiol; 3D cultures

1. Introduction

A wide range of negative impacts on aquatic species has been claimed by endocrine-disrupting chemicals (EDCs), namely estrogenic compounds [1]. In fish, estrogens may cause changes in lipid and steroid hormone profiles [2], disruptions in the biotransformation metabolism [2,3]), and even behavioural and body phenotype alterations [4]. In salmonids, the liver effects associated with the classic endocrine disruptor 17α-ethinylestradiol (EE2) have been intensely discussed and investigated using both in vivo [5–7] and in vitro [8–11] models. Transcriptomics has often been explored to study the impacts of EE2, as reviewed by Martyniuk et al. [12], unveiling estrogen-regulated genes. As an example, according to Hultman et al. [9], the microarray analysis of rainbow trout (*Oncorhynchus mykiss*) primary hepatocytes after EE2 exposure revealed gene expression alterations in distinct biological pathways related to estrogen receptor (ER) regulation, biotransformation, lipid metabolism, and cellular growth. In accordance, the EE2 treatment of liver slices of Atlantic

cod (*Gadus morhua*) upregulated vitellogenin (*Vtg*) and zona pellucida (*ZP*) genes [13], both recognized as estrogenic biomarkers [14,15].

In mammals, three-dimensional (3D) hepatic models are increasingly being used as alternatives to in vivo assays for investigating metabolism [16,17], hepatic diseases [18], and hepatotoxicity [19], and even for testing new drug candidates [20].

While research on 3D systems in fish is not as advanced as that in mammals, studies in recent years have contributed to the establishment of experimental approaches for the maintenance of viable and functional hepatocytes from a variety of fish species [21–25]. There is an enormous potential for using 3D liver models in the context of environmental toxicology. In this line, spheroids from a clearfin livebearer (*Poeciliopsis lucida*) hepatocellular carcinoma (PLHC-1) cell line were used to test the effects of a mixture of plastic additives (1 to 50 μM) and revealed a liver-like lipid profile phenotype [23]. Further, PLHC-1 spheroids exposed to benzo(a)pyrene (1 nM to 5 μM) showed *Cyp1a* induction and cellular alterations, evidencing its high potential for screening the induction of xenobiotic metabolism and tissue damage [26].

Estrogenic compounds were already tested in fish hepatocyte spheroids. For example, Park et al. [25] found upregulations of *Vtg5* mRNA expressions in zebrafish liver (ZFL) cell line spheroids stimulated with 1 nM of 17β-estradiol (E2) for 24 h. Additionally, an increase in *ER* and *Vtg* mRNA levels was observed in rainbow trout hepatocyte spheroids from day 1 to day 8 in culture after 24 h exposure to 1 μM of E2 [27].

Primary hepatocyte brown trout spheroids were previously characterized in terms of viability, morphological parameters, histomorphology, and basal gene expression [21,22]. The present study aimed to test the applicability of those spheroids by exposing them to environmentally relevant concentrations of EE2 (1 to 100 ng/L). Gene expression analyses of a selection of target genes and immunohistochemistry were used to assess effects. To our knowledge, this is the first study using 3D cultures of fish primary hepatocytes under environmentally relevant concentrations of EE2. It uncovers innovative findings and sets baselines to enable further advances for implementing 3D cultures in fish toxicity assays.

2. Materials and Methods

2.1. Fish

A stock of sexually immature brown trout (*Salmo trutta*) of 12 (±2) months—mean (±SD)—was obtained from the Aquaculture Station of Torno (Amarante, Portugal). The animals were randomly distributed (maximum of 5 fish per tank) in 6 independent 100 L fiberglass tanks under a continuous dechlorinated water recirculation system and acclimatized for at least two weeks before use in diverse experiments. For this study, 6 animals were sampled from the different tanks. The fish were maintained under a photoperiod of 12 h light/12 h dark and fed daily ad libitum (Trout Plus 4, AquaSoja), except before isolations. The fish were visually inspected daily and did not have lack of appetite or any common stress behaviours. Finally, no gross lesions were noted, either when living or after sacrifice. Fish used in this study had a mean weight of 49.0 (±26.1) g and a mean total length of 16.3 (±2.9) cm.

The water physicochemical parameters were analysed at least once a week using commercial test kits to measure ammonium/ammonia and nitrates/nitrites (Prodac, Cittadella, Italy): ammonium and ammonia—0.0 (±0.0) mg/L, nitrates—35.4 (±4.2) mg/L, and nitrites—0.05 (±0.02) mg/L. Water temperature—19.3 (±1.4) °C and oxygen (O_2)—90.1 (±1.5)% were determined using a portable instrument (DO210, VWR International, Leuven, Belgium), and pH levels—7.9 (±0.3) were measured using a pH reader (WTW pH530, Oberbayern, Germany).

2.2. Hepatocyte Isolation

Six fish were independently used for primary hepatocyte isolation. The fish were euthanized with an aqueous solution (0.6 mL/L) of ethylene glycol monophenyl ether (Merck KGaA, Darmstadt, Germany). All experimental procedures followed the Portuguese Decree-Law No. 113/2013, implementing EU Directive No. 2010/63 on animal protection

for scientific purposes and respecting animal handling. The blood (±1 mL) was collected using insulin syringes through the caudal vein in order to minimize the amount of blood in the liver. After the liver was sampled, primary hepatocytes were isolated by ex situ collagenase perfusion using Hanks' Balanced Salt Solution (HBSS), as previously described in detail [11]. Cell viability was checked in all experiments using an automatic cell counter (Invitrogen™, Countess™ Automated Cell Counter) based on the trypan blue exclusion assay; cell viability was 76% (±7.0).

2.3. Exposure Assays

Hepatocytes were cultured on four plates per fish at a cell density of 5×10^5 cells/mL (total volume of 3 mL/well), using 6-well non-tissue culture treated sterile plates with flat bottom and low evaporation lid (351146, Falcon, Corning, New York, NY, USA). The culture medium consisted of Dulbecco's modified Eagle medium/nutrient mixture F-12 (DMEM/F-12) (GE Healthcare Life Sciences, South Logan, UT, USA) with 10% fetal bovine serum (FBS) (Merck KGaA, Darmstadt, Germany), 15 mM of 2-[4-(2hydroxyethyl)1-piperazinyl]-ethanesulfonic acid (HEPES) (Merck KGaA, Darmstadt, Germany), and 10 mL/L of antibiotic/antimycotic solution (Merck KGaA, Darmstadt, Germany), since it has already proven to be ideal for cultures of brown trout primary hepatocyte spheroids (PHS) [21,22]. The culture medium (1.5 mL/well) was changed every 48 h. Hepatocytes were maintained at 18 °C, without an additional supply of O_2/CO_2, and at constant orbital agitation (~100 rpm) (IKA® MTS 2/4 digital microtiter shaker, Higashiosaka, Japan). At the 12th day post-isolation, the spheroids were exposed (on the same initial plates) until the 18th day post-isolation to different conditions: control—C (DMEM/F-12 with 15 mM HEPES, 10 mL/L of antibiotic/antimycotic solution, and charcoal-stripped FBS 10%, *v*/*v*), solvent control—SC (0.1% ethanol in supplemented DMEM/F-12 medium), and four EE2 concentrations, 1—1 ng/L (0.003 nM), 10—10 ng/L (0.033 nM), 50—50 ng/L (0.169 nM), and 100—100 ng/L (0.337 nM) in supplemented DMEM/F-12 medium. Medium changes were performed on alternate days (total volume changed on the 14th and 16th days post-isolation), as previously established [21]. On the 18th day post-isolation, spheroids generated from each independent fish were sampled for cell viability (lactate dehydrogenase—LDH and resazurin assays), morphological parameters (area, equivalent diameter and sphericity), morphology, and molecular analyses.

2.4. Spheroids Morphological Parameters

For each experiment on the 18th day post-isolation, brown trout PHS were photographed (n = 30 spheroids/condition) under a 10× objective lens in an Olympus CKX41 light microscope connected to an M5C-CYL-PL-D685CU Pixelink® camera (Barrington, NJ, USA). Spheroid photos were analysed using AnaSP software version 2.0 to obtain the area, equivalent diameter, and sphericity [28].

2.5. Lactate Dehydrogenase (LDH) Assay

An LDH Cytotoxicity WST Assay Kit (ENZ-KIT157, Enzo Life Sciences, New York, NY, USA) was used to determine the LDH leakage in cell culture supernatants derived from each well housing the spheroids, across various experimental conditions. For each experiment on the 18th day post-isolation, 100 µL of cell culture supernatants per well (total of 4 replicates per fish, 1 from each plate/condition), previously centrifuged at 1500 rpm (0.2 rcf) for 5 min, were transferred to 96-well microplates (351172, non-tissue culture treated sterile plate with a flat bottom and low evaporation lid, Falcon, Corning, New York, NY, USA). Background controls were also included by adding 100 µL of fresh culture medium (n = 8 wells). Then, all wells received 100 µL of working solution, and the plate was incubated for 30 min at room temperature (±20 °C), protected from light. Absorbances were measured at 490 nm after stopping the reaction in a Multiskan™ GO microplate spectrophotometer (Thermo Scientific, Vantaa, Finland). Background subtraction was performed, and data were plotted for each condition.

2.6. AlamarBlue™ HS Cell Viability Reagent Assay

A total of 8 spheroids (total of 4 replicates per fish, 1 from each plate per condition) were transferred individually to a 96-well microplate (351172, non-tissue culture treated sterile plate with a flat bottom and low evaporation lid, Falcon, Corning, New York, NY, USA). After transfer, 90 µL of the fresh culture medium was added to each well, followed by 10 µL of the AlamarBlue™ HS Cell Viability Reagent (A50101, Invitrogen, Thermo Fisher Scientific, Life Technologies Corporation, Eugene, OR, USA). Blanks (n = 8 wells) were performed using the same amount of the corresponding medium but without spheroids. The plates were incubated at 18 °C for 24 h, protected from light, and at constant agitation (~100 rpm) (IKA® MTS 2/4 digital microtiter shaker). The fluorescence was read at 550 nm and 588 nm (excitation and emission lengths, respectively) in a microplate Biotek Synergy™ HTX multimode reader (Agilent, Santa Clara, CA, USA) with the software Gen5 version 3.05.11 (Agilent, Santa Clara, CA, USA). The fluorescence values of each sample were adjusted by blank subtraction and plotted for each condition.

2.7. Spheroids Morphology

For each experiment on the 18th day, spheroids (n = 6 per condition per fish) were transferred individually into 1.5 mL microtubes. The fixation was conducted using 500 µL of 10% buffered formalin (Epredia, Breda, The Netherlands) at room temperature. After 24 h, the fixative was changed to 70% ethanol. Richard-Allan Scientific HistoGel (HG-4000, Epredia, Breda, The Netherlands) was used to embed the spheroids. Dehydration, clearing, and paraffin impregnation were carried out over 12 h in an automatic processor (TP 1020, Leica Biosystems, Wetzlar, Germany). Posteriorly, the samples were embedded in paraffin (Histoplast, Epredia, Breda, The Netherlands) using an embedding station (EG1140C, Leica Biosystems, Wetzlar, Germany). After embedding, 1 spheroid/fish per exposure condition was sectioned with a thickness of 3 µm in a fully automated rotary microtome (RM2255, Leica Biosystems, Wetzlar, Germany). Sections were stained with hematoxylin and eosin (H&E), and their visualization and photographs were obtained using a light microscope (BX50, Olympus, Tokyo, Japan) coupled with a digital camera (EP50, Olympus, Tokyo, Japan).

2.8. RNA Extraction and cDNA Synthesis

One pool of spheroids per condition was obtained on the 18th day post-isolation for each independent experiment. The minimum number of brown trout PHS required to obtain the pellet was previously optimized [21]. Spheroids were transferred into 1.5 mL microtubes, centrifuged at 1500 rpm for 5 min, and the pellets were snap-frozen in liquid nitrogen and stored at –80 °C. Total RNA was extracted with an illustra™ RNAspin Mini RNA Isolation Kit (GE Healthcare, Chicago, IL, USA), which involves a step of treating with DNase I to prevent contamination from genomic DNA. RNA quantification and purity were determined using a Multiskan™ GO microplate spectrophotometer (Thermo Scientific, Vantaa, Finland) with a µDrop™ Plate and a SkanIt Microplate Reader software version 4.1. The cDNA synthesis was performed using the iScript™ Reverse Transcription Supermix kit (Bio-Rad, Hercules, CA, USA), using 300 ng of total RNA for a total volume of 20 µL.

2.9. Quantitative Real-Time Polymerase Chain Reaction (RT-qPCR)

The CFX Connect real-time PCR detection system and CFX Manager software version 3.1 (Bio-Rad, Hercules, CA, USA) were used for RT-qPCR. Reactions included 5 µL of cDNA (diluted 1:5), 10 µL of iQ™ SYBR® Green Supermix (Bio-Rad, Hercules, CA, USA), and 200 nM of each primer (total volume of 20 µL). Duplicates of cDNA samples and no-template controls were always included in each analysis. A melt curve was used to assess the product's specificity.

For the relative gene quantification, the Pfaffl method was used [29], and the normalization was performed using the geometric mean of the two most stable reference genes (*glyceraldehyde-3-phosphate dehydrogenase—gapdh* and *ribosomal protein l8—rpl8*), based on the

NormFinder algorithm [30]. Target genes included *acyl-CoA long chain synthetase 1* (*Acsl1*), *apolipoprotein AI* (*ApoAI*), *catalase* (*Cat*), *estrogen receptor α* (*ERα*), *estrogen receptor β* (*ERβ*), *fatty acid binding protein 1* (*Fabp1*), *urate oxidase* (*Uox*), *vitellogenin A* (*VtgA*), *zona pellucida glycoprotein 2.5* (*ZP2.5*), and *zona pellucida glycoprotein 3a.2* (*ZP3a.2*). The conditions and primer sequences are in Table 1.

Table 1. Primer sequences, annealing temperature (AT), and efficiencies (E).

Gene	Abbreviation	Primer Sequences	AT (°C)	E (%)	References
Acyl-CoA long chain synthetase 1	*Acsl1*	F: 5′-CGACCAAGCCGCTATCTC-3′ R: 5′-CCAACAGCCTCCACATCC-3′	55.0	97.8	[6]
Apolipoprotein AI	*ApoAI*	F: 5′-ATGAAATTCCTGGCTCTTG-3′ R: 5′-TACTCTTTGAACTCTGTGTC-3′	55.0	89.9	[31]
Catalase	*Cat*	F: 5′-CACTGATGAGGGCAACTGGG-3′ R: 5′-CTTGAAGTGGAACTTGCAG-3′	58.0	91.4	[32]
Estrogen receptor α	*ERα*	F: 5′-GACATGCTCCTGGCCACTGT-3′ R: 5′-TGGCTTTGAGGCACACAAAC-3′	61.6	91.2	[5]
Estrogen receptor β	*ERβ*	F: 5′-TGTGGACCTGTGCCTGTTC-3′ R: 5′-ACATGAGCCCTAGCATCAGC-3′	66.5	103.3	[5]
Fatty acid binding protein 1	*Fabp1*	F: 5′-GTCCGTCACCAACTCCTTC-3′ R: 5′-GCGTCTCAACCATCTCTCC-3′	57.0	97.7	[31]
Urate oxidase	*Uox*	F: 5′-CTTCCGAGACCGCTTCAC-3′ R: 5′-CATTCTGGACCTTGTTGTAGC-3′	59.0	90.6	[5]
Vitellogenin A	*VtgA*	F: 5′-AACGGTGCTGAATGTCCATAG-3′ R: 5′-ATTGAGATCCTTGCTCTTGGTC-3′	62.9	99.0	[5]
Zona pellucida glycoprotein 2.5	*ZP2.5*	F: 5′-ATCAATAACCACAGCCACAATG-3′ R: 5′-ACCAGGGACAGCCAATATG-3′	55.0	99.0	[33]
Zona pellucida glycoprotein 3a.2	*ZP3a.2*	F: 5′-AACTACACTCCACTTCATC-3′ R: 5′-CACATCTCCTTCATCTTCA-3′	54.5	101.8	[33]
Glyceraldehyde-3-phosphate dehydrogenase	*Gapdh*	F: 5′-CCACCTATGTAGTTGAGTC-3′ R: 5′-ACCTTGAGGGAGTTATCG-3′	55.0	92.8	[34]
Ribosomal protein l8	*rpl8*	F: 5′-TCAGCTGAGCTTTCTTGCCAC-3′ R: 5′-AGGACTGAGCTGTTCATTGCG-3′	59.0	93.8	[5]

2.10. Immunohistochemistry

The histological slides were deparaffinized with xylene (2 × 10 min) and hydrated using a series of ethanol (100%, 95%, and 70%). Then, two antigen retrieval protocols were followed according to the specific antibody. For Vtg, the sections were immersed in Tris/EDTA, pH 9.0, and heated for 15 min in a microwave (700 W) after boiling. For ZP, the antigen retrieval was performed by immersing the slides in citrate buffer 0.01 M, pH 6, and heating them in a pressure cooker for 3 min after reaching the maximum pressure. All slides were then left to cool to room temperature. Next, a solution of 3% hydrogen peroxide (Merck KGaA, Darmstadt, Germany) in methanol was used to block the endogenous peroxidase over 10 min. The following protocol steps followed the NovoLink™ Max Polymer Detection Kit (RE7280-K, Leica Biosystems, Newcastle, UK) recommendations. For the Vtg and ZP immunohistochemistry procedures, the sections were incubated for 2 h (at ±20 °C) in a humidified chamber with a polyclonal rabbit anti-Arctic char Vtg, PO-1 (V01409201, Biosense Laboratories AS, Bergen, Norway) antibody, and a polyclonal rabbit anti-salmon zona radiata protein, O-146 antibody (Z03402202, Biosense Laboratories AS, Bergen, Norway), respectively. The Vtg and ZP antibodies were used at a dilution of 1:2500 and 1:3000, respectively, in phosphate-buffered saline (PBS) with 5% bovine serum albumin (BSA) (NZYTech, Lisbon, Portugal), as previously implemented in brown trout [35]. Negative controls were incubated in PBS with BSA 5% (NZYTech, Lisbon, Portugal), and positive controls were liver sections from a mature female brown trout. The 3,3′-diaminobenzidine (DAB) was used as chromogen, and counterstaining was achieved with Mayer's hematoxylin (Merck KGaA, Darmstadt, Germany) for 1 min. The slides

were dehydrated in ethanol, cleared in xylene, and mounted with Q Path® Coverquick 2000 media (VWR Chemicals, Fontenay-sous-Bois, France). A light microscope (BX50, Olympus, Tokyo, Japan) and a digital camera (EP50, Olympus, Tokyo, Japan) were used to photograph the spheroid sections.

2.11. Statistical Analyses

Descriptive and inferential statistics and graphs were created using Past 3 software version 3.25 [36] and the GraphPad Prism version 8.0.1, respectively. Shapiro–Wilk and Levene's tests checked the assumptions of normality and homogeneity of variance of data sets, respectively. A one-way analysis of variance (ANOVA) was followed by Tuckey's pairwise comparison post-hoc test. The non-parametric Kruskal–Wallis ANOVA and the Mann–Whitney pairwise comparison post-hoc test with sequential Bonferroni corrections were used in a few cases where the mentioned assumptions were not verified, even after data transformation. The differences were considered significant for $p < 0.05$.

3. Results

3.1. Morphological Parameters

Bright-field images showed compact spheroids in all conditions with well-defined limits (Figure 1). For all experimental conditions, the area, equivalent diameter, and sphericity of the spheroids were not significantly influenced by EE2 exposures (Figure 1).

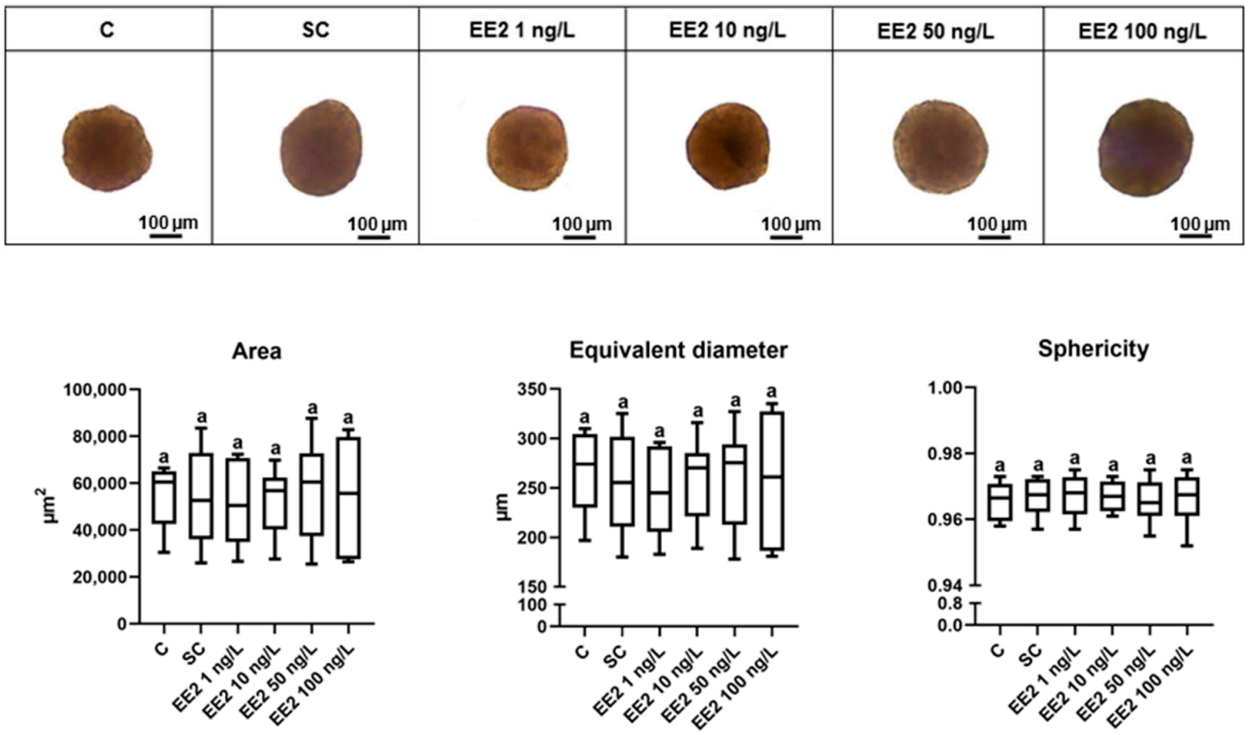

Figure 1. Light microscopy images, area, equivalent diameter, and sphericity of brown trout PHS (total of 6 independent fish, $n = 30$ spheroids per condition) after 6 days exposure (12th to 18th post-isolation day) to distinct conditions: C—control (supplemented DMEM/F-12 medium), SC—solvent control (0.1% ethanol in supplemented DMEM/F-12 medium), EE2 1 ng/L—1 ng/L of EE2 in supplemented DMEM/F-12 medium, EE2 10 ng/L—10 ng/L of EE2 in supplemented DMEM/F-12 medium, EE2 50 ng/L—50 ng/L of EE2 in supplemented DMEM/F-12 medium, and EE2 100 ng/L—100 ng/L of EE2 in supplemented DMEM/F-12 medium. Data correspond to median, minimum, maximum, 25th, and 75th percentiles. Common lower-case letters indicate no significant differences ($p > 0.05$) between conditions.

3.2. Viability—LDH and Resazurin Assays

The LDH and resazurin assays did not evidence significant differences between exposure conditions, as shown in Figure 2.

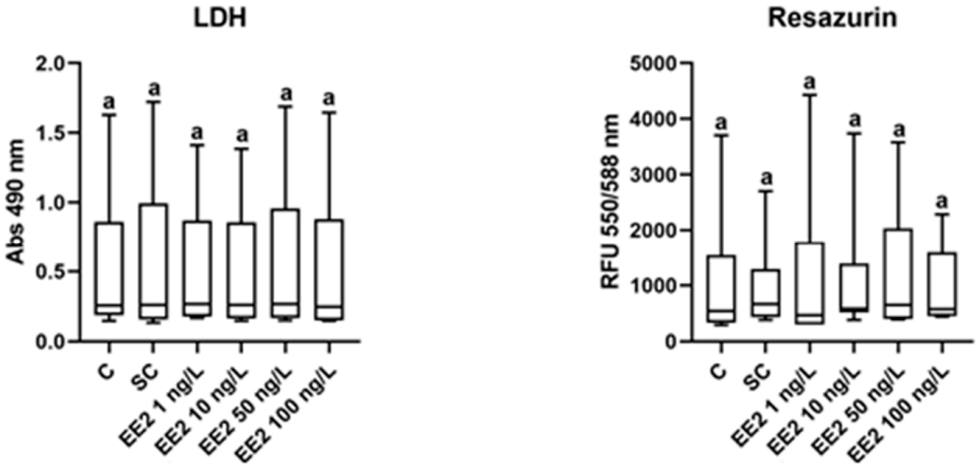

Figure 2. LDH and resazurin assays from brown trout PHS (total of 6 independent fish, n = 8 spheroids per condition) after 6 days of exposure (12th to 18th post-isolation day) to distinct conditions: C—control (supplemented DMEM/F-12 medium), SC—solvent control (0.1% ethanol in supplemented DMEM/F-12 medium), EE2 1 ng/L—1 ng/L of EE2 in supplemented DMEM/F-12 medium, EE2 10 ng/L—10 ng/L of EE2 in supplemented DMEM/F-12 medium, EE2 50 ng/L—50 ng/L of EE2 in supplemented DMEM/F-12 medium, and EE2 100 ng/L—100 ng/L of EE2 in supplemented DMEM/F-12 medium. Absorbance values at 490 nm and relative fluorescence units (RFU 550/588 nm) were plotted against each condition. Data correspond to median, minimum, maximum, 25th, and 75th percentiles. Common lower-case letters indicate no significant differences ($p > 0.05$) between conditions.

3.3. Morphology

No evident alterations were noted in the general structure of PHS between exposure conditions (Figure 3). Overall, spheroids showed a spherical/elliptical shape in all conditions. Hepatocytes had well-defined cellular limits and an intact nucleus (Figure 3).

3.4. RT-qPCR

The lipid metabolism- and peroxisome-related genes were not significantly influenced by EE2 exposure (Figure 4). Regarding the direct estrogen-related genes, the *ZP3a.2*, *ERα*, and *ERβ* showed stable mRNA levels, while *VtgA* and *ZP2.5* expressions were dose-responsive and significantly upregulated at the highest concentration (100 ng/L) (Figure 4).

3.5. Immunohistochemistry

Overall, for both antibodies used, the C and SC conditions showed no significant immunostaining (Figure 5), whereas EE2 exposure resulted in positive labelling, which was classified into three levels of intensity (in particular for Vtg): low, moderate, and strong. Vtg and ZP immunostaining were both cytoplasmic and varied between diffuse and a granular pattern homogeneously distributed throughout the spheroids. Despite inter-animal variability, the overall pattern showed weaker immunostaining signals in spheroids exposed to EE2 concentrations of 1 ng/L and 10 ng/L (Figure 5). Moderate to strong immunolabelling was noticed for EE2 at 50 ng/L and 100 ng/L (Figure 5), respectively. The pattern obtained with both antibodies was well-defined, especially for the 100 ng/L condition. Negative controls did not show immunostaining.

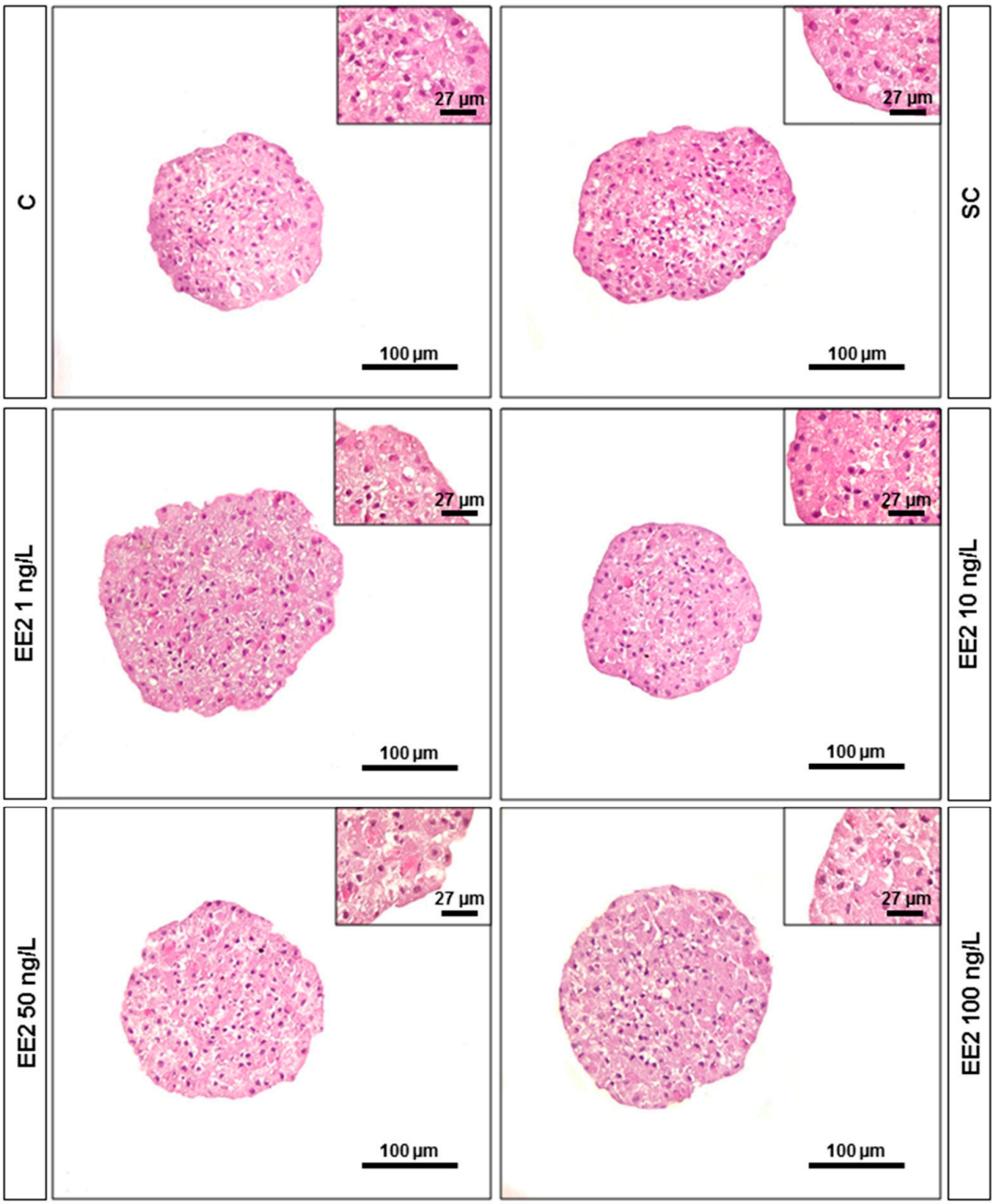

Figure 3. Hematoxylin and eosin (H&E) stained histological sections of brown trout PHS (total of 6 independent fish, n = 6 spheroids per condition) after 6 days exposure (12th to 18th post-isolation day) to distinct conditions. C—control (supplemented DMEM/F-12 medium); SC—solvent control (0.1% ethanol in supplemented DMEM/F-12 medium), EE2 1 ng/L—1 ng/L of EE2 in supplemented DMEM/F-12 medium, EE2 10 ng/L—10 ng/L of EE2 in supplemented DMEM/F-12 medium, EE2 50 ng/L—50 ng/L of EE2 in supplemented DMEM/F-12 medium, and EE2 100 ng/L—100 ng/L of EE2 in supplemented DMEM/F-12 medium.

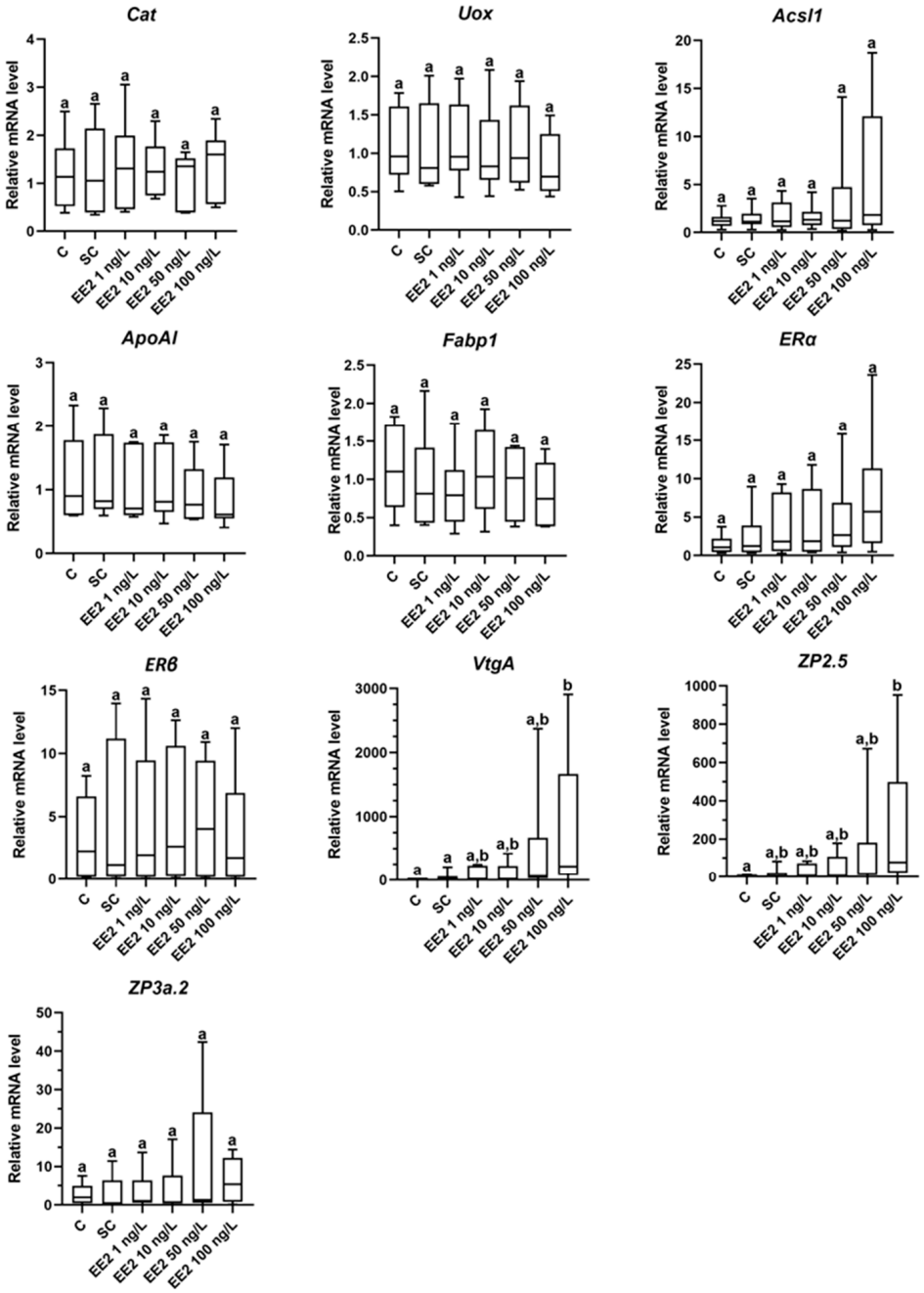

Figure 4. Relative mRNA levels of peroxisomal (*Cat* and *Uox*), lipid (*Acsl1*, *ApoAI* and *Fabp1*), and estrogen-related target (*ERα*, *ERβ*, *VtgA*, *ZP2.5* and *ZP3a.2*) genes of brown trout PHS (total of 6 independent fish, n = 1 pools of spheroids per condition) after 6 days of exposure (12th to 18th post-isolation day) to distinct conditions: C—control (supplemented DMEM/F-12 medium), SC—solvent control (0.1% ethanol in supplemented DMEM/F-12 medium), EE2 1 ng/L—1 ng/L of EE2 in supplemented DMEM/F-12 medium, EE2 10 ng/L—10 ng/L of EE2 in supplemented DMEM/F-12 medium, EE2 50 ng/L—50 ng/L of EE2 in supplemented DMEM/F-12 medium, and EE2 100 ng/L—100 ng/L of EE2 in supplemented DMEM/F-12 medium. Data correspond to median, minimum, maximum, 25th, and 75th percentiles. Conditions not showing common letters differ significantly (a vs. b, $p < 0.05$). Significant differences ($p < 0.05$) between groups are represented by different letters. *Cat—catalase*; *Uox—urate oxidase*; *Acsl1—acyl-CoA long chain synthetase 1*; *ApoAI—apolipoprotein AI*; *Fabp1– fatty acid binding protein 1*; *ERα—estrogen receptor alpha*; *ERβ—estrogen receptor beta*; *VtgA—vitellogenin A*; *ZP2.5—zona pellucida glycoprotein 2.5*; and *ZP3a.2—zona pellucida glycoprotein 3.2*.

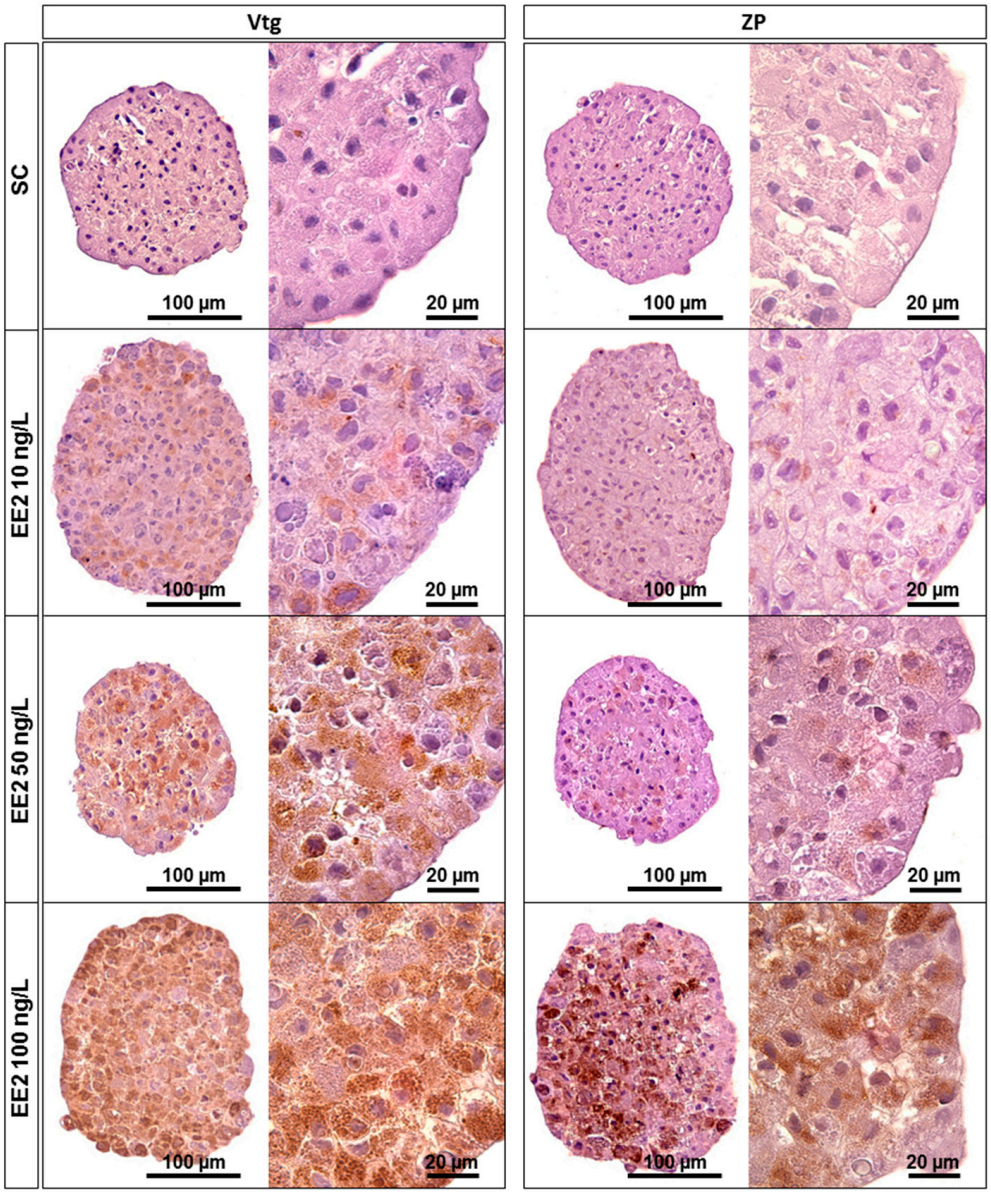

Figure 5. Immunohistochemistry staining for Vtg and ZP on 18-day-old spheroids from brown trout PHS after 6 days of exposure (12th to 18th day post-isolation) to distinct conditions: SC—solvent control (supplemented DMEM/F-12 medium), EE2 10 ng/L—10 ng/L of EE2 in supplemented DMEM/F-12 medium, EE2 50 ng/L—50 ng/L of EE2 in supplemented DMEM/F-12 medium, and EE2 100 ng/L—100 ng/L of EE2 in supplemented DMEM/F-12 medium. Positive immunolabelling corresponds to a brown colour signal.

4. Discussion

Like in other research areas, the practice in ecotoxicology has been to limit the number of animals killed. In mammals, 3D hepatocyte cultures remain viable with morphological and functional capacities closer to in vivo liver and over extended periods more than the ones reported in two-dimensional (2D) cultures [18].

Hence, 3D cultures have recently been explored for developing and characterising new fish models [37–39]. In this context, environmentally realistic conditions must be evaluated in 3D fish models before these can be adopted as accurate alternatives to in vivo studies. As such, the present study is a step toward determining the potential of using fish 3D models by testing environmental exposure concentrations. Using a previously developed spheroid

model of primary brown trout hepatocytes, this study investigated the effects of EE2 at low, medium, and high environmental concentrations on estrogen-related targets.

EE2 environmental levels are variable, ranging from 0.002 ng/L [40] to 45 µg/L [41]. The goal here was to test four concentrations of EE2, three of which were within the range of levels most frequently detected in the environment, as well as a concentration of 100 ng/L; although above the average, environmental monitoring also found such levels [41–43].

The morphological parameters (area, equivalent diameter, and sphericity) of 18-day-old brown trout PHS were not influenced by any EE2 concentration. Compact spheroids were observed in all conditions, which indicates that these EE2 levels did not compromise the cell–cell interactions and, consequently, the 3D structure of spheroids. Viable and metabolically competent brown trout PHS were observed in all conditions and resembled the biometric and morphological characteristics previously described for these spheroids with the same days in culture [22].

The genes selected here to evaluate the effect of EE2 were based on in vivo and in vitro assays, using liver or 2D hepatocytes isolated from brown trout, respectively [6,31,35]. In these studies, the target genes associated with various pathways, including estrogenic, peroxisome, and lipid-related pathways, exhibited estrogen-specific responses.

Here, there were no significant differences in the mRNA levels of the selected peroxisomal and lipid metabolism-related genes after 6 days of exposure to EE2. Lipid-related pathways are frequently listed as estrogen-responsive in fish [3,44,45]. Therefore, the absence of changes in the genes tested here may be related to the model, the doses, exposure time, and/or selected targets. For instance, in zebrafish liver, the expression of *ApoAI* was significantly downregulated in response to 10 ng/L of EE2 for 21 days [46]. According to Madureira et al. [6], the same peroxisomal (*Cat* and *Uox*) and lipid (*Fabp1* and *ApoAI*) target genes in brown trout liver showed a decrease or an increase (*Acsl1*) in gene expression after 28 days of in vivo exposure to EE2 (50 µg/L) [6]. However, it should be noted that in the latter example, the selected concentration is approximately 5000-fold times higher than the usual environmental range (using a concentration of 10 ng/L as reference). A distinct profile was found regarding the expression of the *VtgA* and *ZP2.5* genes, both widely accepted as estrogenic markers [47]. In this study, the *VtgA* and *ZP2.5* mRNA levels were significantly higher after exposure to EE2 at 100 ng/L compared to the other groups. An increasing trend was evident following exposure to 50 ng/L of EE2, although statistical significance was not proved. Data from in vivo EE2 experiments with different fish species support our results with brown trout PHS. For instance, increases in *Vtg* gene expression were observed in rainbow trout and male medaka (*Oryzias latipes*) after water exposure to 125 ng/L and 100 ng/L of EE2 over 61 days [7] and 4 weeks [48], respectively. Uren Webster et al. [33] found a significant upregulation of *vtg1*, *ZP2.5*, and *ZP3a.2* genes after 4 days of water treatment with 34.4 ng/L of E2. Interestingly, *ZP2.5* transcript was more responsive to E2 than *ZP3a.2*, which aligns with our results. Also, in brown trout, low doses of EE2 (3 ng/L) for 21 days caused a *Vtg* mRNA induction in vivo [5], but this did not happen in PHS, at least for the exposure time tested here. Evidence linked *Vtg* induction in trout to *ER* expression [49], but the *ERα* and *ERβ* mRNA levels did not change significantly in the present study. Mortensen and Arukwe [50] showed that liver *ERα* and *ERβ* mRNA levels significantly decreased, while *Vtg* and *ZP* increased at day 3 after EE2 exposures (50 ng/L) in juvenile Atlantic salmon. It was suggested by the authors that basal *ER* levels may be sufficient to trigger *Vtg* and *ZP* gene inductions, which may justify here the steady *ER* expression with increases of *VtgA* and *ZP2.5* mRNA levels. Further, prior studies demonstrated a peak induction of *ERα* mRNA levels in less than 48 h after EE2 exposure in rainbow trout [7]. As a result, we cannot rule out the possibility that we did not assess (at least) *ERα* expression at its maximum induction time.

In vitro studies with hepatocyte cell cultures also corroborate the *VtgA* and *ZP2.5* gene expression patterns obtained in this study. In rainbow trout primary hepatocytes exposed to EE2 for 48 h, there was a dose–effect concentration on the upregulation of *vtg1*, *zrp3*, and *zrp4* levels for concentrations above 88.9 ng/L (0.3 nM) [9]. In fish hepatocyte

spheroid cultures, estrogenic stimulation has also been tested but, so far, in unrealistic environmental concentrations [25,27,51,52]. For instance, according to Pelissero et al. [52], EE2 highly increased the Vtg concentrations in the culture medium of rainbow trout hepatocyte aggregates at the 296,400—29,640,000 ng/L (1000–100,000 nM) range, although minimal induction was measured at 296.4 ng/L (1 nM). Flouriot et al. [27] described that the *Vtg* mRNA induction was caused by exposure to 272,380 ng/L (1 μM) of 17β-estradiol (E2) during 24 h in male rainbow trout hepatocyte spheroids. Also, in the zebrafish liver (ZFL) cell line, the *Vtg5* mRNA expression was upregulated after exposure to E2 (1 nM = 272.38 ng/L) [25].

Within the present study, EE2 also caused a specific induction of Vtg and ZP protein expression, as already evidenced in the liver of Atlantic salmon exposed to other estrogenic compounds [53,54]. The positive control labelling for Vtg and ZP protein was cytoplasmic, as previously reported for both antibodies in brown trout hepatocytes [35]. Here, immunohistochemistry corroborated gene expression, showing a consistent increase in Vtg and ZP proteins, particularly after exposure to 100 ng/L of EE2. Immunolabelling was weaker and variable across the fish for lower EE2 concentrations (1 and 10 ng/L). The effect concentration that caused a 10-fold Vtg protein induction in rainbow trout hepatocytes was 71.7 ng/L (2.42×10^{-10} mol/L) [8], which aligns with the data obtained here.

5. Conclusions

The present study revealed the applicability, sensitivity, and specific responsiveness to EE2 of primary brown trout hepatocyte spheroids under distinct environmentally relevant levels. At 100 ng/L, remarkable effects were detected, particularly the stimulation of *Vtg* and *ZP* genes and protein expression. Lipid target genes did not change, even at the higher EE2 concentration, under the tested conditions. Given the published evidence from in vivo and 2D in vitro research, the model used here could serve as an alternate diagnostic tool for uncovering some effects arising from exposure to estrogen-disrupting compounds. However, further studies should be considered to disclose the EE2 effects at environmentally relevant levels in brown trout PHS and its applicability as an alternative model in ecotoxicology.

Author Contributions: Conceptualization, E.R. and T.V.M.; formal analysis, R.F.A., E.R. and T.V.M.; funding acquisition, E.R.; investigation, R.F.A., C.L., E.R. and T.V.M.; methodology, R.F.A., C.L., E.R. and T.V.M.; supervision, E.R. and T.V.M.; writing—original draft, R.F.A. and T.V.M.; writing—review and editing, R.F.A., C.L., E.R. and T.V.M. All authors have read and agreed to the published version of the manuscript.

Funding: This work was conducted in the frame of the project ATLANTIDA—Platform for the monitoring of the North Atlantic Ocean and tools for the sustainable exploitation of the marine resources (NORTE-01-0145-FEDER-000040), supported by Norte Portugal Regional Operational Programme (NORTE 2020), under the PORTUGAL 2020 Partnership Agreement, through the European Regional Development Fund (ERDF). The Strategic Funding UIDB/04423/2020 and UIDP/04423/2020 also supported this research through national funds provided by FCT and ERDF to CIIMAR/CIMAR in the framework of the PT2020 program. The ICBAS—U.Porto provided additional funding.

Institutional Review Board Statement: The animal study protocol was approved by the Ethics Committee of ICBAS (Ref. 2021-CE-P020-P360-CETI, 21 July 2021).

Informed Consent Statement: Not applicable.

Data Availability Statement: Available from the corresponding author upon reasonable request.

Conflicts of Interest: The authors declare no conflicts of interest.

References

1. Ciślak, M.; Kruszelnicka, I.; Zembrzuska, J.; Ginter-Kramarczyk, D. Estrogen pollution of the european aquatic environment: A critical review. *Water Res.* **2023**, *229*, 119413. [CrossRef]
2. Sun, S.X.; Wu, J.L.; Lv, H.B.; Zhang, H.Y.; Zhang, J.; Limbu, S.M.; Qiao, F.; Chen, L.Q.; Yang, Y.; Zhang, M.L.; et al. Environmental estrogen exposure converts lipid metabolism in male fish to a female pattern mediated by AMPK and mTOR signaling pathways. *J. Hazard. Mater.* **2020**, *394*, 122537. [CrossRef] [PubMed]

3. Voisin, A.S.; Kültz, D.; Silvestre, F. Early-life exposure to the endocrine disruptor 17-α-ethinylestradiol induces delayed effects in adult brain, liver and ovotestis proteomes of a self-fertilizing fish. *J. Proteom.* **2019**, *194*, 112–124. [CrossRef] [PubMed]
4. Goundadkar, B.B.; Katti, P. Environmental estrogen(s) induced swimming behavioural alterations in adult zebrafish (*Danio rerio*). *Environ. Toxicol. Pharmacol.* **2017**, *54*, 146–154. [CrossRef] [PubMed]
5. Körner, O.; Kohno, S.; Schönenberger, R.; Suter, M.J.; Knauer, K.; Guillette, L.J., Jr.; Burkhardt-Holm, P. Water temperature and concomitant waterborne ethinylestradiol exposure affects the vitellogenin expression in juvenile brown trout (*Salmo trutta*). *Aquat. Toxicol.* **2008**, *90*, 188–196. [CrossRef]
6. Madureira, T.V.; Malhão, F.; Simões, T.; Pinheiro, I.; Lopes, C.; Gonçalves, J.F.; Urbatzka, R.; Castro LF, C.; Lemos MF, L.; Rocha, E. Sex-steroids and hypolipidemic chemicals impacts on brown trout lipid and peroxisome signaling—Molecular, biochemical and morphological insights. *Comp. Biochem. Physiol. Part C Toxicol. Pharmacol.* **2018**, *212*, 1–17. [CrossRef]
7. Skillman, A.D.; Nagler, J.J.; Hook, S.E.; Small, J.A.; Schultz, I.R. Dynamics of 17alpha-ethynylestradiol exposure in rainbow trout (*Oncorhynchus mykiss*): Absorption, tissue distribution, and hepatic gene expression pattern. *Environ. Toxicol. Chem.* **2006**, *25*, 2997–3005. [CrossRef]
8. Hultman, M.T.; Rundberget, J.T.; Tollefsen, K.E. Evaluation of the sensitivity, responsiveness and reproducibility of primary rainbow trout hepatocyte vitellogenin expression as a screening assay for estrogen mimics. *Aquat. Toxicol.* **2015**, *159*, 233–244. [CrossRef]
9. Hultman, M.T.; Song, Y.; Tollefsen, K.E. 17α-Ethinylestradiol (EE2) effect on global gene expression in primary rainbow trout (*Oncorhynchus mykiss*) hepatocytes. *Aquat. Toxicol.* **2015**, *169*, 90–104. [CrossRef]
10. Finne, E.F.; Cooper, G.A.; Koop, B.F.; Hylland, K.; Tollefsen, K.E. Toxicogenomic responses in rainbow trout (Oncorhynchus mykiss) hepatocytes exposed to model chemicals and a synthetic mixture. *Aquat. Toxicol.* **2007**, *81*, 293–303. [CrossRef]
11. Madureira, T.V.; Malhão, F.; Pinheiro, I.; Lopes, C.; Ferreira, N.; Urbatzka, R.; Castro, L.F.; Rocha, E. Estrogenic and anti-estrogenic influences in cultured brown trout hepatocytes: Focus on the expression of some estrogen and peroxisomal related genes and linked phenotypic anchors. *Aquat. Toxicol.* **2015**, *169*, 133–142. [CrossRef] [PubMed]
12. Martyniuk, C.J.; Feswick, A.; Munkittrick, K.R.; Dreier, D.A.; Denslow, N.D. Twenty years of transcriptomics, 17alpha-ethinylestradiol, and fish. *Gen. Comp. Endocrinol.* **2020**, *286*, 113325. [CrossRef] [PubMed]
13. Yadetie, F.; Zhang, X.; Hanna, E.M.; Aranguren-Abadía, L.; Eide, M.; Blaser, N.; Brun, M.; Jonassen, I.; Goksøyr, A.; Karlsen, O.A. RNA-Seq analysis of transcriptome responses in Atlantic cod (*Gadus morhua*) precision-cut liver slices exposed to benzo[a]pyrene and 17α-ethynylestradiol. *Aquatic Toxicology* **2018**, *201*, 174–186. [CrossRef] [PubMed]
14. Mcgovarin, S.; Nishikawa, J.; Metcalfe, C.D. Vitellogenin induction in mucus from brook trout (*salvelinus fontinalis*). *Bull. Environ. Contam. Toxicol.* **2022**, *108*, 878–883. [CrossRef] [PubMed]
15. Berg, A.H.; Westerlund, L.; Olsson, P.E. Regulation of arctic char (*Salvelinus alpinus*) egg shell proteins and vitellogenin during reproduction and in response to 17beta-estradiol and cortisol. *Gen. Comp. Endocrinol.* **2004**, *135*, 276–285. [CrossRef]
16. Kozyra, M.; Johansson, I.; Nordling, Å.; Ullah, S.; Lauschke, V.M.; Ingelman-Sundberg, M. Human hepatic 3D spheroids as a model for steatosis and insulin resistance. *Sci. Rep.* **2018**, *8*, 14297. [CrossRef] [PubMed]
17. Kanebratt, K.P.; Janefeldt, A.; Vilén, L.; Vildhede, A.; Samuelsson, K.; Milton, L.; Björkbom, A.; Persson, M.; Leandersson, C.; Andersson, T.B.; et al. Primary human hepatocyte spheroid model as a 3D in vitro platform for metabolism studies. *J. Pharm. Sci.* **2021**, *110*, 422–431. [CrossRef] [PubMed]
18. Bell, C.C.; Hendriks, D.F.; Moro, S.M.; Ellis, E.; Walsh, J.; Renblom, A.; Fredriksson, P.L.; Dankers, A.C.; Jacobs, F.; Snoeys, J.; et al. Characterization of primary human hepatocyte spheroids as a model system for drug-induced liver injury, liver function and disease. *Sci. Rep.* **2016**, *6*, 25187. [CrossRef] [PubMed]
19. Foster, A.J.; Chouhan, B.; Regan, S.L.; Rollison, H.; Amberntsson, S.; Andersson, L.C.; Srivastava, A.; Darnell, M.; Cairns, J.; Lazic, S.E.; et al. Integrated in vitro models for hepatic safety and metabolism: Evaluation of a human Liver-Chip and liver spheroid. *Arch. Toxicol.* **2019**, *93*, 1021–1037. [CrossRef]
20. Song, Y.; Kim, N.; Heo, J.; Shum, D.; Heo, T.; Seo, H.R. Inhibition of DNMT3B expression in activated hepatic stellate cells overcomes chemoresistance in the tumor microenvironment of hepatocellular carcinoma. *Sci. Rep.* **2024**, *14*, 115. [CrossRef]
21. Pereira, I.L.; Lopes, C.; Rocha, E.; Madureira, T.V. Establishing brown trout primary hepatocyte spheroids as a new alternative experimental model–Testing the effects of 5α-dihydrotestosterone on lipid pathways. *Aquat. Toxicol.* **2022**, *253*, 106331. [CrossRef] [PubMed]
22. Alves, R.F.; Lopes, C.; Rocha, E.; Madureira, T.V. A step forward in the characterization of primary brown trout hepatocytic spheroids as experimental models. *Animals* **2023**, *13*, 2277. [CrossRef] [PubMed]
23. Wang, T.; Desmet, J.; Pérez-Albaladejo, E.; Porte, C. Development of fish liver PLHC-1 spheroids and its applicability to investigate the toxicity of plastic additives. *Ecotoxicol. Environ. Saf.* **2023**, *259*, 115016. [CrossRef] [PubMed]
24. Lammel, T.; Tsoukatou, G.; Jellinek, J.; Sturve, J. Development of threedimensional (3D) spheroid cultures of the continuous rainbow trout liver cell line RTLW1. *Ecotoxicol. Environ. Saf.* **2019**, *167*, 250–258. [CrossRef] [PubMed]
25. Park, C.G.; Ryu, C.S.; Sung, B.; Manz, A.; Kong, H.; Kim, Y.J. Transcriptomic and physiological analysis of endocrine disrupting chemicals impacts on 3D zebrafish liver cell culture system. *Aquat. Toxicol.* **2022**, *245*, 106105. [CrossRef] [PubMed]
26. Rodd, A.L.; Messier, N.J.; Vaslet, C.A.; Kane, A.B. A 3D fish liver model for aquatic toxicology: Morphological changes and Cyp1a induction in PLHC-1 microtissues after repeated benzo(a)pyrene exposures. *Aquat. Toxicol.* **2017**, *186*, 134–144. [CrossRef] [PubMed]

27. Flouriot, G.; Vaillant, C.; Salbert, G.; Pelissero, C.; Guiraud, J.M.; Valotaire, Y. Monolayer and aggregate cultures of rainbow trout hepatocytes: Long-term and stable liver-specific expression in aggregates. *J. Cell Sci.* **1993**, *105*, 407–416. [CrossRef]
28. Piccinini, F. AnaSP: A software suite for automatic image analysis of multicellular spheroids. *Comput. Methods Programs Biomed.* **2015**, *119*, 43–52. [CrossRef] [PubMed]
29. Pfaffl, M.W. A new mathematical model for relative quantification in real-time RTPCR. *Nucleic Acids Res.* **2001**, *29*, e45. [CrossRef]
30. Andersen, C.L.; Jensen, J.L.; Ørntoft, T.F. Normalization of real-time quantitative reverse transcription-PCR data: A model-based variance estimation approach to identify genes suited for normalization, applied to bladder and colon cancer data sets. *Cancer Res.* **2004**, *64*, 5245–5250. [CrossRef]
31. Madureira, T.V.; Pinheiro, I.; Malhão, F.; Lopes, C.; Urbatzka, R.; Castro LF, C.; Rocha, E. Cross-interference of two model peroxisome proliferators in peroxisomal and estrogenic pathways in brown trout hepatocytes. *Aquat. Toxicol.* **2017**, *187*, 153–162. [CrossRef] [PubMed]
32. Batista-Pinto, C. Peroxisomes in Brown trout (*Salmo trutta f. fario*): Regulation by Estrogens. Ph.D Thesis, Institute of Biomedical Sciences Abel Salazar, Porto, Portugal, 2007.
33. Uren Webster, T.M.; Shears, J.A.; Moore, K.; Santos, E.M. Identification of conserved hepatic transcriptomic responses to 17β-estradiol using high-throughput sequencing in brown trout. *Physiol. Genom.* **2015**, *47*, 420–431. [CrossRef] [PubMed]
34. Madureira, T.V.; Pinheiro, I.; De Paula Freire, R.; Rocha, E.; Castro, L.F.; Urbatzka, R. Genome specific PPARαB duplicates in salmonids and insights into estrogenic regulation in brown trout. *Comp. Biochem. Physiol. Part B Biochem. Mol. Biol.* **2017**, *208*, 94–101. [CrossRef] [PubMed]
35. Lopes, C.; Madureira, T.V.; Gonçalves, J.F.; Rocha, E. Disruption of classical estrogenic targets in brown trout primary hepatocytes by the model androgens testosterone and dihydrotestosterone. *Aquat. Toxicol.* **2020**, *227*, 105586. [CrossRef] [PubMed]
36. Hammer, Ø.; Harper, D.A.; Ryan, P.D. PAST: Paleontological statistics software package for education and data analysis. *Palaeontol. Electron.* **2001**, *4*, 9.
37. Alves, R.F.; Rocha, E.; Madureira, T.V. Fish hepatocyte spheroids—A powerful (though underexplored) alternative in vitro model to study hepatotoxicity. *Comp. Biochem. Physiol. Part C Toxicol. Pharmacol.* **2022**, *262*, 109470. [CrossRef] [PubMed]
38. Park, C.G.; Jun, I.; Lee, S.; Ryu, C.S.; Lee, S.A.; Park, J.; Han, H.S.; Park, H.; Manz, A.; Shin, H.; et al. Integration of bioinspired fibrous strands with 3D spheroids for environmental hazard monitoring. *Small* **2022**, *18*, e2200757. [CrossRef] [PubMed]
39. Langanl, M.; Dodd, N.J.; Owen, S.F.; Purcell, W.M.; Jackson, S.K.; Jha, A.N. Direct measurements of oxygen gradients in spheroid culture system using electron parametric resonance oximetry. *PLoS ONE* **2016**, *11*, e0149492. [CrossRef]
40. Avar, P.; Zrínyi, Z.; Maász, G.; Takátsy, A.; Lovas, S.; G-Tóth, L.; Pirger, Z. β-Estradiol and ethinyl-estradiol contamination in the rivers of the Carpathian Basin. *Environ. Sci. Pollut. Res. Int.* **2016**, *23*, 11630–11638. [CrossRef]
41. Griffero, L.; Alcántara-Durán, J.; Alonso, C.; Rodríguez-Gallego, L.; Moreno-González, D.; García-Reyes, J.F.; Molina-Díaz, A.; Pérez-Parada, A. Basin-scale monitoring and risk assessment of emerging contaminants in South American Atlantic coastal lagoons. *Sci. Total Environ.* **2019**, *697*, 134058. [CrossRef]
42. Valdés, M.E.; Marino, D.J.; Wunderlin, D.A.; Somoza, G.M.; Ronco, A.E.; Carriquiriborde, P. Screening concentration of E1, E2 and EE2 in sewage effluents and surface waters of the "Pampas" region and the "Río de la Plata" estuary (Argentina). *Bull. Environ. Contam. Toxicol.* **2015**, *94*, 29–33. [CrossRef] [PubMed]
43. Klaic, M.; Jirsa, F. 17α-Ethinylestradiol (EE2): Concentrations in the environment and methods for wastewater treatment—An update. *RSC Adv.* **2022**, *12*, 12794–12805. [CrossRef] [PubMed]
44. Zhang, X.; Zhong, H.; Han, Z.; Tang, Z.; Xiao, J.; Guo, Z.; Wang, F.; Luo, Y.; Zhou, Y. Effects of waterborne exposure to 17β-estradiol on hepatic lipid metabolism genes in tilapia (*Oreochromis niloticus*). *Aquac. Rep.* **2020**, *17*, 100382. [CrossRef]
45. Lourenço, T.; Rocha, E.; Gonçalves, J.F.; Rocha, M.J.; Madureira, T.V. A proof-of-concept for a hypolipidemic brown trout model. *Toxics* **2024**, *12*, 219. [CrossRef] [PubMed]
46. Martyniuk, C.J.; Gerrie, E.R.; Popesku, J.T.; Ekker, M.; Trudeau, V.L. Microarray analysis in the zebrafish (*Danio rerio*) liver and telencephalon after exposure to low concentration of 17alpha-ethinylestradiol. *Aquat. Toxicol.* **2007**, *84*, 38–49. [CrossRef] [PubMed]
47. Celius, T.; Matthews, J.B.; Giesy, J.P.; Zacharewski, T.R. Quantification of rainbow trout (*Oncorhynchus mykiss*) zona radiata and vitellogenin mRNA levels using real-time PCR after in vivo treatment with estradiol-17 beta or alpha-zearalenol. *J. Steroid Biochem. Mol. Biol.* **2000**, *75*, 109–119. [CrossRef] [PubMed]
48. Scholz, S.; Kordes, C.; Hamann, J.; Gutzeit, H.O. Induction of vitellogenin in vivo and in vitro in the model teleost medaka (*Oryzias latipes*): Comparison of gene expression and protein levels. *Mar. Environ. Res.* **2004**, *57*, 235–244. [CrossRef] [PubMed]
49. Leaños-Castañeda, O.; Van Der Kraak, G. Functional characterization of estrogen receptor subtypes, ERalpha and ERbeta, mediating vitellogenin production in the liver of rainbow trout. *Toxicol. Appl. Pharmacol.* **2007**, *224*, 116–125. [CrossRef] [PubMed]
50. Mortensen, A.S.; Arukwe, A. Effects of 17alpha-ethynylestradiol on hormonal responses and xenobiotic biotransformation system of Atlantic salmon (*Salmo salar*). *Aquat. Toxicol.* **2007**, *85*, 113–123. [CrossRef]
51. Sullivan, K.M.; Park, C.G.; Ito, J.D.; Kandel, M.; Popescu, G.; Kim, Y.J.; Kong, H. Matrix softness-mediated 3D zebrafish hepatocyte modulates response to endocrine disrupting chemicals. *Environ. Sci. Technol.* **2020**, *54*, 13797–13806. [CrossRef]
52. Pelissero, C.; Flouriot, G.; Foucher, J.L.; Bennetau, B.; Dunoguès, J.; Le Gac, F.; Sumpter, J.P. Vitellogenin synthesis in cultured hepatocytes; an in vitro test for the estrogenic potency of chemicals. *J. Steroid Biochem. Mol. Biol.* **1993**, *44*, 263–272. [CrossRef] [PubMed]

53. Arukwe, A.; Røe, K. Molecular and cellular detection of expression of vitellogenin and zona radiata protein in liver and skin of juvenile salmon (*Salmo salar*) exposed to nonylphenol. *Cell Tissue Res.* **2008**, *331*, 701–712. [CrossRef] [PubMed]
54. Arukwe, A.; Nilsen, B.M.; Berg, K.; Goksoyr, A. Immunohistochemical analysis of the vitellogenin response in the liver of Atlantic salmon exposed to environmental oestrogens. *Biomarkers* **1999**, *4*, 373–380. [CrossRef]

Journal of
Xenobiotics

MDPI

Article

Aquatic Fate and Ecotoxicology Effect of ZnS:Mn Quantum Dots on *Chlorella vulgaris* in Fresh Water

Bingbing Deng [1,*], Rania Maaloul [1], Sophie Nowak [1], Yann Sivry [2], Claude Yéprémian [3], Souad Ammar [1], Fayna Mammeri [1,*] and Roberta Brayner [1,†]

[1] ITODYS, Université Paris Cité, CNRS, F-75013 Paris, France; ammarmer@univ-paris-diderot.fr (S.A.)
[2] IPGP, Université Paris Cité, CNRS, F-75005 Paris, France
[3] CNRS, Molécules de Communication & Adaptation des Microorganismes MCAM, Museum National d'Histoire Naturelle, F-75005 Paris, France; claude.yepremian@mnhn.fr
* Correspondence: dengbingbcugb@163.com (B.D.); fayna.mammeri@u-paris.fr (F.M.)
† In memoriam.

Abstract: With the increasing integration of nanomaterials into daily life, the potential ecotoxicological impacts of nanoparticles (NPs) have attracted increased attention from the scientific community. This study assessed the ecotoxicity of ZnS quantum dots (QDs) doped with varying molar concentrations of Mn^{2+} on *Chlorella vulgaris*. The ZnS:Mn QDs were synthesized using the polyol method. The size of the ZnS:Mn QDs ranged from approximately 1.1 nm to 2 nm, while the aggregation size in Seine River water was 341 nm at pH 6 and 8. The presence of ZnS:Mn (10%) NPs exhibited profound toxicity to *Chlorella vulgaris*, with immediate reductions in viability (survival cells) from 71%, 60% to 51%, 52% in BG11 and Seine River water, respectively, at a concentration of 100 mg L^{-1} of ZnS:Mn (10%) NPs. Additionally, the ATP content in *Chlorella vulgaris* significantly decreased in Seine River water (by 20%) after 3 h of exposure to ZnS:Mn (10%) NPs. Concurrently, SOD activity significantly increased in Seine River water, indicating that the ZnS:Mn (10%) NPs induced ROS production and triggered an oxidative stress response in microalgae cells.

Keywords: nanoparticles; toxicological impact; toxicity; quantum dots; behavior; dissolution; risk; fate

1. Introduction

The release of engineered materials into the environment may negatively affect living organisms in the ground, rivers, and oceans. Despite the growing prevalence of nanomaterials in various devices, research on the degradation of these materials remains scant, while numerous studies have focused on their impact on plants and potential incorporation into the food chain. With increasing apprehensions about nanotechnologies, the drive to comprehend the biological and environmental repercussions of manufactured materials is intensifying [1]. Enhancing our understanding of ecotoxicological mechanisms is crucial not only for environmental conservation but also for advancing chemistry by developing more nature-friendly protocols. For this, conducting physicochemical studies is vital for understanding the behavior of these materials, as well as their uptake and distribution within microorganisms [2–4]. Environmental risk assessments of nanoparticles should consider both environmental exposure (dissolution/aggregation) and hazards, such as ecotoxicity.

Among various manufactured nanomaterials, II-VI semiconducting nanocrystals stand out for their quantum confinement, enabling the tailoring of electronic and optical properties by adjusting particle size [5,6]. ZnS nanoparticles (NPs), recognized for their application in displays [7], can display different colors when doped [8–13], as dopants serve as emitting centers within the quantum-confined crystalline structure of the quantum dots (QDs) [14,15]. To generate an orange wavelength (580–590 nm), manganese is a prevalent dopant in ZnS; Mn^{2+} can replace zinc in the blende lattice as a divalent cation. The emission

peak is typically attributed to the electronic transition between 4T1 and 6A1 energy levels of tetrahedral $[MnS4]^{6-}$ molecular species [9]. However, as the exploration of the potential of ZnS nanoparticles continues, so does the imperative to understand their environmental impact and potential toxicity.

To evaluate the toxicity of ZnS quantum dots doped with Mn^{2+} and conduct ecotoxicological assays, selecting an appropriate natural setting and an aquatic model organism is crucial. Microalgae serve as excellent aquatic models due to their ability to proliferate in nutrient-rich lakes and seas, conducive to microalgae cultivation. Seine River water, known for its high mineral salt content [16–18], is ideal for culturing microorganisms. Microalgae are utilized in wastewater treatment [19,20] and have demonstrated proficiency in assimilating nutrients from such sources. Their ease of cultivation, relatively short growth period (<1 week), and sensitivity to pollutants [21–23] make them valuable for ecotoxicological studies. Certain algal species have shown remarkable abilities to eliminate some kinds of environmental pollutants (such as metal pollutants or biodegradable NPs) [24–26]. *Chlorella vulgaris*, recognized for its sensitivity and crucial role as a primary producer in aquatic ecosystems, has become a key organism in ecotoxicology [27–29]. This microalga, prevalent in diverse aquatic environments, is highly sensitive to environmental shifts. For instance, exposure to pollutants can lead to observable toxicological symptoms in *C. vulgaris* within 72–96 h, establishing it as a potent bioindicator for NP toxicity evaluation [30–32]. Moreover, the easy culture and maintenance of *C. vulgaris* in laboratory conditions, allowing large-scale, controlled cultivation, enhances the reproducibility of toxicological studies and minimizes logistical hurdles.

Microorganisms in natural environments are often the initial points of contact with functional engineered nanomaterials. Nonetheless, the toxicity mechanisms of NPs, such as ZnS:Mn NPs, have not yet been fully explored. While extensive research has been conducted on the toxicity of cadmium-based NPs (e.g., CdSe, CdS, CdTe) [33–36] and oxides (like ZnO NPs, TiO_2 NPs, SiO_2 NPs) [37–39], studies investigating the ecotoxicity of low-dose Mn-doped ZnS NPs to aquatic algae remain relatively scarce.

In this study, we aim to evaluate the ecotoxicity of ZnS:Mn nanoparticles (synthesized via the polyol process) when interacting with *Chlorella vulgaris* in Seine River water [16]. The ecotoxic effects of ZnS NPs with varying Mn^{2+} dopant concentrations on microalgae were investigated. Specifically, we examined the impact of ZnS:Mn NPs on mitochondrial activity (Adenosine TriPhosphate (ATP) content), superoxide dismutase (SOD) activity, photosynthetic activity, and microalgae viability. Notably, Mn^{2+} can dissolve in the aquatic system and may pose toxicity to *C. vulgaris*. The dissolved Mn^{2+} or ZnS:Mn NPs, once internalized by algal cells, could affect the functionality of chloroplasts and mitochondria. This is primarily achieved through the induction of reactive oxygen species (ROS), potentially leading to cell death.

2. Materials and Methods

2.1. Synthesis of Mn-Doped ZnS Quantum Dots Using the Polyol Method

All chemicals are of analytical grade and were used without any further purification. Manganese acetate tetrahydrate ($\geq$99%, $Mn(CH_3COO)_2{\cdot}4H_2O$), trioctylphosphine oxide (TOPO, $(CH_3(CH_2)_7)_3PO$), and diethylene glycol (DEG) ($OH(CH_2)_2O(CH_2)_2OH$) were purchased from Sigma-Aldrich, Saint-Quentin Fallavier, France; thiourea (99%, $SC(NH_2)_2$) was purchased from Alfa Aesar, Paris, France; and zinc acetate dihydrate (98 + %, $Zn(CH_3COO)_2{\cdot}2H_2O$) was purchased from Acros Organics, Illkirch, France.

Zinc acetate dihydrate ($Zn(CH_3COO)_2{\cdot}2H_2O$, 87.8 mg) and manganese acetate tetrahydrate ($Mn(CH_3COO)_2{\cdot}4H_2O$, 1.0 mg, 4.1 mg, 8.5 mg and 24.5 mg) were mixed in a three-neck flask with 80 mL of diethylene glycol (DEG) to synthesize ZnS:Mn (0.5%), ZnS:Mn (2.0%), ZnS:Mn (4.0%), and ZnS:Mn (10%) in presence of thiourea (38.8 mg) and TOPO (193.3 mg). All the reagents were dissolved in DEG with 20 min of sonication, and then the solutions were heated to 180 °C for 30 min; after that, ZnS:Mn (0.5%), ZnS:Mn (2.0%),

ZnS:Mn (4.0%); ZnS:Mn (10%) NPs were recovered after 3 cycles of centrifugation (at 22,000× *g* rpm) and washing with ethanol, and then dried at 60 °C overnight.

2.2. Characterization of ZnS:Mn QDs

The crystalline structure of the synthesized ZnS:Mn NPs was analyzed using XRD with a X'Pert Pro Pananalytical diffractometer (Panalytical, Almelo, The Netherlands), employing Co Kα radiation over a range of 10–80° (2θ) with a scan step of 0.016°. Peak indexing was executed utilizing Highscore Plus software (version 5.2, Panalytical, The Netherlands) and the ICSD-Panalytical Database. Cell parameters and coherent diffraction domain size were determined using MAUD software (version 2.92, Trento, Italy) [40], based on the Rietveld method.

The surface chemical composition analysis of the NPs was performed through XPS using a Thermo VG ESCALAB 250 instrument (ThermoFisher Scientific, East-Grinstead, UK) equipped with a micro-focused monochromatic Al Kα X-ray source (1486.6 eV) and a magnetic lens. The X-ray spot size was 500 µm (15 kV, 150 W). Spectra were collected in constant analyzer energy mode with pass energies of 100 and 40 eV for survey spectra and high-resolution regions, respectively. Data acquisition and processing were conducted using "Avantage" software (version 4.67). The C1s peak at 285 eV, attributed to adventitious contamination, served as a reference for binding energy calibration and charge correction.

Mn, Zn, and S ratios were determined by XRF spectrometry (Panalytical, Almelo, The Netherlands). Nanopowders were dispersed in demineralized water, and 20 µL of aliquots was deposited on clean polycarbonate membranes and dried. The membranes were then analyzed using an Epsilon 3XL (Panalytical) XRF spectrometer equipped with a silver X-ray tube. Operating conditions varied: 20 kV and 15 µA for Mn, 50 kV and 6 µA for Zn, and 10 kV and 30 µA for S. A certified solution of Mn, Zn, and S (Inorganic Ventures 1 g/L) was utilized for calibration under identical conditions, within a range from 0 to 30 µg.

The morphology of the NPs was assessed by transmission electron microscopy (TEM) using a JEOL-100 CX II microscope (JEOL, Tokyo, Japan) at 100 kV. The mean diameter and standard deviation were derived from an image analysis of approximately 250 particles, conducted using ImageJ software (Version 1.53).

Dynamic light scattering (DLS) and zetametry were utilized to assess the size distribution and surface charge of the NPs using a Zetasizer (Spectris plc., London, UK) from Malvern. The ζ potential was measured at room temperature, beginning with their aqueous solution (1 g L^{-1}) after vigorous sonication for 10 min. The concentration of these solutions was 0.1 mg mL^{-1}, with pH levels of 2, 4, 6, 8, and 10, respectively.

The dissolution concentrations of Mn and Zn were quantified via inductively coupled plasma–atomic emission spectroscopy (ICP-AES) (ICAP 6200 Thermo Fisher, Thermo Fisher Scientific, Waltham, MA, USA). Detection and quantification limits were 0.20 ppb and 0.67 ppb for Zn, and 0.02 ppb and 0.07 ppb for Mn, respectively. The standard deviation associated with these measurements was less than 5%. The concentration of solutions used for ICP-AES was 0.01 mg mL^{-1}.

2.3. Chlorella vulgaris Culture

C. vulgaris were sourced from the Museum National d'Histoire Naturelle (MNHN) Culture Collection. *C. vulgaris*, a planktonic eukaryotic single-cell green alga, was cultivated in 75 cm^2 cell culture flasks purchased from Thermo Fisher in (i) sterile BG11 medium (pH 7.30) and (ii) Seine River water (SRW, pH 8.11). Then, 15 mL of *C. vulgaris* culture was mixed with 45 mL of various media, and then all cultures were maintained at a controlled temperature of 25 °C and a daily light cycle of 16 h of luminosity (50–80 µmol m^{-2} s^{-1} photosynthetic photon flux, PPF) in an ambient CO_2 environment. The live cell concentration in these media (BG11, SRW) was approximately 8.84 × 10^6 cells mL^{-1} and 5.59 × 10^6 cells mL^{-1}, before commencing the experiments.

Seine River water was taken from the river close to Université Paris Diderot, France (GPS: 48.828335° N, 2.385351° E), immediately filtered with a 0.22 µm acetate membrane (Millipore)(Sigma-Aldrich, Saint-Quentin Fallavier, France), autoclaved (121 °C for 20 min), and then stored at 4 °C in a fridge. The average chemical composition of Seine River water is shown in Table 1.

Table 1. Chemical composition of Seine River water [16].

$\times 10^{-3}$ mol/L	Na^+	Mg^{2+}	Ca^{2+}	K^+	Cl^-	Alkalinity	SO_4^{2-}	NO_3^-	SiO_2	pH	DOC (mg/L)
Seine River water	0.429	0.189	2.366	0.077	0.617	3.807	0.334	0.382	0.06	8.05	2.445

2.4. Ecotoxicity Assessments

Survival viability was assessed using the Cellometer Auto T4 (Nexcelom, Lawrence, KS, USA). SOD (superoxide dismutase) enzymatic activity was measured using the 19,160 SOD Determination Kit from Sigma-Aldrich (Saint-Quentin-Fallavier, France). SOD activity was colorimetrically evaluated through a kinetic method and readings were taken at 450 nm using an Envision Multilabel Plate Reader (Perkin-Elmer, Waltham, MA, USA).

ATP levels in the samples were detected using the luciferase–luciferin enzymatic assay kit BacTiter-Glo™ from Progema (Charbonnières-les-Bains, France). This kit facilitates the release of ATP from algal cells through cell lysis, negating the need for cell washing or medium removal. The reagent can be directly added to the microplate well. ATP quantitation was performed using an Envision Multilabel Plate Reader (Perkin-Elmer, Waltham, MA, USA) equipped with a luminescent optical filter. All assays were conducted in triplicate, and the test reagents used in the ecotoxicity assessments are also from the same batch.

Biomass transmission electron microscopy (TEM) studies were carried out using a Hitachi H-700 (Tokyo, Japan) at 80 kV, equipped with a Hamatsu camera (Massy, France). The microalgae were initially fixed with a mixture containing 2% glutaraldehyde and picric acid in a Sorengën phosphate buffer (0.1 M, pH 7.4). Cells were contrasted with 0.5% osmium tetroxide. Dehydration was then achieved through a series of ethanol baths, after which the samples were processed for flat embedding in Supper resin. Ultrathin sections of the samples in resin were then produced using a Reicherd E Young Ultracut ultramicrotome (Leica, Wetzlar, Germany).

2.5. Statistical Analysis

Statistical analyses were performed using SPSS v.26.0. For comparisons among control and treatments, one-way analysis of variance (ANOVA) test followed by Tukey's post hoc test was conducted for the variables that met the criteria of normality (Shapiro–Wilk test, $p > 0.05$), homoscedasticity (variance homogeneity, Levene test, $p > 0.05$) and independence (Durbin Watson test, p~2.0). For the variables that did violate the assumptions for ANOVA validity, a non-parametric Kruskal–Wallis test was conducted. Differences between groups were considered statistically significant when $p \leq 0.05$ and marginally significant when $0.05 < p \leq 0.1$.

3. Results and Discussion

3.1. Structural Characterization of ZnS:Mn NPs

X-ray diffraction (XRD) patterns of the ZnS:Mn NPs are illustrated in Figure 1. The diffraction peaks observed at 33°, 56°, and 67° correspond to the (111), (220), and (311) crystalline planes of the cubic ZnS phase (COD no. 5000088), indicating the presence of a singular phase, and thus the high purity of the ZnS:Mn NPs, despite their small size. The breadth of the peaks suggests the nanocrystalline nature of the samples [41]. The crystal sizes were computationally determined through Rietveld refinements using MAUD software (Materials Analysis Using Diffraction, Version 2.998), ranging between 1.1 and

1.5 nm. The average crystalline size of these ZnS NPs was further estimated using the full width at half maximum (FWHM) of the diffraction peaks and applying the Debye–Scherrer formula [41,42]:

$$D = \frac{k\lambda}{\beta cos\theta}$$

where D is the average size of the particles, k is the particles' shape factor (0.89), λ is the X-ray wavelength (0.17889 nm), β is the FWHM of the diffraction peak, θ is the diffraction Bragg angle. The calculated average crystalline sizes of ZnS:Mn (0.5%, 2.0%, 4.0%, and 10%) NPs ranged from 2.3 nm to 2.5 nm. This range aligns well with the average diameter deduced from the TEM analysis (2.3 ± 0.5 nm), as shown in Figure 4. It is worth noting that the Debye–Scherrer formula was used to calculate size, and the TEM statistical size was slightly larger than the actual crystal size, which can be attributed to the 2θ measurement boundary and other factors.

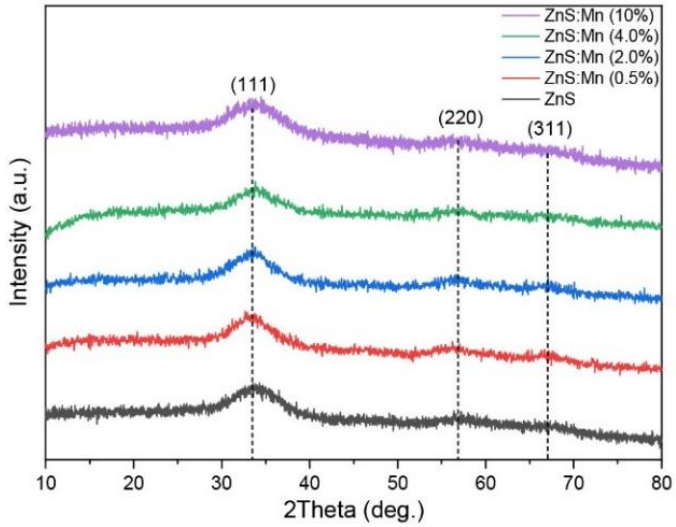

Figure 1. XRD patterns of all the produced ZnS:Mn NPs.

Table 2 gathers the elemental compositions of ZnS:Mn nanoparticles deduced from XRF analysis: the Mn content in the synthesized NPs increased from 0.002 to 0.168, while increasing the theoretical molar concentration of Mn ($Mn/(Mn + Zn)_{exp}$ from 0.005 to 0.100, although this does not match well with the expected molar concentration of Mn.

Table 2. Elemental composition XRF of all the produced ZnS: Mn NPs, deduced by XRF.

NPs		Zn	S	Mn	$Mn/(Mn + Zn)_{exp}$	$Mn/(Mn + Zn)_{XRF}$
ZnS:Mn (0.5%)	mass (µg)	32.315	11.034	0.048		
	%mol	58.9	41.0	0.10	0.005	0.002
ZnS:Mn (2.0%)	mass (µg)	46.842	14.838	0.668		
	%mol	60.1	38.8	1.1	0.020	0.018
ZnS:Mn (4.0%)	mass (µg)	22.464	8.427	0.427		
	%mol	55.9	42.8	1.3	0.040	0.023
ZnS:Mn (10%)	mass (µg)	8.336	3.5	1.420		
	%mol	48.6	41.6	9.8	0.100	0.168

The surface chemical composition of the NPs was examined through an XPS analysis. The survey spectra of ZnS:Mn (0.5%, 2.0%, 4.0%, and 10%) NPs are displayed in Figure 2. The binding energies for Zn $2p_{1/2}$ and Zn $2p_{3/2}$ were identified at 1045.8 eV and 1022.9 eV,

respectively, confirming the presence of Zn solely in the Zn^{2+} state. The S 2p peak at 161.4 eV is characteristic of the S^{2-} species [43,44]. Semi-quantitative XPS data revealed atomic Zn/S ratios of 1:0.9, 1:1, 1:1, and 1:0.9 for the 0.5%, 2.0%, 4.0%, and 10% samples, respectively, approximating the ideal 1:1 ratio for each sample. Peaks indicative of C and O adventitious contaminations were also observed in all spectra. The slight deviation in the Zn/S ratio to 0.9 might suggest the possible oxidation of the NPs. Nevertheless, the O 1s peak at 532.0 eV is not indicative of O atoms in a ZnO crystalline system, as signals from ZnO would manifest at 530 eV. Thus, the O 1s peak at 532 eV is likely attributable to chemisorbed oxygen species [43].

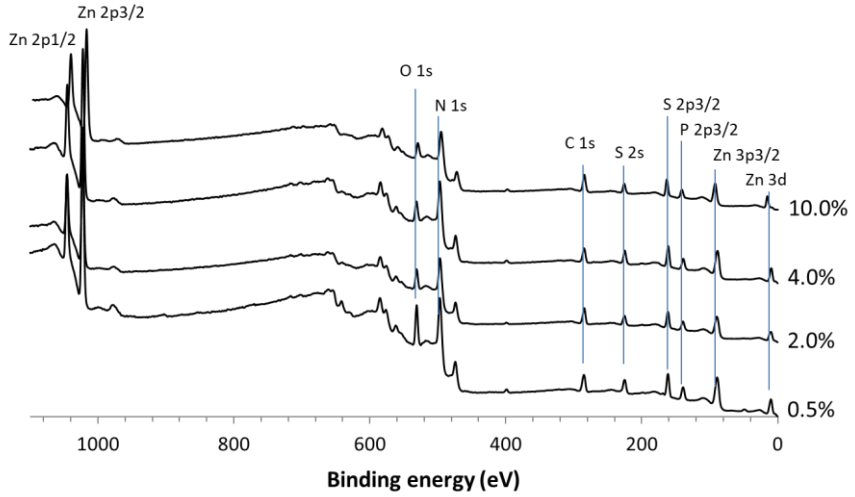

Figure 2. XPS survey spectra of ZnS:Mn (0.5%, 2.0%, 4.0% and 10%) NPs, the spectra were calibrated by setting the main C 1s at 285 eV.

The high-resolution spectra of S 2p, Mn 2p, and Zn 2p elements are depicted in Figure 3. The spin–orbit splitting peaks' intensity ratio for S $2p_{3/2}$ and S $2p_{1/2}$ was approximately 2:1, consistent with the presence of Zn^{2+} exclusively bonded to S atoms [45]. The asymmetric spectra of S 2p for ZnS:Mn (10%) NPs could be deconvoluted into two components, each with two peaks corresponding to S $2p_{3/2}$ and S $2p_{1/2}$. The binding energies at 158–159 eV stemmed from S^{2-} within the ZnS structure, while the subpeak around 160–161 eV might be attributable to surface defects of S–S species in the ZnS shell layer, as previously reported for ZnS nanorods [46]. Additionally, a less intense S 2p peak at 167.9 eV, indicative of the oxidized $SO_4{}^{2-}$ form, was observed [47], suggesting the slight and negligible surface oxidation of ZnS:Mn NPs. As the Mn content increased, the spectra became progressively less noisy [48–50]. The Mn $2p_{3/2}$ peak, centered at approximately 642 eV, corresponded to Mn^{2+} [51]. The binding energies for Zn $2p_{1/2}$ and Zn $2p_{3/2}$ were identified at 1045.8 eV and 1022.9 eV, respectively, affirming Zn in the Zn^{2+} state. Semi-quantitative XPS data presented atomic Mn/S ratios of 0.02:1, 0.03:1, 0.04:1, and 0.08:1 for the 0.5%, 2.0%, 4.0%, and 10% samples, respectively, closely aligning with the ideal ratios for each sample.

Transmission electron microscopy (TEM) images, as shown in Figure 4, Figures S1 and S2, displayed different molar concentrations of Mn-doped ZnS NPs. The TEM images provided lattice information and confirmed the blende structure of crystallized ZnS:Mn (0.5%, 2.0%, 4.0%, and 10%). Statistical analysis of the NP size distribution indicated an average size of approximately 2.3 ± 0.5 nm. Furthermore, an energy-dispersive X-ray (EDX) analysis revealed the primary constituents of these NPs to be Mn, Zn, and S elements. Cu was identified as a component of the grid, and Cr originated from the TEM machine, suggesting the absence of impurities in the ZnS:Mn NPs.

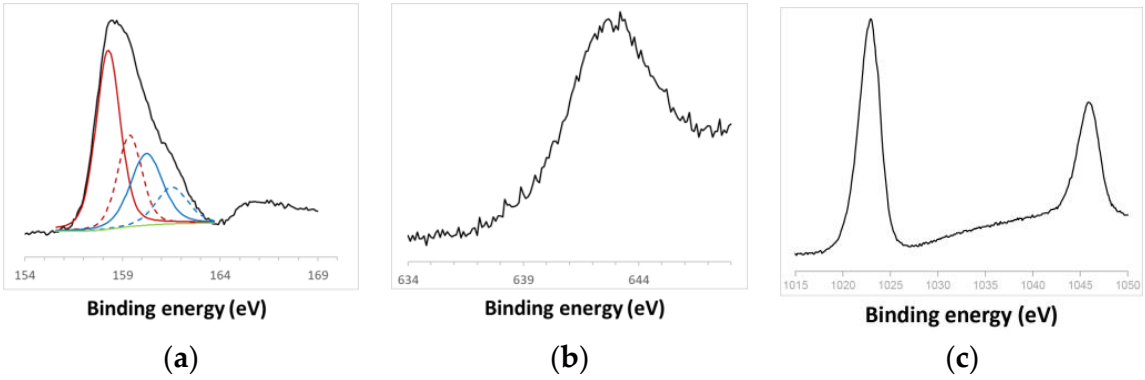

Figure 3. High-resolution spectra of (**a**) S 2p, (**b**) Mn 2p and (**c**) Zn 2p signals recorded on ZnS:Mn NPs with 10% Mn.

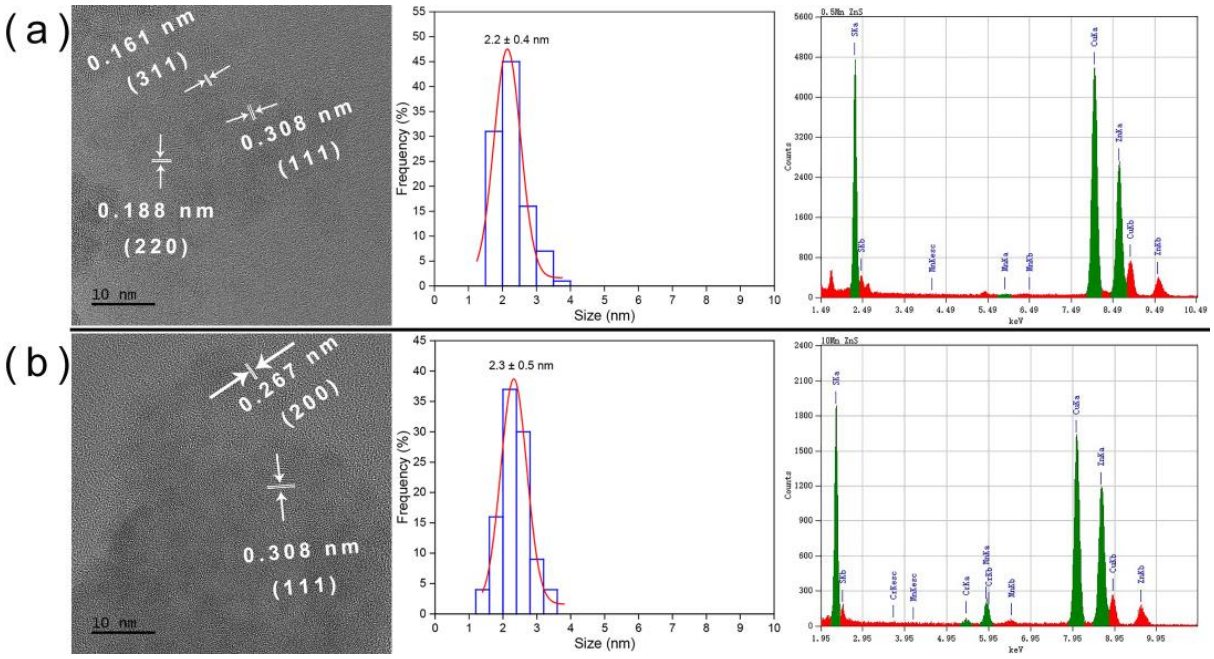

Figure 4. TEM image, size distribution and EDS of (**a**) 0.5% ZnS:Mn and (**b**) 10% ZnS:Mn. (2.0% and 4.0% Mn doped ZnS are shown in Figure S1).

The size and colloidal stability of the NPs were assessed using dynamic light scattering (DLS) in BG11 and Seine River water across varying pH levels (Figures 5 and S3). Irrespective of the medium and pH, the NPs aggregated to varying extents. In BG11 (or fresh) water at pH 2, all NPs formed smaller aggregates with colloidal sizes of around 340 nm for ZnS:Mn (0.5%) and ZnS:Mn (4.0%) NPs, and 460 nm and 400 nm for ZnS:Mn (2.0%) and ZnS:Mn (10%), respectively. In more basic conditions (pH 8), the colloidal size of almost all samples exceeded 1000 nm, except for ZnS:Mn (4.0%) which remained below 340 nm. In Seine River water, the colloids were relatively stable, exhibiting sizes between 340 nm and 530 nm across different pH levels, except for ZnS:Mn (4.0%) NPs, which formed aggregates of 220 nm at pH 4 and larger than 2000 nm at pH 10. Overall, NP aggregate sizes were more stable in BG11 under acidic conditions. In Seine River water, colloids maintained stability (300 to 500 nm) regardless of the medium being acidic or alkaline, with the exception of ZnS:Mn (4.0%) NPs, which tended to aggregate more readily when the pH varied from 6 to 8. Additionally, the size of ZnS:Mn (10%) NPs in Milli-Q water was 440 nm (at pH 6.89, Figure S4). It is important to note that the pH of *Chlorella vulgaris* cultures in different water systems ranges from 7.4 to 8.7.

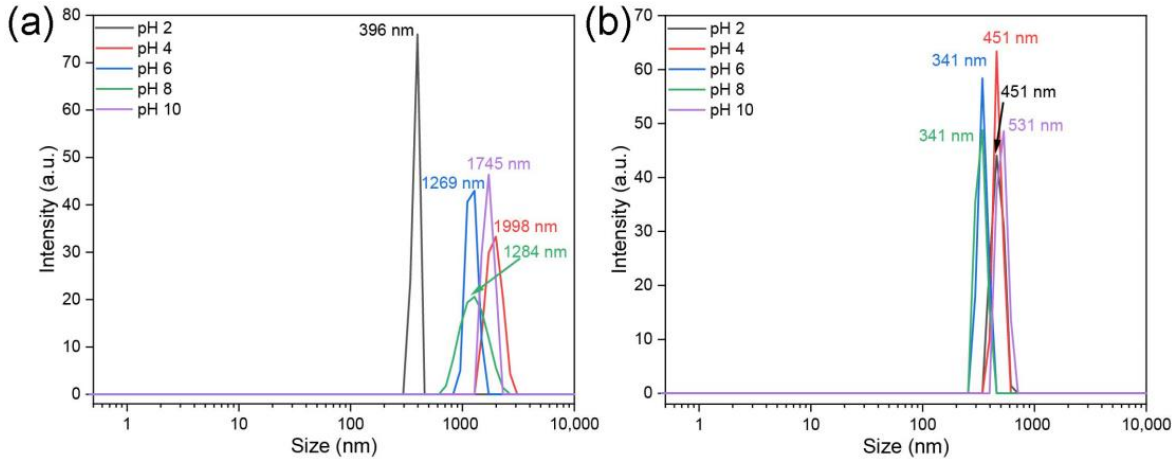

Figure 5. Size of ZnS:Mn (10%) NPs in (**a**) BG11 and (**b**) Seine River water: (0.5%, 2.0% and 4.0% Mn doped ZnS NPs are shown in Figure S3).

Figure 6 and Figure S5 illustrate the zeta potential measurements of all produced NPs in these two water systems across varying pH levels. It was noted that the zeta potential values of the NPs in fresh water (BG11) and Seine River water were approximately or greater than 20 in alkaline conditions (pH: 8 to 10), indicating the relative stability of the NPs in alkaline media in both BG11 and Seine River water. In all aquatic environments, NPs were negatively charged when pH ranged from 6 to 8. Furthermore, the zeta potential value of ZnS:Mn (10%) NPs in Milli-Q water was recorded as −2.67, denoting instability in pure water, while indicating relative stability in mildly acidic or alkaline environments. Given that the zeta potential of algal cells is 8.82, nanoparticles and algae would likely repel each other electrostatically, impeding the internalization of NPs by the cells [52,53].

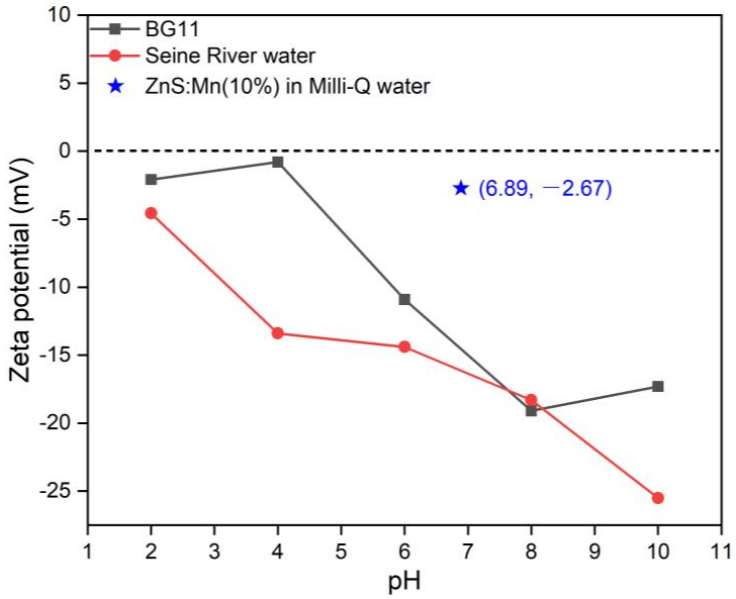

Figure 6. Zeta potential of ZnS:Mn (10%) NPs in different water systems: (0.5%, 2.0% and 4.0% Mn doped ZnS NPs are shown in Figure S3).

Despite the tendency of NPs to aggregate in water across pH levels, dissolution is possible. Hence, the dissolution of ZnS:Mn (10%) was monitored by ICP-AES. Figure 7 displays the concentrations of Mn^{2+} and Zn^{2+} in these two water systems after dissolving ZnS:Mn (10%) NPs. Mn^{2+} dissolution was generally higher in Seine River water compared to Milli-Q water. In Milli-Q water, peak Mn^{2+} dissolution occurred on the 2nd day, whereas

it reached its zenith on the 5th day in Seine River water. Interestingly, Zn^{2+} dissolution exhibited distinct behavior: in Seine River water and Milli-Q water, Zn^{2+} dissolution persisted and intensified over time.

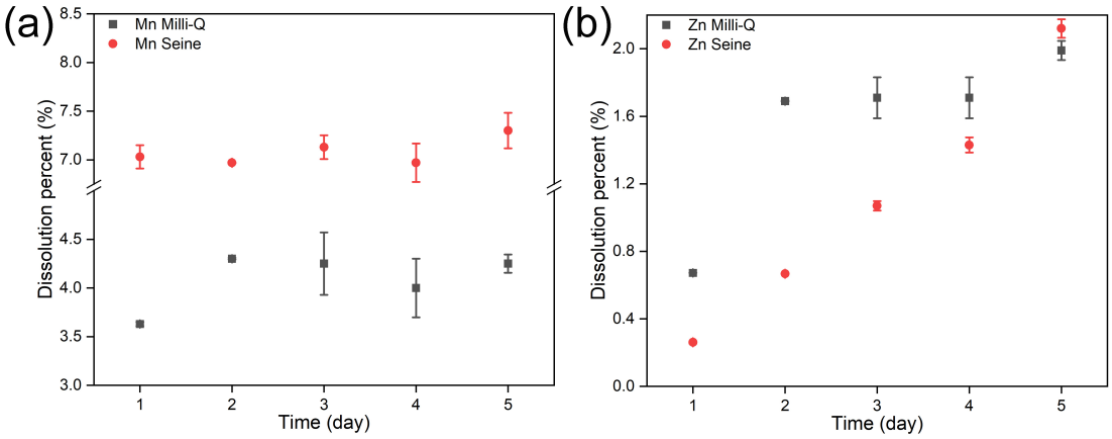

Figure 7. Dissolution of ZnS:Mn (10%) NPs in different water systems: monitoring of (**a**) Mn^{2+} and (**b**) Zn^{2+} concentrations in different water systems.

3.2. Assessment of the Toxicity of ZnS:Mn Nanoparticles

The toxicity of ZnS:Mn NPs to *Chlorella vulgaris* may be influenced by various factors, including composition, nanoparticle size, concentration, surface coating, and exposure duration. Unlike their bulk counterparts, nanomaterials like ZnS:Mn NPs have the potential to distinctively interact with living organisms due to their unique nanoscale properties. The exposure of *C. vulgaris* to nanoparticles can affect several biological processes, such as cellular uptake, oxidative stress, and alterations in biochemical pathways. These interactions may lead to consequences such as inhibited growth, reduced photosynthesis, lower cell viability, and altered metabolic functions.

To discern whether toxicity originated from Mn^{2+} ions or the NPs themselves, $Mn(CH_3COO)_2{\cdot}4H_2O$ salt, pure ZnS NPs, and ZnS:Mn NPs were introduced into two different culture media of *C. vulgaris*: BG11 and Seine River water (SRW). After one week, varying concentrations of NPs (20 mg L^{-1}, 50 mg L^{-1}, and 100 mg L^{-1}) were administered to the aquatic media, with each medium represented in four culture flasks (three experimental groups and one control group). Relative toxicity indicators, such as cell viability, superoxide dismutase (SOD) activity, and mitochondrial activity, were monitored for five consecutive days following exposure to the NP environment. This approach facilitated the evaluation of NP toxicity by comparison with the control group.

3.2.1. Toxicity of ZnS NPs

Figure 8 illustrates the viability of *Chlorella vulgaris* in different aqueous media when exposed to ZnS NPs. In both BG11 and SRW media, a notable decline in viability (about 3%) was observed from the initial day of exposure, persisting until the test's conclusion, relative to the control group. However, a recovery in viability was noted 48 h later at lower NP concentrations (20 mg L^{-1} and 50 mg L^{-1}). In Seine River water, viability decreased during the initial days of testing at higher NP concentrations (50 mg L^{-1} and 100 mg L^{-1}), with the exception of the fourth day. Moreover, algae exhibited a substantially reduced viability (below 40%) in SRW media, even in the control group, and this reduction may be attributed either to the media's influence on cell membrane protein expression [54] or to the significant aggregation of ZnS NPs on the algal surface, potentially disrupting cellular membrane transport functions and consequently reducing the nutrient availability essential for algal growth. Thus, it can be inferred that ZnS NPs exert a weak toxic impact on *C. vulgaris*, corroborating findings from previous studies [55,56]. As expected, higher NP concentrations manifested greater toxicity compared to lower concentrations.

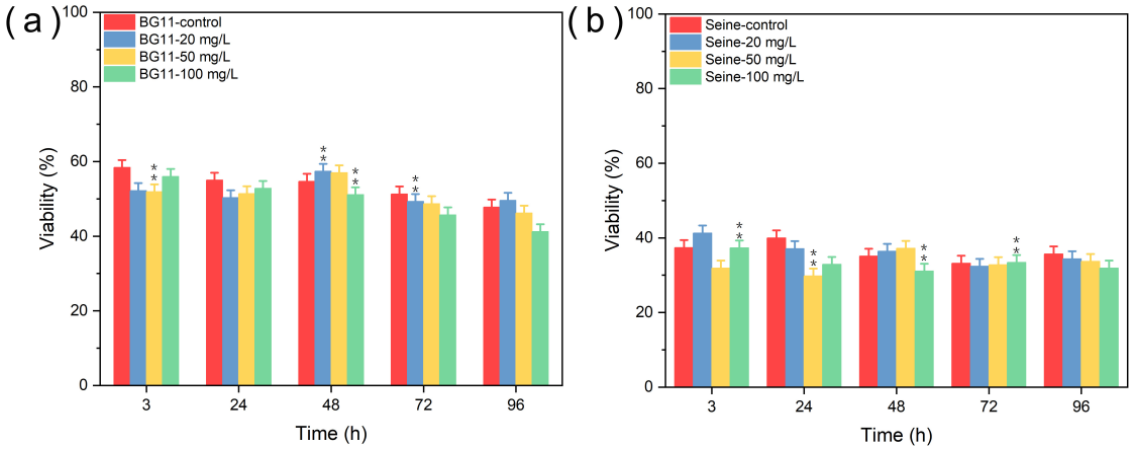

Figure 8. Viability (survival) tests of *Chlorella vulgaris* in (**a**) BG11, (**b**) SRW culture media contacted with pure ZnS NPs. Values represent mean ± standard deviation (n = 3). Differences among groups are indicated by an asterisk (marginally significant, $0.05 < p \leq 0.1$) or double asterisk (significant, $p \leq 0.05$). Double asterisk indicates that the difference between groups is statistically significant.

3.2.2. Toxicity of Mn^{2+}

The toxicity of Mn^{2+} was investigated by introducing Mn^{2+} solutions at concentrations of 20 mg L^{-1}, 50 mg L^{-1}, and 100 mg L^{-1}. Figure S6 depicts the state of *Chlorella vulgaris* cultures in the presence of Mn^{2+} ions 96 h post-introduction. The cultures in Seine River water containing Mn^{2+} ions exhibited a notably darker color compared to the control groups, especially in the culture medium containing high concentrations of Mn^{2+} (100 mg L^{-1}).

Figure 9 presents the viability of *C. vulgaris*: in BG11 media, viability was nearly stable at Mn^{2+} concentrations up to 100 mg L^{-1}. However, at 100 mg L^{-1} of Mn^{2+}, a significant reduction in viability was noted during the first four days of testing. In SRW media, viability decreased variably, likely due to nutrient deficiencies, such as nitrates, phosphates, or carbon sources (e.g., glucose), which are lacking in Seine River water [38]. As a result, the physiological condition of the algae deteriorated owing to nutrient scarcity, making them more susceptible to the adverse conditions of the water or the potentially toxic effects of Mn^{2+} ions. In contrast, algae in BG11 water, supplied with adequate nutrients, exhibited a markedly different response. Thus, high concentrations of Mn^{2+} ions (e.g., 100 mg L^{-1}) were profoundly toxic to *C. vulgaris* across all culture media, with the toxicity being particularly pronounced in SRW medium.

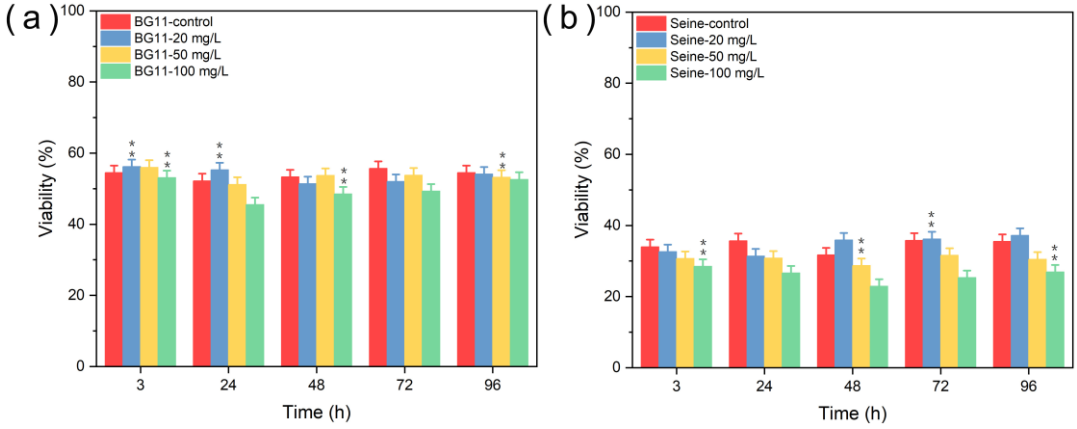

Figure 9. Viability (survival) tests of *Chlorella vulgaris* in (**a**) BG11 and (**b**) SRW culture media contacted with Mn^{2+} salt. Values represent mean± standard deviation (n = 3). Differences among groups are indicated by asterisk (marginally significant, $0.05 < p \leq 0.1$) or double asterisk (significant, $p \leq 0.05$). Double asterisk indicates that the difference between groups is statistically significant.

3.2.3. Toxicity of ZnS:Mn (10%) NPs

The doping of nanoparticles with transition metal cations, such as manganese, can alter their toxicity and interactions with living organisms compared to their undoped counterparts. Specifically, a transition metal cation like Mn^{2+}, not originally present in the base nanoparticles, is incorporated into the crystal lattice during the synthesis process. Consequently, the toxicity of ZnS:Mn (10%) NPs was evaluated (results detailing the toxicity of ZnS:Mn (0.5%), ZnS:Mn (2.0%), and ZnS:Mn (4.0%) are illustrated in Figures S7–S12).

Figure 10 shows a significant decrease in *Chlorella vulgaris* viability immediately following exposure to 100 mg L^{-1} of ZnS:Mn (10%) NPs in these aqueous media; the viability was approximately 50% in BG11 and SRW. At a 50 mg L^{-1} NP concentration, the viability in BG11 significantly decreased during the initial three days of testing before gradually returning to normal levels [57]. At a concentration of 20 mg L^{-1}, viability also slightly declined, notably in BG11 from 3 h to 72 h. These observations lead to the conclusion that a concentration of 100 mg L^{-1} of ZnS:Mn (10%) NPs poses a significant threat to the survival of *C. vulgaris*, and even lower concentrations of these NPs manifest toxicity to *C. vulgaris* in BG11. Interestingly, while viability decreased, photosynthetic activity did not show a corresponding decline (as seen in Figure S13). This resilience might be attributed to a protective mechanism involving carotenoids, a type of non-enzymatic antioxidants, which possibly act as singlet oxygen quenchers, thus safeguarding photosynthetic machinery [58].

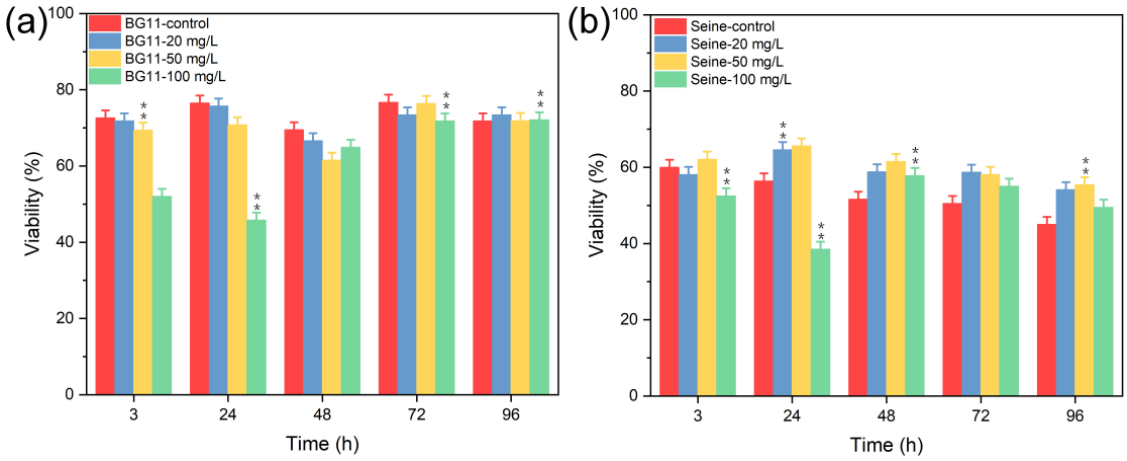

Figure 10. Viability (survival) tests of *Chlorella vulgaris* in (**a**) BG11 and (**b**) SRW culture media contacted with ZnS:Mn (10%) NPs. Values represent mean± standard deviation (n = 3). Differences among groups are indicated by an asterisk (marginally significant, $0.05 < p \leq 0.1$) or double asterisk (significant, $p \leq 0.05$). Double asterisk indicates that the difference between groups is statistically significant.

The impact of NPs on the mitochondrial activity of algal cells was gauged through the intracellular adenosine triphosphate (ATP) content, as depicted in Figure 11. In BG11, ATP content experienced a decline after 24 h of exposure compared to the control group, and this effect was more pronounced at a concentration of 50 mg L^{-1} after 72 h. While mitochondrial activity significantly decreased post 3 h of exposure in SRW, the detrimental impact on mitochondria persisted over an extended period. The reduction in ATP content indicates a decrease in mitochondrial activity, signifying that ZnS:Mn NPs (10%) disrupted the energy metabolism of the algae. Superoxide dismutase (SOD) activity, as shown in Figure 11, exhibited a marginal increase in BG11 after 48 h, particularly at a concentration of 100 mg L^{-1} of NPs. Moreover, SOD activity significantly rose in SRW after 24 h, and in the group with 100 mg L^{-1} of NPs, the SOD activity has always been at a high level. These observations suggest that NPs triggered the production of reactive oxygen species (ROS), especially in SRW, impacting mitochondrial activity. This led to a notable reduction in ATP production, which consequently influenced photosynthetic activity and cell viability.

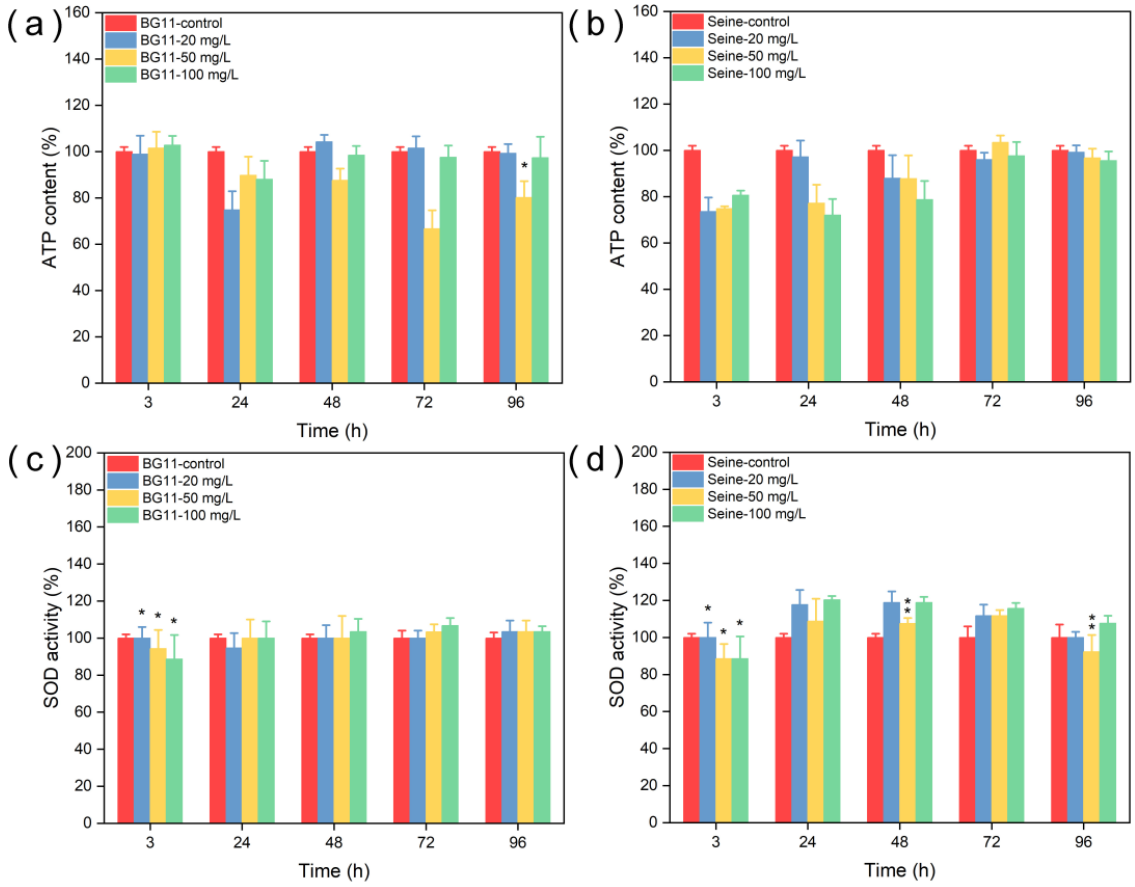

Figure 11. ATP (**a**,**b**) and SOD (**c**,**d**) tests of *Chlorella vulgaris* in different culture media contacted with ZnS: Mn (10%) NPs. Values represent mean ± standard deviation (n = 3). Differences among groups are indicated by asterisk (marginally significant, $0.05 < p \leq 0.1$) or double asterisk (significant, $p \leq 0.05$).

Thin-section TEM images, presented in Figures 12 and S14, showcase *Chlorella vulgaris* cells with and without exposure to ZnS:Mn (10%) NPs. In the absence of NPs, the integrity of the cell wall and the clarity of the cytoplasm are evident across all aqueous media. Conversely, the presence of ZnS:Mn (10%) NPs resulted in noticeable damage to the cell wall and/or cytoplasm. In BG11, dark, circular, and spherical NP aggregates are visibly attached to the cell wall, with a pronounced separation between the cytoplasm and cell wall. In SRW, smaller NPs were also observed within the cytoplasm, accompanied by the breakdown of the cell wall. The images further reveal numerous aggregated NPs within the algal cell, the disappearance of the cytoplasm, and the presence of NPs (circled in the image) outside the algal cell. Although the precise mechanisms of algal cell NP uptake remain unconfirmed, the following mechanisms are proposed: direct contact of NPs with the cell membrane, leading to interactions with lipid molecule groups and subsequent pore formation, and the internalization of NPs by cells through endocytosis [59]. Regardless of the mechanism, NPs inside algal cells can cause the destruction of the cytoplasm and cell wall, posing a lethal threat to the cells.

In this study, the synthesis of ZnS and ZnS:Mn NPs with Mn^{2+} concentrations ranging from 0.5% to 10% was detailed. All synthesized particles exhibited uniform diameters. DLS analysis revealed that these NPs tend to aggregate variably between pH 6 and 8, with the degree of aggregation dependent on the specific aqueous medium. The NPs demonstrated better dispersion in SRW compared to freshwater. Zeta potential measurements indicated good stability in freshwater and Seine River water, although in all environments, the NPs were negatively charged, posing challenges for internalization from the outset.

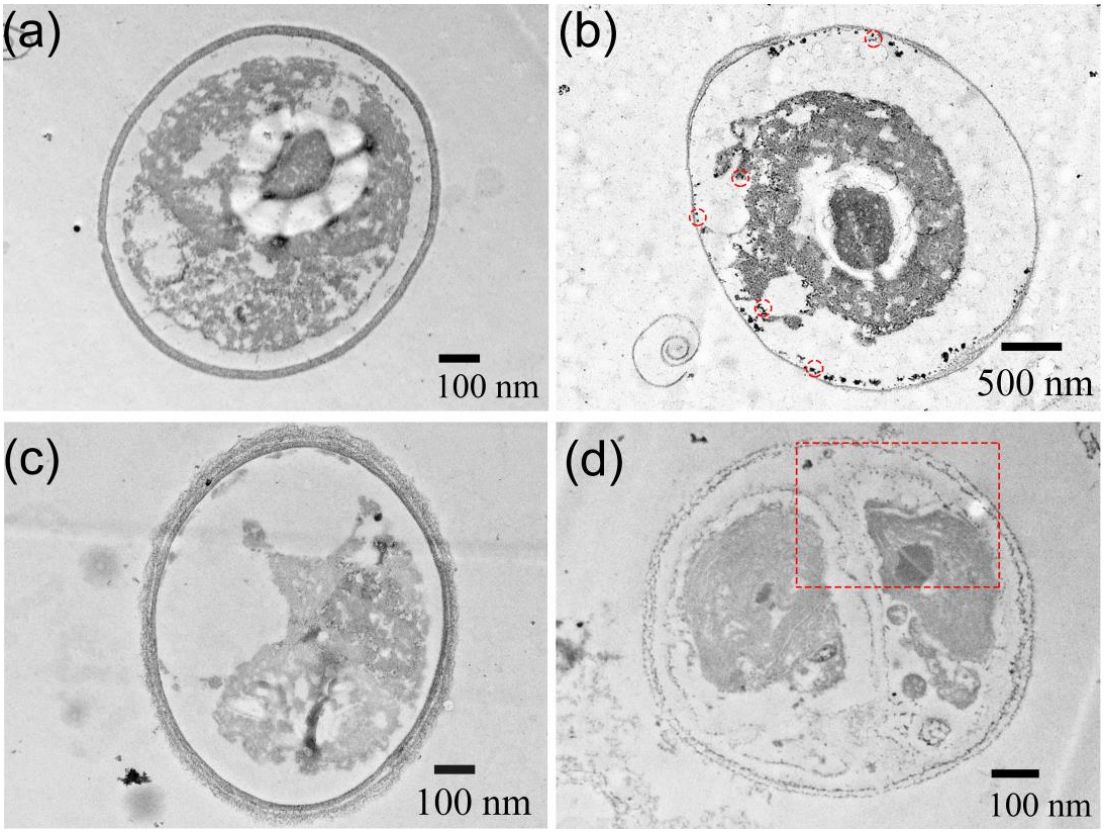

Figure 12. TEM images of thin sections of *Chlorella vulgaris* in different media: (**a**,**c**) in BG11 and in SRW; (**b**,**d**) show the thin sections of *Chlorella vulgaris* after exposure to 100 mg L^{-1} of ZnS:Mn (10%) NPs. Areas with red dotted lines mean that there are many NPs in the algal cell.

Focusing on particles with 10% Mn^{2+}, an ICP-AES analysis indicated the substantial dissolution of Mn^{2+} ions in Seine River water, whereas Zn^{2+} ions showed a higher dissolution rate in freshwater and Seine River water. Toxicity assays revealed that ZnS NPs had a poor toxicity to *Chlorella vulgaris* across all water types. Observations based on the color of solutions suggested that Mn^{2+} ions exhibited toxicity at 100 mg L^{-1} concentrations, with a milder toxicity noted in Seine River water. Similarly, ZnS:Mn NPs demonstrated pronounced toxicity at concentrations around 100 mg L^{-1}, and a partial toxic effect on *Chlorella vulgaris* may stem from ZnS:Mn NPs dissolving Mn^{2+} in the culture medium; with some dissolved ions (presumably Zn^{2+} ions) potentially serving as nutrients in Seine River water.

A marked reduction in ATP content was noted in freshwater and Seine River water, indicating a significant disruption of algal energy metabolism by ZnS:Mn (10%) NPs. However, a subsequent increase in ATP content in SRW media suggests that algae may adapt to the medium and restore ATP production.

SOD content almost remained stable in freshwater, only slightly increased 48 h later, and showed a significant increase in SRW media before stabilizing. This suggests that NPs induced ROS production, impairing mitochondrial activity and consequently reducing ATP production. This, in turn, affected photosynthetic activity and cell viability. However, with the enhancement of the SOD activity in the algae cells, ROS productions are gradually cleared, which alleviates the oxidative stress response in the algae cells. Subsequently, ATP levels slowly recovered, and cell viability almost returns to normal levels after 96 h. The growth of the algal community in the medium appears to be recovered.

Hence, ZnS:Mn NPs activate an antioxidant defense system within the algal cell, which may not always successfully counteract these assaults. Subcellular organelle degradation, as observed in TEM images, and oxidative stress are primary outcomes of NP toxicity.

This toxicity can be ascribed to several factors including the size of the aggregates, their composition, and their ion dissolution stability. Investigations on manganese salt indicate that Mn^{2+} ions must reach very high concentrations before transitioning from a nutrient to a toxin. Conversely, ZnS NPs were identified as having a poor toxicity. Additionally, the natural organic matter present in aquatic environments may modulate NP toxicity due to its heterogeneous composition and numerous functional groups [60], potentially altering NP behavior in aquatic settings and mitigating the toxicity of ZnS:Mn NPs [61]. The interplay between natural organic matter in natural water environments and the toxicity of ZnS:Mn NPs warrants further exploration.

In conclusion, nanoparticles can be considered toxic to *Chlorella vulgaris* via an oxidative stress mechanism. The high surface-to-volume ratio of NPs enables them to encircle the algal cell, despite general aggregation, thereby reducing the nutrient exchange surface of algal cells, in addition to facilitating NP internalization.

4. Conclusions

In this study, the synthesis of ZnS:Mn NPs (0.5%, 2%, 4%, and 10%) via the polyol method was detailed. The NPs exhibited a zinc blende structure with relatively small sizes, ranging from approximately 1.1 nm to 2 nm. When introduced into aqueous systems, these NPs were prone to aggregation, potentially impacting nutrient uptake by *Chlorella vulgaris*. Furthermore, these NPs influenced the SOD activity, ATP content, and viability of *C. vulgaris*, and could even lead to algal cell death. Notably, in Seine River water, a significant reduction in ATP content and an increase in SOD activity were observed. This suggests that NPs can create an oxidative stress environment, affecting mitochondrial activity and resulting in cell death. Additionally, in BG11 medium, the biological activity of *C. vulgaris* was also affected, with a substantial decline in viability was observed at a ZnS:Mn (10%) NP concentration of 100 mg L^{-1}.

The potential toxicity of manufactured nanoparticles is multifaceted and is compounded by the complexity and diversity of biological environments, which can result in variable responses among algal cultures. Fortunately, *C. vulgaris* demonstrated consistent behavior, allowing us to conclude that while the toxicity of manganese-doped ZnS nanoparticles is evident, it is less severe than the toxicity induced by Mn^{2+} ion concentrations of 100 mg L^{-1}. Consequently, the integration of these particles into miniaturized devices can be considered with a degree of confidence.

Supplementary Materials: The following supporting information can be downloaded at: https://www.mdpi.com/article/10.3390/jox14020028/s1. Table S1: Preparation of stock solutions. Table S2: Preparation of BG11 medium. Table S3: pH of the aqueous media containing various amounts of ZnS:Mn (4.0%). Figure S1: TEM image, size distribution and EDS of (a) ZnS: Mn (2.0%) and (b) ZnS:Mn (4.0%) NPs. Figure S2: TEM image (a) ZnS: Mn (0.5%) and (b) ZnS:Mn (10%) NPs. Figure S3: Size of ZnS:Mn (0.5%, 2.0%, 4.0%) NPs, (a–c) in BG11 and (d–f) in SRW. Figure S4: Size of ZnS:Mn (10%) NPs in Milli-Q water. Figure S5: Zeta potential of (a) ZnS:Mn (0.5%) NPs, (b) ZnS:Mn (2.0%) NPs, and (c) ZnS:Mn (4.0%) NPs. Figure S6: Chlorella vulgaris in the presence of Mn^{2+}. Figure S7: PAM and viability of ZnS:Mn (0.5%) NPs. Figure S8: ATP and SOD activity of ZnS:Mn (0.5%) NPs. Figure S9: PAM and viability of ZnS:Mn (2.0%) NPs. Figure S10: ATP and SOD activity of ZnS:Mn (2.0%) NPs. Figure S11: PAM and viability of ZnS:Mn (4.0%) NPs. Figure S12: ATP and SOD activity of ZnS:Mn (4.0%) NPs. Figure S13: Photosynthetic activity of ZnS:Mn (10%) NPs. Figure S14: The Chlorella vulgaris thin sections after exposure to 100 mg L-1 ZnS:Mn (10%) NPs, (a) BG11, and (b) SRW.

Author Contributions: B.D., investigation and methodology; R.M., S.N., Y.S. and C.Y., formal analysis; R.B., conceptualization; F.M., S.A. and R.B., supervision, B.D. and F.M., writing—original draft preparation; R.B. and F.M., project administration. All authors have read and agreed to the published version of the manuscript.

Funding: ANR (Agence Nationale de la Recherche) and CGI (Commissariat à l'Investissement d'Avenir) are gratefully acknowledged for their financial support of this work through Labex SEAM

(Science and Engineering for Advanced Materials and devices), ANR-10-LABX-096 and ANR-18-IDEX-0001. B.D. thanks the China Scholarship Council (CSC no. 201806400081) for the financial support.

Institutional Review Board Statement: Not applicable.

Informed Consent Statement: Not applicable.

Data Availability Statement: Data is contained within the article or/and supplementary material.

Acknowledgments: B.D. acknowledges Chakib Djediat for his technical support for TEM observations at MNHN and Philippe Decorse for his technical support for XPS analysis. Part of this research was supported by IPGP multidisciplinary program PARI, and by Paris–IdF region SESAME Grant no. 1201590.

Conflicts of Interest: The authors declare no conflicts of interest.

References

1. Nel, A.; Xia, T. Toxic Potential of Materials at the Nanolevel. *Science* **2006**, *311*, 622–627. [CrossRef]
2. Mueller, N.C.; Nowack, B. Exposure Modeling of Engineered Nanoparticles in the Environment. *Environ. Sci. Technol.* **2008**, *42*, 4447–4453. [CrossRef] [PubMed]
3. Gottschalk, F.; Sonderer, T.; Scholz, R.W.; Nowack, B. Modeled Environmental Concentrations of Engineered Nanomaterials (TiO_2, ZnO, Ag, CNT, Fullerenes) for Different Regions. *Environ. Sci. Technol.* **2009**, *43*, 9216–9222. [CrossRef] [PubMed]
4. Nowack, B. The Behavior and Effects of Nanoparticles in the Environment. *Environ. Pollut.* **2009**, *157*, 1063–1064. [CrossRef] [PubMed]
5. Wang, Y.; Herron, N. Nanometer-Sized Semiconductor Clusters: Materials Synthesis, Quantum Size Effects, and Photophysical Properties. *J. Phys. Chem.* **1991**, *95*, 525–532. [CrossRef]
6. Longo, A.V.; Notebaert, B.; Gaceur, M.; Patriarche, G.; Sciortino, A.; Cannas, M.; Messina, F.; von Bardeleben, H.J.; Battaglini, N.; Ammar, S. Photo-Activated Phosphorescence of Ultrafine ZnS:Mn Quantum Dots: On the Lattice Strain Contribution. *J. Phys. Chem. C* **2022**, *126*, 1531–1541. [CrossRef]
7. Chen, W.; Wang, Z.; Lin, Z.; Lin, L. Absorption and Luminescence of the Surface States in ZnS Nanoparticles. *J. Appl. Phys.* **1997**, *82*, 3111–3115. [CrossRef]
8. Biswas, S.; Kar, S.; Chaudhuri, S. Optical and Magnetic Properties of Manganese-Incorporated Zinc Sulfide Nanorods Synthesized by a Solvothermal Process. *J. Phys. Chem. B* **2005**, *109*, 17526–17530. [CrossRef] [PubMed]
9. Datta, A.; Biswas, S.; Kar, S.; Chaudhuri, S. Multicolor Luminescence from Transition Metal Ion (Mn^{2+} and Cu^{2+}) Doped ZnS Nanoparticles. *J. Nanosci. Nanotech.* **2007**, *7*, 3670–3676. [CrossRef]
10. Mishra, P.; Ojha, K.S.; Khare, A. Structural and Optical Study of Copper-Doped Zinc Sulfide Nanoparticles. *J. Appl. Spectrosc.* **2018**, *85*, 743–748. [CrossRef]
11. Manzoor, K.; Vadera, S.R.; Kumar, N.; Kutty, T.R.N. Multicolor Electroluminescent Devices Using Doped ZnS Nanocrystals. *Appl. Phys. Lett.* **2004**, *84*, 284–286. [CrossRef]
12. Mei, S.; Zhang, G.; Yang, W.; Wei, X.; Zhang, W.; Zhu, J.; Guo, R. A Facile Route for Highly Efficient Color-Tunable Cu-Ga-Se/ZnSe Quantum Dots. *Appl. Surf. Sci.* **2018**, *456*, 876–881. [CrossRef]
13. Wei, X.; Mei, S.; Zhang, G.; Su, D.; Xie, F.; Zhang, W.; Guo, R. Enhanced Tunable Dual Emission of Cu:InP/ZnS Quantum Dots Enabled by Introducing Ag Ions. *Appl. Surf. Sci.* **2019**, *493*, 605–612. [CrossRef]
14. Chung, J.H.; Ah, C.S.; Jang, D.-J. Formation and Distinctive Decay Times of Surface- and Lattice-Bound Mn^{2+} Impurity Luminescence in ZnS Nanoparticles. *J. Phys. Chem. B* **2001**, *105*, 4128–4132. [CrossRef]
15. Xu, S.J.; Chua, S.J.; Liu, B.; Gan, L.M.; Chew, C.H.; Xu, G.Q. Luminescence Characteristics of Impurities-Activated ZnS Nanocrystals Prepared in Microemulsion with Hydrothermal Treatment. *Appl. Phys. Lett.* **1998**, *73*, 478–480. [CrossRef]
16. Rocha, A.D.; Sivry, Y.; Gelabert, A.; Beji, Z.; Benedetti, M.F.; Menguy, N.; Brayner, R. The Fate of Polyol-Made ZnO and CdS Nanoparticles in Seine River Water (Paris, France). *J. Nanosci. Nanotechnol.* **2015**, *15*, 3900–3908. [CrossRef] [PubMed]
17. Planchon, M.; Jittawuttipoka, T.; Cassier-Chauvat, C.; Guyot, F.; Gelabert, A.; Benedetti, M.F.; Chauvat, F.; Spalla, O. Exopolysaccharides Protect Synechocystis against the Deleterious Effects of Titanium Dioxide Nanoparticles in Natural and Artificial Waters. *J. Colloid Interface Sci.* **2013**, *405*, 35–43. [CrossRef] [PubMed]
18. Planchon, M.; Léger, T.; Spalla, O.; Huber, G.; Ferrari, R. Metabolomic and Proteomic Investigations of Impacts of Titanium Dioxide Nanoparticles on Escherichia Coli. *PLoS ONE* **2017**, *12*, e0178437. [CrossRef] [PubMed]
19. Kube, M.; Mohseni, A.; Fan, L.; Roddick, F. Impact of Alginate Selection for Wastewater Treatment by Immobilised *Chlorella vulgaris*. *Chem. Eng. J.* **2019**, *358*, 1601–1609. [CrossRef]
20. Gao, F.; Cui, W.; Xu, J.-P.; Li, C.; Jin, W.-H.; Yang, H.-L. Lipid Accumulation Properties of *Chlorella vulgaris* and Scenedesmus Obliquus in Membrane Photobioreactor (MPBR) Fed with Secondary Effluent from Municipal Wastewater Treatment Plant. *Renew. Energy* **2019**, *136*, 671–676. [CrossRef]
21. Wang, F.; Guan, W.; Xu, L.; Ding, Z.; Ma, H.; Ma, A.; Terry, N. Effects of Nanoparticles on Algae: Adsorption, Distribution, Ecotoxicity and Fate. *Appl. Sci.* **2019**, *9*, 1534. [CrossRef]

22. Qiu, R.; Gao, S.; Lopez, P.A.; Ogden, K.L. Effects of pH on Cell Growth, Lipid Production and CO_2 Addition of Microalgae *Chlorella sorokiniana*. *Algal Res.* **2017**, *28*, 192–199. [CrossRef]
23. Zhuang, D.; He, N.; Khoo, K.S.; Ng, E.-P.; Chew, K.W.; Ling, T.C. Application Progress of Bioactive Compounds in Microalgae on Pharmaceutical and Cosmetics. *Chemosphere* **2022**, *291*, 132932. [CrossRef]
24. Dahoumane, S.A.; Yéprémian, C.; Djédiat, C.; Couté, A.; Fiévet, F.; Coradin, T.; Brayner, R. A Global Approach of the Mechanism Involved in the Biosynthesis of Gold Colloids Using Micro-Algae. *J. Nanopart. Res.* **2014**, *16*, 2607. [CrossRef]
25. Prasad, K.; Jha, A.K. ZnO Nanoparticles: Synthesis and Adsorption Study. *Nat. Sci.* **2009**, *1*, 129–135. [CrossRef]
26. Pimprikar, P.S.; Joshi, S.S.; Kumar, A.R.; Zinjarde, S.S.; Kulkarni, S.K. Influence of Biomass and Gold Salt Concentration on Nanoparticle Synthesis by the Tropical Marine Yeast Yarrowia Lipolytica NCIM 3589. *Colloids Surf. B Biointerfaces* **2009**, *74*, 309–316. [CrossRef] [PubMed]
27. Sathasivam, R.; Radhakrishnan, R.; Hashem, A.; Abd_Allah, E.F. Microalgae Metabolites: A Rich Source for Food and Medicine. *Saudi J. Biol. Sci.* **2019**, *26*, 709–722. [CrossRef]
28. Mishra, B.; Tiwari, A.; Mahmoud, A.E.D. Microalgal Potential for Sustainable Aquaculture Applications: Bioremediation, Biocontrol, Aquafeed. *Clean Technol. Environ. Policy* **2023**, *25*, 675–687. [CrossRef]
29. Mapelli-Brahm, P.; Gómez-Villegas, P.; Gonda, M.L.; León-Vaz, A.; León, R.; Mildenberger, J.; Rebours, C.; Saravia, V.; Vero, S.; Vila, E.; et al. Microalgae, Seaweeds and Aquatic Bacteria, Archaea, and Yeasts: Sources of Carotenoids with Potential Antioxidant and Anti-Inflammatory Health-Promoting Actions in the Sustainability Era. *Mar. Drugs* **2023**, *21*, 340. [CrossRef] [PubMed]
30. Dziwulska, U.; Bajguz, A.; Godlewska-Żyłkiewicz, B. The Use of Algae *Chlorella vulgaris* Immobilized on Cellex-T Support for Separation/Preconcentration of Trace Amounts of Platinum and Palladium before GFAAS Determination. *Anal. Lett.* **2004**, *37*, 2189–2203. [CrossRef]
31. Kaplan, D.; Heimer, Y.M.; Abeliovich, A.; Goldsbrough, P.B. Cadmium Toxicity and Resistance in *Chlorella* sp. *Plant Sci.* **1995**, *109*, 129–137. [CrossRef]
32. Kim, J.; Lingaraju, B.P.; Rheaume, R.; Lee, J.-Y.; Siddiqui, K.F. Removal of Ammonia from Wastewater Effluent by *Chlorella vulgaris*. *Tinshhua Sci. Technol.* **2010**, *15*, 391–396. [CrossRef]
33. Zhou, C.; Vitiello, V.; Pellegrini, D.; Wu, C.; Morelli, E.; Buttino, I. Toxicological Effects of CdSe/ZnS Quantum Dots on Marine Planktonic Organisms. *Ecotoxicol. Environ. Saf.* **2016**, *123*, 26–31. [CrossRef] [PubMed]
34. Chakraborty, D.; Ethiraj, K.R.; Chandrasekaran, N.; Mukherjee, A. Mitigating the Toxic Effects of CdSe Quantum Dots towards Freshwater Alga Scenedesmus Obliquus: Role of Eco-Corona. *Environ. Pollut.* **2021**, *270*, 116049. [CrossRef]
35. Pikula, K.; Mintcheva, N.; Kulinich, S.A.; Zakharenko, A.; Markina, Z.; Chaika, V.; Orlova, T.; Mezhuev, Y.; Kokkinakis, E.; Tsatsakis, A.; et al. Aquatic Toxicity and Mode of Action of CdS and ZnS Nanoparticles in Four Microalgae Species. *Environ. Res.* **2020**, *186*, 109513. [CrossRef]
36. Yu, Z.; Hao, R.; Zhang, L.; Zhu, Y. Effects of TiO_2, SiO_2, Ag and CdTe/CdS Quantum Dots Nanoparticles on Toxicity of Cadmium towards Chlamydomonas Reinhardtii. *Ecotoxicol. Environ. Saf.* **2018**, *156*, 75–86. [CrossRef]
37. Suman, T.Y.; Radhika Rajasree, S.R.; Kirubagaran, R. Evaluation of Zinc Oxide Nanoparticles Toxicity on Marine Algae *Chlorella Vulgaris* through Flow Cytometric, Cytotoxicity and Oxidative Stress Analysis. *Ecotoxicol. Environ. Saf.* **2015**, *113*, 23–30. [CrossRef]
38. Planchon, M.; Ferrari, R.; Guyot, F.; Gélabert, A.; Menguy, N.; Chanéac, C.; Thill, A.; Benedetti, M.F.; Spalla, O. Interaction between Escherichia Coli and TiO_2 Nanoparticles in Natural and Artificial Waters. *Colloids Surf. B Biointerfaces* **2013**, *102*, 158–164. [CrossRef]
39. Liu, Y.; Wang, S.; Wang, Z.; Ye, N.; Fang, H.; Wang, D. TiO_2, SiO_2 and ZrO_2 Nanoparticles Synergistically Provoke Cellular Oxidative Damage in Freshwater Microalgae. *Nanomaterials* **2018**, *8*, 95. [CrossRef]
40. Lutterotti, L. MAUD Tutorial—Instrumental Broadening Determination. Available online: https://www.researchgate.net/publication/228868859_MAUD_tutorial-Instrumental_Broadening_Determination (accessed on 26 August 2023).
41. Murugadoss, G. Synthesis and Photoluminescence Properties of Zinc Sulfide Nanoparticles Doped with Copper Using Effective Surfactants. *Particuology* **2013**, *11*, 566–573. [CrossRef]
42. Sakthivel, P.; Prasanna Venkatesan, G.K.D.; Subramaniam, K.; Muthukrishnan, P. Structural, Optical, Photoluminescence and Electrochemical Behaviours of Mg, Mn Dual-Doped ZnS Quantum Dots. *J. Mater. Sci. Mater. Electron.* **2019**, *30*, 11984–11993. [CrossRef]
43. Zhu, Y.-P.; Li, J.; Ma, T.-Y.; Liu, Y.-P.; Du, G.; Yuan, Z.-Y. Sonochemistry-Assisted Synthesis and Optical Properties of Mesoporous ZnS Nanomaterials. *J. Mater. Chem. A* **2014**, *2*, 1093–1101. [CrossRef]
44. Do, Y.R.; Park, D.H.; Yang, H.G.; Park, W.; Wagner, B.K.; Yasuda, K.; Summers, C.J. Uniform Nanoscale SiO_2 Encapsulation of ZnS Phosphors for Improved Aging Properties under Low Voltage Electron Beam Excitation. *J. Electrochem. Soc.* **2001**, *148*, G548–G551. [CrossRef]
45. Labiadh, H.; Sellami, B.; Khazri, A.; Saidani, W.; Khemais, S. Optical Properties and Toxicity of Undoped and Mn-Doped ZnS Semiconductor Nanoparticles Synthesized through the Aqueous Route. *Opt. Mater.* **2017**, *64*, 179–186. [CrossRef]
46. Zhou, D.-J.; Xie, X.-Y.; Zhang, Y.; Guo, D.-Y.; Zhou, Y.-J.; Xie, J.-F. Facile Synthesis of ZnS Nanorods in PEG and Their Spectral Performance. *Mater. Res. Express* **2016**, *3*, 105023. [CrossRef]
47. Liu, W.; Chen, S. An Investigation of the Tribological Behaviour of Surface-Modified ZnS Nanoparticles in Liquid Paraffin. *Wear* **2000**, *238*, 120–124. [CrossRef]

48. Geszke, M.; Murias, M.; Balan, L.; Medjahdi, G.; Korczynski, J.; Moritz, M.; Lulek, J.; Schneider, R. Folic Acid-Conjugated Core/Shell ZnS:Mn/ZnS Quantum Dots as Targeted Probes for Two Photon Fluorescence Imaging of Cancer Cells. *Acta Biomater.* **2011**, *7*, 1327–1338. [CrossRef]
49. Kolmykov, O.; Coulon, J.; Lalevée, J.; Alem, H.; Medjahdi, G.; Schneider, R. Aqueous Synthesis of Highly Luminescent Glutathione-Capped Mn^{2+}-Doped ZnS Quantum Dots. *Mater. Sci. Eng. C* **2014**, *44*, 17–23. [CrossRef]
50. Bwatanglang, I.B.; Mohammad, F.; Yusof, N.A.; Abdullah, J.; Hussein, M.Z.; Alitheen, N.B.; Abu, N. Folic Acid Targeted Mn:ZnS Quantum Dots for Theranostic Applications of Cancer Cell Imaging and Therapy. *Int. J. Nanomed.* **2016**, *11*, 413–428. [CrossRef]
51. Sumboja, A.; Ge, X.; Goh, F.W.T.; Li, B.; Geng, D.; Hor, T.S.A.; Zong, Y.; Liu, Z. Manganese Oxide Catalyst Grown on Carbon Paper as an Air Cathode for High-Performance Rechargeable Zinc–Air Batteries. *ChemPlusChem* **2015**, *80*, 1341–1346. [CrossRef]
52. Munk, M.; Brandão, H.M.; Nowak, S.; Mouton, L.; Gern, J.C.; Guimaraes, A.S.; Yéprémian, C.; Couté, A.; Raposo, N.R.B.; Marconcini, J.M.; et al. Direct and Indirect Toxic Effects of Cotton-Derived Cellulose Nanofibres on Filamentous Green Algae. *Ecotoxicol. Environ. Saf.* **2015**, *122*, 399–405. [CrossRef] [PubMed]
53. Ding, H.; Ma, Y. Controlling Cellular Uptake of Nanoparticles with pH-Sensitive Polymers. *Sci. Rep.* **2013**, *3*, 2804. [CrossRef] [PubMed]
54. Haniu, H.; Saito, N.; Matsuda, Y.; Tsukahara, T.; Maruyama, K.; Usui, Y.; Aoki, K.; Takanashi, S.; Kobayashi, S.; Nomura, H.; et al. Culture Medium Type Affects Endocytosis of Multi-Walled Carbon Nanotubes in BEAS-2B Cells and Subsequent Biological Response. *Toxicol. In Vitro* **2013**, *27*, 1679–1685. [CrossRef]
55. Gaceur, M.; Giraud, M.; Hemadi, M.; Nowak, S.; Menguy, N.; Quisefit, J.P.; David, K.; Jahanbin, T.; Benderbous, S.; Boissière, M.; et al. Polyol-Synthesized $Zn_{0.9}Mn_{0.1}S$ Nanoparticles as Potential Luminescent and Magnetic Bimodal Imaging Probes: Synthesis, Characterization, and Toxicity Study. *J. Nanoparticle Res.* **2012**, *14*, 1–5. [CrossRef]
56. Jahanbin, T.; Gaceur, M.; Gros-Dagnac, H.; Benderbous, S.; Merah, S.A. High Potential of Mn-Doped ZnS Nanoparticles with Different Dopant Concentrations as Novel MRI Contrast Agents: Synthesis and in Vitro Relaxivity Studies. *J. Nanoparticle Res.* **2015**, *17*, 258. [CrossRef]
57. da Rocha, A.; Menguy, N.; Yéprémian, C.; Couté, A.; Brayner, R. Ecotoxicological Studies of ZnO and CdS Nanoparticles on *Chlorella vulgaris* Photosynthetic Microorganism in Seine River Water. *Nanomaterials* **2020**, *10*, 227. [CrossRef]
58. Furger, C. Live Cell Assays for the Assessment of Antioxidant Activities of Plant Extracts. *Antioxidants* **2021**, *10*, 944. [CrossRef]
59. Mahana, A.; Guliy, O.I.; Mehta, S.K. Accumulation and Cellular Toxicity of Engineered Metallic Nanoparticle in Freshwater Microalgae: Current Status and Future Challenges. *Ecotoxicol. Environ. Saf.* **2021**, *208*, 111662. [CrossRef]
60. Wang, X.; Liang, D.; Wang, Y.; Peijnenburg, W.J.G.M.; Monikh, F.A.; Zhao, X.; Dong, Z.; Fan, W. A Critical Review on the Biological Impact of Natural Organic Matter on Nanomaterials in the Aquatic Environment. *Carbon Res.* **2022**, *1*, 13. [CrossRef]
61. Arvidsson, R.; Hansen, S.F.; Baun, A. Influence of Natural Organic Matter on the Aquatic Ecotoxicity of Engineered Nanoparticles: Recommendations for Environmental Risk Assessment. *NanoImpact* **2020**, *20*, 100263. [CrossRef]

Journal of *Xenobiotics*

MDPI

Review

Bamboo-Based Biochar: A Still Too Little-Studied Black Gold and Its Current Applications

Silvana Alfei [1,*] and Omar Ginoble Pandoli [1,2,*]

[1] Department of Pharmacy (DIFAR), University of Genoa, Viale Cembrano, 4, 16148 Genoa, Italy
[2] Departamento de Química, Pontifícia Universidade Católica, Rua Marquês de São Vincente, 225, Rio de Janeiro 22451-900, Brazil
* Correspondence: alfei@difar.unige.it (S.A.); omar.ginoblepandoli@unige.it or omarpandoli@puc-rio.br (O.G.P.)

Abstract: Biochar (BC), also referred to as "black gold", is a carbon heterogeneous material rich in aromatic systems and minerals, preparable by the thermal decomposition of vegetable and animal biomasses in controlled conditions and with clean technology. Due to its adsorption ability and presence of persistent free radicals (PFRs), BC has demonstrated, among other uses, great potential in the removal of environmental organic and inorganic xenobiotics. Bamboo is an evergreen perennial flowering plant characterized by a short five-year growth period, fast harvesting, and large production in many tropical and subtropical countries worldwide, thus representing an attractive, low-cost, eco-friendly, and renewable bioresource for producing BC. Due to their large surface area and increased porosity, the pyrolyzed derivatives of bamboo, including bamboo biochar (BBC) or activated BBC (ABBC), are considered great bio-adsorbent materials for removing heavy metals, as well as organic and inorganic contaminants from wastewater and soil, thus improving plant growth and production yield. Nowadays, the increasing technological applications of BBC and ABBC also include their employment as energy sources, to catalyze chemical reactions, to develop thermoelectrical devices, as 3D solar vapor-generation devices for water desalination, and as efficient photothermal-conversion devices. Anyway, although it has great potential as an alternative biomass to wood to produce BC, thus paving the way for new bio- and circular economy solutions, the study of bamboo-derived biomasses is still in its infancy. In this context, the main scope of this review was to support an increasing production of BBC and ABBC and to stimulate further studies about their possible applications, thus enlarging the current knowledge about these materials and allowing their more rational, safer, and optimized application. To this end, after having provided background concerning BC, its production methods, and its main applications, we have reviewed and discussed the main studies on BBC and ABBC and their applications reported in recent years.

Keywords: biochar (BC); pyrolysis; hydrothermal carbonization; bamboo biomass; bamboo-derived BC (BBC); activated BBC (ABBC); environmental xenobiotics removal; circular economy solutions

1. Introduction: Biochar (BC)

According to the definition provided by the International Biochar Initiative (IBI), biochar (BC) is "the solid material obtained from the thermochemical conversion of biomass in an oxygen-limited environment" [1]. Practically, BC is the lightweight black residue made mainly of carbon and ashes but also rich in aromatic systems and minerals produced by the thermal decomposition of organic material biomass, including wood, manure, leaves, waste, etc., under limited supply or in absence of oxygen (O_2). Such a thermal decomposition process is referred to as pyrolysis. The most commonly used pyrolysis temperature is in the range of 400–600 °C [2], but a larger range of 200–1000 °C is reported [3]. When the thermal decomposition temperature is over 1000 °C and up to1600 °C, the process is named gasification. Pyrolysis comprises slow pyrolysis, fast pyrolysis, and flash pyrolysis,

depending on the working temperature, the heating rate, and the residence time of the organic matter at a fixed temperature [4]. Upon the pyrolysis of biomass, three types of products with different physical states can form simultaneously in different concentrations. The solid residue comprises BC, which could contain ash and soot, bio-oils represent the liquid product, and the gaseous ones consist of syngas [4]. The relative yields of such products depend mainly on the pyrolysis temperature and heating rate, as shown in Figure 1.

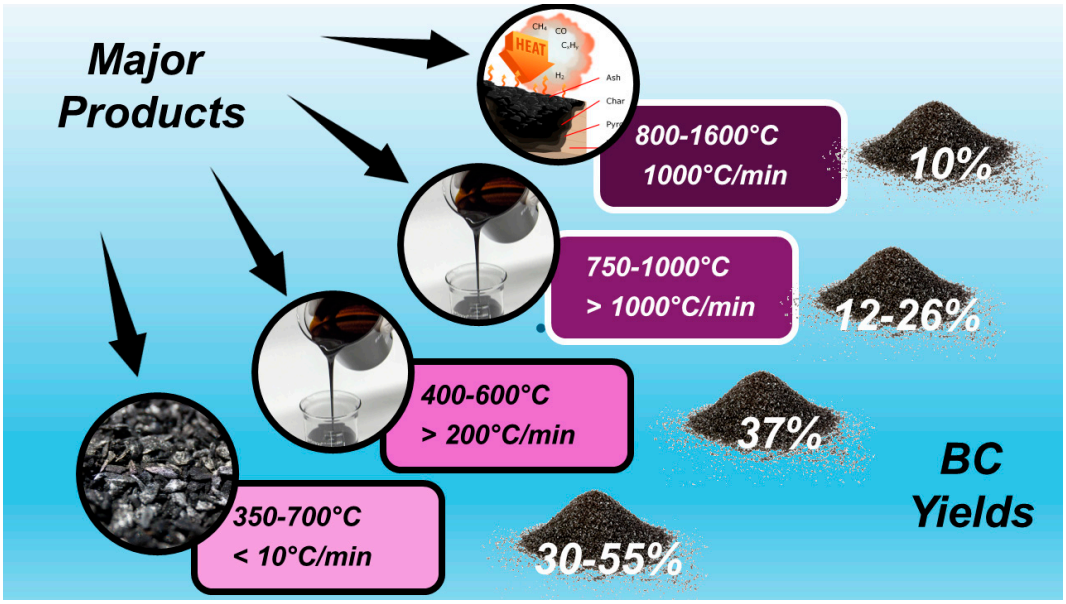

Figure 1. Influence of temperature of thermal degradation process on BC yield and that of by-products.

In conditions of slow pyrolysis (350–700 °C, heating rate < 10 °C/min), the major compound is BC; bio-oils are instead the most abundant products in conditions of flash and fast pyrolysis (400–600 °C, heating > 200 °C/min and 750–1000 °C, heating > 1000 °C/min, respectively), and syngas becomes the major product when gasification conditions are applied (800–1600 °C, heating 1000 °C/min) [5–9]. Syngas consists of a gas mixture whose composition can vary significantly depending on the feedstock type and gasification condition. However, typically, syngas is 30–60% carbon monoxide (CO), 25–30% hydrogen (H_2), 0–5% methane (CH_4), and 5–15% carbon dioxide (CO_2), plus a lesser or greater amount of water vapor, smaller amounts of sulfur compounds such as hydrogen sulfide (H_2S) and carbonyl sulfide (COS), and finally, some ammonia and other trace contaminants [10]. As for bio-oils, their production could be an appealing strategy for generating fuel from biomass, allowing a reduction in the global dependence on fossil fuels to produce energy [11]. Bio-oil has a higher heating value when compared to its original feedstock, and when burned, it can potentially generate a lower amount of greenhouse gas when compared to fossil fuels [12]. Consequently, even if its most studied application is still as a burning fuel, other applications are emerging due to its composition, as in the case of foams and resins [13]. Moreover, the latter applications emphasize the potential of bio-oil as a source of value-added chemicals [11].

The treatment of biomass at 200–300 °C heating at <50 °C/min is named torrefaction, leading to a torrefied biomass with a high content of BC (69–80%), while hydrothermal carbonization (HTC) in the presence of oxygen, carried out at 400–1000 °C and a very low heating rate (<1 °C/min), leads to the obtainment of hydro char (HC) (50–70% BC), also referred to as HTC material [3]. HC is a solid material distinct from BC due to its production process and properties [14]. Typically, HC has higher H/C ratios and lower aromatic systems than BC, as well as little or no fused aromatic ring structures. The

pyrolytic process leading to BC echoes that which yields charcoal, which is the most ancient industrial technology developed by humankind. Anyway, although very similar and of analogous origin, while charcoal is used mainly as a fuel, the primary application of BC was for soil amendment, aiming at improving soil characteristics and functions, as well as at preventing the natural degradation of biomass to greenhouse gases by sequestrating carbon, thus reducing gas emissions in the atmosphere and mitigating climate change [4]. As mentioned above, BC could contain other solids such as soot and ash. While soot is a secondary pyrogenic carbonaceous material (PCM) identified as a separate component resulting from gas condensation processes, ash typically includes inorganic oxides and carbonates not containing organic carbon. Figure 2 shows the main possible thermal treatment of biomass and the related main products of decomposition.

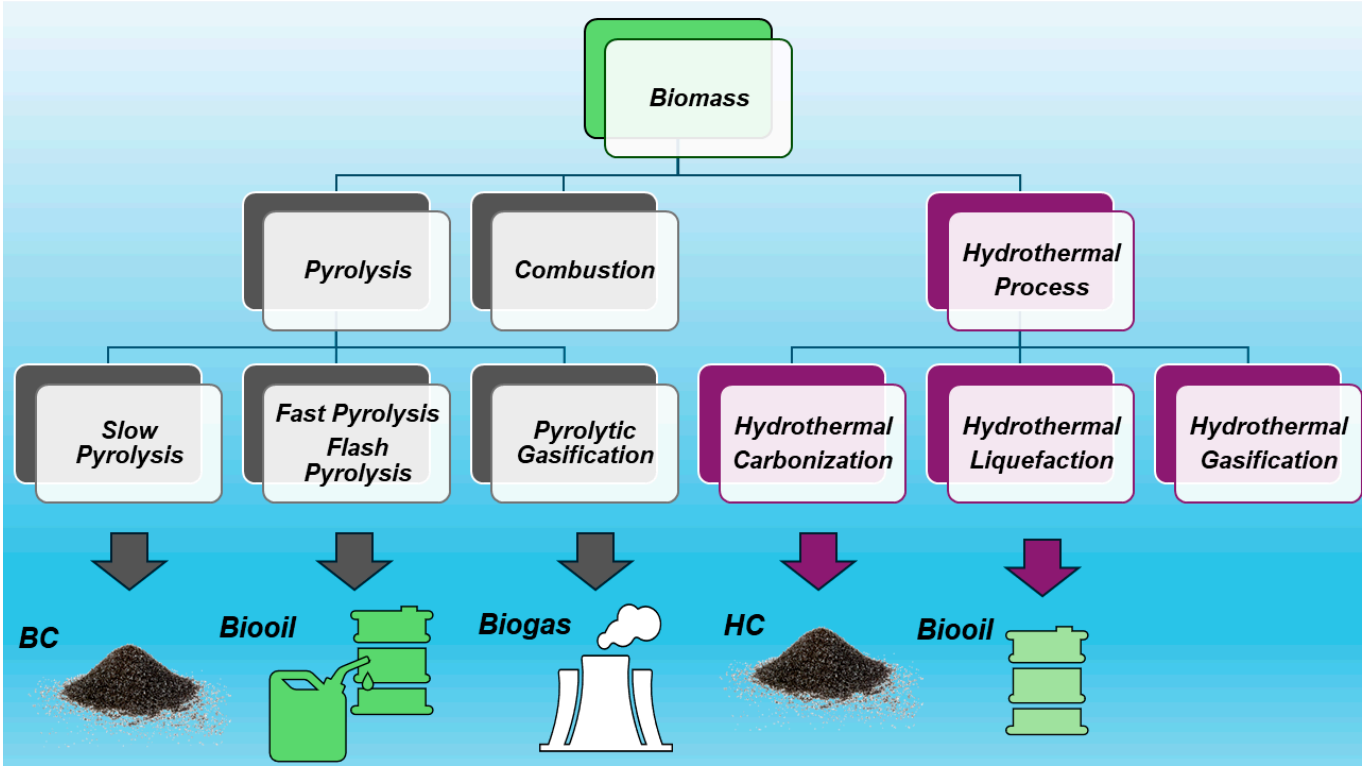

Figure 2. Main possible thermal treatment of biomass and the related products of decomposition.

An alternative method to produce BC consists of thermocatalytic depolymerization (TCD), which utilizes microwaves. It has been used to efficiently convert organic matter to BC on an industrial scale, producing ≈ 50% char [15,16].

2. What Can Biochar Do?

Biochar (BC) is a sustainable, cost-effective, eco-friendly material that is also endowed with reusability, which is increasingly gaining the attention of many researchers [4]. In addition to other possible applications, simply by its production, BC allows for the reduction of agricultural and other types of waste. According to Table 1, among the biomass waste materials, crop residues from agriculture, forestry, municipal solid waste, and food and animal manures have a high potential and are appropriate for BC production [17–22].

Table 1. Main sources and general applications of BCs.

Source Biomass	Ref.	Application	Refs.
Crop residue	[23]	Carbon sequestration	[24]
Kitchen waste	[35]	Soil amendment	[25]
Forestry	[36]	Composting	[26]
Agricultural waste	[37]	Wastewater treatment	[27]
Sugar beet tailings	[38]	Concrete additive	[28,29]
Forest residues	[39]	Adsorbing xenobiotics	[30]
Waste wood	[40]	Reducing greenhouse gas emissions	[31]
Bioenergy crops	[41]	Pollutant degradation	[32]
Municipal solid waste	[42]	Catalysis	[33]
Wheat straw	[43]	Stock fodder	[34]
Rice straw	[44]		
Food manure	[45]		
Animal manure	[46]		
Corn cob	[47]		

BC possesses several properties, including large surface area, high porosity, presence of functional groups, high cation exchange capacity (CEC), high water-holding capacity (WHC), strong stability, etc., which make it suitable for various applications, as reported and summarized in Table 1 [4]. Particularly, in the first column of Table 1 (source biomass), we have reported the biomasses that are commonly used to produce BC along with related references (column two), while in the third column (applications), the most common uses of BCs, which can be derived from all biomasses reported in column one, have been included along with related references (column four).

More specifically, Table 2 reports the environmental applications of BC and the related mechanisms.

Table 2. Main environmental applications of BC and related mechanisms.

Application	Mechanisms	Refs.
Climate change mitigation	Sequestering carbon in soil, ⇓ CO_2 emissions ⇓ NO_2 emissions, ⇓ CH_4 emissions Tackling 12% of current anthropogenic carbon emissions	[31]
Soil improvement	⇑ Physicochemical and biological properties ⇑ Water retention capacity, ⇓ nutrient leaching ⇓ Acids, ⇑ microbial population and microbial activity Positive impacts on earthworm population Preventing desiccation	[25]
Waste management	Simply by pyrolyzing waste biomass *	[48]
Energy production	By conversion of waste biomass to BC **, providing liquid fuel (bio-oil)	[49]
Capturing contaminants	By adsorption of both organic xenobiotics and metal ions present in soil and water	[30,32]
Composting	⇑ Physicochemical properties of composting ⇑ Enhance composting microbial activities ⇑ Organic matter decomposition	[26,32]

* Including crop residues, forestry waste, animal manure, food processing waste, paper mill waste, municipal solid waste, and sewage sludge; ** mainly by fast pyrolysis; ⇓ low, lower, reduced, minor; ⇑ high, higher, increased, major.

By using BC, it is possible to fight global warming by reducing greenhouse gas emissions, such as CO_2, NO_2, and CH_4, and sequestering carbon [31]. Interestingly, BC has been estimated to be capable of tackling 12% of the current anthropogenic carbon emissions [4]. Concurrently, the process of pyrolysis manages to balance fossil fuel consumption by producing clean and renewable energy (bioenergy) [49]. Due to its high content of

carbon, BC can work as a soil conditioner, mainly by improving the physicochemical and biological properties of soils, increasing its WHC by ~18%, reducing nutrient leaching, and neutralizing acidic soils, thus enhancing plant productivity, seed germination, plant growth, and crop yields [25]. Especially when wet BC is applied, soil desiccation is prevented [4]. In some BC systems, all these objectives can be met, while in others, a combination of two or more objectives will be obtained. Interestingly, BC has been used in animal feed for centuries. Doug Pow, a Western Australian farmer, who won the Australian Government Innovation in Agriculture Land Management Award at the 2019 Western Australian Landcare Awards for his studies and innovations, explored the use of BC mixed with molasses as stock fodder for ruminants [50]. The study demonstrated that BC-assisted digestion was improved, and methane production was reduced. On-farm evidence indicated that the fodder led to improvements of liveweight gain in Angus-cross cattle [50]. Additionally, the production of BC by solid waste can help in solving the problem of waste management [48]. The production of the cement known as ordinary Portland cement (OPC), which is an essential component of concrete mix, is energy- and emissions-intensive and accounts for around 8% of global CO_2 emissions. To limit this issue, the concrete industry has increasingly moved toward the use of supplementary cementitious materials (SCMs) and additives to both reduce the volume of OPC in the concrete mix and maintain or improve concrete properties [51–53]. BC has been shown to be an effective SCM, reducing concrete production emissions while maintaining the required strength and ductility properties [28,29]. Studies have been carried out demonstrating that a 1–2% wt. concentration of BC is excellent for use in concrete mixes, both in terms of low cost and good strength [28]. Moreover, the addition of a 2% wt. BC solution in the concrete mix resulted in an increased concrete flexural strength by 15% in a three-point bending test conducted after 7 days, compared to the traditional OPC-based concrete [29]. BC-based concrete also showed higher temperature resistance and reduced permeability [28]. Compared to other SCMs from industrial waste streams (such as fly ash and silica fume), BC also demonstrated decreased toxicity. Additionally, BC has been demonstrated to be capable of catalyzing chemical reactions and removing hazardous organic and inorganic pollutants from water soil and atmosphere, including antibiotics, thus reducing the emergence of microbial resistance [4]. Batch and column sorption experiments have shown that certain types of BCs have good sorption performance for heavy metals, dyes, or phosphate from aqueous solution and are being investigated as cost-effective, promising, and eco-friendly alternative materials for producing adsorbent materials [54–60].

2.1. BC as Climate and Soil Improver

As mentioned above, by its carbon sequestration action, BC performs climate remediation.

The refractory stability of BC leads to the concept of pyrogenic carbon capture and storage (PyCCS) [61], or rather, the sequestration of carbon in the form of BC [16]. Due to this potential, BC may be a means of mitigating climate change [62,63]. Due to its alkalinity, BC can increase the soil fertility of acidic soils and improve agricultural productivity [4]. When used for soil application, BC has been demonstrated to improve soil nutrient availability, aeration in soil, and soil water filtration. A large body of peer-reviewed literature exists assessing and describing the crop yield benefits of BC-amended soil [25]. Several field trials using BC conducted in the tropics have shown positive results on crop yields when BC was applied to field soils, and nutrients were managed appropriately. The most well-known example of the beneficial action of BC application to soil is the fertile Terra Preta soils in Brazil, but Japan also has a long tradition of using charcoal in soil [64,65]. Such a tradition is being revived and has been exported over the past 20 years to countries such as Costa Rica. The Brazilian and Japanese traditions together provide long-term evidence of positive BC impact on soils. Figure 3 summarizes the ways by which BC can improve soil quality.

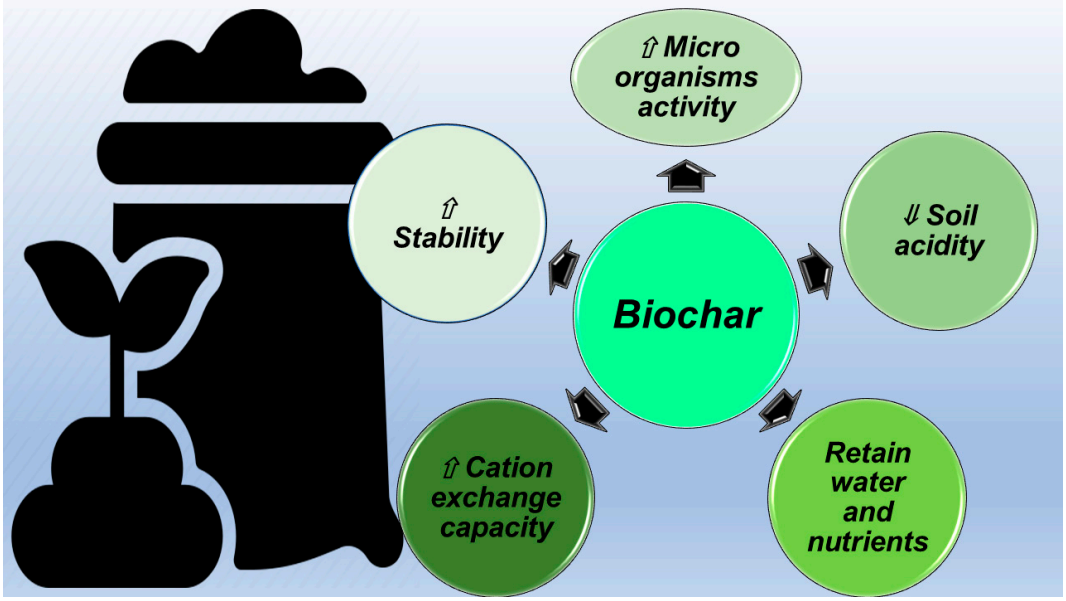

Figure 3. Ways by which BC acts as a soil improver. ⇓ low, lower, reduced, minor; ⇑ high, higher, increased, major.

Particularly, BC stimulates the activity of a variety of agriculturally important soil microorganisms by providing them with a suitable habitat and by protecting them from predation and drying while addressing many of their diverse carbon (C), energy, and mineral nutrient needs [66]. BC reduces soil acidity by means of the negative charges present on its surface and attracts and holds soil nutrients by the same mechanism [66]. BC has a high CEC, by which it retains positively charged ions, such as calcium (Ca^{2+}), potassium (K^{+}), and magnesium (Mg^{2+}), thus improving soil fertility and exchanging them with plant roots. BC mineralizes in soils much more slowly than its uncharred precursor material (feedstock). Moreover, although most BC has a small labile (easily decomposed) fraction of carbon, typically a much larger recalcitrant (stable) fraction composes it [25]. Scientists have shown that the mean residence time (the estimated amount of time that biochar carbon will persist in soils) of this recalcitrant fraction ranges from decades to millennia [25].

The long persistence of BC when incorporated into soils is of paramount importance because it determines how long BC can provide benefits to soil and water quality.

Critical Considerations

While the larger questions concerning overall BC benefits to soils and climate have received affirmative responses, significant questions remain to be answered, including the need for a better understanding of some of the details of BC production and characterization. Although BC is widely viewed as an environmentally positive material for soil, it is crucial to also take into account the potential adverse effects of BC, including disturbing soil pH levels or introducing harmful chemical characteristics that cause problems at the micro dimensions. Therefore, caution should be exercised when considering the extensive application of BC, as the research exploring its positive and negative effects is currently ongoing.

Dust is certainly a concern associated with BC application, but best practices require that BC application be done during periods of low wind to prevent the blowing of fine particulates. Agricultural techniques already exist for applying powdered fertilizers and other amendments. Several techniques are available to help keep wind losses to a minimum, including that BC can be pelleted, prilled, mixed into a slurry with water or other liquids, mixed with manure and/or compost, or banded in rows. The optimization of BC application to soil is important, and the farm technology and methods are available to do the job.

2.2. Xenobiotics Removal by Biochar (BC)

BC is a material possessing a large surface area and high porosity based on the conditions of the pyrolysis process and the physicochemical characteristics of the original biomass [4] that allow it to interact with beneficial molecules, including water and water nutrients, as well as hazardous inorganic metal cations and organic pollutants [4]. Due to its enriched porous structure, high surface area, functional groups, and the possibility of interlacing π–π interactions and mineral components, BC is an excellent material for absorbing solutes from aqueous and organic solutions. Moreover, its naturally acquired adsorption capacity (3.6–6.3 g/g for BC prepared at a temperature range of 300–700 °C) [67] can further be enhanced by modifying its physicochemical properties through acid, alkali, or oxidizing treatments, and its surface area can be improved using acid treatments [68–70]. BC can absorb inorganic and organic contaminants, such as polycyclic aromatic hydrocarbons (PAHs), phenols and phthalate derivatives, and antibiotics and other drugs, and can aid in improving the treatment of sewage wastewater containing organic contaminants [71]. Table 3 reports the main mechanisms by which BC captures inorganic or organic pollutants.

Table 3. Main mechanisms by which BC can capture inorganic or organic contaminants (reproduced by our recent paper [4]).

Catching Mechanism	Influencing Factors [#], Details [°], Examples [§]	Ref.
Adsorption *	⇑ Surface area [#] Microporosity of BC [#] pH [#]	[71]
Hydrogen bond formation **	For polar compounds [°,**]	
Electrostatic attraction/repulsion	For cationic compounds [°] Interaction between positively charged cationic organic contaminants and negatively charged BC surfaces [°,**]	
Electrostatic outer sphere complexation	Due to metallic exchange with K^+ and Na^+ available in BC [°,**]	
Hydrophobic interactions ***	For non-polar compounds [°]	
Diffusion	Non-ionic compounds can diffuse into the non-carbonized and carbonized fractions of BC [°]	
Formation of surface complexes **	pH [#] Ionic radius [#] Between metal cations and -OH, -COOH on BCs [°]	
Precipitation	Lead precipitates as lead-phosphate-silicate in BC [§] Co-precipitates and inner-sphere complexes can form between metals and organic matter/mineral oxides of BC [§]	

* From water/soil onto biochar; ** for BCs produced at relatively lower temperatures; *** for BCs produced at higher temperatures; ⇑ = high, higher, improved, enhanced.

BCs produced at higher temperatures exhibited higher adsorption capacity in the remediation of both organic contaminants and metal cations from soil and water, due to their higher porosity and surface area. Additionally, the adsorption capacity of organic pollutants by BC is superior to that of inorganic ones, which strongly depends on the ionic radius of metals.

Xenobiotics Removal by Degradative Oxidation

The mechanism recognized for years by which BC removes toxic heavy metals and organic xenobiotics from wastewater and contaminated soil is adsorption, whose efficiency mainly depends on the type and number of functional groups, surface area, CEC, etc. Nevertheless, more research studies have evidenced on the surface or inside the BC particles the presence of free radicals, known as permanent free radicals (PFRs) due to their very long lifetime, which may be generated during the pyrolysis of biomass [72]. PFRs

can exist in the air for months or even years. PFR lifetime depends mainly on the type of PFR, their possible complexation with metals or metal oxides, and their carbonaceous structure, as well as their concentration [72]. As recently reported, PFRs' nature depends strongly on pyrolysis conditions, while their formation and characteristics differ based on feedstock types [4]. PFRs are classified into three categories, including oxygen-centered PFRs (OCPFRs), carbon-centered PFRs (CCPFRs), and oxygenated carbon-centered radicals (CCPFRs-O) [4], including, in turn, semiquinone radicals (oxygen-centered), phenoxy radicals (oxygenated carbon-centered radicals), and cyclopentadienyls (carbon-centered radicals) [4]. Several recent studies have mainly investigated the possible contribution of BC-bound PFRs in the removal of several organic xenobiotics through oxidative degradation by electron transfer-dependent production of reactive oxygen species (ROS) [73–83]. The degradation of hazardous cations, including As (III) and Cr (VI), by PFRs via electron transfer has also been extensively reported [84–88], as well as that of biological samples, including hormones and extracellular DNA (eDNA) [89–93]. Odinga et al. reviewed the application of BC-derived PFRs in the remediation of several environmental pollutants [94], while Fang et al. explored the reactivity of PFRs in BC and their catalytic ability to activate persulfate to degrade pollutants [95]. On the other hand, Odinga et al. also considered and commented on the possible ROS-mediated environmental risks of PFRs from BCs, mainly associated with the generation of oxidative stress, which represent the shadows associated with these chemicals and indicate they need further study, more knowledge, and regulation before their extensive application [94].

3. Bamboo-Derived Biochar (BBC)

To date, the types of biomasses used to prepare BC and involved in the investigation of BC-bound PFRs mainly include lignocellulosic biomasses, such as pine needles, wheat straw, lignin, waste wood, cow manure, rice husk, and maize straw [23,35–47]. Lignocellulosic biomasses are made of hemicellulose, cellulose, and lignin. Despite the fact that bamboo may be a starting material almost perfect for synthesizing BC (BBC) and activated BBC (ABBC) due to its low cost, high biomass yield, and significantly accelerated growth rate, few researchers and scientists have used bamboo as a source for developing BC, as established by the number of publications on bamboo-derived BCs from the year 2013 until now (351) vs. those on BCs derived from different sources (14560) (Figure 4).

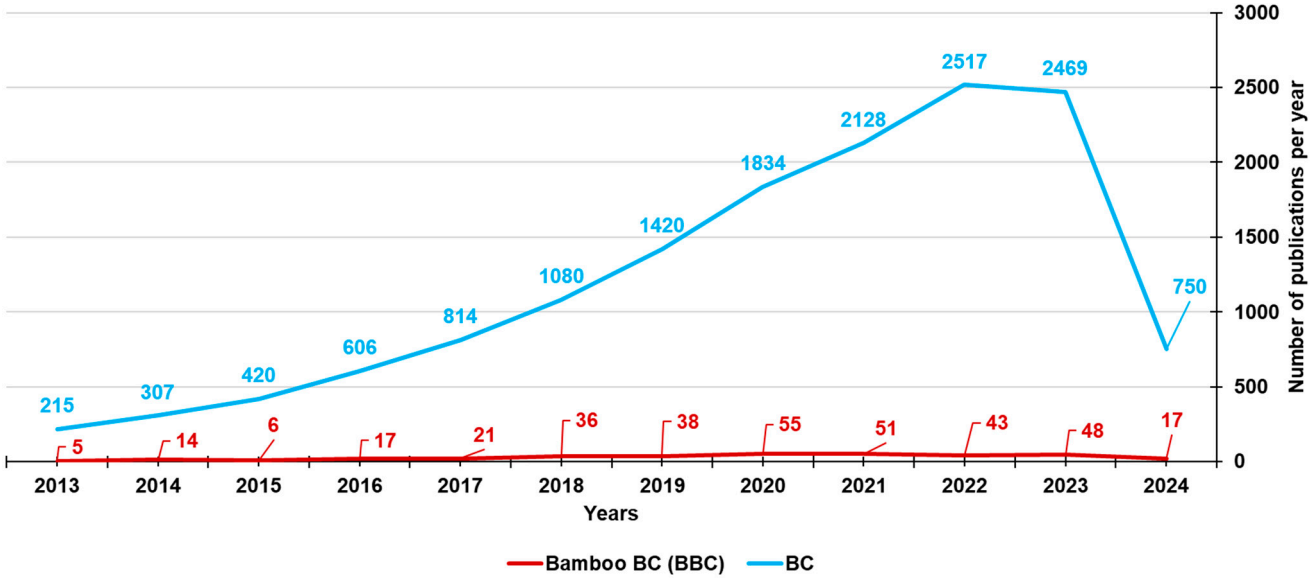

Figure 4. Number of papers on BCs and BBCs published from the year 2013 until now, according to the PubMed dataset. The survey was carried out using the keywords biochar (light blue line) and bamboo biochar (red line).

Among the 351 papers on BBC, the majority concerned its adsorption activity (128), followed by its degradation capacity (96), while fewer were studies on its possible toxic action (29) (Figure 5).

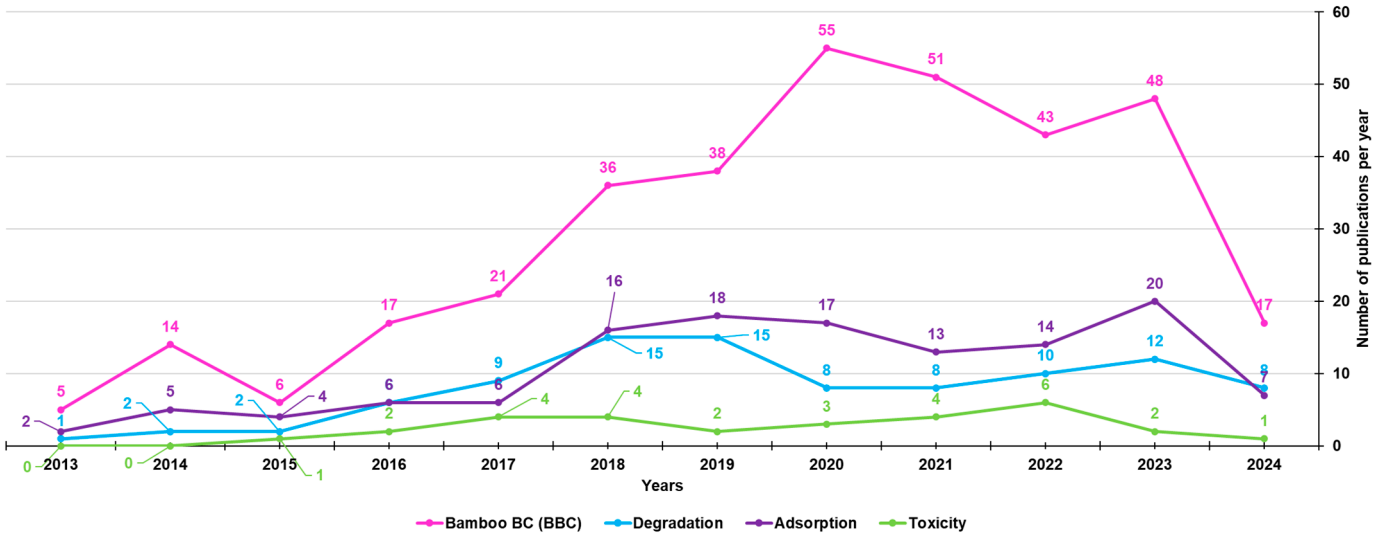

Figure 5. Number of papers on BBCs, as well as on BBC absorption, degradation and toxic properties, published from the year 2013 until now, according to the PubMed dataset. The survey was carried out using the keywords bamboo biochar (pink line); bamboo biochar AND adsorption (purple line); bamboo biochar AND degradation (light blue line); bamboo biochar AND toxicity (light green line).

To support and sustain further research on BBCs, the possible associated PFRs, and its possible applications, the following sections of this paper first review the general characteristics of bamboo biomass and the main reported characteristics of BBCs. Secondly, the current applications of BBCs and the PFR-mediated applications of BBCs are reported and discussed.

3.1. The Use of Bamboo Biomass to Prepare BC: A Plethora of Advantages over Wood

Bamboo is a woody grass belonging to the Poaceae family, extensively occurring both in forests and in rural areas, as well as in farmlands and riverbanks [96]. Bamboo, due to its growth form, acts as a natural environmental shield and has been used as food and to construct tools and musical instruments. Moreover, bamboo has been exploited as a construction material, as an alternative to wood fuel, as a substitute for wood, and even as a substitute for non-wood forest products [96]. Due to its strength and durability, the latter applications of bamboo are typical in those world areas where the supply of wood no longer manages to meet the demand [97]. Anyway, only in recent years the interest in agricultural bamboo has exploded in Africa, North America, and even Europe. Collectively, as a regenerative agriculture and as a renewable source of energy, bamboo represents a wonder crop for producing BC. It has minimal nutrient needs, it is relatively quick to get established, and once established, it grows with unmatched vigor, using its tenacious roots to raise the water table and curb erosion [96]. Due to these characteristics and mainly thanks to its fast growth with respect to woody plants, bamboo is an optimal source of BC, more efficient and eco-friendlier than wood [97]. Bamboo is capable of proliferating without the necessity of following stringent rules for growing, harvesting, propagating and cutting [98]. Bamboo can tolerate a wide range of temperatures (−28–38 °C), is able to efficiently exploit water and soil at its disposition, and does not need fertilizers or pesticides. It is known that the possible amount of carbon content in BC deriving from a certain plant depends directly on its metabolic activity (photosynthesis), through which it ingests CO_2 and releases oxygen (>30%) back into the atmosphere, thus reducing global warming. In this regard, due to its unequaled growth rate, bamboo yields more biomass and captures more atmospheric

carbon per hectare than anything, thus removing more carbon from the sky and adding it to the soil. Although the usefulness of bamboo as an absorbent is not very well known, that which is cultivated in tropical and subtropical regions worldwide can be used as a renewable feedstock, as already occurs in many countries, especially in Asia (China, India, and Thailand), Central America (Costa Rica, Mexico, and Honduras), and South America (Peru, Ecuador, and Colombia) [99–105]. It has been reported that bamboo plantations can store four times more carbon than timber forests and that they are therefore considered as a potential alternative as a durable carbon stock [106]. Bamboo, like wood, is a promising natural template for biobased devices that take advantage of its hierarchical architecture, microarray channels, and anisotropic mechanical and electrical properties [107]. Bamboo charcoal has been recognized as a cost-effective and environmentally friendly regenerative physio-sorbing material for carbon capture [108]. Additionally, BBC, being a growing porous carbonous material with high surface area, has been used for biomass fuel, carbon capture, and containment adsorption [109]. Through pyrolysis, up to 50% of the carbon can be transferred from plant tissue to the BC, with the remaining 50% used to produce energy and fuels [110]. However, bamboo-derived biochar has not been comprehensively reported despite its good CO_2 uptake [111]. Compared to wood composition, the lamellation of bamboo fiber has different fibrillar orientations surrounded by alternating narrow and broad layers [112]. The secondary cell wall is mainly made up of cellulose and lignin, with covalent linkage binding lignin phenolic acids to polysaccharide materials [112]. Bamboo culms grow and mature in a very short period of time, which can enable a continuous supply of fiber, giving it an advantage over trees. Bamboo's mechanical and thermal properties increase its competitiveness against other forms of woody biomasses [113]. For various reasons, bamboo is a superior option to other wood planks to prepare BC, including strength, environmental friendliness, water resistance, cost, soil protection, and contribution to air quality. These benefits were the driving force behind several uses for this material, including blood purification, electromagnetic wave absorbers, and water purifiers. These benefits are influenced by the activation and carbonization procedures used to make bamboo charcoal. Green bamboo wood is roasted to a constant temperature to create activated charcoal when charcoal is exposed to oxygen by using the pyrolysis method.

3.2. Composition of Bamboo

The anatomical and chemical components of a plant, especially the plant cell wall thickness and the lignin content, are correlated with its physical and mechanical properties, which can be improved by saturated steam heat treatments [114,115], in turn influencing the characteristics of the derived BC [116,117]. In sight of having to use bamboo to produce BBC with several possible applications, it is important to have more information about bamboo chemical components.

3.2.1. Chemical Composition of Bamboo

Table 4 summarizes the main constituents of bamboo.

Table 4. Main constituents of bamboo.

Components	Chemical Structure/Class of Substances	Description	(%)	Refs.
Cellulose	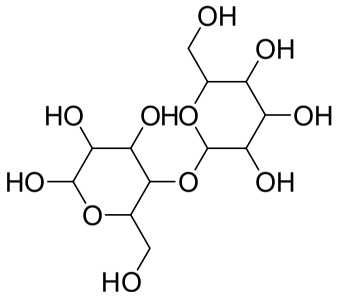 Portion of cellulose	Main material responsible for fibers' stability and mechanical strength, allowing the formation of compact fibers Higher thermal stability and resistance to mechanical stresses in comparison to other non-cellulosic plant fiber components Exhibit areas with a flexible structure (amorphous cellulose) and areas with an ordinated, rigid, and non-flexible structure (crystalline cellulose)	40–60 *	[118–121]
Hemicellulose (xylan) **	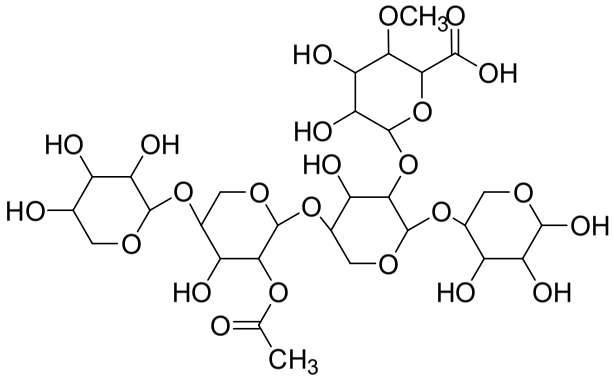 The most present hemicellulose in bamboo	Consists of a heterogeneous group of polysaccharides not forming a well-arranged fibrous network (amorphous structure) Low polymerization degree Easily absorbs water	25 §	[116,122]

Table 4. *Cont.*

Components	Chemical Structure/Class of Substances	Description	(%)	Refs.
Lignin	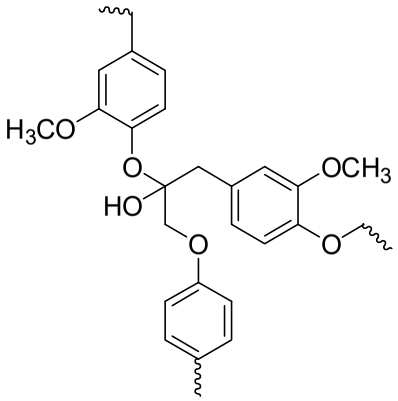 Portion of lignin	Amorphous phenolic macromolecule composed of phenyl propane units (C6-C3) No crystalline structure High resistance Cellulose and hemicellulose cells constitute the wall matrix Prevents cellulose and hemicellulose degradation, providing strength and rigidity to plant tissues Energy storage Polymerization degree (PD) > 15,000 High molecular weight	20–30	[116,120,121, 123]
Extractives	N.R.	Aromatic organic compounds, including fatty acids, terpenes, flavonoids, and steroids	N.R.	[120,122,124]
Ash	N.R.	Mainly in the interior of the stem	1–5	N.R.
Starch	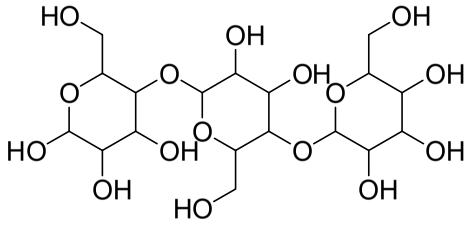 Portion of starch	Production by the cellular activity of chlorophyllized vegetables Attractive for xylophagous organisms, especially for *Dinoderus minutus*	2–5	[124]
Moisture	N.R.	N.R.	6.1	N.R.
Proteins	N.R.	N.R.	1.5–6	[124]
Glucose	N.R.	N.R.	2	[124]
Waxes, Resins	N.R.	N.R.	2–3.5	[124]
Silica	N.R.	Mainly in the epidermis, increasing from bottom to top Nonexistent in the internode tissues	1–6	N.R.

* Along with hemicellulose and lignin content, represents more than 90% of the total weight; ** 90% of hemicelluloses in bamboo; § of bamboo cell wall; N.R. Not reported.

The cellulose content in bamboo stem is in the range of 40–60%, while bamboo hemicellulose (25%) is composed of more than 90% xylan (4-O-acetyl-4-O-methyl-D-glucuronoxylan, shown in Table 4), a linear short-chain polymer with a polymerization degree of 200 [116]. Xylans constitute 25% of the bamboo cell wall, which is classified between hardwood and softwood, thus being endowed with a very particular structure [120]. Lignin (20%) occurs in the compound middle lamella as well as in the primary wall structure [123]. Lignin is considered a set of correlated materials responsible for transferring the stress between fibers, which promotes traction resistance, flexibility, and rigidity to the stem longitudinal section, being a supporting element. Lignin exhibits a high molecular weight and is the second most abundant component in bamboo, emerging from several stages of lignification that are related to the plant age. However, bamboo reaches a final height between 3 and 6 months during its growth process. While the process of lignification occurs in the longitudinal direction (in the top-down direction on bamboo length) in the internodes, it occurs in the transversal direction in the inner layer of the region closest to the bark, thus completing the whole process of the growth stage. The lignin and carbohydrate proportion varies during the maturation process and tends to stabilize when the plant is about 1 year old [120]. Secondary elements in bamboo chemical composition are represented by extractives, ash, waxes, resins, and silica. The compounds known as extractives consist of aromatic organic compounds, including fatty acids, terpenes (essential oils), flavonoids, and steroids, that are distributed in the leaf, shell, stem, and other parts of the plant but do not constitute the cell wall. The variation of these secondary components is related to the plant species, age, season, and weather conditions, as well as to the soil nutrient availability and diversity and the presence of water [120,122,124]. Collectively, the content of cellulose, hemicellulose, and lignin in bamboo is similar to that of wood, while the extractives, ashes, and silica contents are higher. The soluble substances (resins, fatty acids, essential oil, tannins, etc.), ashes (inorganic substances such as potassium, calcium, silicon, and magnesium), and lignin (a polymer responsible for the plant elasticity and resistance properties) contents in nodes are lower than in the internodes. For the cellulose content, the opposite occurs [120,121].

3.2.2. Elemental Composition of Bamboo

The elemental composition of a material relates to the average contents of carbon (C), hydrogen (H), nitrogen (N), and oxygen (O), and the H/C and O/C ratios of different bamboo and other lignocellulosic species are given in Table 5.

Table 5. Elemental composition of bamboo, wood, and other materials.

Biomass	C	H	N	O	H/C	O/C	Sources
Bambusa vulgaris	49.60	6.10	0.40	44.00	0.12	0.89	[125]
Bambusa vulgaris	46.80	6.38	0.22	46.60	0.14	0.99	[126]
Dendrocalamus giganteus	44.26	5.48	0.46	42.66	0.12	0.96	[127]
Dendrocalamus latiflorus	44.22	6.10	0.07	45.63	0.14	1.03	[128]
Phyllostachys makinoi	43.90	6.06	0.06	41.47	0.14	0.94	[128]
Phyllostachys pubescens	45.25	5.71	0.08	43.89	0.13	0.97	[128]
Wood *	45.68	6.30	0.30	47.42	0.14	1.04	[129]
Forest residue	51.40	6.00	0.50	40.00	0.12	0.78	[129]
Pine	47.79	5.80	0.10	45.31	0.12	0.95	[129]
Rice husk	47.30	6.10	0.90	45.70	0.13	0.97	[125]
Sugar cane bagasse	48.10	5.90	0.50	45.50	0.12	0.95	[125]
Jatropha bark	50.80	6.50	1.50	41.30	0.13	0.81	[125]
Elephant grass	49.20	6.10	1.10	43.60	0.12	0.89	[125]

C = carbon; H = hydrogen; N = nitrogen; O = oxygen; * Average values for different species.

The biomasses reported in Table 5 show very similar H/C ratios (from 0.12 to 0.14), indicating that they are highly carbonized. Otherwise, the average O/C ratio of bamboo species (0.96) is lower than the O/C ratio of wood biomass (1.04), indicating a higher

hydrophobicity on their surfaces, which makes bamboo biomass more stable against degradation than wood-based biomass. The average oxygen content of the bamboo species (44.04%) is lower than that of wood (47.42%), thus indicating a lower reactivity. Nevertheless, the presence of a high content of oxygen could decrease the energy density as well as the miscibility in hydrocarbon fuels. The biomass nitrogen content ranged from 0.1 to 12%, and the bamboo species had very low nitrogen content that ranged from 0.06 to 0.46%. The lowest content of nitrogen is important for environmental protection since NOx production, when burning the material, promotes environmental damage.

3.3. Bamboo-Derived Biochar (BBC)

In the last few years, researchers and scientists have used bamboo biomass from different species as a source for developing BC. Bamboo species like *Dendrocalamus giganteus, Dendrocalamus latiforus Munro, Dendrocalamus asper, Phyllostachys pubescens Mazel*, *Phyllostachys edulis*, *Phyllostachys virdiglaucesons*, Moso bamboo, and others have been carbonized in different conditions and in several cases chemically activated to obtain activated bamboo biochar (ABBC), which demonstrated different characteristics and properties and was studied for different applications. Table 6 summarizes useful information on the preparation of these materials and their possible uses.

Table 6. BBCs and activated BBCs (ABBCs) developed in recent years and their applications.

Bamboo Biomass	Pyrolysis Conditions	Reactor	Char (%) Other (%)	Characteristics Applications	Refs.
Dendrocalamus giganteus	300 °C Slow pyrolysis	Fixed bad type	BC 80% ## Oil 35% $ Gas 40% @	⇑ Porosity ⇑ Carbon concentration As AC after chemical/physical modification Similar to wood biochar Energy source Soil ameliorant	[127]
	200–1000 °C	Tube furnace (MTI)	N.R.	700 °C ⇑ Resistivity ⇑ Thermal conductivity ⇑ Thermal heating rate As a 3D microfluidic heater	[130]
				1000 °C ⇑ Electric conductivity As working electrode	
Phyllostachy edulis	N.R.	N.R.	N.R.	Ag-carbon electrodes for energy device applications	[131]
Bamboo waste	$KHCO_3$ 400 °C/3 h	Muffle furnace	N.R.	Excellent electrochemical performance as supercapacitor electrode materials	[132]
Bamboo chopsticks	800 °C/2 h (alkali)	N.R.	N.R.	Sustainable anodes for Li-ion batteries	[133]
Bamboo powder waste (alkali-activated)	1000 °C/15 min	Tube furnace	N.R.	Sustainable anodes for Na-ion batteries	[134]
Dendrocalamus asper	400 700 800 900 °C	N.R.	N.R.	N.R.	[135]
Phyllostachys pubescens Mazel	900 °C	Tube furnace	N.R.	BCT-derived air cathode for microbial fuel cells	[136]
Phyllostachys edulis	350 °C/60 min 500 °C/40 min 900 °C/240 min	N.R.	N.R.	3D solar vapor-generation device for water desalination	[137]
Local defoliated bamboo	Surface-carbonized	N.R.	N.R.	Efficient photothermal-conversion devices	[138]
Agricultural by-product (BSS) [d] *(D. latiforus Munro)*	300 °C to 500 °C	Tubular furnace	48%	As AC when chemically/physically modified soil ameliorant ⇑ Porosity ⇑ Carbon concentration	[139]

Table 6. *Cont.*

Bamboo Biomass	Pyrolysis Conditions	Reactor	Char (%) Other (%)	Characteristics Applications	Refs.
Dry bamboo stalks	400 °C to 600 °C Slow pyrolysis	Muffle furnace	32% to 27%	In place of industrially produced AC ⇑ Porosity ⇑ Carbon concentration	[113]
Bamboo waste	500 °C	Fabricated close tank	N.R.	⇑ Soil fertility and crop growth	[140]
Bamboo tick (*P. praecox*)	700 °C/4 h	Closed container	N.R.	⇑ Soil acidification ⇑ Soil C and nutrient retention ⇑ Microbial community abundance ⇓ CO_2	[141]
Bamboo	500 °C	N.R.	N.R.	⇓ NO_2 emissions in thermophilic phase of composting ⇑ nosZ-carrying denitrifying bacteria	[142]
Commercial BBC	N.R.	N.R.	N.R.	⇑ Humidification during pig manure composting ⇑ Humic acid (HA) ⇑ HA/Fulvic acid (FA) ratio ⇑ Bacteria transforming organic matter	[143]
Residual bamboo biomass	450–550 °C	N.R.	N.R.	Soil amendment	[144]
Bamboo waste	N.R.	N.R.	N.R.	Improving yield of pakchoy plant	[145]
Bamboo feedstock	300–600 °C	Furnace apparatus	N.R.	⇑ Tomato plant growth ⇑ Fruit quality	[146]
Bamboo stems (culms) [a]	400 °C/30 min	Sealed metallic kiln	N.R.	⇑ Physicochemical properties of SL, SiL ⇑ Tomato productivity	[147]
N.R.	500 °C/2 h	N.R.	N.R.	⇓ Cu uptake in roots ⇓ Solubility of soil heavy metals	[148]
N.R.	N.R.	N.R.	N.R.	⇑ pH in red soil ⇑ Soil nutrients ⇑ Abundance of *Basidiomycota Mucoromycota, Chytridiomycota*	[149]
N.R.	<500 °C	N.R.	N.R.	⇓ Mobile Cd, Cu, Mn, Ni, Zn ⇓ Pb, Mn, Cd, Zn, Cu, Ni uptake in soybean shoots ⇑ Root nodulation ⇑ Soybean growth ⇑ Plant K and Mo uptake ⇑ Soybean physiological performance	[150]

Table 6. *Cont.*

Bamboo Biomass	Pyrolysis Conditions	Reactor	Char (%) Other (%)	Characteristics Applications	Refs.
Bamboo chips	300 °C/1 h 450 °C/1 h 600 °C/1 h	Muffle furnace	N.R.	Remediation of As-contaminated paddy soil via iron–organic ligand complexation	[151]
Bamboo charcoal particles [b]	600 °C	N.R.	N.R.	As stabilizer for heavy metals Nitrogen retention in sludge composting	[152]
Bamboo sawdust	1000 °C	N.R.	N.R.	For CO_2 capturing ⇓ Regeneration temperature Excellent adsorption capacity	[153]
Bamboo carbon	600 °C/2 h	Muffle furnace	N.R.	BBC [§]-immobilized *Paracoccus* sp. YF1 for nitrates remediation	[154]
P. virdiglaucesons	460 °C Slow pyrolysis	Rotary furnace	50%	Nitrate absorption from wastewater or industrial effluents *	[155]
Residual of Moso bamboo manufacturing	900 °C/1 h	Electric furnace	N.R.	Nitrate-nitrogen adsorption	[156]
Giant timber bamboo (*P. bambusoides*)	400, 700, 1000 °C/1 h	Charcoal kiln	N.R.	Ammonia absorption	[157]
Healthy dried stems without leaves of bamboo	500 °C/20 min	Muffle furnace	N.R.	Modulate the toxic effects of chromium	[158]
Offcuts of bamboo [c]	900 °C/4 h	Vacuum annealing furnace	N.R.	Remediation of Cd (II) in water	[159]
Bamboo residues	400 °C	N.R.	N.R.	Restoration of acidic Cd-contaminated soil	[160]
Local bamboo	600 °C/4 h	N.R.	N.R.	Cu adsorption from soil ⇓ Cu accumulation in lettuce	[161]
Bamboo pieces	600 °C/5 h	Tube furnace	N.R.	Cu absorption from soil ⇓ Soil acidity ⇓ Zn and Pb	[162]
Bamboo shoot shells	500 °C/3 h	Muffle furnace	N.R.	Removal of Ag (I) and Pd (II) Removal of TC and MB	[163]
N.R.	N.R.	N.R.	N.R.	Removal of elemental mercury	[164]
N.R. °°°	N.R.	N.R.	N.R.	Removal of Cd (II) ions from water	[165]

Table 6. *Cont.*

Bamboo Biomass	Pyrolysis Conditions	Reactor	Char (%) Other (%)	Characteristics Applications	Refs.
Makino bamboo (*P. makinoi Hayata*) [d]	800–900 °C/2 h	Furnace	N.R.	Removal of heavy metal ions from water	[166]
Moso (*P. pubescens*) and Ma (*D. latiflorus*) bamboo slices [e]	800 °C/1 h	Furnace	N.R.	Removal of heavy metal ions from water	[167]
B. vulgaris striata [f]	650 °C/2 h	N.R.	N.R.	Adsorption of Cd (II), Hg (II), and Zn (II) from aqueous solution	[168]
Bundles of bamboo culms (*Melocanna baccifera*) [g]	N.R./2–4 h	Kiln	N.R.	Removal of Ni (II) and Zn (II) from aqueous solutions	[169]
Commercial bamboo charcoal	>450 °C	N.R.	N.R.	Activated by NaOH treatment ⇑ Percentage of surface graphitic carbon ⇑ Oxygen-containing groups ⇑ π–π interactions Adsorptive removal of chloramphenicol	[170]
Bamboo pieces	550 °C	Fluidized bed reactor	N.R.	100% Furfural removal	[171]
Bamboo	600 °C/1 h	Tube furnace	N.R.	Removal of MB by electrostatic interactions	[172]
Bamboo from authors' campus (Jiangsu University, China)	200 °C/6 h 180 °C/3 h	Teflon-lined stainless steel autoclave	N.R.	As core–shell non-metallic photocatalysts for the photocatalytic decomposition of tetracyclines	[173]
Bamboo sawdust	500 °C	N.R.	N.R.	Removal of fluoroquinolone antibiotics	[174]
Bamboo waste	600 °C	N.R.	N.R.	In situ remediation of PCP	[175]
Bamboo waste	1000 °C	N.R.	N.R.	Removal of MCAB-172	[176]
Bamboo waste	820 °C	Stainless steel vessel	N.R.	⇓ Bioavailability of DEP	[177]
Moso (*P. pubescens*) bamboo	800 °C Fast pyrolysis	N.R.	N.R.	Removal of pyridine, indole, quinoline	[178]
Bundles of bamboo culms (*Melocanna baccifera*) [h]	800 °C Fast pyrolysis	N.R.	N.R.	Removal of MB and AO7	[109]
Bamboo dust [i]	240 °C/2 h	Tube furnace	N.R.	Removal of MB	[179]
Bamboo [g]	700 °C/1 h (1st pyrolysis) 850 °C/2 h (activation)	Tube furnace	N.R.	Removal of MB	[180]
Moso (*P. pubescens*) bamboo sections	700 °C Fast pyrolysis	N.R.	N.R.	Removal of CAF and TC	[181]

Table 6. *Cont.*

Bamboo Biomass	Pyrolysis Conditions	Reactor	Char (%) Other (%)	Characteristics Applications	Refs.
Bamboo waste (China)	650 °C/1 h	Muffle furnace	N.R.	CdSe quantum dots/porous channel BBC for improved photocatalytic degradation of TC	[182]
Purchased BBC	N.R.	N.R.	N.R.	Removal of DBT	[183]
Bamboo sawdust [g]	873.15 K/1 h (carbonization) 1073 K/0.5 h (activation)	Tube furnace	N.R.	Removal of NVP	[184]
Bamboo waste	25 °C up to 850 °C	Microwave (2450 MHz)	N.R.	Absorption of toluene and benzene ⇑ Humidity resistance	[185]
Bamboo	N.R.	N.R.	N.R.	Extraction and determination of coumarins from *Angelicae pubescentis* Radix	[186]
Bamboo wood (KOH-activated)	500–700 °C/60–120 min	Vacuum pyrolysis machine	29–34% char 37–39% oil 26–33% gas	Adsorption of CO_2 and $PM_{2.5}$	[187]
Bamboo power *	450–600 °C	2 L Cylindrical reactor	9–29.82% ** 0.91–2.41% ***	As BC-supported sulfonic acid catalyst for cellulose hydrolysis	[188]
Phyllostachys edulis	353 K/3 h	N.R.	N.R.	BBC sulfonic acid bearing polyamide for microwave-assisted hydrolysis of cellulose	[189]
Bamboo waste	600 °C/30 min Fast pyrolysis	Fixed-bed system	84.7 wt% °°	To prepare phenols	[190]
Bamboo waste #	600 °C/30 min	Fixed-bed reactor	Char 19% Oil 42% H_2O 18% Gas 18%	Formation of aromatics and phenols	[191]
Bamboo waste °	600 °C/30 min	Fixed-bed reactor	N.R.	Formation of phenols (67%)	[192]
Bamboo activated carbon (BAC)	N.R.	N.R.	N.R.	Sulfonated BAC-based catalyst for oleic acid esterification	[193]

* From a bamboo processing factory (Zhejiang province, China) pretreated with alkaline carbonates; ** char; *** ash; °°° bamboo charcoal was provided by the Department of Material Science and Engineering, Tsinghua University; HTC = hydrothermal carbonization; § BBC improved the grow of immobilized bacterial cells; # catalytic deoxygenation co-pyrolysis of bamboo wastes and microalgae with biochar catalyst; ° pyrolyzed in absence or presence of activated BBC catalysts (activation with KOH, K_2CO_3, $KHCO_3$, or CH_3COOK at 800 °C/30 min); °° carbon content; ## 300 °C; $ over 500 °C; @ 600 °C; [a] *Guadua Angustifolia Kunth*; [b] Yaoshi Charcoal Production Company, Hangz; [c] *Phyllostachys heterocycla* (Carr.), *Mitford cv. Pubescens*; [d] CO_2- or water steam-activated; [e] water-activated; [f] water steam-activated; [g] raw or KOH-activated BBC; [h] not-activated and microwave-activated ABBC; [i] ammonium persulfate- and potassium persulfate-pretreated bamboo and then activated by cold alkali; BSS = bamboo shoot shell; ⇑ = high, higher, improved, enhanced; the symbol = means similar, like, comparable; BCT = bamboo charcoal tube; ⇓ = low, lower, reduced, decreased; DBT = dibenzo thiophen; CAF = chloramphenicol; TC = tetracycline; MB = methylene blue; PCP = pentachlorophenol; DEP = diethyl phthalate; MCAB-172 = metal-complex dye acid black 172; NVP = N-vinyl pyrrolidone; SL = sandy loam; SiL = silt loam; $PM_{2.5}$ = fine dust; N.R. = not reported.

The studies reported in Table 6 are related to the transformation of the lignocellulose bamboo biomass into pyrolyzed bamboo BCs (BBCs) in a nitrogen atmosphere. In several cases, BBCs were chemically treated with alkali, acid, and oxidant solutions to increase their porosity and add new chemical functional groups, thus achieving activated BBC, namely ABBC. In the studies, BBC and ABBC were used for metal removal in an aqueous solution or gas phase for ameliorating soil quality by reducing acidity and absorbing heavy metals, as catalysts for organic chemical reactions, as energy sources, and as thermoelectrical devices, as well as for the adsorption of organic compounds, such as dyes, drugs, and aromatic compounds. To limit the problem of deforestation and to meet the pressure of avoiding the use of native forest resources for the production of BC, a woody bamboo (species *Dendrocalamus giganteus Munro*) was pyrolyzed by Hernandez-Mena et al. as a renewable material, and the properties of bamboo-derived BC (BBC) were studied [127]. To this end, the fast-growth bamboo was slow-pyrolyzed in a fixed-bed reactor at temperatures ranging from 300 to 600 °C and at a 10 °C/min heating rate [127]. The obtained BC was analyzed by different analytical techniques, and according to the reported results, the pyrolysis of bamboo yielded both biochar and bio-oil, thus representing a low-cost and sustainable strategy for producing energy and for agricultural applications. Using different bamboo species, including *Dendrocalamus giganteus*, *Phyllostachys edulis*, *D. asper*, *P. pubescens Mazel*, and *P. edulis*, and different parts of the plant as bamboo chopsticks and defoliated bamboo and even bamboo waste, BBCs were produced with electrical, electrochemical, and thermal properties [130–133,135–138]. Particularly, depending on the temperature of the pyrolysis process (700 °C), BBCs demonstrated high resistivity, thermal conductivity, and thermal heating rate, being suitable as a 3D microfluidic heater. Otherwise, BBCs obtained at 1000 °C proved to have high electric conductivity, thus being suitable as working electrodes [130]. Also, other bamboo-derived BCs were proposed as Ag-carbon electrodes for energy device applications [131]. BBCs obtained in specific conditions demonstrated excellent electrochemical performance [132] and were usable as supercapacitor electrode materials [132], as sustainable anodes for Li-ion batteries [133], as anodes for Na-ion batteries [134], as BCT-derived air cathodes for microbial fuel cells [136], as 3D solar vapor-generation devices for water desalination [137], and as efficient photothermal conversion devices [138]. The shoot shell of *D. latiflorus Munro* was used to produce BBCs at temperatures ranging from 300 °C to 500 °C. BBC derived at 400 °C demonstrated the best properties in soil improvement in terms of water-holding capacity (WHC), bulk density, iodine sorption, and metal adsorption. Particularly, soil adsorption capacities of Pb (II), Cr (III), and Cd (II) were improved by approximately 27%, 21%, and 29% with the addition of 2.5% wt. BBC [139]. Aiming at preparing BBCs to be used as soil improvers again, Sahoo and co-workers characterized and compared BCs obtained by pyrolysis at different temperatures (400, 500, and 600 °C) of bamboo biomass (BBCs) with those achieved by pyrolyzing pigeon pea stalk under the same conditions [113]. Briefly, the BC yield, which decreased with increasing temperature, was higher in bamboo than in pigeon pea stalk biomass due to more lignin content and low volatile matter in the former. Both BCs were shown to be highly carbonized and hydrophobic and to have low volatile matter, high porosity, and high fixed carbon, as well as proved to be beneficial for agricultural application, as they had high ash recovery [113]. The pyrolysis temperature of 600 °C was the most effective one in terms of surface area, total pore volume, and high mass fraction of carbon and fixed carbon for both the biomass materials [113]. Other authors, by pyrolyzing bamboo waste, bamboo tick, residual bamboo biomass, and bamboo agricultural by-products at temperatures ranging from 300 °C to 700 °C, prepared BBCs that were successful in enhancing soil fertility, crop growth [140], and soil acidification. Such BBCs have been demonstrated to be efficient in improving soil carbon content, promoting nutrient retention, improving microbial community abundance, and reducing CO_2 emissions [141], thus being suitable for soil amendment [144]. Yanan et al. prepared three types of biochar (corn stalk biochar (CSB), rape straw biochar (RSB), and bamboo charcoal (BC)) to investigate the relationship between N_2O emissions from composting

and denitrifying bacterial communities on compost and BC particles [142]. The results showed that N_2O emissions rates were higher in the thermophilic phase of composting and that the average emissions rate was lower upon BC treatment than after treatment with CSB and RSB [142]. The nosZ-carrying denitrifying bacterial community played a key role in reducing N_2O emissions, and the study indicated that BC enhanced the efficiency of N_2O emission reduction by enhancing the abundance of these key genera [142]. In another recent study by the same authors, the effects of bamboo charcoal (BC) and wheat straw biochar (WSB) on the humic acid (HA) and fulvic acid (FA) contents during pig manure composting were investigated [143]. The results evidenced that BC enhanced humification more than WSB and significantly increased the HA content and HA/FA ratio [143]. As in the study previously reported, the bacterial community structure under BC treatment differed from those under the other treatments. Particularly, BC increased the abundance of bacteria associated with the transformation of organic matter, thus influencing HA and FA concentration and improving the humification process during composting [143]. By the application of BBCs to soil obtained by the combustion of bamboo feedstocks, the quality and performance of different plants were enhanced. Particularly, the growth of mustard plants [194] and the yield of pakchoy plants [145], as well as the growth of tomato plants and the quality of their fruits, were improved [146,147]. Villagra-Mendoza et al. reported that the physicochemical changes that occurred in loam soils amended with BBC obtained by the pyrolysis of bamboo stems at 400 °C determined a significant improvement in tomato production yield [147]. Wang et al. demonstrated that the application of 5% bamboo biochar to soil reduced Cu uptake in the roots of Moso bamboo (*Phyllostachys pubescens*) and ameliorated soil physical properties and heavy metal solubility in soil [148]. Applications of biochar have significantly reduced the solubility of soil heavy metals. Authors evidenced that the application of BBC to soils ameliorated the quality of soils in terms of improved pH, nutrients, and abundance of beneficial fungi of *Basidiomycota, Mucoromycota,* and *Chytridiomycota* species [149], as well as reduced mobile Cd, Cu, Mn, Ni, Zn, reduced Pb, Mn, Cd, Zn, Cu, and Ni uptake in soybean shoots, and increased root nodulation, soybean growth, K and Mo uptake, and physiological performance of soybean plants [150]. Very recently, Tang et al. prepared BBCs at different pyrolysis temperatures (BB300, BB450, and BB600), which were successful in reducing As availability in paddy soil by adsorption and promoted the complexation of HCl-extractable Fe (III)/(II) and the formation of amorphous iron oxides, which, in turn, facilitated the formation of ternary complex (As-Fe-DOM) with highly stability [151]. Moreover, the abundance of *Geobacteraceae* and *Xanthomonadaceae*, which are common electroactive bacteria, was promoted in the BB450-treated paddy soil, which assisted in forming amorphous iron oxides [151]. Also, Hua et al. evidenced that the incorporation of bamboo charcoal particles prepared at 600 °C into the sludge composting material significantly reduced nitrogen loss (64.1%) and lessened the mobility of Cu and Zn [152]. Furthermore, a BBC with high adsorption capacity for CO_2 capture and for low-temperature heat utilization was developed by Ji et al. by pyrolyzing bamboo sawdust at 1000 °C [153]. BBCs were also used for nitrate remediation and for the removal/degradation of hazardous inorganic pollutants. Particularly, Liu et al. immobilized a *Paracoccus* sp. strain YF1 on bamboo carbon obtained at 600°C to be assessed for denitrification. The results showed that denitrification was significantly improved using immobilized bacteria compared to that of free cells, where denitrification time decreased from 24 h (free cells) to 15 h (immobilized cells) [154]. Aiming at further improving the sorption characteristics of BBC in the denitrification process, a BBC/montmorillonite composite was produced in an experimental pyrolysis reactor using bamboo (*P. virdiglaucesons*) as biomass feedstock by Viglašová et al. This composite was successful in removing nitrates from aqueous solutions, being 1.8-fold more efficient than BBC without montmorillonite [155]. In the past, the efficient removal of nitrogen in the form of nitrate and ammonia using BBCs obtained by pyrolyzing Moso and Giant timber bamboo at temperatures in the range of 400–1000 °C in a tube furnace and charcoal kiln, respectively, have been reported by Mizuta et al. [156] and Asada et al. [157]. Particularly,

the BBC prepared in the study by Asaka et al. was more efficient than commercial activated carbon in removing ammonia from water solution, and its performance improved further upon acidic treatment [157]. Concerning the environmental removal of hazardous metals, healthy dried stems without leaves of bamboo were converted in BBC in a muffle furnace at 500 °C to modulate the toxic effects of chromium on wheat plants [158], while offcuts of bamboo and bamboo residues were pyrolyzed at 900 °C and 400 °C, respectively, obtaining BBCs that were successful in the remediation of Cd (II) in Cd (II)-contaminated water and in the restoration of acidic Cd-contaminated soil [159,160]. Very recently, Ma et al. prepared BBCs and magnetic BBCs by the pyrolysis of bamboo at 600 °C and applied them for copper (Cu) immobilization in agricultural lands [161]. Particularly, magnetic BBC increased the maximum adsorption capacity and mitigated copper accumulation in lettuce. The major adsorption mechanisms of magnetic BBC were chemical precipitation, ion exchange, and metal–π complexation. Soil organic matter (SOM) facilitated the immobilization of activated copper [161]. In the same year, Zhang et al. prepared a ferrate-modified BBC and tested it as a composite system for soil amendment [162]. Particularly, the capacity of Fe-modified BBC to absorb heavy metal Cu and to reduce soil acidity was investigated [162]. An absorption efficiency of 276.12 mg/g due to single-layer surface adsorption and chemisorption processes was evidenced. Pore diffusion, electrostatic interaction, and surface interaction were the other possible mechanisms of Fe–BBC interaction with Cu^{2+} ions [162]. Multilayer self-assembled multifunctional bamboo shoot shell biochar microspheres (BSSBMs) showed a wide range of adsorption capacities, demonstrating the capability of absorbing heavy metals such as Ag (I) and Pd (II), antibiotics such as TC, and dyes such as MB from wastewater [163]. The maximum adsorption amounts of BSSBMs on Pd (II), Ag (I), TC, and MB were 417.3 mg/g, 222.5 mg/g, 97.2 mg/g, and 42.9 mg/g, respectively [163]. Moreover, Tan et al. investigated the adsorptive potential of a bamboo-derived BC (BBC) and of modified BBC using H_2O_2 for elemental mercury removal [164]. The results evidenced that BBC materials have excellent adsorption potential for elemental mercury, especially after being modified by H_2O_2 [164]. Batch adsorption experiments were conducted by Wang et al. to investigate the adsorption capacity of Cd (II) ions from aqueous solutions by BBC [165]. The results showed that the adsorption of Cd (II)ions was very fast initially, and equilibrium was reached after 6 h with an adsorbed capacity of 18 mg/g at pH = 8. Similarly, the batch adsorption capacity of heavy metal ions by CO_2 and water steam-activated or water-activated ABBC was investigated by Wang et al. [166] and by Sheng-Fong Lo et al., respectively [167]. The optimum pH values for the adsorption capacity of heavy metal ions were 5.81–9.82 by bamboo-activated carbons. The optimum soaking time was 2–4 h for Pb^{2+}, 4–8 h for Cu^{2+} and Cd^{2+}, 4 h for Cr^{3+} by *Moso* ABBC, and 1 h for the tested heavy metal ions by Makino ABBC. However, the removal efficiency of heavy metal ions by the tested ABBCs decreased in the order $Pb^{2+} > Cu^{2+} > Cr^{3+} > Cd^{2+}$. Specifically, depending on their interaction with anionic functional groups on the surface of activated ABBC, the adsorption capacity varies from 0.68 to 0.19 mg/g [166,167]. Moreover, water steam-activated mesoporous ABBC from the bamboo species *Bambusa vulgaris striata* achieved high efficiency in the removal of Cd (II), Hg (II), and Zn (II) ions from water solutions [168]. The batch studies suggested the highest adsorption capacities for an activated carbon dose of 0.6 g/L, solution pH = 9 and an equilibrium time of 16 h in static conditions were 240, 248, and 254 mg/g of cadmium, mercury, and zinc, respectively [168]. Other studies using KOH-activated bamboo derivates obtained from *Melocanna baccifera* species were mentioned with lower absorption capacities of 40.5 mg/g of Zn (II) [169]. A number of studies were concerned with the use of commercial bamboo charcoal, as well as that of BBCs prepared by the combustion of bamboo pieces, bamboo sawdust, or bamboo waste at different temperatures (450–1000 °C) in the remediation of hazardous organic compounds, including antibiotics and dyes. Particularly, an NaOH-activated BBC with a high percentage of surface graphitic carbon, oxygen-containing groups, and π–π interactions was used for the adsorptive removal of chloramphenicol [170]. The 100% removal of furfural, as well as the capability of removing MB by electrostatic interac-

tions and decomposing tetracyclines by a photocatalytic process, was demonstrated by BBCs [171–173]. Additionally, the removal of fluoroquinolone antibiotics and MCAB-172, the in situ remediation of PCP, and the reduction of the bioavailability of DEP in soil by BBC applications has also been reported [174–177]. Furthermore, Liao et al. reported the production of not-activated and microwave-activated ABBCs starting from Moso bamboo as biomass feedstock [109,178]. BBCs were obtained by pre-carbonization at 150–270 °C for 2–3 days, carbonization at 270–450 °C for 1–2 days, calcination between 450 and 800 °C for 0.5–1 day, and finally, maintenance at 800 °C for a short time. All the processes were carried out under a nitrogen atmosphere. The obtained materials were successful in the removal of nitrogen-heterocyclic compounds (NHCs), such as pyridine, quinoline, and indole [178], as well as MB and OA7 dyes [109] from water solutions. In the first case, the spent BBC with NHC adsorption was effectively regenerated by MW radiation [178], while microwave-activated ABBCs were remarkably more efficient in removing dyes than the raw BBC (17.32 mg/g vs. 14.99 mg/g for MB and 9.28 mg/g vs. 4.91 mg/g for OA7) [109]. Anyway, a very high maximum monolayer adsorption capacity of 454.2 mg/g for MB was reported previously by Hameed et al. using a KOH-activated ABBC prepared by pyrolyzing in a two-phase process: bamboo biomass first at 700 °C for 1 h and then at 850 °C for 2 h in the presence of KOH [180]. In a recent study, two BBCs were prepared from the torrefaction of ammonium persulfate- and potassium persulfate-pretreated bamboo and then activated by cold alkali, which were named ASBC and KSBC, respectively. The two BBCs demonstrated high adsorption properties (475/881 mg/g at 303 K) over MB, mainly by electrostatic interactions [179]. As previously reported by Fan et al., Liao and colleagues succeeded in removing chloramphenicol (CAF) from water solutions using a BBC obtained from the thermal decomposition of sections of bamboo (Moso bamboo) [181]. Particularly, 4-year-old Moso bamboo cut into different sections was pre-carbonized at 150–250 °C for 1–2 d, carbonized at 250–400 °C for 0.5–1 d, calcined at 400–700 °C for 0.5–1 d, and finally, kept at 700 °C for a short time [180]. In addition to CAF, the obtained BBC was also capable of removing tetracyclines (TCs), both in batch experiments and in fixed-bed column ones [181]. A simple in situ method was used by Men et al. to load CdSe quantum dots (QDs) onto hydrothermal biochar (HTC) obtained by pyrolyzing bamboo to form CdSe/HTC composites [182]. The authors employed the as-obtained BBC-based nanomaterials in the photocatalytic degradation of tetracycline (TC). Compared with pure CdSe quantum dots, the best photocatalytic degradation efficiency of CdSe/HTC complex containing 15% HTC was 73%, which was attributed to the high carrier transport efficiency of HTC and the inhibition reorganization of photogenerated electron-hole pairs [182]. Furthermore, DBT was removed by n-octane by Zhao et al. using a commercial BBC [183], while Li and Umereweneza prepared an ABBC using bamboo sawdust that was carbonized at 873.15 K for 1 h and then activated with alkaline treatment (KOH) at 1073 K for 0.5 h [184]. The as-prepared ABBC was successful in removing NVP from water solutions [184]. The enhanced adsorption capacity towards aromatic volatile organic compounds (VOCs) by hydrophobic porous BBC produced via microwave rapid pyrolysis of bamboo in the presence of $FeCl_3$ was recently reported by Junhao et al. [185]. Particularly, the as-obtained engineered BBC displayed better benzene and toluene adsorption capacity and humidity resistance. A BBC was also employed by Yu et al. to prepare a composite monolithic adsorbent [186]. The prepared composite adsorbent was successfully applied in a column for the reversible absorption of two coumarins from *Angelicae pubescentis* Radix, as well as for their determination [186]. Activated BBC (ABBC) was produced by treating the BBC with KOH, achieving a highly porous structure that was effective in extracting organic and inorganic contaminants from the air [187]. Particularly, ABBC produced at 700 °C demonstrated an air purifier's performance efficiency for removing CO_2 and $PM_{2.5}$ of 91.23 and 89.19%, respectively [187]. Bamboo-derived BCs were also used as hydrolytic catalysts or as catalysts to produce aromatic and phenolic derivatives. Particularly, the combustion by the molten alkali carbonate method of bamboo power at 450–600 °C (450 °C being the optimal temperature) in a 2 L cylindrical reactor yielded a BBC that was used to support

sulfonic acid groups, achieving a BBC-supported sulfonic acid catalyst that performed well in cellulose hydrolysis [188]. Similarly, a bamboo-based biochar sulfonic acid (BCSA) catalyst bearing polyamide moieties (BCSA-PA) with acidic and alkaline sites was prepared by the Yin group; it showed high activity and good selectivity for the conversion of glucose to 5-hydroxymethylfurfural (HMF) in pure water at 90 °C under microwave irradiation [189]. Chen et al. used N-doped BC catalysts derived by the fast pyrolysis (30 min) of bamboo at 600 °C in the presence of variant NH_3 concentrations for the catalytic pyrolysis of bamboo wastes to prepare phenols [190]. High-concentration aromatic and phenolic derivatives were prepared by Chen et al. through the catalytic deoxygenation co-pyrolysis of bamboo wastes and microalgae using a BBC catalyst, in turn achieved by bamboo waste pyrolysis [191]. Similarly, Yang et al. produced high-concentration phenols (67%) through the catalytic fast pyrolysis of bamboo wastes at 600 °C using a BBC catalyst activated with KOH, K_2CO_3, $KHCO_3$, or CH_3COOK at 800 °C, in turn achieved by bamboo waste pyrolysis at 600 °C [192]. Also, Niu et al. prepared a sulfonated heterogeneous acid catalyst from bamboo-activated carbon (BAC) through arylation. This BBC-based catalyst was used in the catalytic esterification of oleic acid with ethanol to produce biodiesel with 96% efficiency [193]. Collectively, information reported in Table 6 has evidenced that the majority of case studies on BBC and ABBC were concerned with their use in the removal of organic and inorganic xenobiotics from wastewater and in soil amendment, followed by their application in developing electrical and photochemical devices. Otherwise, their employment as catalysts for organic chemical reactions remains limited (Figure 6). In fact, unlike BC-based materials obtained from other biomasses, which have been employed as heterogeneous catalysts for organic reactions, including reduction, oxidations, esterification, C-C and C-N coupling, alkylation, epoxidation, cycloadditions, and multi-component reactions [195], the reactions catalyzed by BBCs include only those reported in Table 6, such as cellulose hydrolysis, pyrolytic production of phenols and aromatic compounds, and esterification reactions [188–193].

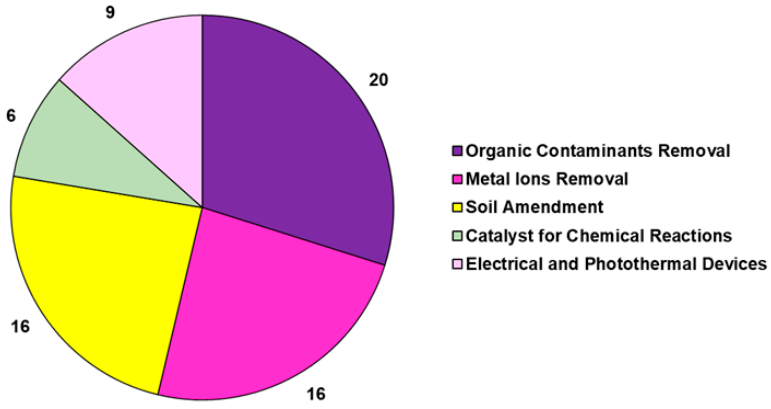

Figure 6. Main relative applications of bamboo-derived BC. Numbers refer to the existing publications reporting that specific application.

4. BBC-Derived Persistent Free Radicals

While the formation and presence of PFRs in the BC produced by several feedstock biomasses has been widely documented and studied since 2014, the literature documentation regarding those found in bamboo-derived biochar (BBC) is limited to four recent publications (Figure 7), which are reported in Table 7.

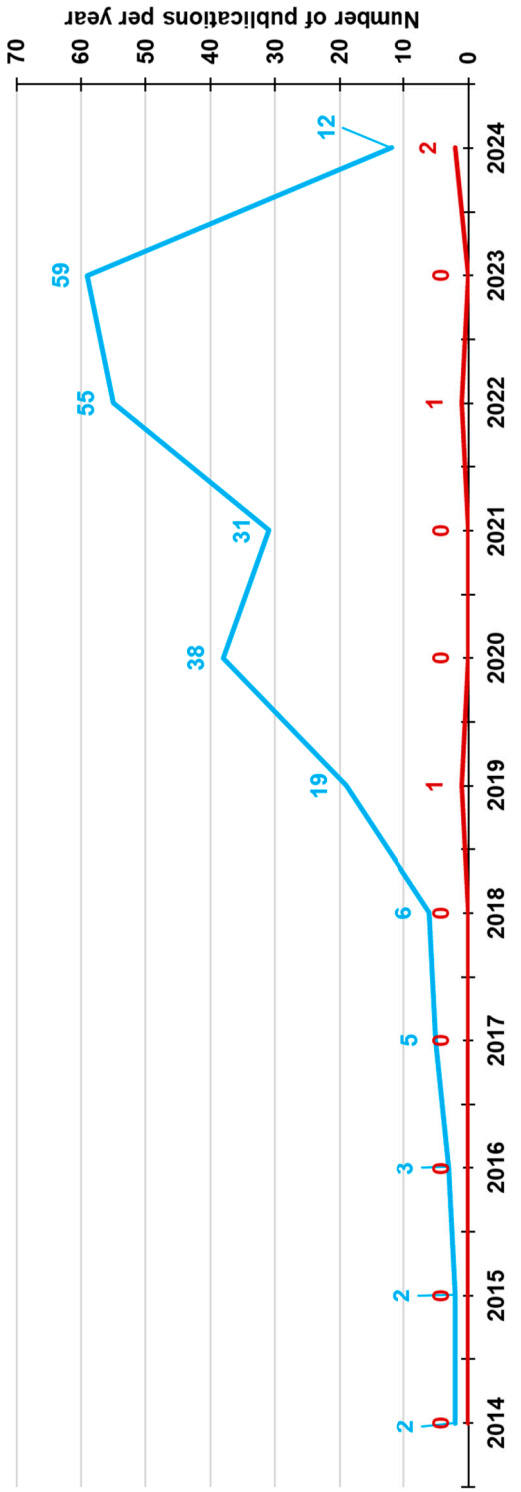

Figure 7. Number of papers on BC-derived PFRs and BBC-derived PFRs from 2014 until now, according to Scopus and PubMed datasets (reviews included). The survey was carried out using the following keywords: persistent AND free AND radicals AND biochar (light blue line) and persistent AND free AND radicals AND biochar AND bamboo (red line).

Table 7. Bamboo-BC (BBC)-derived EPFRs and their applications.

Source of BBC	Application	Process	Radicals Active Site		Radicals	Refs.
Bamboo	Tetracycline degradation	Fenton-like	PFRs		•OH	[196]
Moso bamboo **	PFX, OTC, CTC degradation	Oxidation PDS activation	OCFRs CCFRs-O CCFRs	g2 > 2.0040 2.0030 < g3 < 2.0040 g1 < 2.0030	•OH SO_4•$^-$	[197]
Bamboo chips	PCB28 degradation	Electron transfer * Oxidation *	PFRs *		•OH *	[198]
Bamboo	SMX, TOC degradation	Electron transfer Oxidation PDS activation	PFRs		•OH, SO_4•$^-$ •O_2	[199]

* Refers to degradation of PCB28 adsorbed on BBC obtained at low temperature; ** N-doped (urea), S-doped ($Na_2S_2O_8$), and NS-doped (thiourea); OCFRs = oxygen-centered free radicals; CCFRs-O = carbon-centered radicals with oxygen atoms; CCFRs = carbon-centered free radicals; PFX = pefloxacin; OTC = oxytetracycline; CTC = chloro-tetracycline; PCB28 = 2,4,4′-trichlorobiphenyl; PDS = persulfate.

Briefly, Huang et al., to assess the non-negligible role of biomass types and their compositions on the formation of PFRs in the related BC, selected three different biomass feedstocks, including bamboo [196]. Biomass was pyrolyzed in a tube furnace for 2 h at a temperature of 500 °C, and BBC was stored in an anaerobic glovebox purged with N_2 to avoid the effects of oxygen molecules on the PFR concentrations contained therein. The as-obtained BBC was tested in a BBC/H_2O_2 Fenton-like system to catalyze the oxidative degradation of tetracycline, evidencing high degradation efficiency by an electron transfer pathway via ROS production. The authors demonstrated that the catalytic property of BBC strongly depended on the amounts of PFRs [196]. The second and last experimental work found in literature concerning BBC-related PFRs was that by Zhang et al., who prepared N-doped (NBC), S-doped (SBC), and NS-doped (NSBC) BBC using Moso bamboo [197]. Bamboo biomass was pyrolyzed at temperatures in the range of 300–700 °C, giving the highest concentration of PFRs at 500 °C. The as-prepared BBCs were used to activate persulfate to produce both radical ($SO_4^{\bullet-}$, •OH, and $O_2^{\bullet-}$) and non-radical ($^1O_2$) species, which catalyzed the degradation of different antibiotics. Particularly, both EPFRs enhanced by the N-or S-doping, and non-radical species catalyzed the degradation of different antibiotics, including PFX, OTC, and CTC [197]. More recently, the photodegradation processes under simulated solar illuminations of 2,4,4′-trichlorobiphenyl (PCB28) adsorbed on biochar colloids (BCCs) released from bulk BBCs were studied by Wang et al. as a function of pyrolysis temperature (300, 500, or 700 °C) [198]. It was demonstrated that PCB28 adsorbed on the low-temperature BCCs degraded mainly by accepting electrons from the BBC-associated PFRs. Such electron transfer led to PCB28 dechlorination, followed by ring-opening oxidation through hydroxyl radical attack, ultimately resulting in progressive mineralization [198]. Otherwise, singlet oxygen non-radical mechanisms caused preferential ring opening of adsorbed PCB28 on the high-temperature BCCs, preceding dichlorination [198]. Lignocellulosic bamboo biomass was used as raw material to prepare Fe-N-BBC for persulfate activation and sulfamethoxazole (SMX) and TOC degradation [199]. BBCs were capable of activating peroxydisulfate (PDS) and degraded SMX and TOC, mainly via the oxidative action of four active species, such as •OH, $SO_4^{\bullet-}$, $^{\bullet}O_2$, and $^1O_2$ [199]. Based on these data, if the research on BBC is still limited compared to that on BC, the research studying the possible presence of PFRs in BBC, their characteristics, their possible application, their environmental transformation, and above all, their possible toxicity to humans and the environment is even more minimal (Figure 8).

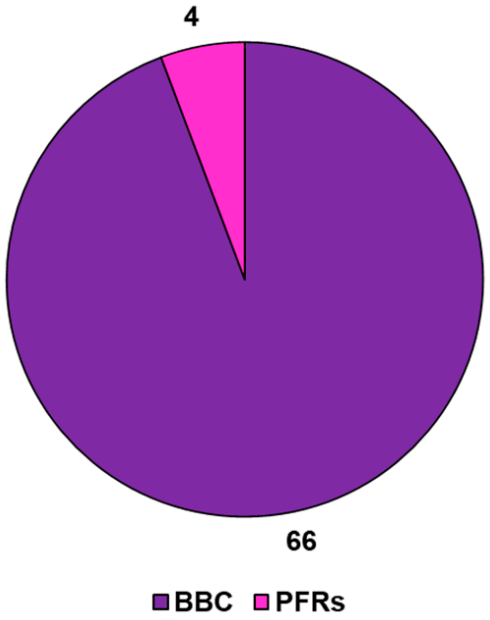

Figure 8. PFR-mediated BBC applications vs. BBC applications according to data reported in Tables 6 and 7. Numbers refer to the existing publications reporting that specific application.

5. Conclusions and Future Perspectives

In this review, the different applications of biochar (BC) and activated BC obtained by the thermal decomposition of several bamboo species (BBC and ABBC) have been schematically highlighted and extensively discussed. *Bambusa vulgaris*, *Gigantochloa albociliata*, Moso bamboo (*Phyllostachys edulis*), *Dendrocalamus giganteus*, *Bamboo Dendrocatiflorus Munro*, dry bamboo stalks, *Phyllostachys virdiglaucesons*, etc. are the most used bamboo species for developing BBC and ABBC. The interest in bamboo as a source for producing BC is quite young and still too limited, as evidenced by the lower number of existing experimental works concerning BBC compared to those concerning the production of BC from other biomasses. Anyway, BBC has revealed to be promising as an electromagnetic wave absorber, for constructing electrodes to be used in dye-sensitized solar cells, and for water and soil purification by absorption of organic xenobiotics and inorganic pollutants. Additionally, BBC has been helpful for the release of nutrients and gas remediation, and it has been largely demonstrated that BBC positively affects soil properties and greenhouse gas emissions, thus representing a nonpareil natural gift source for BC. Anyway, in our perspective, the more extensive use of bamboo and BBC in the urban, green building, and gardening industries to increase the nation's economic aspects and reduce ecotoxicity, the improvement of the properties of BC developable from bamboo, and more in-depth knowledge about the possible existence of BBC-associated PFRs is mandatory. In this context, the main scope of this review was to support increasing production of BBC and ABBC and to stimulate further studies about their possible applications, thus enlarging the current knowledge about these materials and allowing their more rational, safer, and optimized application, especially in the removal of xenobiotics.

Author Contributions: Authors contributed equally to this work. All authors have read and agreed to the published version of the manuscript.

Funding: This work was funded by Fundação Carlos Chagas Filho Amparo à Pesquisa do Estado do Rio de Janeiro (FAPERJ project n.SEI-260003/001227/2020), the European Union—*Next Generation EU*-the Italian Ministry of University (MUR) (PRIN2022, project n. 2022JM3LZ3_(SUST-CARB)).

Institutional Review Board Statement: Not applicable.

Informed Consent Statement: Not applicable.

Data Availability Statement: Data and information reported in this work have been obtained by literature using Scopus, PubMed, and Scifinder databases.

Conflicts of Interest: The authors declare no conflicts of interest.

References

1. International Biochar Initiative. Available online: https://biochar-international.org/about-biochar/faqs/ (accessed on 11 January 2024).
2. Panwar, N.L.; Pawar, A.; Salvi, B.L. Comprehensive Review on Production and Utilization of Biochar. *SN Appl. Sci.* **2019**, *1*, 168. [CrossRef]
3. Danesh, P.; Niaparast, P.; Ghorbannezhad, P.; Ali, I. Biochar Production: Recent Developments, Applications, and Challenges. *Fuel* **2023**, *337*, 126889. [CrossRef]
4. Alfei, S.; Pandoli, O.G. Biochar-Derived Persistent Free Radicals: A Plethora of Environmental Applications in a Lights and Shadows Scenario. *Preprints* **2024**. [CrossRef]
5. Pandey, D.; Daverey, A.; Arunachalam, K. Biochar: Production, Properties and Emerging Role as a Support for Enzyme Immobilization. *J. Clean. Prod.* **2020**, *255*, 120267. [CrossRef]
6. Antal, M.J.; Grønli, M. The Art, Science, and Technology of Charcoal Production. *Ind. Eng. Chem. Res.* **2003**, *42*, 1619–1640. [CrossRef]
7. Bridgwater, A.V. The Production of Biofuels and Renewable Chemicals by Fast Pyrolysis of Biomass. *Int. J. Glob. Energy Issues* **2007**, *27*, 160–203. [CrossRef]
8. DeSisto, W.J.; Hill, N.; Beis, S.H.; Mukkamala, S.; Joseph, J.; Baker, C.; Ong, T.-H.; Stemmler, E.A.; Wheeler, M.C.; Frederick, B.G.; et al. Fast Pyrolysis of Pine Sawdust in a Fluidized-Bed Reactor. *Energy Fuels* **2010**, *24*, 2642–2651. [CrossRef]
9. Al-Rumaihi, A.; Shahbaz, M.; Mckay, G.; Mackey, H.; Al-Ansari, T. A Review of Pyrolysis Technologies and Feedstock: A Blending Approach for Plastic and Biomass towards Optimum Biochar Yield. *Renew. Sustain. Energy Rev.* **2022**, *167*, 112715. [CrossRef]

10. National Energy Technology Laboratory. Syngas Composition. Available online: https://www.netl.doe.gov/research/coal/energy-systems/gasification/gasifipedia/syngas-composition (accessed on 16 January 2024).
11. Machado, H.; Cristino, A.F.; Orišková, S.; Galhano dos Santos, R. Bio-Oil: The Next-Generation Source of Chemicals. *Reactions* **2022**, *3*, 118–137. [CrossRef]
12. Shan Ahamed, T.; Anto, S.; Mathimani, T.; Brindhadevi, K.; Pugazhendhi, A. Upgrading of Bio-Oil from Thermochemical Conversion of Various Biomass—Mechanism, Challenges and Opportunities. *Fuel* **2021**, *287*, 119329. [CrossRef]
13. Hu, X.; Gholizadeh, M. Progress of the Applications of Bio-Oil. *Renew. Sustain. Energy Rev.* **2020**, *134*, 110124. [CrossRef]
14. Masoumi, S.; Borugadda, V.B.; Nanda, S.; Dalai, A.K. Hydrochar: A Review on Its Production Technologies and Applications. *Catalysts* **2021**, *11*, 939. [CrossRef]
15. Karagöz, S.; Bhaskar, T.; Muto, A.; Sakata, Y.; Oshiki, T.; Kishimoto, T. Low-Temperature Catalytic Hydrothermal Treatment of Wood Biomass: Analysis of Liquid Products. *Chem. Eng. J.* **2005**, *108*, 127–137. [CrossRef]
16. Alok, J. 'Biochar' Goes Industrial with Giant Microwaves to Lock Carbon in Charcoal. *The Guardian*. 13 March 2009. Available online: https://www.theguardian.com/environment/2009/mar/13/charcoal-carbon (accessed on 15 January 2024).
17. Ng, W.C.; You, S.; Ling, R.; Gin, K.Y.-H.; Dai, Y.; Wang, C.-H. Co-Gasification of Woody Biomass and Chicken Manure: Syngas Production, Biochar Reutilization, and Cost-Benefit Analysis. *Energy* **2017**, *139*, 732–742. [CrossRef]
18. Cantrell, K.B.; Hunt, P.G.; Uchimiya, M.; Novak, J.M.; Ro, K.S. Impact of Pyrolysis Temperature and Manure Source on Physicochemical Characteristics of Biochar. *Bioresour. Technol.* **2012**, *107*, 419–428. [CrossRef] [PubMed]
19. Funke, A.; Ziegler, F. Hydrothermal Carbonization of Biomass: A Summary and Discussion of Chemical Mechanisms for Process Engineering. *Biofuels Bioprod. Biorefin.* **2010**, *4*, 160–177. [CrossRef]
20. Klinghoffer, N.B.; Castaldi, M.J.; Nzihou, A. Influence of Char Composition and Inorganics on Catalytic Activity of Char from Biomass Gasification. *Fuel* **2015**, *157*, 37–47. [CrossRef]
21. Nunoura, T.; Wade, S.R.; Bourke, J.P.; Antal, M.J. Studies of the Flash Carbonization Process. 1. Propagation of the Flaming Pyrolysis Reaction and Performance of a Catalytic Afterburner. *Ind. Eng. Chem. Res.* **2006**, *45*, 585–599. [CrossRef]
22. Chen, Q.; Zhou, J.; Liu, B.; Mei, Q.; Luo, Z. Influence of Torrefaction Pretreatment on Biomass Gasification Technology. *Chin. Sci. Bull.* **2011**, *56*, 1449–1456. [CrossRef]
23. Smidth, A.N. A New Boost for Biochar as a Natural Climate Solution. 2023. Available online: https://blog.nature.org/science-brief/a-new-boost-for-biochar-as-a-natural-climate-solution/#:~:text=biochar%20is%20a%20type%20of%20charcoal%20made%20from,other%20biomass%20would,%20leading%20to%20more%20carbon%20sequestration (accessed on 27 December 2023).
24. Luo, L.; Wang, J.; Lv, J.; Liu, Z.; Sun, T.; Yang, Y.; Zhu, Y.-G. Carbon Sequestration Strategies in Soil Using Biochar: Advances, Challenges, and Opportunities. *Environ. Sci. Technol.* **2023**, *57*, 11357–11372. [CrossRef]
25. Brassard, P.; Godbout, S.; Lévesque, V.; Palacios, J.H.; Raghavan, V.; Ahmed, A.; Hogue, R.; Jeanne, T.; Verma, M. Biochar for Soil Amendment. In *Char and Carbon Materials Derived from Biomass*; Elsevier: Amsterdam, The Netherlands, 2019; pp. 109–146.
26. Godlewska, P.; Schmidt, H.P.; Ok, Y.S.; Oleszczuk, P. Biochar for Composting Improvement and Contaminants Reduction. A Review. *Bioresour. Technol.* **2017**, *246*, 193–202. [CrossRef]
27. Xiang, W.; Zhang, X.; Chen, J.; Zou, W.; He, F.; Hu, X.; Tsang, D.C.W.; Ok, Y.S.; Gao, B. Biochar Technology in Wastewater Treatment: A Critical Review. *Chemosphere* **2020**, *252*, 126539. [CrossRef]
28. Gupta, S.; Kua, H.W.; Koh, H.J. Application of Biochar from Food and Wood Waste as Green Admixture for Cement Mortar. *Sci. Total Environ.* **2018**, *619–620*, 419–435. [CrossRef]
29. Suarez-Riera, D.; Restuccia, L.; Ferro, G.A. The Use of Biochar to Reduce the Carbon Footprint of Cement-Based Materials. *Procedia Struct. Integr.* **2020**, *26*, 199–210. [CrossRef]
30. Qiu, B.; Shao, Q.; Shi, J.; Yang, C.; Chu, H. Application of Biochar for the Adsorption of Organic Pollutants from Wastewater: Modification Strategies, Mechanisms and Challenges. *Sep. Purif. Technol.* **2022**, *300*, 121925. [CrossRef]
31. Kalu, S.; Kulmala, L.; Zrim, J.; Peltokangas, K.; Tammeorg, P.; Rasa, K.; Kitzler, B.; Pihlatie, M.; Karhu, K. Potential of Biochar to Reduce Greenhouse Gas Emissions and Increase Nitrogen Use Efficiency in Boreal Arable Soils in the Long-Term. *Front. Environ. Sci.* **2022**, *10*, 914766. [CrossRef]
32. Jiang, T.; Wang, B.; Gao, B.; Cheng, N.; Feng, Q.; Chen, M.; Wang, S. Degradation of Organic Pollutants from Water by Biochar-Assisted Advanced Oxidation Processes: Mechanisms and Applications. *J. Hazard. Mater.* **2023**, *442*, 130075. [CrossRef]
33. Lyu, H.; Zhang, Q.; Shen, B. Application of Biochar and Its Composites in Catalysis. *Chemosphere* **2020**, *240*, 124842. [CrossRef]
34. Schmidt, H.-P.; Hagemann, N.; Draper, K.; Kammann, C. The Use of Biochar in Animal Feeding. *PeerJ* **2019**, *7*, e7373. [CrossRef]
35. Yu, D.; Yu, Y.; Tang, J.; Li, X.; Ke, C.; Yao, Z. Application Fields of Kitchen Waste Biochar and Its Prospects as Catalytic Material: A Review. *Sci. Total Environ.* **2022**, *810*, 152171. [CrossRef] [PubMed]
36. Yu, S.; Zhang, W.; Dong, X.; Wang, F.; Yang, W.; Liu, C.; Chen, D. A Review on Recent Advances of Biochar from Agricultural and Forestry Wastes: Preparation, Modification and Applications in Wastewater Treatment. *J. Environ. Chem. Eng.* **2024**, *12*, 111638. [CrossRef]
37. Wijitkosum, S. Biochar Derived from Agricultural Wastes and Wood Residues for Sustainable Agricultural and Environmental Applications. *Int. Soil Water Conserv. Res.* **2022**, *10*, 335–341. [CrossRef]

38. Yao, Y.; Gao, B.; Inyang, M.; Zimmerman, A.R.; Cao, X.; Pullammanappallil, P.; Yang, L. Biochar Derived from Anaerobically Digested Sugar Beet Tailings: Characterization and Phosphate Removal Potential. *Bioresour. Technol.* **2011**, *102*, 6273–6278. [CrossRef] [PubMed]
39. Puettmann, M.; Sahoo, K.; Wilson, K.; Oneil, E. Life Cycle Assessment of Biochar Produced from Forest Residues Using Portable Systems. *J. Clean. Prod.* **2020**, *250*, 119564. [CrossRef]
40. Papageorgiou, A.; Azzi, E.S.; Enell, A.; Sundberg, C. Biochar Produced from Wood Waste for Soil Remediation in Sweden: Carbon Sequestration and Other Environmental Impacts. *Sci. Total Environ.* **2021**, *776*, 145953. [CrossRef] [PubMed]
41. Laird, D. Biochar Amendments Make the Harvesting of Crop Residue for Bioenergy Production Sustainable. *Nutr. Cycl. Agroecosyst.* **2023**. [CrossRef]
42. Li, N.; He, M.; Lu, X.; Yan, B.; Duan, X.; Chen, G.; Wang, S.; Hou, L. Municipal Solid Waste Derived Biochars for Wastewater Treatment: Production, Properties and Applications. *Resour. Conserv. Recycl.* **2022**, *177*, 106003. [CrossRef]
43. Shi, W.; Wang, H.; Yan, J.; Shan, L.; Quan, G.; Pan, X.; Cui, L. Wheat Straw Derived Biochar with Hierarchically Porous Structure for Bisphenol A Removal: Preparation, Characterization, and Adsorption Properties. *Sep. Purif. Technol.* **2022**, *289*, 120796. [CrossRef]
44. Foong, S.Y.; Chan, Y.H.; Chin, B.L.F.; Lock, S.S.M.; Yee, C.Y.; Yiin, C.L.; Peng, W.; Lam, S.S. Production of Biochar from Rice Straw and Its Application for Wastewater Remediation—An Overview. *Bioresour. Technol.* **2022**, *360*, 127588. [CrossRef]
45. Gunamantha, I.M.; Widana, G.A.B. Characterization the Potential of Biochar from Cow and Pig Manure for Geoecology Application. *IOP Conf. Ser. Earth Environ. Sci.* **2018**, *131*, 012055. [CrossRef]
46. Rathnayake, D.; Schmidt, H.; Leifeld, J.; Mayer, J.; Epper, C.A.; Bucheli, T.D.; Hagemann, N. Biochar from Animal Manure: A Critical Assessment on Technical Feasibility, Economic Viability, and Ecological Impact. *GCB Bioenergy* **2023**, *15*, 1078–1104. [CrossRef]
47. Drané, M.; Zbair, M.; Hajjar-Garreau, S.; Josien, L.; Michelin, L.; Bennici, S.; Limousy, L. Unveiling the Potential of Corn Cob Biochar: Analysis of Microstructure and Composition with Emphasis on Interaction with NO_2. *Materials* **2023**, *17*, 159. [CrossRef] [PubMed]
48. Sudarsan, J.S.; Prasanna, K.; Shiam Babu, R.; Sai Krishna, V.M.V. Biochar: A Sustainable Solution for Organic Waste Management a Way Forward towards Circular Economy. In *Recent Trends in Solid Waste Management*; Elsevier: Amsterdam, The Netherlands, 2023; pp. 215–230.
49. Rawat, S.; Wang, C.-T.; Lay, C.-H.; Hotha, S.; Bhaskar, T. Sustainable Biochar for Advanced Electrochemical/Energy Storage Applications. *J. Energy Storage* **2023**, *63*, 107115. [CrossRef]
50. Daly, J. Poo-Eating Beetles and Charcoal Used by WA Farmer to Combat Climate Change. *ABC RURAL*. 18 October 2019. Available online: https://www.abc.net.au/news/rural/2019-10-18/wa-farmer-uses-beetles-and-charcoal-to-combat-climate-change/11613846 (accessed on 16 January 2024).
51. Making Concrete Change: Innovation in Low-Carbon Cement and Concrete. Chatham House—International Affairs Think Tank. Available online: https://www.chathamhouse.org/2018/06/making-concrete-change-innovation-low-carbon-cement-and-concrete (accessed on 22 January 2024).
52. Arvaniti, E.C.; Juenger, M.C.G.; Bernal, S.A.; Duchesne, J.; Courard, L.; Leroy, S.; Provis, J.L.; Klemm, A.; De Belie, N. Physical Characterization Methods for Supplementary Cementitious Materials. *Mater. Struct.* **2015**, *48*, 3675–3686. [CrossRef]
53. Gupta, S.; Kua, H.W.; Pang, S.D. Effect of Biochar on Mechanical and Permeability Properties of Concrete Exposed to Elevated Temperature. *Constr. Build. Mater.* **2020**, *234*, 117338. [CrossRef]
54. Varjani, S.; Kumar, G.; Rene, E.R. Developments in Biochar Application for Pesticide Remediation: Current Knowledge and Future Research Directions. *J. Environ. Manag.* **2019**, *232*, 505–513. [CrossRef]
55. Bridgwater, A.V. Review of Fast Pyrolysis of Biomass and Product Upgrading. *Biomass Bioenergy* **2012**, *38*, 68–94. [CrossRef]
56. Premarathna, K.S.D.; Rajapaksha, A.U.; Sarkar, B.; Kwon, E.E.; Bhatnagar, A.; Ok, Y.S.; Vithanage, M. Biochar-Based Engineered Composites for Sorptive Decontamination of Water: A Review. *Chem. Eng. J.* **2019**, *372*, 536–550. [CrossRef]
57. Beesley, L.; Moreno-Jiménez, E.; Gomez-Eyles, J.L.; Harris, E.; Robinson, B.; Sizmur, T. A Review of Biochars' Potential Role in the Remediation, Revegetation and Restoration of Contaminated Soils. *Environ. Pollut.* **2011**, *159*, 3269–3282. [CrossRef]
58. Jeffery, S.; Verheijen, F.G.A.; van der Velde, M.; Bastos, A.C. A Quantitative Review of the Effects of Biochar Application to Soils on Crop Productivity Using Meta-Analysis. *Agric. Ecosyst. Environ.* **2011**, *144*, 175–187. [CrossRef]
59. Kinney, T.J.; Masiello, C.A.; Dugan, B.; Hockaday, W.C.; Dean, M.R.; Zygourakis, K.; Barnes, R.T. Hydrologic Properties of Biochars Produced at Different Temperatures. *Biomass Bioenergy* **2012**, *41*, 34–43. [CrossRef]
60. Qin, Y.; Li, G.; Gao, Y.; Zhang, L.; Ok, Y.S.; An, T. Persistent Free Radicals in Carbon-Based Materials on Transformation of Refractory Organic Contaminants (ROCs) in Water: A Critical Review. *Water Res.* **2018**, *137*, 130–143. [CrossRef] [PubMed]
61. Werner, C.; Schmidt, H.-P.; Gerten, D.; Lucht, W.; Kammann, C. Biogeochemical Potential of Biomass Pyrolysis Systems for Limiting Global Warming to 1.5 °C. *Environ. Res. Lett.* **2018**, *13*, 044036. [CrossRef]
62. Yousaf, B.; Liu, G.; Wang, R.; Abbas, Q.; Imtiaz, M.; Liu, R. Investigating the Biochar Effects on C-mineralization and Sequestration of Carbon in Soil Compared with Conventional Amendments Using the Stable Isotope ($\delta^{13}C$) Approach. *GCB Bioenergy* **2017**, *9*, 1085–1099. [CrossRef]
63. Woolf, D.; Amonette, J.E.; Street-Perrott, F.A.; Lehmann, J.; Joseph, S. Sustainable Biochar to Mitigate Global Climate Change. *Nat. Commun.* **2010**, *1*, 56. [CrossRef] [PubMed]

64. Cocora, L.; Brand, K.; Cocora, L.; Brand, K. United Nations University: Japan's Charcoal Making Traditions Still Alive. Available online: https://ourworld.unu.edu/en/japans-charcoal-making-traditions-still-alive (accessed on 16 January 2024).
65. Arshad, U.; Altaf, M.T.; Liaqat, W.; Ali, M.; Shah, M.N.; Jabran, M.; Ali, M.A. Biochar: Black Gold for Sustainable Agriculture and Fortification Against Plant Pathogens—A Review. *Gesunde Pflanz.* **2023**. [CrossRef]
66. Hamidzadeh, Z.; Ghorbannezhad, P.; Ketabchi, M.R.; Yeganeh, B. Biomass-Derived Biochar and Its Application in Agriculture. *Fuel* **2023**, *341*, 127701. [CrossRef]
67. Nguyen, H.N.; Pignatello, J.J. Laboratory Tests of Biochars as Absorbents for Use in Recovery or Containment of Marine Crude Oil Spills. *Environ. Eng. Sci.* **2013**, *30*, 374–380. [CrossRef]
68. Jothirani, R.; Kumar, P.S.; Saravanan, A.; Narayan, A.S.; Dutta, A. Ultrasonic Modified Corn Pith for the Sequestration of Dye from Aqueous Solution. *J. Ind. Eng. Chem.* **2016**, *39*, 162–175. [CrossRef]
69. Suganya, S.; Senthil Kumar, P.; Saravanan, A.; Sundar Rajan, P.; Ravikumar, C. Computation of Adsorption Parameters for the Removal of Dye from Wastewater by Microwave Assisted Sawdust: Theoretical and Experimental Analysis. *Environ. Toxicol. Pharmacol.* **2017**, *50*, 45–57. [CrossRef]
70. Saravanan, A.; Kumar, P.S.; Renita, A.A. Hybrid Synthesis of Novel Material through Acid Modification Followed Ultrasonication to Improve Adsorption Capacity for Zinc Removal. *J. Clean. Prod.* **2018**, *172*, 92–105. [CrossRef]
71. Luo, Z.; Yao, B.; Yang, X.; Wang, L.; Xu, Z.; Yan, X.; Tian, L.; Zhou, H.; Zhou, Y. Novel Insights into the Adsorption of Organic Contaminants by Biochar: A Review. *Chemosphere* **2022**, *287*, 132113. [CrossRef]
72. Tao, W.; Zhang, P.; Li, H.; Yang, Q.; Oleszczuk, P.; Pan, B. Generation Mechanism of Persistent Free Radicals in Lignocellulose-Derived Biochar: Roles of Reducible Carbonyls. *Environ. Sci. Technol.* **2022**, *56*, 10638–10645. [CrossRef] [PubMed]
73. He, W.; Zhu, Y.; Zeng, G.; Zhang, Y.; Wang, Y.; Zhang, M.; Long, H.; Tang, W. Efficient Removal of Perfluorooctanoic Acid by Persulfate Advanced Oxidative Degradation: Inherent Roles of Iron-Porphyrin and Persistent Free Radicals. *Chem. Eng. J.* **2020**, *392*, 123640. [CrossRef]
74. Cao, W.; Zeng, C.; Guo, X.; Liu, Q.; Zhang, X.; Mameda, N. Enhanced Electrochemical Degradation of 2,4-Dichlorophenol with the Assist of Hydrochar. *Chemosphere* **2020**, *260*, 127643. [CrossRef] [PubMed]
75. Xu, H.; Zhang, Y.; Li, J.; Hao, Q.; Li, X.; Liu, F. Heterogeneous Activation of Peroxymonosulfate by a Biochar-Supported Co_3O_4 Composite for Efficient Degradation of Chloramphenicols. *Environ. Pollut.* **2020**, *257*, 113610. [CrossRef]
76. Li, X.; Jia, Y.; Zhou, M.; Su, X.; Sun, J. High-Efficiency Degradation of Organic Pollutants with Fe, N Co-Doped Biochar Catalysts via Persulfate Activation. *J. Hazard. Mater.* **2020**, *397*, 122764. [CrossRef] [PubMed]
77. Xie, Y.; Hu, W.; Wang, X.; Tong, W.; Li, P.; Zhou, H.; Wang, Y.; Zhang, Y. Molten Salt Induced Nitrogen-Doped Biochar Nanosheets as Highly Efficient Peroxymonosulfate Catalyst for Organic Pollutant Degradation. *Environ. Pollut.* **2020**, *260*, 114053. [CrossRef] [PubMed]
78. Yan, J.; Yang, L.; Qian, L.; Han, L.; Chen, M. Nano-Magnetite Supported by Biochar Pyrolyzed at Different Temperatures as Hydrogen Peroxide Activator: Synthesis Mechanism and the Effects on Ethylbenzene Removal. *Environ. Pollut.* **2020**, *261*, 114020. [CrossRef] [PubMed]
79. Mian, M.M.; Liu, G.; Zhou, H. Preparation of N-Doped Biochar from Sewage Sludge and Melamine for Peroxymonosulfate Activation: N-Functionality and Catalytic Mechanisms. *Sci. Total Environ.* **2020**, *744*, 140862. [CrossRef]
80. da Silva Veiga, P.A.; Schultz, J.; da Silva Matos, T.T.; Fornari, M.R.; Costa, T.G.; Meurer, L.; Mangrich, A.S. Production of High-Performance Biochar Using a Simple and Low-Cost Method: Optimization of Pyrolysis Parameters and Evaluation for Water Treatment. *J. Anal. Appl. Pyrolysis* **2020**, *148*, 104823. [CrossRef]
81. Sun, P.; Zhang, K.-K.; Zhang, Y.; Zhang, Y.-R. Sunflower-Straw-Derived Biochar-Enhanced Fe(III)/$S_2O_8^{2-}$ System for Degradation of Benzoic Acid. *Huan Jing Ke Xue* **2020**, *41*, 2301–2309. [CrossRef]
82. Zeng, L.; Chen, Q.; Tan, Y.; Lan, P.; Zhou, D.; Wu, M.; Liang, N.; Pan, B.; Xing, B. Dual Roles of Biochar Redox Property in Mediating 2,4-Dichlorophenol Degradation in the Presence of Fe^{3+} and Persulfate. *Chemosphere* **2021**, *279*, 130456. [CrossRef]
83. Yang, F.; Zhu, Q.; Gao, Y.; Jian, H.; Wang, C.; Sun, H. Effects of Biochar-Dissolved Organic Matter on the Photodegradation of Sulfamethoxazole and Chloramphenicol in Biochar Solutions as Revealed by Oxygen Reduction Performances and Free Radicals. *Sci. Total Environ.* **2021**, *781*, 146807. [CrossRef]
84. Zhong, D.; Jiang, Y.; Zhao, Z.; Wang, L.; Chen, J.; Ren, S.; Liu, Z.; Zhang, Y.; Tsang, D.C.W.; Crittenden, J.C. PH Dependence of Arsenic Oxidation by Rice-Husk-Derived Biochar: Roles of Redox-Active Moieties. *Environ. Sci. Technol.* **2019**, *53*, 9034–9044. [CrossRef] [PubMed]
85. Zhang, K.; Sun, P.; Zhang, Y. Decontamination of Cr(VI) Facilitated Formation of Persistent Free Radicals on Rice Husk Derived Biochar. *Front. Environ. Sci. Eng.* **2019**, *13*, 22. [CrossRef]
86. Zhu, S.; Huang, X.; Yang, X.; Peng, P.; Li, Z.; Jin, C. Enhanced Transformation of Cr(VI) by Heterocyclic-N within Nitrogen-Doped Biochar: Impact of Surface Modulatory Persistent Free Radicals (PFRs). *Environ. Sci. Technol.* **2020**, *54*, 8123–8132. [CrossRef] [PubMed]
87. Wang, X.; Xu, J.; Liu, J.; Liu, J.; Xia, F.; Wang, C.; Dahlgren, R.A.; Liu, W. Mechanism of Cr(VI) Removal by Magnetic Greigite/Biochar Composites. *Sci. Total Environ.* **2020**, *700*, 134414. [CrossRef] [PubMed]
88. Tang, Z.; Kong, Y.; Zhao, S.; Jia, H.; Vione, D.; Kang, Y.; Gao, P. Enhancement of Cr(VI) Decontamination by Irradiated Sludge Biochar in Neutral Conditions: Evidence of a Possible Role of Persistent Free Radicals. *Sep. Purif. Technol.* **2021**, *277*, 119414. [CrossRef]

89. Yu, J.; Zhu, Z.; Zhang, H.; Chen, T.; Qiu, Y.; Xu, Z.; Yin, D. Efficient Removal of Several Estrogens in Water by Fe-Hydrochar Composite and Related Interactive Effect Mechanism of H_2O_2 and Iron with Persistent Free Radicals from Hydrochar of Pinewood. *Sci. Total Environ.* **2019**, *658*, 1013–1022. [CrossRef] [PubMed]
90. Zhu, N.; Li, C.; Bu, L.; Tang, C.; Wang, S.; Duan, P.; Yao, L.; Tang, J.; Dionysiou, D.D.; Wu, Y. Bismuth Impregnated Biochar for Efficient Estrone Degradation: The Synergistic Effect between Biochar and Bi/Bi_2O_3 for a High Photocatalytic Performance. *J. Hazard. Mater.* **2020**, *384*, 121258. [CrossRef]
91. Chen, Y.; Duan, X.; Zhang, C.; Wang, S.; Ren, N.; Ho, S.-H. Graphitic Biochar Catalysts from Anaerobic Digestion Sludge for Nonradical Degradation of Micropollutants and Disinfection. *Chem. Eng. J.* **2020**, *384*, 123244. [CrossRef]
92. Xu, H.; Han, Y.; Wang, G.; Deng, P.; Feng, L. Walnut Shell Biochar Based Sorptive Remediation of Estrogens Polluted Simulated Wastewater: Characterization, Adsorption Mechanism and Degradation by Persistent Free Radicals. *Environ. Technol. Innov.* **2022**, *28*, 102870. [CrossRef]
93. Wang, T.; Zheng, J.; Cai, J.; Liu, Q.; Zhang, X. Visible-Light-Driven Photocatalytic Degradation of Dye and Antibiotics by Activated Biochar Composited with K^+ Doped g-C_3N_4: Effects, Mechanisms, Actual Wastewater Treatment and Disinfection. *Sci. Total Environ.* **2022**, *839*, 155955. [CrossRef] [PubMed]
94. Odinga, E.S.; Waigi, M.G.; Gudda, F.O.; Wang, J.; Yang, B.; Hu, X.; Li, S.; Gao, Y. Occurrence, Formation, Environmental Fate and Risks of Environmentally Persistent Free Radicals in Biochars. *Environ. Int.* **2020**, *134*, 105172. [CrossRef] [PubMed]
95. Fang, G.; Liu, C.; Gao, J.; Dionysiou, D.D.; Zhou, D. Manipulation of Persistent Free Radicals in Biochar To Activate Persulfate for Contaminant Degradation. *Environ. Sci. Technol.* **2015**, *49*, 5645–5653. [CrossRef] [PubMed]
96. Ahmad, Z.; Upadhyay, A.; Ding, Y.; Emamverdian, A.; Shahzad, A. Bamboo: Origin, Habitat, Distributions and Global Prospective. In *Biotechnological Advances in Bamboo*; Springer: Singapore, 2021; pp. 1–31.
97. Yadav, M.; Mathur, A. Bamboo as a Sustainable Material in the Construction Industry: An Overview. *Mater. Today Proc.* **2021**, *43*, 2872–2876. [CrossRef]
98. Chaturvedi, K.; Singhwane, A.; Dhangar, M.; Mili, M.; Gorhae, N.; Naik, A.; Prashant, N.; Srivastava, A.K.; Verma, S. Bamboo for Producing Charcoal and Biochar for Versatile Applications. *Biomass Convers. Biorefin.* **2023**. [CrossRef]
99. Lou, Z.; Wang, Q.; Sun, W.; Zhao, Y.; Wang, X.; Liu, X.; Li, Y. Bamboo Flattening Technique: A Literature and Patent Review. *Eur. J. Wood Wood Prod.* **2021**, *79*, 1035–1048. [CrossRef]
100. Yang, L.; Lou, Z.; Han, X.; Liu, J.; Wang, Z.; Zhang, Y.; Wu, X.; Yuan, C.; Li, Y. Fabrication of a Novel Magnetic Reconstituted Bamboo with Mildew Resistance Properties. *Mater. Today Commun.* **2020**, *23*, 101086. [CrossRef]
101. da Silveira, E.S.; Roel, A.R.; dos Santos Brito, V.H.; Pistori, H.; Cereda, M.P. Influência de Espécies de Bambu Como Alimento No Crescimento Populacional e Na Preferência Alimentar Do Caruncho-Do-Bambu. I. In *Bambus no Brasil: Da Biologia à Tecnologia*; Drumond, P.M., Wiedman, G., Eds.; Instituto Ciência Hoje—ICH: Rio de Janeiro, Brazil, 2017; pp. 130–144.
102. Darabant, A.; Haruthaithanasan, M.; Atkla, W.; Phudphong, T.; Thanavat, E.; Haruthaithanasan, K. Bamboo Biomass Yield and Feedstock Characteristics of Energy Plantations in Thailand. *Energy Procedia* **2014**, *59*, 134–141. [CrossRef]
103. Romero Millán, L.M.; Sierra Vargas, F.E.; Nzihou, A. Characterization of Steam Gasification Biochars from Lignocellulosic Agrowaste towards Soil Applications. *Waste Biomass Valoriz.* **2021**, *12*, 4141–4155. [CrossRef]
104. Masís-Meléndez, F.; Segura-Chavarría, D.; García-González, C.A.; Quesada-Kimsey, J.; Villagra-Mendoza, K. Variability of Physical and Chemical Properties of TLUD Stove Derived Biochars. *Appl. Sci.* **2020**, *10*, 507. [CrossRef]
105. Patel, B.; Patel, M.; Gami, B.; Patel, A. Cultivation of Bioenergy Crops in Gujarat State: A Consultative Survey Process to Understand the Current Practices of Landowners. *Environ. Dev. Sustain.* **2021**, *23*, 8991–9013. [CrossRef]
106. Odega, C.A.; Ayodele, O.O.; Ogutuga, S.O.; Anguruwa, G.T.; Adekunle, A.E.; Fakorede, C.O. Potential Application and Regeneration of Bamboo Biochar for Wastewater Treatment: A Review. *Adv. Bamboo Sci.* **2023**, *2*, 100012. [CrossRef]
107. Ginoble Pandoli, O.; Santos de Sá, D.; Nogueira Barbosa Junior, M.; Paciornik, S. Bamboo-Based Lignocellulose Biomass as Catalytic Support for Organic Synthesis and Water Treatments. In *Bamboo Science and Technology*; Springer: Singapore, 2023; pp. 297–327. [CrossRef]
108. Kawakami, M.; Karato, T.; Takenaka, T.; Yokoyama, S. Structure Analysis of Coke, Wood Charcoal and Bamboo Charcoal by Raman Spectroscopy and Their Reaction Rate with CO_2. *ISIJ Int.* **2005**, *45*, 1027–1034. [CrossRef]
109. Liao, P.; Malik Ismael, Z.; Zhang, W.; Yuan, S.; Tong, M.; Wang, K.; Bao, J. Adsorption of Dyes from Aqueous Solutions by Microwave Modified Bamboo Charcoal. *Chem. Eng. J.* **2012**, *195–196*, 339–346. [CrossRef]
110. Lehmann, J. Bio-Energy in the Black. *Front. Ecol. Environ.* **2007**, *5*, 381–387. [CrossRef]
111. Wei, H.; Deng, S.; Hu, B.; Chen, Z.; Wang, B.; Huang, J.; Yu, G. Granular Bamboo-Derived Activated Carbon for High CO_2 Adsorption: The Dominant Role of Narrow Micropores. *ChemSusChem* **2012**, *5*, 2354–2360. [CrossRef]
112. Liu, D.; Song, J.; Anderson, D.P.; Chang, P.R.; Hua, Y. Bamboo Fiber and Its Reinforced Composites: Structure and Properties. *Cellulose* **2012**, *19*, 1449–1480. [CrossRef]
113. Sahoo, S.S.; Vijay, V.K.; Chandra, R.; Kumar, H. Production and Characterization of Biochar Produced from Slow Pyrolysis of Pigeon Pea Stalk and Bamboo. *Clean. Eng. Technol.* **2021**, *3*, 100101. [CrossRef]
114. Wang, Q.; Wu, X.; Yuan, C.; Lou, Z.; Li, Y. Effect of Saturated Steam Heat Treatment on Physical and Chemical Properties of Bamboo. *Molecules* **2020**, *25*, 1999. [CrossRef] [PubMed]
115. Lou, Z.; Yuan, T.; Wang, Q.; Wu, X.; Hu, S.; Hao, X.; Liu, X.; Li, Y. Fabrication of Crack-Free Flattened Bamboo and Its Macro-/MicroMorphological and Mechanical Properties. *J. Renew. Mater.* **2021**, *9*, 959–977. [CrossRef]

116. Liese, W. *The Anatomy of Bamboo Culms*; INBAR: Beijing, China, 1998; 208p.
117. Lee, C.-H.; Chung, M.-J.; Lin, C.-H.; Yang, T.-H. Effects of Layered Structure on the Physical and Mechanical Properties of Laminated Moso Bamboo (*Phyllosachys edulis*) Flooring. *Constr. Build. Mater.* **2012**, *28*, 31–35. [CrossRef]
118. Wastowski, A.D. *Química Da Madeira Editora Interciência*, 1st ed.; Editora Interciência: Rio de Janeiro, Brazil, 2018; 556p.
119. Yan, L.; Kasal, B.; Huang, L. A Review of Recent Research on the Use of Cellulosic Fibres, Their Fibre Fabric Reinforced Cementitious, Geo-Polymer and Polymer Composites in Civil Engineering. *Compos. B Eng.* **2016**, *92*, 94–132. [CrossRef]
120. Liese, W.; Tang, T.K.H. Properties of the Bamboo Culm. In *Bamboo*; Springer: Cham, Switzerland, 2015; pp. 227–256. [CrossRef]
121. Nayak, L.; Mishra, S.P. Prospect of Bamboo as a Renewable Textile Fiber, Historical Overview, Labeling, Controversies and Regulation. *Fash. Text.* **2016**, *3*, 2. [CrossRef]
122. Wan, J.; Wang, Y.; Xiao, Q. Effects of Hemicellulose Removal on Cellulose Fiber Structure and Recycling Characteristics of Eucalyptus Pulp. *Bioresour. Technol.* **2010**, *101*, 4577–4583. [CrossRef]
123. Mohamad Ibrahim, M.N.; Zakaria, N.; Sipaut, C.S.; Sulaiman, O.; Hashim, R. Chemical and Thermal Properties of Lignins from Oil Palm Biomass as a Substitute for Phenol in a Phenol Formaldehyde Resin Production. *Carbohydr. Polym.* **2011**, *86*, 112–119. [CrossRef]
124. Nogueira, C.d.L. Painel de Bambu Laminado Colado Estrutural. Master's Thesis, Universidade de São Paulo, Piracicaba, Brazil, 2008.
125. Macedo, L.A.; Rousset, P.L.A.; Vale, A.T. Influência Da Composição Da Biomassa No Rendimento Em Condensáveis Da Torrefação de Resíduos Vegetais. *Pesqui. Florest. Bras.* **2014**, *34*, 417–424. [CrossRef]
126. Rousset, P.; Aguiar, C.; Labbé, N.; Commandré, J.-M. Enhancing the Combustible Properties of Bamboo by Torrefaction. *Bioresour. Technol.* **2011**, *102*, 8225–8231. [CrossRef]
127. Hernandez-Mena, L.E.; Pécoraa, A.A.B.; Beraldo, A.L. Slow Pyrolysis of Bamboo Biomass: Analysis of Biochar Properties. *Chem. Eng. Trans.* **2014**, *37*, 115–120. [CrossRef]
128. Lin, L.-D.; Chang, F.-C.; Ko, C.-H.; Wang, C.-T. Bamboo-Derived Fuel from *Dendrocalamus latiflorus*, *Phyllostachys makinoi*, and *Phyllostachys pubescens* Waste. *Bioresources* **2016**, *11*, 8425–8434. [CrossRef]
129. Neves, D.; Thunman, H.; Matos, A.; Tarelho, L.; Gómez-Barea, A. Characterization and Prediction of Biomass Pyrolysis Products. *Prog. Energy Combust. Sci.* **2011**, *37*, 611–630. [CrossRef]
130. Gontijo, L.O.L.; Junior, M.N.B.; de Sá, D.S.; Letichevsky, S.; Pedrozo-Peñafiel, M.J.; Aucélio, R.Q.; Bott, I.S.; Diniz Lopes Alves, H.; Fragneaud, B.; Oliveira Maciel, I.; et al. 3D Conductive Monolithic Carbons from Pyrolyzed Bamboo for Microfluidic Self-Heating System. *Carbon* **2023**, *213*, 118214. [CrossRef]
131. Lin, Q.; Gao, R.; Li, D.; Lu, Y.; Liu, S.; Yu, Y.; Huang, Y.; Yu, W. Bamboo-Inspired Cell-Scale Assembly for Energy Device Applications. *NPJ Flex. Electron.* **2022**, *6*, 13. [CrossRef]
132. Deng, J.; Xiong, T.; Xu, F.; Li, M.; Han, C.; Gong, Y.; Wang, H.; Wang, Y. Inspired by Bread Leavening: One-Pot Synthesis of Hierarchically Porous Carbon for Supercapacitors. *Green Chem.* **2015**, *17*, 4053–4060. [CrossRef]
133. Jiang, J.; Zhu, J.; Ai, W.; Fan, Z.; Shen, X.; Zou, C.; Liu, J.; Zhang, H.; Yu, T. Evolution of Disposable Bamboo Chopsticks into Uniform Carbon Fibers: A Smart Strategy to Fabricate Sustainable Anodes for Li-Ion Batteries. *Energy Environ. Sci.* **2014**, *7*, 2670–2679. [CrossRef]
134. Yin, T.; Zhang, Z.; Xu, L.; Li, C.; Han, D. Preparation of Green High-performance Biomass-Derived Hard Carbon Materials from Bamboo Powder Waste. *ChemistryOpen* **2024**. [CrossRef]
135. Subyakto, S.; Budiman, I.; Pari, G. Effects of Temperature and Time of Carbonization on the Properties of Bamboo (*Dendrocalamus asper*) Carbon. *Wood Res. J.* **2017**, *4*, 68–73. [CrossRef]
136. Yang, W.; Li, J.; Zhang, L.; Zhu, X.; Liao, Q. A Monolithic Air Cathode Derived from Bamboo for Microbial Fuel Cells. *RSC Adv.* **2017**, *7*, 28469–28475. [CrossRef]
137. Bian, Y.; Du, Q.; Tang, K.; Shen, Y.; Hao, L.; Zhou, D.; Wang, X.; Xu, Z.; Zhang, H.; Zhao, L.; et al. Carbonized Bamboos as Excellent 3D Solar Vapor-Generation Devices. *Adv. Mater. Technol.* **2019**, *4*, 1800593. [CrossRef]
138. Liu, J.; Yao, J.; Yuan, Y.; Liu, Q.; Zhang, W.; Zhang, X.; Gu, J. Surface-Carbonized Bamboos with Multilevel Functional Biostructures Deliver High Photothermal Water Evaporation Performance. *Adv. Sustain. Syst.* **2020**, *4*, 2000126. [CrossRef]
139. Ye, L.; Zhang, J.; Zhao, J.; Luo, Z.; Tu, S.; Yin, Y. Properties of Biochar Obtained from Pyrolysis of Bamboo Shoot Shell. *J. Anal. Appl. Pyrolysis* **2015**, *114*, 172–178. [CrossRef]
140. Aggangan, N.S.; Cortes, A.D.; Reaño, C.E. Growth Response of Cacao (*Theobroma cacao* L.) Plant as Affected by Bamboo Biochar and Arbuscular Mycorrhizal Fungi in Sterilized and Unsterilized Soil. *Biocatal. Agric. Biotechnol.* **2019**, *22*, 101347. [CrossRef]
141. Chen, J.; Li, S.; Liang, C.; Xu, Q.; Li, Y.; Qin, H.; Fuhrmann, J.J. Response of Microbial Community Structure and Function to Short-Term Biochar Amendment in an Intensively Managed Bamboo (*Phyllostachys praecox*) Plantation Soil: Effect of Particle Size and Addition Rate. *Sci. Total Environ.* **2017**, *574*, 24–33. [CrossRef]
142. Yin, Y.; Gu, M.; Zhang, W.; Yang, C.; Li, H.; Wang, X.; Chen, R. Relationships between Different Types of Biochar and N_2O Emissions during Composting Based on Roles of NosZ-Carrying Denitrifying Bacterial Communities Enriched on Compost and Biochar Particles. *Bioresour. Technol.* **2024**, *394*, 130214. [CrossRef] [PubMed]
143. Yin, Y.; Tao, X.; Du, Y.; Li, M.; Yang, S.; Zhang, W.; Yang, C.; Li, H.; Wang, X.; Chen, R. Biochar Improves the Humification Process during Pig Manure Composting: Insights into Roles of the Bacterial Community and Metabolic Functions. *J. Environ. Manag.* **2024**, *355*, 120463. [CrossRef] [PubMed]

144. Cruz-Méndez, A.S.; Ortega-Ramírez, E.; Lucho-Constantino, C.A.; Arce-Cervantes, O.; Vázquez-Rodríguez, G.A.; Coronel-Olivares, C.; Beltrán-Hernández, R.I. Bamboo Biochar and a Nopal-Based Biofertilizer as Improvers of Alkaline Soils with Low Buffer Capacity. *Appl. Sci.* **2021**, *11*, 6502. [CrossRef]
145. Situmeang, Y.P.; Sudewa, K.A.; Holo, P.P. Utilization Biochar of Bamboo and Compost in Improving Yield of Pakchoy Plant. *J. Biol. Chem. Res.* **2017**, *34*, 713–722.
146. Suthar, R.; Wang, C.; Nunes, M.; Chen, J.; Sargent, S.; Bucklin, R.; Gao, B. Bamboo Biochar Pyrolyzed at Low Temperature Improves Tomato Plant Growth and Fruit Quality. *Agriculture* **2018**, *8*, 153. [CrossRef]
147. Villagra-Mendoza, K.; Masís-Meléndez, F.; Quesada-Kimsey, J.; García-González, C.A.; Horn, R. Physicochemical Changes in Loam Soils Amended with Bamboo Biochar and Their Influence in Tomato Production Yield. *Agronomy* **2021**, *11*, 2052. [CrossRef]
148. Wang, Y.; Zhong, B.; Shafi, M.; Ma, J.; Guo, J.; Wu, J.; Ye, Z.; Liu, D.; Jin, H. Effects of Biochar on Growth, and Heavy Metals Accumulation of Moso Bamboo (*Phyllostachy pubescens*), Soil Physical Properties, and Heavy Metals Solubility in Soil. *Chemosphere* **2019**, *219*, 510–516. [CrossRef]
149. Tarin, M.W.K.; Fan, L.; Xie, D.; Tayyab, M.; Rong, J.; Chen, L.; Muneer, M.A.; Zheng, Y. Response of Soil Fungal Diversity and Community Composition to Varying Levels of Bamboo Biochar in Red Soils. *Microorganisms* **2021**, *9*, 1385. [CrossRef]
150. Wang, C.; Alidoust, D.; Yang, X.; Isoda, A. Effects of Bamboo Biochar on Soybean Root Nodulation in Multi-Elements Contaminated Soils. *Ecotoxicol. Environ. Saf.* **2018**, *150*, 62–69. [CrossRef]
151. Tang, L.; Xiong, L.; Zhang, H.; Joseph, A.; Wang, Y.; Li, J.; Yuan, X.; Rene, E.R.; Zhu, N. Reduced Arsenic Availability in Paddy Soil through Fe-Organic Ligand Complexation Mediated by Bamboo Biochar. *Chemosphere* **2024**, *349*, 140790. [CrossRef]
152. Hua, L.; Wu, W.; Liu, Y.; McBride, M.B.; Chen, Y. Reduction of Nitrogen Loss and Cu and Zn Mobility during Sludge Composting with Bamboo Charcoal Amendment. *Environ. Sci. Pollut. Res.* **2009**, *16*, 1–9. [CrossRef]
153. Ji, Y.; Zhang, C.; Zhang, X.J.; Xie, P.F.; Wu, C.; Jiang, L. A High Adsorption Capacity Bamboo Biochar for CO_2 Capture for Low Temperature Heat Utilization. *Sep. Purif. Technol.* **2022**, *293*, 121131. [CrossRef]
154. Liu, Y.; Gan, L.; Chen, Z.; Megharaj, M.; Naidu, R. Removal of Nitrate Using *Paracoccus* sp. YF1 Immobilized on Bamboo Carbon. *J. Hazard. Mater.* **2012**, *229–230*, 419–425. [CrossRef] [PubMed]
155. Viglašová, E.; Galamboš, M.; Danková, Z.; Krivosudský, L.; Lengauer, C.L.; Hood-Nowotny, R.; Soja, G.; Rompel, A.; Matík, M.; Briančin, J. Production, Characterization and Adsorption Studies of Bamboo-Based Biochar/Montmorillonite Composite for Nitrate Removal. *Waste Manag.* **2018**, *79*, 385–394. [CrossRef] [PubMed]
156. Mizuta, K.; Matsumoto, T.; Hatate, Y.; Nishihara, K.; Nakanishi, T. Removal of Nitrate-Nitrogen from Drinking Water Using Bamboo Powder Charcoal. *Bioresour. Technol.* **2004**, *95*, 255–257. [CrossRef] [PubMed]
157. Asada, T.; Ohkubo, T.; Kawata, K.; Oikawa, K. Ammonia Adsorption on Bamboo Charcoal with Acid Treatment. *J. Health Sci.* **2006**, *52*, 585–589. [CrossRef]
158. Deng, P.; Wan, W.; Azeem, M.; Riaz, L.; Zhang, W.; Yang, Y.; Li, C.; Yuan, W. Characterization of Biochar Derived from Bamboo and Its Application to Modulate the Toxic Effects of Chromium on Wheat Plant. *Biomass Convers. Biorefin.* **2024**, *14*, 7643–7658. [CrossRef]
159. Huang, A.; Bai, W.; Yang, S.; Wang, Z.; Wu, N.; Zhang, Y.; Ji, N.; Li, D. Adsorption Characteristics of Chitosan-Modified Bamboo Biochar in Cd(II) Contaminated Water. *J. Chem.* **2022**, *2022*, 6303252. [CrossRef]
160. Mohamed, I.; Zhang, G.; Li, Z.; Liu, Y.; Chen, F.; Dai, K. Ecological Restoration of an Acidic Cd Contaminated Soil Using Bamboo Biochar Application. *Ecol. Eng.* **2015**, *84*, 67–76. [CrossRef]
161. Ma, W.; Han, R.; Zhang, W.; Zhang, H.; Chen, L.; Zhu, L. Magnetic Biochar Enhanced Copper Immobilization in Agricultural Lands: Insights from Adsorption Precipitation and Redox. *J. Environ. Manag.* **2024**, *352*, 120058. [CrossRef]
162. Zhang, X.; Xue, J.; Han, H.; Wang, Y. Study on Improvement of Copper Sulfide Acid Soil Properties and Mechanism of Metal Ion Fixation Based on Fe-Biochar Composite. *Sci. Rep.* **2024**, *14*, 247. [CrossRef] [PubMed]
163. Yang, J.; Long, Q.; Zhu, Y.; Lin, C.; Xu, X.; Pan, B.; Shi, W.; Guo, Y.; Deng, J.; Yao, Q.; et al. Multifunctional Self-Assembled Adsorption Microspheres Based on Waste Bamboo Shoot Shells for Multi-Pollutant Water Purification. *Environ. Res.* **2024**, *249*, 118452. [CrossRef]
164. Tan, Z.; Qiu, J.; Zeng, H.; Liu, H.; Xiang, J. Removal of Elemental Mercury by Bamboo Charcoal Impregnated with H_2O_2. *Fuel* **2011**, *90*, 1471–1475. [CrossRef]
165. Wang, F.Y.; Wang, H.; Ma, J.W. Adsorption of Cadmium (II) Ions from Aqueous Solution by a New Low-Cost Adsorbent—Bamboo Charcoal. *J. Hazard. Mater.* **2010**, *177*, 300–306. [CrossRef]
166. Wang, S.Y.; Tsai, M.H.; Lo, S.F.; Tsai, M.J. Effects of Manufacturing Conditions on the Adsorption Capacity of Heavy Metal Ions by Makino Bamboo Charcoal. *Bioresour. Technol.* **2008**, *99*, 7027–7033. [CrossRef]
167. Lo, S.-F.; Wang, S.-Y.; Tsai, M.-J.; Lin, L.-D. Adsorption Capacity and Removal Efficiency of Heavy Metal Ions by Moso and Ma Bamboo Activated Carbons. *Chem. Eng. Res. Des.* **2012**, *90*, 1397–1406. [CrossRef]
168. González, P.G.; Pliego-Cuervo, Y.B. Adsorption of Cd(II), Hg(II) and Zn(II) from Aqueous Solution Using Mesoporous Activated Carbon Produced from *Bambusa vulgaris* Striata. *Chem. Eng. Res. Des.* **2014**, *92*, 2715–2724. [CrossRef]
169. Lalhruaitluanga, H.; Prasad, M.N.V.; Radha, K. Potential of Chemically Activated and Raw Charcoals of *Melocanna baccifera* for Removal of Ni(II) and Zn(II) from Aqueous Solutions. *Desalination* **2011**, *271*, 301–308. [CrossRef]
170. Fan, Y.; Wang, B.; Yuan, S.; Wu, X.; Chen, J.; Wang, L. Adsorptive Removal of Chloramphenicol from Wastewater by NaOH Modified Bamboo Charcoal. *Bioresour. Technol.* **2010**, *101*, 7661–7664. [CrossRef]

171. Li, Y.; Shao, J.; Wang, X.; Deng, Y.; Yang, H.; Chen, H. Characterization of Modified Biochars Derived from Bamboo Pyrolysis and Their Utilization for Target Component (Furfural) Adsorption. *Energy Fuels* **2014**, *28*, 5119–5127. [CrossRef]
172. Yao, Y.; Gao, B.; Fang, J.; Zhang, M.; Chen, H.; Zhou, Y.; Creamer, A.E.; Sun, Y.; Yang, L. Characterization and Environmental Applications of Clay–Biochar Composites. *Chem. Eng. J.* **2014**, *242*, 136–143. [CrossRef]
173. Wang, T.; Liu, X.; Ma, C.; Liu, Y.; Dong, H.; Ma, W.; Liu, Z.; Wei, M.; Li, C.; Yan, Y. A Two Step Hydrothermal Process to Prepare Carbon Spheres from Bamboo for Construction of Core–Shell Non-Metallic Photocatalysts. *New J. Chem.* **2018**, *42*, 6515–6524. [CrossRef]
174. Wang, Y.; Lu, J.; Wu, J.; Liu, Q.; Zhang, H.; Jin, S. Adsorptive Removal of Fluoroquinolone Antibiotics Using Bamboo Biochar. *Sustainability* **2015**, *7*, 12947–12957. [CrossRef]
175. Xu, T.; Lou, L.; Luo, L.; Cao, R.; Duan, D.; Chen, Y. Effect of Bamboo Biochar on Pentachlorophenol Leachability and Bioavailability in Agricultural Soil. *Sci. Total Environ.* **2012**, *414*, 727–731. [CrossRef] [PubMed]
176. Yang, Y.; Lin, X.; Wei, B.; Zhao, Y.; Wang, J. Evaluation of Adsorption Potential of Bamboo Biochar for Metal-Complex Dye: Equilibrium, Kinetics and Artificial Neural Network Modeling. *Int. J. Environ. Sci. Technol.* **2014**, *11*, 1093–1100. [CrossRef]
177. Zhang, X.; Sarmah, A.K.; Bolan, N.S.; He, L.; Lin, X.; Che, L.; Tang, C.; Wang, H. Effect of Aging Process on Adsorption of Diethyl Phthalate in Soils Amended with Bamboo Biochar. *Chemosphere* **2016**, *142*, 28–34. [CrossRef]
178. Liao, P.; Yuan, S.; Xie, W.; Zhang, W.; Tong, M.; Wang, K. Adsorption of Nitrogen-Heterocyclic Compounds on Bamboo Charcoal: Kinetics, Thermodynamics, and Microwave Regeneration. *J. Colloid Interface Sci.* **2013**, *390*, 189–195. [CrossRef]
179. Liu, X.-M.; Huan, W.-W.; Kang, Y.; Guo, J.-Z.; Wang, Y.-X.; Li, F.-H.; Li, B. Effects of Cation Types in Persulfate on Physicochemical and Adsorptive Properties of Biochar Prepared from Persulfate-Pretreated Bamboo. *Bioresour. Technol.* **2024**, *393*, 130140. [CrossRef]
180. Hameed, B.H.; Din, A.T.M.; Ahmad, A.L. Adsorption of Methylene Blue onto Bamboo-Based Activated Carbon: Kinetics and Equilibrium Studies. *J. Hazard. Mater.* **2007**, *141*, 819–825. [CrossRef] [PubMed]
181. Liao, P.; Zhan, Z.; Dai, J.; Wu, X.; Zhang, W.; Wang, K.; Yuan, S. Adsorption of Tetracycline and Chloramphenicol in Aqueous Solutions by Bamboo Charcoal: A Batch and Fixed-Bed Column Study. *Chem. Eng. J.* **2013**, *228*, 496–505. [CrossRef]
182. Men, Q.; Wang, T.; Ma, C.; Yang, L.; Liu, Y.; Huo, P.; Yan, Y. In-Suit Preparation of CdSe Quantum Dots/Porous Channel Biochar for Improving Photocatalytic Activity for Degradation of Tetracycline. *J. Taiwan Inst. Chem. Eng.* **2019**, *99*, 180–192. [CrossRef]
183. Zhao, D.; Zhang, J.; Duan, E.; Wang, J. Adsorption Equilibrium and Kinetics of Dibenzothiophene from N-Octane on Bamboo Charcoal. *Appl. Surf. Sci.* **2008**, *254*, 3242–3247. [CrossRef]
184. Li, S.; Umereweneza, D. Adsorption of N-Vinylpyrrolidone from Polyvinylpyrrolidone Solution onto Bamboo-Based Activated Carbon. *Sep. Sci. Technol.* **2012**, *47*, 104–111. [CrossRef]
185. Lin, J.; Xu, Z.; Zhang, Q.; Cao, Y.; Mašek, O.; Lei, H.; Tsang, D.C.W. Enhanced Adsorption of Aromatic VOCs on Hydrophobic Porous Biochar Produced via Microwave Rapid Pyrolysis. *Bioresour. Technol.* **2024**, *393*, 130085. [CrossRef] [PubMed]
186. Yu, C.; Xie, T.; Liu, S.; Bai, L. Fabrication of a Biochar-Doped Monolithic Adsorbent and Its Application for the Extraction and Determination of Coumarins from *Angelicae pubescentis* Radix. *J. Chromatogr. A* **2024**, *1714*, 464564. [CrossRef] [PubMed]
187. Jagnade, P.; Panwar, N.L. Experiment Investigation on the Performance of Activated Bamboo Biochar for the Adsorption of CO_2 and $PM_{2.5}$. *Emergent Mater.* **2024**. [CrossRef]
188. Wei, Y.; Shen, C.; Xie, J.; Bu, Q. Study on Reaction Mechanism of Superior Bamboo Biochar Catalyst Production by Molten Alkali Carbonates Pyrolysis and Its Application for Cellulose Hydrolysis. *Sci. Total Environ.* **2020**, *712*, 136435. [CrossRef] [PubMed]
189. Chen, Z.; Li, Q.; Xiao, Y.; Zhang, C.; Fu, Z.; Liu, Y.; Yi, X.; Zheng, A.; Li, C.; Yin, D. Acid–Base Synergistic Catalysis of Biochar Sulfonic Acid Bearing Polyamide for Microwave-Assisted Hydrolysis of Cellulose in Water. *Cellulose* **2019**, *26*, 751–762. [CrossRef]
190. Chen, W.; Fang, Y.; Li, K.; Chen, Z.; Xia, M.; Gong, M.; Chen, Y.; Yang, H.; Tu, X.; Chen, H. Bamboo Wastes Catalytic Pyrolysis with N-Doped Biochar Catalyst for Phenols Products. *Appl. Energy* **2020**, *260*, 114242. [CrossRef]
191. Chen, W.; Li, K.; Xia, M.; Yang, H.; Chen, Y.; Chen, X.; Che, Q.; Chen, H. Catalytic Deoxygenation Co-Pyrolysis of Bamboo Wastes and Microalgae with Biochar Catalyst. *Energy* **2018**, *157*, 472–482. [CrossRef]
192. Yang, H.; Chen, Z.; Chen, W.; Chen, Y.; Wang, X.; Chen, H. Role of Porous Structure and Active O-Containing Groups of Activated Biochar Catalyst during Biomass Catalytic Pyrolysis. *Energy* **2020**, *210*, 118646. [CrossRef]
193. Niu, S.; Ning, Y.; Lu, C.; Han, K.; Yu, H.; Zhou, Y. Esterification of Oleic Acid to Produce Biodiesel Catalyzed by Sulfonated Activated Carbon from Bamboo. *Energy Convers. Manag.* **2018**, *163*, 59–65. [CrossRef]
194. Situmeang, Y.P. The Use of Bamboo Biochar as a Soil Improver on the Growth and Yield of Mustard Plants. *Agriwar J.* **2022**, *2*, 14–18. [CrossRef]
195. Zhang, S.-Z.; Cui, Z.-S.; Zhang, M.; Zhang, Z.-H. Biochar-Based Functional Materials as Heterogeneous Catalysts for Organic Reactions. *Curr. Opin. Green Sustain. Chem.* **2022**, *38*, 100713. [CrossRef]
196. Huang, D.; Luo, H.; Zhang, C.; Zeng, G.; Lai, C.; Cheng, M.; Wang, R.; Deng, R.; Xue, W.; Gong, X.; et al. Nonnegligible Role of Biomass Types and Its Compositions on the Formation of Persistent Free Radicals in Biochar: Insight into the Influences on Fenton-like Process. *Chem. Eng. J.* **2019**, *361*, 353–363. [CrossRef]
197. Zhang, Y.; Xu, M.; He, R.; Zhao, J.; Kang, W.; Lv, J. Effect of Pyrolysis Temperature on the Activated Permonosulfate Degradation of Antibiotics in Nitrogen and Sulfur-Doping Biochar: Key Role of Environmentally Persistent Free Radicals. *Chemosphere* **2022**, *294*, 133737. [CrossRef] [PubMed]

198. Wang, Z.; Lin, X.; Yang, K.; Lin, D. Differential Photodegradation Processes of Adsorbed Polychlorinated Biphenyls on Biochar Colloids with Various Pyrolysis Temperatures. *Water Res.* **2024**, *251*, 121174. [CrossRef] [PubMed]
199. Lin, Y.; Ge, Q.; Wan, J.; Wang, Y.; Zhu, C. Insights into the Influence and Mechanism of Biomass Substrate and Thermal Conversion Conditions on Fe N Doped Biochar as a Persulfate Activator for Sulfamethoxazole Removal. *Sci. Total Environ.* **2024**, *907*, 168101. [CrossRef] [PubMed]

MDPI AG
Grosspeteranlage 5
4052 Basel
Switzerland
Tel.: +41 61 683 77 34

Journal of Xenobiotics Editorial Office
E-mail: jox@mdpi.com
www.mdpi.com/journal/jox

Academic Open
Access Publishing

mdpi.com

ISBN 978-3-7258-4614-6